

Special Issue

Polymer materials and composites
Polimerni materiali in kompoziti

Guest Editor:

Miran Mozetič

MATER. TEHNOL.	LETNIK VOLUME	45	ŠTEV. NO.	3	STR. P.	167–292	LJUBLJANA SLOVENIJA	MAY–JUNE 2011
-------------------	------------------	----	--------------	---	------------	---------	------------------------	------------------

VSEBINA – CONTENTS

Predgovor/Foreword

M. Mozetič	171
------------------	-----

*IZVIRNI ZNANSTVENI ČLANKI – ORIGINAL SCIENTIFIC ARTICLES***Microwave-assisted non-aqueous synthesis of ZnO nanoparticles**

Sinteza nanodelcev ZnO v nevodnem mediju pod vplivom mikrovalov G. Ambrožič, Z. Crnjak Orel, M. Žigon	173
--	-----

Removal of a thin hydrogenated carbon film by oxygen plasma treatment

Odstranjevanje tanke plasti hidrogeniranega ogljika s kisikovo plazmo U. Cvelbar	179
---	-----

Low temperature destruction of bacteria *Bacillus stearothermophilus* by weakly ionized oxygen plasma

Nizkotemperaturno uničevanje bakterij <i>Bacillus stearothermophilus</i> s šibko ionizirano kisikovo plazmo M. Mozetič	185
---	-----

Surface characterization of polymers by XPS and SIMS techniques

Analiza površine polimerov z metodama XPS in SIMS J. Kovač	191
---	-----

Modification of PET-polymer surface by nitrogen plasma

Modifikacija površine PET-polimera z dušikovo plazmo R. Zaplotnik, M. Kolar, A. Doliška, K. Stana-Kleinschek	199
---	-----

Functionalization of AFM tips for use in force spectroscopy between polymers and model surfaces

Funkcionalizacija AFM-konic za uporabo v spektroskopiji sil med polimeri in modelnimi površinami T. Maver, K. Stana - Kleinschek, Z. Peršin, U. Maver	205
--	-----

A novel approach for qualitative determination of residual tin based catalyst in poly(lactic acid) by X-ray photoelectron spectroscopy

Nov način kvalitativne določitve vsebnosti katalizatorja kositra v polilaktični kislini z rentgensko fotoelektronsko spektroskopijo V. Sedlařík, A. Vesel, P. Kucharczyk, P. Urbánek	213
---	-----

Hydrophobization of polymer polystyrene in fluorine plasma

Hidrofobizacija polimera polistiren s fluorovo plazmo A. Vesel	217
---	-----

Plasma treatment of biomedical materials

Plazemska obdelava biomedicinskih materialov I. Junkar, U. Cvelbar, M. Lehocky	221
---	-----

Radiofrequency induced plasma in large-scale plasma reactor

Radiofrekvenčno inducirana plazma v reaktorju velikih dimenzij R. Zaplotnik, A. Vesel	227
--	-----

Modification of surface morphology of graphite by oxygen plasma treatment

Sprememba morfologije grafita med obdelavo s kisikovo plazmo K. Eleršič, I. Junkar, M. Modic, R. Zaplotnik, A. Vesel, U. Cvelbar	233
---	-----

Properties of particleboards made by using an adhesive with added liquefied wood

Lastnosti ivernih plošč, izdelanih z uporabo lepila z dodanim utekočinjenim lesom N. Čuk, M. Kunaver, S. Medved	241
--	-----

Poly(styrene-CO-divinylbenzene-CO-2-ethylhexyl)acrylate membranes with interconnected macroporous structure

Poli(stiren-KO-divinilbenzen-KO-2-etilheksil)akrilatne membrane s povezano porozno strukturo U. Sevšek, S. Seifried, Č. Stropnik, I. Pulko, P. Krajnc	247
--	-----

Modification of non-woven cellulose for medical applications using non-equilibrium gaseous plasma

Modifikacija celuloznih kopren, uporabljenih v medicinske namene, z neravnovesno plinsko plazmo K. Stana - Kleinschek, Z. Peršin, T. Maver	253
---	-----

Use of AFM force spectroscopy for assessment of polymer response to conditions similar to the wound, during healing Uporaba AFM-spektroskopije sil za spremljanje odziva polimernih molekul na v rani podobna okolja med celjenjem U. Maver, T. Maver, A. Žnidaršič, Z. Peršin, M. Gaberšček, K. Stana-Kleinschek	259
Biodegradable polymers from renewable resources: effect of proteinic impurity on polycondensation products of 2-hydroxypropanoic acid Biorazgradljivi polimeri iz obnovljivih virov: vpliv proteinskih nečistot na produkte polikondenzacije 2-hidroksipropanojske kisline I. Poljanšek, P. Kucharczyk, V. Sedlařík, V. Kašpárková, A. Šalaková, J. Drbohlav	265
Submikrometrski in nano ZnO kot polnilo v PMMA-materialih Sub micrometer and nano ZnO as filler in PMMA materials A. Anžlovar, Z. Crnjak Orel, M. Žigon	269
Tuning of poly(ethylene terephthalate) (PET) surface properties by oxygen plasma treatment Prilagoditev lastnosti površine polietilen tereftalata (PET) z obelavo v kisikovi plazmi A. Doliška, M. Kolar	275
Probability of recombination and oxidation of O atoms on a-C:H surface Verjetnost za rekombinacijo in oksidacijo za atome kisika na površini a-C:H A. Drenik, K. Eleršič, M. Modic, P. Panjan	281
Hydrothermal growth of Zn₅(OH)₆(CO₃)₂ and its thermal transformation into porous ZnO film used for dye-sensitized solar cells Hidrotermalna rast Zn ₅ (OH) ₆ (CO ₃) ₂ s termično transformacijo v porozno plast ZnO, uporabljeno za elektrokemijske sončne celice M. Bitenc, Z. Crnjak Orel	287
19. KONFERENCA O MATERIALIH IN TEHNOLOGIJAH, 21. – 23. november 2011, Portorož, Slovenija 19th CONFERENCE ON MATERIALS AND TECHNOLOGY, November 21–23, 2011, Portorož, Slovenia	293

MISLI GOSTUJOČEGA UREDNIKA

FOREWORD

Posebno izdajo naše znanstvene revije namenimo polimerom in materialom, ki vsebujejo polimere. Tovrstne materiale srečujemo povsod okoli nas, od nekaterih naravnih organskih materialov do visokotehnoloških biočipov. Hitra rast uporabe polimernih materialov je vedno nov izziv za razvoj naprednih izdelkov in tehnologij za modifikacijo površinskih lastnosti, ki v vedno večji meri temeljijo na sodobnih neravnovesnih postopkih. Ta izdaja naše revije obsega nekatere vidike polimerov in polimernih kompozitov od nanokompozitov do hidrogeniranega ogljika v sodobnih fuzijskih reaktorjih. Tematski sklopi, ki so predstavljeni v tej izdaji, spadajo med raziskovalne aktivnosti Centra odličnosti "Polimerni materiali in tehnologije", ki je bil ustanovljen leta 2010 z namenom združevanja raziskav na tem področju in uporabnikov tovrstnih materialov.

This special issue is devoted to polymers and polymer-containing materials. They are found everywhere around us in various forms ranging from some natural organic materials to sophisticated biochips. Rapidly growing applications dictate development of novel materials with improved characteristics as well as innovative techniques for surface modification – many are based on application of advanced non-equilibrium processing. The present issue covers some scientific aspects of polymers and polymer composites, from nanocomposites to hydrogenated carbon in fusion reactors. The topics presented in the issue are essentially research activities performed within the Centre of excellence "Polymer materials and technologies" established in 2010 in order to unite Slovenian research centers and users of such materials.

Gostujoči urednik:
prof. dr. Miran Mozetič,
vodja projekta
Center odličnosti PoliMaT

Guest Editor
Prof. Dr. Miran Mozetič
Project manager
Centre of excellence PoliMaT

MICROWAVE-ASSISTED NON-AQUEOUS SYNTHESIS OF ZnO NANOPARTICLES

SINTEZA NANODELCEV ZnO V NEVODNEM MEDIJU POD VPLIVOM MIKROVALOV

Gabriela Ambrožič, Zorica Crnjak Orel, Majda Žigon

Center of Excellence for Polymer Materials and Technologies, Tehnološki park 24, SI-1000 Ljubljana, Slovenia.
gabriela.ambrozic@ki.si

Prejem rokopisa – received: 2011-02-14; sprejem za objavo – accepted for publication: 2011-04-12

In this work, the microwave-assisted non-aqueous synthesis of ZnO nanoparticles is reviewed. In comparison with the "classical" (conductive) heating, the microwave method provides for a better control over experimental parameters and, therefore, opens exciting opportunities for a better understanding of the influence of the reaction conditions on the reaction and growth mechanisms of ZnO particles. As the morphology and size determine the physicochemical behavior of ZnO, a variety of polymer-ZnO nanomaterials with tunable optoelectrical and mechanical properties can be *in-situ* or *ex-situ* prepared by the microwave-assisted synthesis.

In the article, a special attention is devoted to investigations performed in our laboratory on the systems of zinc acetylacetonate as a precursor and 1-butanol as media as well as oxygen supplier. Contrary to analogous syntheses performed under reflux conditions, we showed that under microwave conditions the precursor's initial amount exerts a tremendous effect on the morphology and size of ZnO particles.

Keywords: ZnO nanoparticles, microwave chemistry, non-aqueous synthesis, crystal growth

V delu podajamo pregled sinteze nanodelcev ZnO v nevodnem mediju pod vplivom mikrovalov. V primerjavi s segrevanjem s konvekcijo mikrovalovno segrevanje omogoča boljši nadzor nad eksperimentalnimi parametri in tako ponuja zanimive priložnosti za boljše razumevanje vpliva reakcijskih pogojev na mehanizem in rast delcev ZnO. Ker pa velikost in oblika delcev določata fizikalno-kemijske lastnosti ZnO-nanomateriala, bo mikrovalovna sinteza v prihodnosti omogočila *in-situ* ali *ex-situ* pripravo širokega spektra nanokompozitov ZnO/polimer z nastavljivimi optoelektronskimi in mehanskimi lastnostmi.

V članku je posebna pozornost namenjena raziskavam, ki smo jih opravili v našem laboratoriju na sistemu cinkovega acetilacetonata kot prekurzorja in 1-butanola kot medija in donorja kisika. V nasprotju s prejšnjimi študijami na analognem sistemu pod pogoji refluxa smo pokazali, da pod mikrovalovnimi vplivi začetna količina prekurzorja ključno vpliva na morfologijo in velikost delcev ZnO.

Ključne besede: ZnO-nanodelci, mikrovalovna kemija, brezvodna sinteza, rast kristalov

1 INTRODUCTION

The unique and fascinating properties of nanostructured materials have triggered tremendous motivation among scientists to explore and understand their formation and growth processes as well as their subsequent implementation in the steady and fast growing research on the preparation of new polymer composite nanomaterials, which can exhibit new functionalities based on nanoparticle's optical and electrical properties.¹ Due to the fact that morphologies and sizes of inorganic particles determine the properties and applications of the polymer nanocomposites, the possibility to tune the physical and chemical properties of nanoscale materials through varying the crystal size and shape is a major driving force in nanoparticle research.

In general, three types of processes are applied for the synthesis of metal oxide particles in solution: the "classical" synthesis under reflux conditions, the autoclave synthesis and, the most recent microwave-assisted synthesis.²

In the oil bath synthesis, where the walls of the reactor are heated by convection or conduction, the core

of the sample needs longer time to achieve the target temperature and this may result in inhomogeneous temperature profiles within the reaction flask.

One possibility to overcome this problem is the use of microwave or dielectric heating, which is becoming an increasingly popular synthetic method for organic^{3, 4} as well as inorganic materials.⁵ Microwave process enables the rapid and homogeneous heating of the reaction mixture to the desired temperature without heating the entire furnace or oil bath, which saves time and energy.

The microwave heating is based on two mechanisms of the conversion of the electromagnetic radiation into heat energy, namely dipolar rotation and ionic conduction (**Figure 1**). The dipolar rotation (**Figure 1a**) occurs when polar molecules having an electrical dipole moment align with the oscillating electromagnetic field. In this process, energy is lost as heat due to the molecular friction and dielectric loss.

The ionic conduction heating mechanism (**Figure 1b**) results from the dissolved (dissociated) charged particles (ions). In dependence from the charge, the ions oscillate back and forth under the influence of the electric component of microwave radiation. In comparison with the

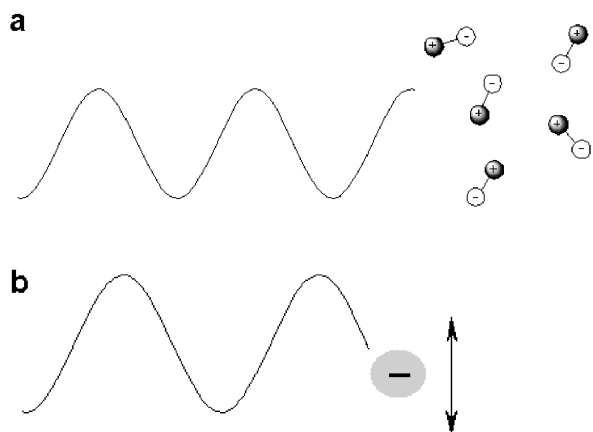


Figure 1: Microwave-mediated heating process: a) dipolar rotation and b) ionic conduction

Slika 1: Proces segrevanja pod vplivom mikrovalov: a) dipolarna rotacija in b) ionska prevodnost

former mechanism, the absorption of microwave irradiation by this mechanism is more efficient and the energy transfer is faster.

Due to the fact that different compounds convert microwave radiation to heat to different extents, i.e., they have different microwave absorbing properties, microwave radiation allows a selective heating of compounds in the reaction mixture.

Therefore, the general advantages of microwave-mediated synthesis over conventional heating are (**Figure 2**): a) reaction rate acceleration as a consequence of high heating rates, b) versatility of applied reaction conditions, i.e. mild conditions (low-power/low-temperature synthesis) or autoclave conditions (high temperatures and pressures), c) higher chemical yields with less by-products, d) different reaction selectivity due to different microwave absorbing properties, e) better reproducibility (excellent control over reaction conditions), f) easy handling, which allows fast and easy optimization of the experimental parameters.

However, there are few disadvantages of microwave over the conventional heating. The monitoring of the reaction course or, in the case of inorganic species, the time-dependent monitoring of the particles growth can not be performed. Furthermore, the microwave synthesis reactor is expensive in comparison with glassware equipment used for conventional (oil-bath) synthesis

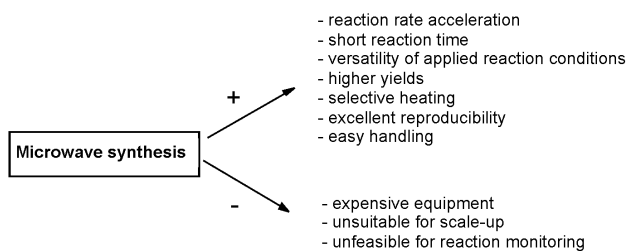


Figure 2: Pros (+) and cons (-) of the microwave-assisted synthesis.

Slika 2: Prednosti (+) in pomanjkljivosti (-) sintez pod vplivom mikrovalov

and, up-to-now, the microwave-mediated scale-up production has not yet reached the production quantities of the "classical" reactors.

Nevertheless, the microwave synthesis promise to offer many new benefits in the field of inorganic nanoparticle precipitations, and, particularly in gaining an insight into the dynamics of the formation of inorganic nanoparticles under defined experimental conditions. Given that microwave-mediated synthesis of inorganic materials offer even better control over reaction parameters that conventional approach, methodological investigations are indispensable to explore the full potential of this synthetic method.

The purpose of this article is first a brief review of the state-of-the art of the ZnO microwave synthesis using organic solvents, particularly alcohols, and second, to report on our own results of the non-aqueous microwave-mediated synthesis of ZnO nanoparticles from zinc acetylacetonate hydrate ($\text{Zn}(\text{acac})_2 \cdot \text{xH}_2\text{O}$) in 1-butanol.

2 MICROWAVE HEATING IN THE SYNTHESIS OF ZNO NANOPARTICLES

As a wide band gap II–VI semiconductor (3.37 eV), zinc oxide (ZnO) is promising material for numerous applications, such as gas sensors, transparent electrodes, pH sensors, biosensors, acoustic wave devices, and UV photodiodes.⁶ Its extraordinary properties makes it one of the most intensively studied materials and, as so, there is a rapid growth in number of recent publications concerning the synthesis performed under microwave conditions (**Figure 3**).

The investigations on the solution-based microwave-assisted growth of ZnO were mainly performed in the water systems.^{7–10}

In nonaqueous routes, the organic reaction mechanisms play a dominant role in ZnO formation. The organic species (i.e., the solvent and the organic ligands in the precursor) undergo chemical reactions that are responsible for supplying the monomers for nucleation

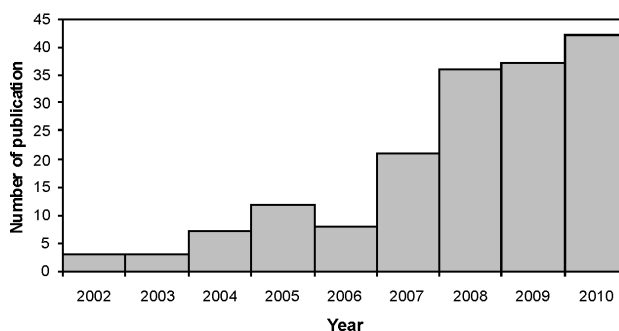


Figure 3: Number of publication per year on the solution-phase (aqueous and non-aqueous) microwave-assisted synthesis of ZnO particles (source ISI Web of Knowledge).

Slika 3: Število objav na leto o sintezi ZnO-delcev v vodnem ali nevodnem mediju pod vplivom mikrovalov (vir ISI Web of Knowledge)

and growth of ZnO nanoparticles. Therefore, in these systems, a high sensitivity of both the organic reactions and the crystal growth towards microwave irradiation can be expected. Because of the fact that species differ in their microwave absorption behavior, a selective heating in a homogeneous or heterogeneous system might lead to diverse morphology and size of the ZnO particles.

The wide parameter window for controlling the microwave-assisted synthesis of ZnO has been investigated in numerous of alcohol reaction systems. Hu et al.¹¹ reported on the rapid microwave-polyol process that leads to the formation of monodisperse spherical ZnO clusters, which average size can be tuned by the amount of the precursor (zinc acetate). The striking effects of the microwave heating parameters and the solvent composition on morphology hierarchical ZnO nanostructures were demonstrated in ethylene glycol-water systems.^{12,13} Straw-bundle-like, wide chrysanthemum-like and oat-rista-like morphologies and microspheres were prepared on the basis of the applied cycling mode, which determine the growth of the particles in the nucleation stage, whereas T-like, X-like and cross-like linked hexagonal prisms were observed by changing the volume ratio of ethylene glycol to water.

Bilecka et al.^{14,15} studied in details the kinetic and thermodynamic aspects of microwave-assisted synthesis of ZnO nanoparticles from zinc acetate and benzyl alcohol. It was concluded that microwave radiation drastically accelerated the particle formation by enhancing the dissolution of the precursor in alcohol as well as increasing the rate constants of the esterification reaction and the crystal growth.

3 SYNTHESIS OF ZnO BY MICROWAVE HEATING USING ZINC ACETYLACETONATE

The syntheses were carried out in a Milestone MEGA 1200 laboratory microwave oven. The precursor (2.3, 4.6 and 6.9) mmol was initially dispersed in 17 mL of

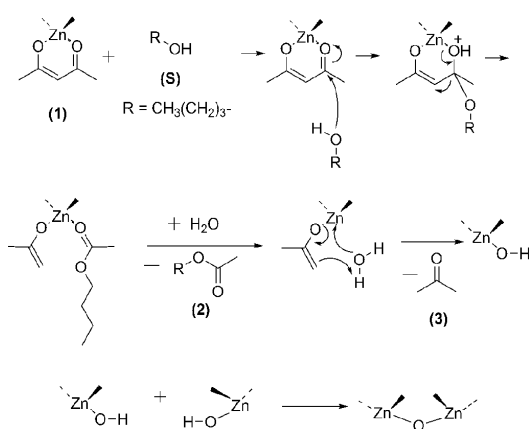


Figure 4: Reaction mechanism of ZnO formation from zinc acetylacetonate and 1-butanol.¹⁶

Slika 4: Mehanizem nastanka ZnO iz cinkovega acetilacetonata in 1-butanol.¹⁶

1-butanol and heated in 2 min to 120 °C. Samples were irradiated for 30 min with 250 W pulsed microwave irradiation power. After irradiation, the samples were cooled to room temperature, centrifuged and vacuum dried at 40 °C.

The mechanism of the zinc acetylacetonate conversion into ZnO¹⁶ relies on the nucleophilic attack of the alcohol to the carbonyl group of the acetylacetonate ligand and subsequent hydrolytic formation of the reactive Zn-OH intermediates, which polycondensate forming repeating -Zn-O-Zn- bonds. (**Figure 4**).

For the microwave-assisted synthesis, besides the alcohol reactivity, the crucial property of the alcohol as a medium is its ability to convert effectively the electromagnetic energy into heat energy. Based on the experimental data¹⁷, 1-butanol is efficient microwave absorbing solvent so under the microwave conditions the transformation of zinc acetylacetonate into ZnO occurs in an excellent yield (up to 85 %).

FTIR spectra (Perkin Elmer's Spectrum One spectrometer) and XRD diffractograms (Bruker AXS D4 Endeavor diffractometer with Cu K α radiation and a Sol-X energy-dispersive detector) of the precipitates obtained from 2.3 mmol and 6.9 mmol of initial amount of zinc acetylacetonate are shown in **Figure 5**. Both of the FTIR spectra (**Figures 5a and 5b**) consist of bands

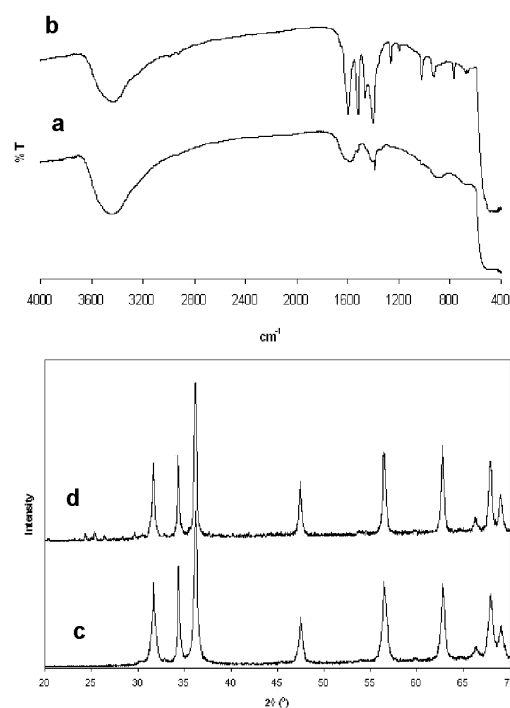


Figure 5: FTIR spectra and XRD diffractograms of the as-prepared ZnO particles obtained from 2.3 (curves a and c) and 6.9 mmol (curves b and d) of initial amount of zinc acetylacetonate in 17 mL of 1-butanol. The samples were exposed for 30 min with 250 W pulsed microwave irradiation at 120 °C.

Slika 5: FTIR-spektra in XRD-difraktograma ZnO-delcev, pripravljenih iz 2.3 mmol (krivulji a in c) in 6.9 mmol (krivulji b and d) cink acetilacetonata v 17 mL 1-butanol. Vzorci so bili 30 min izpostavljeni pulznemu mikrovalovnemu sevanju z močjo 250 W pri 120 °C.

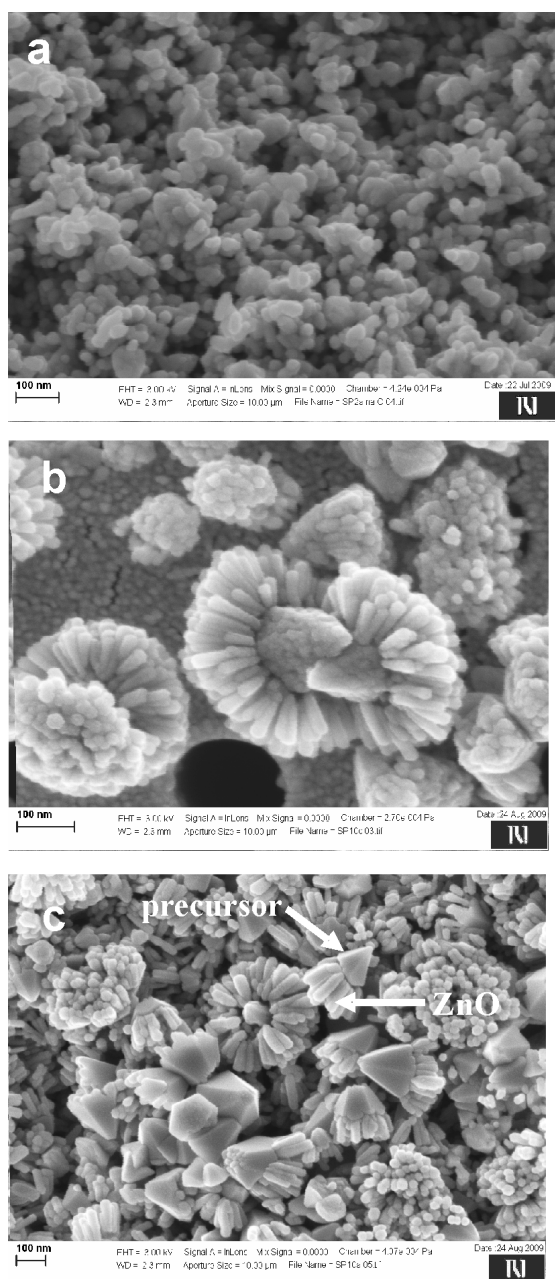


Figure 6: FE-SEM images of as-prepared ZnO particles synthesized from a) 2.3, b) 4.6 and c) 6.9 mmol of zinc acetylacetonate in 17 ml of 1-butanol. The samples were exposed for 30 min with 250 W pulsed microwave irradiation at 120 °C.

Slika 6: FE-SEM-mikrografije ZnO-delcev pripravljenih iz a) 2.3 mmol, b) 4.6 mmol in c) 6.9 mmol cink acetilacetonata v 17 mL 1-butanol. Vzorci so bili 30 min izpostavljeni pulznemu mikrovalovnemu sevanju z močjo 250 W pri 120 °C.

representing Zn-O stretching vibration at approximately 450 cm^{-1} and diffuse signals at cca. 3400 cm^{-1} attributed to water molecules adsorbed on the ZnO surface. The FTIR spectrum of as-prepared precipitate obtained from higher amount of zinc acetylacetonate (**Figure 5b**) shows also numerous signals of unreacted precursor. Correspondingly, besides the intensive zincite reflections, the XRD pattern in **Figure 5d** shows additional

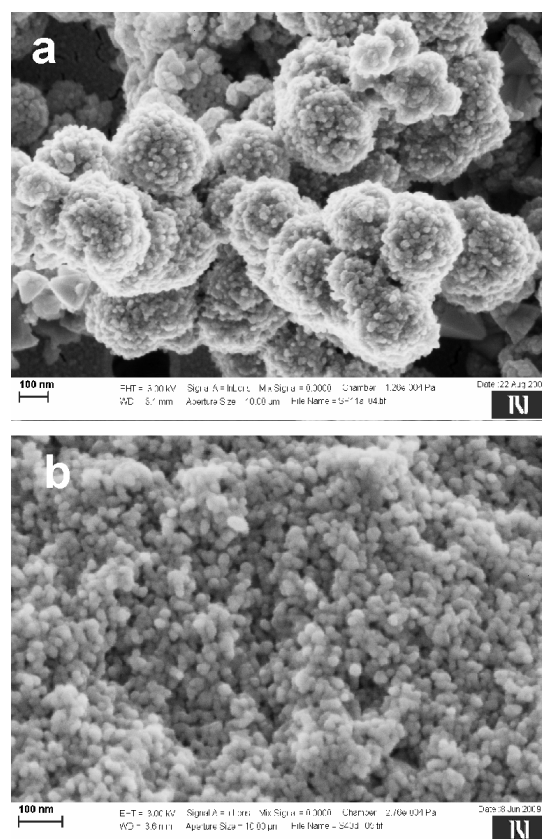


Figure 7: FE-SEM images of as-prepared ZnO nanoparticles synthesized from 2.3 mmol of zinc acetylacetonate and 1.16 mmol of 1-hexadecyl-3-methyl imidazole chloride monohydrate in 17 ml of 1-butanol under a) 250 W pulsed microwave irradiation microwave conditions (30 min, 120 °C) and b) reflux conditions after 3 h.

Slika 7: FE-SEM-mikrografije ZnO-nanodelcev, pripravljenih iz 2.3 mmol cink acetilacetonata in 1.16 mmol 1-heksadecil-3-metil imidazol klorid monohidrata v 17 mL 1-butanol. Vzorci so bili 30 min izpostavljeni pulznemu mikrovalovnemu sevanju z močjo 250 W pri 120 °C.

low intensity signals in the low-angle region representing the crystalline phase of the precursor.

Figure 6 shows FE-SEM images (FE-SEM SUPRA 35VP (Carl Zeiss) equipped with an energy-dispersive spectrometer (EDXS, Inca 400, Oxford Instruments)) of as-prepared ZnO nanoparticles synthesized from different amounts of zinc acetylacetonate (2.3, 4.6 and 6.9) mmol in 17 mL of 1-butanol. It was observed that the initial quantity of the precursor exerts a tremendous effect on the morphology of the particles, similarly to the reported ethylene-glycol-water systems.^{12,13} Contrary to the mentioned microwave-assisted ZnO preparation, in the syntheses performed under reflux conditions by using analogous concentration of the precursor in 1-butanol, the rod-shaped ZnO particles were formed from all of the investigated solution meaning that in this case the product shape is concentration-independent.¹⁶

The particles in **Figure 6a** are approximately 10 nm to 60 nm in size, while the complex ZnO architectures in **Figure 6b** consist of a few-nanometers-large ZnO

crystallites, which form approximately 100-nm-long nanorods growing on one side of the agglomerated, densely packed, quasi-spherical ZnO particles. In accordance with FTIR and XRD data (**Figures 5b and 5d**), in the case of 6.9 mmol of precursor, the micrograph in Figure 6c shows that after 30 min of microwave exposure approximately 100 nm long ZnO nanorods formed close to the surface of the undissolved pyramidal precursor. The similar phenomenon was observed during the monitoring of the ZnO growth from the oversaturated solution of zinc acetylacetonate in 1-butanol under the reflux conditions, where, due to the local supersaturation of the reactive monomer species, the initial formation of ZnO occurs around the solid precursor.¹⁶

Ionic liquids are particularly interesting species in microwave chemistry not only as they can act as template to control the particle shape and assembly behaviour, but also their ionic properties can drastically enhance the microwave absorbance of the system. For that mean, we have performed the microwave assisted synthesis of ZnO from the 1-butanol solution of zinc acetylacetonate in the presence of 1-hexadecyl-3-methyl imidazole chloride monohydrate. Contrary to the reactions carried out under "classical" reflux conditions (**Figure 7a**), under microwave radiation the product precipitates in form of round-shape architectures, which are formed by the aggregation of ZnO nanocrystals (**Figure 7b**). The similar effect of ionic liquid on the aggregation of primary ZnO nanoparticles was already reported in the microwave irradiated system of tetrabutylammonium hydroxide hydrate and zinc acetate dehydrate.¹⁸ The formation of thermodynamically favorable spherical shape was attributed to the electrostatic interactions of polar charges in small ZnO particles, which uncontrolled growth is prevented by the absorption of charged species of the ionic liquid. This shows that microwaves can be used to influence and control the oriented attachment process, so new exciting opportunities for the assembly of ZnO nanoparticles could be opened.

4 CONCLUSIONS

The application of microwave radiation for the preparation of metal oxides under aqueous and non-aqueous conditions, especially relevant for the preparations of polymer/ZnO nanocomposites, has been shown to be a versatile approach to the design on novel nanoparticles' morphologies. Particularly the fast reaction rates (short reaction times), better product yields and the possibility to automatically combine different experimental parameters makes microwave-assisted

synthesis suitable for the studies of the influences of the reaction conditions on the morphology and sizes of ZnO particles, which determine its properties and applications.

The different examples of the microwave-assisted synthesis of ZnO described in this article show that the general rules of the influence of the reaction parameters on the mechanism of the particle growth in microwave processes are not yet fully understand. This opens new research challenges in designing the nanoparticles with defined sizes, morphologies and complex architectures by using different experimental conditions.

ACKNOWLEDGEMENT

The authors acknowledge the financial support from the Ministry of Higher Education, Science and Technology of the Republic of Slovenia through the contract No. 3211-10-000057 (Center of Excellence for Polymer Materials and Technologies).

5 REFERENCES

- G. R. Patzke, Y. Zhou, R. Kontic, F. Conrad, *Angewandte Chemie International Edition*, 50 (2011), 826
- I. Bilecka, M. Niederberger, *Electrochimica Acta*, 55 (2010), 7717
- V. Polshettiwar, R. S. Varma, *Accounts of Chemical Research*, 41 (2008), 629
- C. O. Kappe, *Angewandte Chemie International Edition*, 43 (2004), 6250
- I. Bilecka, M. Niederberger, *Nanoscale*, 2 (2010), 1358
- M. Ahmad, J. Zhu, *Journal of Material Chemistry*, 21 (2011), 599
- S. C. Padmanabhan, D. Ledwith, S. C. Pillai, D. E. McCormack, J. M. Kelly, *Journal of Material Chemistry*, 19 (2009), 9250
- W.-W. Wang, Y.-J. Zhu, *Inorganic Chemistry Communication*, 7 (2004), 1003
- M.-G. Ma, Y.-J. Zhu, G.-F. Cheng, Y.-H. Huang, *Materials Letters*, 62 (2008), 507
- X.-L. Hu, Y.-J. Zhu, S.-W. Wang, *Materials Chemistry and Physics*, 88 (2004), 421
- X. Hu, J. Gong, L. Zhang, J. C. Yu, *Advanced Materials*, 20 (2008), 4845
- P. Zhu, J. Zhang, Z. Wu, Z. Zhang, *Crystal Growth & Design*, 8 (2008), 3148
- L. Zhang, Y.-J. Zhu, *Applied Physics A*, 97 (2009), 847
- I. Bilecka, P. Elser, M. Niederberger, *ACS Nano*, 3 (2009), 467
- I. Bilecka, I. Djerdj, M. Niederberger, *Chemical Communication*, (2008), 886
- G. Ambrožič, S. D. Škapin, M. Žigon, Z. C. Orel, *Journal of Colloid and Interface Science*, 346 (2010), 317
- Hayes, B., *Microwave Synthesis*, CEM Publishing, Matthews, NC, 2002, Chapter 2
- H. Zou, Z. Li, Y. Luan, T. Mu, Q. Wang, L. Li, J. Ge, G. Chen, *Current Opinion in Solid State & Materials Science*, 14 (2010), 75

REMOVAL OF A THIN HYDROGENATED CARBON FILM BY OXYGEN PLASMA TREATMENT

ODSTRANJEVANJE TANKE PLASTI HIDROGENIRANEGA OGLJIKA S KISIKOVO PLAZMO

Uroš Cvelbar

Center of Excellence for Polymer Materials and Technologies, Tehnološki park 24, 1000 Ljubljana, Slovenia
uro.cvelbar@ijs.si

Prejem rokopisa – received: 2011-02-15; sprejem za objavo – accepted for publication: 2011-03-09

Capability of low pressure oxygen as a medium for removal of hydrogenated carbon thin films is demonstrated. The film was deposited onto polished iron discs by CVD method. Discs were mounted into a discharge chamber which was evacuated to the ultimate pressure of about 5 Pa. Methane of commercial purity was leaked into the chamber during continuous pumping so the pressure of 100 Pa was established. Weakly ionized plasma was then created in the chamber by an inductively coupled RF generator operating at the frequency of 27.12 MHz and the power of about 200 W. The methane molecules dissociated in the plasma forming CH_3 radicals that adsorbed on the sample surface causing formation of a thin film of hydrogenated carbon. AES depth profiling showed that a 3 nm thick film was formed after 200 s of plasma treatment. Samples were then exposed to oxygen plasma in the same chamber, and characterized by AES as well as water drop contact angle. After 12 s of oxygen plasma treatment the samples were visually free of carbon and the AES depth profiling proved it. The contact angle of a water drop decreased from initial 80° to about 10° indicating a rapid transformation of the surface properties from hydrophobic to hydrophilic character. The experiments allowed for estimation of the cleaning efficiency which was about 0.25 nm/s.

Keywords: hydrogenated carbon, gaseous plasma, methane, oxygen, Auger electron spectroscopy, hydrophilic

Prispevek opisuje možnosti, ki jih daje kisikova plazma pri odstranjevanju tankih plasti hidrogeniranega ogljika. Plasti so bile pripravljene na železnih poliranih vzorcih z nanosom iz parne faze. Vzorci so bili postavljeni v razelektritveno posodo vakuumskega sistema. Sistem je bil najprej izčrpan do končnega tlaka okoli 5 Pa, potem pa smo ob stalnem črpanju dovajali metan pri tlaku 100 Pa. V metanu smo ustvarili plinsko plazmo z razelektritvijo, ki smo jo vzbujali z radiofrekvenčnim generatorjem moči okoli 200 W in frekvence 27,12 MHz. Molekule metana v plazmi disociirajo, nastali radikali CH_3 pa se lahko vežejo na površino vzorca in počasi tvorijo tanko plast hidrogeniranega ogljika. Profilna analiza s spektroskopijo Augerjevih elektronov (AES) je pokazala, da je po 200 s obdelave nastala plast debeline okoli 3 nm. Vzorci so bili potem izpostavljeni delovanju kisikove plazme v istem reaktorju. Po izpostavitvi so bili analizirani z AES, izmerili pa smo tudi kontaktne kote vodnih kapljic v odvisnosti od časa izpostavitve kisikovi plazmi. Globinski profili AES so pokazali izredno veliko stopnjo čistosti vzorcev po okoli 12-sekundni obdelavi. Kontaktni kot vodne kapljice je bil sprva 80° , kar kaže na hidrofobnost plasti hidrogeniranega ogljika. Že po 1 s obdelave s kisikovo plazmo pa se je zmanjšal na okoli 10° , kar kaže na hitro funkcionalizacijo s polarnimi skupinami. Rezultati raziskav so omogočili izračun hitrosti jedkanja, ki je za navedene vzorce okoli 0,25 nm/s.

Ključne besede: hidrogenirani ogljik, plinska plazma, metan, kisik, spektroskopija Augerjevih elektronov, hidrofilizacija

1 INTRODUCTION

Energy supply is a major global consideration of future generations. Currently, the majority of energy is supplied by burning fossil fuels. The problem of this energy source is not only that it will be exhausted sooner or later, but the burning also causes release of huge quantities of greenhouse gases, such as CO_2 , which contributes to the heating of Earth's atmosphere. Moreover, as recent history shows, the availability of energy sources is often subject to local political situation. The future energy sources should therefore be both friendly to the environment and independent from local political situation. While many methods for energy production have been invented, none of them is effective enough to be a suitable replacement of carbon fuels as the consumption of energy is expected to grow continuously due to the expected growth of population as well as higher consumption per capita in third world countries.

The most natural solution of the problem is usage of energy arising from our Sun. The Sun is a rather young star and is expected to supply energy for the next billion years. The temperature on the Sun surface is close to 6 000 K so it radiates energy as a black body covering a broad range from IR to UV part of the spectrum. The majority of energy reaching the Earth is in the visible range, i. e. photons of the energy of few eV. The Earth receives the energy flux of close to 1000 W/m^2 . Taking into account the Earth diameter which is about 12 700 km one can calculate the power reaching the earth

$$P = \frac{1}{4} \pi d^2 E_0 = 4 \times 10^{17} \text{ W} \quad (1)$$

Here d is the Earth's diameter and E_0 the flux of energy from the Sun at the Earth distance (close to 1000 W/m^2). The current needs of all population are approximately $3 \times 10^{10} \text{ W}$ so the energy coming from the Sun is 10 million times the needs of the population. The humans therefore use only a negligible fraction of available energy.

The problem arises from the fact that the energy in the form of visible light photons does not cover all of humanity's energy needs. Beside visible light, we need other forms of energy, such as electricity. Not surprisingly, efforts have been made worldwide to develop methods for conversion energy from visible light photons to electricity. Solar panels have been developed decades ago and are currently being used, but only a small fraction of the globally consumed energy comes from this source. There are several reasons that prevent general adoption of solar cells including geographic (climate) reasons, high investment costs, rather poor efficiency, and aging effects. Also, it seems that contamination of the panel surface by dust is far from a minor problem, especially in the deserts where other conditions are favorable. Although recent results in development of new generation of solar cells with quantum dots or nanowires¹⁻⁵ are promising, their application is still questionable.

The original source of energy from our Sun are not photons of visible light. Sun makes energy from nuclear fusion (reactions between hydrogen isotopes). Huge amount of energy is released by fusion. At the reaction



an amount of energy equal to almost 18 MeV is released. The majority of energy (more than 14 MeV) is taken by the neutron in terms of its kinetic energy, and the rest is taken by the He nucleus, also in terms of the kinetic energy. This reaction is really energetic: 1 kg of fuel (hydrogen isotopes) produces about $100 \cdot 10^6$ kW h of energy. A kilogram of coal, on the other hand, gives only about 5 kW h – 8 orders of magnitude less energy.

Nuclear fusion is possible only at extremely high temperatures, because a substantial amount of energy (0.4 MeV) has to be invested in the pair of nuclei in order to overcome the electrostatic energy barrier. Such high temperature is not available at the sun surface, but only in the Sun core. The temperature in the Sun centre is estimated to $15 \cdot 10^6$ K. This is obviously enough for fusion reactions heating our Sun. Extremely fast neutrons and helium nuclei formed at fusion reactions collide with other nuclei and are thermalized (achieve Maxwell – Boltzmann kinetic energy distribution function) so they cannot reach the Sun surface. Strong convection allows for transfer of energy from the Sun core toward the surface. Adiabatic cooling occurs on the way so the Sun crust is not as hot as the core. Finally, the Sun surface emits photons according to the Stefan – Boltzmann law and what we get at the Earth surface is a flux of mostly visible light photons at the value close to 1000 W/m².

Since the early 1940s, scientists began experimenting with nuclear fusion on Earth, as the energetic neutrons produced in the reaction are more promising particles for energy production than the photons of visible light. Recent results are encouraging so the international community is making many efforts to bring the idea of

having a small Sun here on Earth into fruition. Extremely high temperatures that should be achieved in human-made fusion devices bring many technical problems; a major one is deposition of hydrogenated carbon layers in experimental fusion devices. They are formed when protective graphite coatings, needed due to extremely high temperatures, are eroded by hydrogen atoms. Several research groups worldwide are therefore involved in development of methods for removal of the deposits.

An original approach for removal of hydrogenated carbon deposits is application of thermodynamically non-equilibrium gases, especially oxygen. Such a state of oxygen is obtained by passing molecular gas through a gaseous discharge⁶⁻¹¹. Oxygen molecules in the discharge are partly ionized, dissociated and excited, and the resultant particles are chemically very reactive¹¹⁻¹⁶. A unique property of such particles is that they are very selective – they do interact with certain polymers even at room temperature, but the interaction with graphite is poor¹⁷⁻²³. Exposure of fusion reactors to such oxygen particles would therefore lead to removal of hydrogenated carbon deposits while leaving the massive graphite blocks of protective coatings in fusion reactors rather intact.

Although it is well known that oxygen particles interact chemically with hydrocarbons including polymers²⁴⁻³⁰, very little work has been performed on quantification of results for hydrogenated carbon deposits prepared by plasma deposition. The present paper reports recent results on this phenomenon.

2 EXPERIMENTAL

Experiments were performed in a plasma reactor explained to details elsewhere³⁰⁻³⁴. The reactor is made from glass in order to prevent heterogeneous surface recombination of neutral oxygen atoms so a rather high dissociation fraction is obtained already at a rather low power. The dissociation fraction of 10 % is typical³⁵⁻³⁹. The original experimental setup was modified for current experiments. Two different gases were leaked into the system – methane and oxygen. Methane was used to deposit a thin film of hydrogenated carbon, and oxygen for its removal.

Samples were iron discs with a diameter of 10 mm and a thickness of 0.5 mm. The discs were polished and cleaned by chemical methods. The appearance of hydrogenated film during treatment with methane plasma was observed by a naked eye, but some quantification was performed by Auger Electron Spectroscopy (AES) depth profiling. A classical AES device with a rather poor lateral resolution was applied. The primary electron beam has the diameter of about 40 μm. The samples were sputtered by argon ions in order to measure the depth profiles. The ions had the kinetic energy of 3 keV and were rastered over the surface area of about 5 mm x

5 mm. The sputtering rate for hydrogenated carbon deposits was estimated previously using standard samples and the value was about 2 nm/min.

Water drop contact angle measurements were used in order to determine the surface conditions. A home-made device comprising a CCD camera and a computer with appropriate software was used to measure contact angles of a drop of distilled water with the volume of 3 μ L.

3 RESULTS

The discharge chamber was first cleaned by a brief exposure to oxygen plasma, then evacuated to ultimate pressure of about 5 Pa. Methane was leaked continuously during pumping so a stable working pressure of 100 Pa was obtained. Samples were exposed to methane plasma for 200 s and removed from the discharge system. A typical AES depth profile of a sample is presented in **Figure 1**. Samples were then mounted back into the system individually. Oxygen plasma was used to remove the hydrogenated carbon deposits. Samples were visually clean after about 10 s of treatment with oxygen plasma. A depth profile of a sample treated for 12 s is presented in **Figure 2**. Many samples were exposed to plasma for different periods. These samples were characterized by the water drop contact angle method. The contact angle versus plasma treatment time is presented in **Figure 3**.

4 DISCUSSION

The depth profile of a sample presented in **Figure 1** indicates formation of a thin carbon film. Unfortunately, the AES technique does not recognize hydrogen but since methane was used to deposit the film it is expected that it contains much hydrogen. Namely, methane molecules entering the discharge are not only partially ionized but also well-dissociated. The dissociation products are neutral H atoms and CH_x radicals. Since our plasma is not powerful, full dissociation is unlikely to

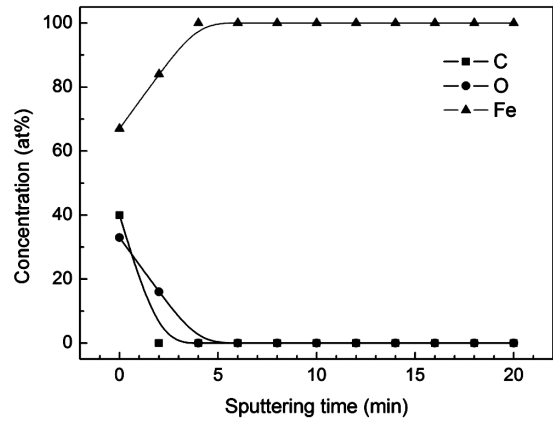


Figure 2: AES depth profile of an iron sample after exposure to methane plasma for 200s and subsequently to oxygen plasma for 12 s
Slika 2: AES profilni diagram jeklenega vzorca po izpostavi metanovi plazmi za 200 s in nato kisikovi plazmi za 12 s

occur. The CH_x radicals stick on the surfaces forming a thin film of hydrogenated carbon. The appearance of the film is easily observed with a naked eye because it is black. The thickness of the layer cannot be determined by the eye but AES depth profile gives a good approximation. The thickness is calculated from the **Figure 1** by taking into account approximate sputtering yield which was determined previously with standard samples. In our case, the thickness is estimated to about 3 nm. The deposition rate is pretty low, what can be explained either by low deposition rate or by spontaneous removal of formed layer by neutral hydrogen atoms and hydrogen ions. Namely, these particles cause slow erosion of carbon in fusion reactors⁴⁰⁻⁴⁵ and it was already shown that hydrogen plasma was suitable for removal of hydrogenated carbon prepared by other techniques⁴⁶⁻⁴⁸.

It is interesting that the oxygen concentration at the interface between iron and carbon in **Figure 1** is pretty small. According to the literature, iron tends to form a thin native oxide film spontaneously⁴⁹⁻⁵¹. The absence of

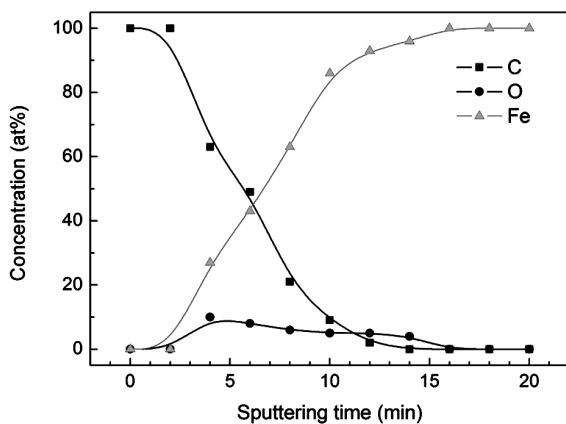


Figure 1: AES depth profile of an iron sample after exposure to methane plasma for 200 s

Slika 1: AES profilni diagram jeklenega vzorca po izpostavi metanovi plazmi za 200 s

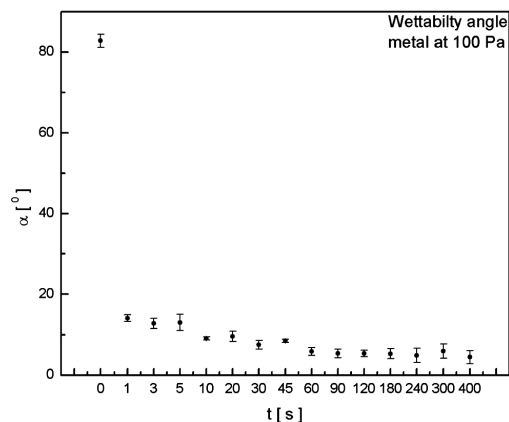


Figure 3: Contact angle of a water drop on iron samples with hydrogenated carbon deposits versus oxygen plasma treatment time.

Slika 3: Kontaktni kot vodne kapljice na jeklenih vzorcih s plastjo hydrogeniranega ogljika v odvisnosti od časa obdelave s kisikovo plazmo

rather large oxygen concentration is thus explained by effects of methane plasma. As already mentioned, lots of H atoms are created in methane plasma and these atoms cause reduction of metal oxide thin films^{52–55}. The first effect of iron exposure to methane plasma is thus reduction of the native oxide film.

Once the film is reduced the deposition of hydrogenated carbon is observed. This film is removed rather efficiently by oxygen plasma treatment as demonstrated in **Figure 2**. This sample is almost free from carbon (a small concentration is observed only at the surface and this is probably due to contamination on the way from the plasma lab to the surface characterization lab. The oxide film is now present on the surface as expected since iron is quickly oxidized after exposure to air.

Figure 3 represents results of the water drop contact angle measurements. Metals have large surface energy so the contact angle on pure metal should be very low. Samples with hydrogenated carbon deposits, however, exhibit a high contact angle, which indicates hydrophobic character of the deposits. The result is not surprising – all oxygen-free polymers are hydrophobic^{55–59}. The contact angle quickly drops at exposure to oxygen plasma as shown in **Figure 3**. The huge decrease of the contact angle after 1s of plasma treatment cannot be attributed to removal of the film, since the sample is still black. The effect is rather explained by surface functionalization of the hydrogenated carbon film. Numerous authors have shown that even a brief exposure of polymer to oxygen plasma causes an appearance of oxygen-rich functional groups on the surface of a polymer^{60–64}. These functional groups are extremely polar and the surface functionalized by them is usually hydrophilic. The contact angle shown in **Figure 3** keeps decreasing with increasing oxygen plasma treatment time and finally stabilizes at the value of approximately 10°, typical of very clean metals.

Knowing the thickness of the original hydrogenated carbon films, Δz , and length of oxygen plasma processing needed for complete removal of the film, Δt , allows for an estimation of the removal rate. The removal rate is

$$\Delta z/\Delta t = 3 \text{ nm}/12 \text{ s} = 0.25 \text{ nm/s} \quad (3)$$

This value is approximate since the removal is not all homogeneous. Also, the estimation of the film thickness is not very accurate, and finally, it is worth mentioning that this value holds for room temperature. It has been shown that removal rates of amorphous carbon deposits increase with temperature²³, so we expect that this removal rate would also be higher at elevated temperature.

5 CONCLUSION

The experimental results presented in this paper clearly show that weakly ionized oxygen plasma created in inductively coupled radiofrequency discharge is a

suitable medium for removal of hydrogenated carbon thin films. The films that were deposited by CVD using methane as precursor were effectively removed in about 10 s which makes this technique suitable for cleaning of large areas. The removal rate was estimated to about 0.25 nm/s. This value may be somewhat too small for application in fusion reactors, but it should be stressed that modern fusion devices operate at elevated temperature of few 100 °C where the removal rate is expected to be much higher.

ACKNOWLEDGEMENT

The authors acknowledge the financial support from the Ministry of Higher Education, Science and Technology of the Republic of Slovenia through the contract No. 3211-10-000057 (Center of Excellence Polymer Materials and Technologies).

6 REFERENCES

- K. Ostrikov, *J. Phys. D: Appl. Phys.*, **44** (2011) in press
- J. Baxter et al, *Energy Environ. Sci.*, **2** (2009), 559
- A. Akimov Yu, W. S. Koh, K. Ostrikov, *Optics Express* **17** (2009), 10195
- S. Gubbala, V. Chakrapani, V. Kumar, M. K. Sunkara, *Adv. Func. Mater.* **18** (2008), 2411
- V. Svrcek, D. Mariotti, Y. Shibata, M. Kondo, *J. Phys. D: Appl. Phys.*, **43** (2010), 415402
- M. Mozetič, A. Vesel, M. Gaillard, A. Ricard, *Plasmas polym.*, **6** (2001) 1/2, 493–495
- N. Krstulović et al, *Mater. Tehnol.*, **38** (2004), 1/2, 51–54
- A. Vesel et al., *Mater. Tehnol.*, **38** (2004) 3/4, 177–180
- U. Cvelbar, M. Mozetič, A. Ricard, *IEEE Trans. Plasma Sci.*, **33** (2005) 2, 236–237
- A. Drenik, U. Cvelbar, A. Vesel, M. Mozetič, *Inf. Midem*, **35** (2005), 85–91
- M. Tadokoro, A. Itoh, N. Nakano, Z- Lj. Petrovic, T. Makabe, *IEEE Trans Plasma. Sci.*, **26** (1998), 1724–1732
- Z. Lj. Petrović, B. M. Jelenković, A. V. Phelps, *Phys. Rev. Lett.*, **68** (1992), 325
- N. Krstulović et al., *J. Phys. D: Appl. Phys.*, **39** (2006), 3799–3804
- A. Vesel et al., *Plasma Chem. Plasma Process.*, **26** (2006), 577–584
- D. Vujošević, M. Mozetič, U. Cvelbar, S. Milošević, *J. Appl. Phys.*, **101** (2007) 10, 13305
- K. Ostrikov, *Rev. Moder. Phys.*, **77** (2005) 2, 489–511
- M. Kunaver, M. Klanjšek - Gunde, M. Kunaver, A. Horvat, *Surf. Coat. Int., Part B Coat. Trans.*, **86** (2003) B3, 175–179
- M. Kunaver, M. Klanjšek - Gunde, M. Mozetič, A. Horvat, *Dyes Pig.*, **57** (2003) 3, 235–243
- U. Cvelbar, S. Pejovnik, M. Mozetič, A. Zalar, *App. Surf. Sci.*, **210** (2003), 255–261
- I. Junkar, U. Cvelbar, A. Vesel, N. Hauptman, M. Mozetic, *Plasma Proces. Polym.*, **6** (2009) 10, 667–675
- U. Cvelbar, M. Mozetič, M. Klanjšek - Gunde, *IEEE Trans. Plasma Sci.*, **33** (2005) 2, 236–237
- I. Junkar, N. Hauptman, K. Rener - Sitar, M. Klanjšek - Gunde, U. Cvelbar, *Inf. Midem*, **38** (2008) 4, 266–271
- A. Drenik, A. Vesel, M. Mozetič, *J. Nucl. Mater.*, **286–388** (2009), 893–895
- A. Vesel, M. Mozetič, A. Zalar, *Surf. Interface Anal.*, **40** (2008) 3/4, 661–663

- ²⁵ A. Vesel, I. Junkar, U. Cvelbar, J. Kovač, M. Mozetič, *Surf. Interface Anal.*, 40 (2008) 11, 1444–1453
- ²⁶ T. Vrlinič et al., *Surf. Interface Anal.*, 39 (2007) 6, 476–481
- ²⁷ I. Junkar, A. Vesel, U. Cvelbar, M. Mozetič, S. Strnad, *Vacuum*, 84 (2010) 1, 83–85
- ²⁸ U. Cvelbar et al., *Appl. Surf. Sci.*, 253 (2007) 21, 8669–8673
- ²⁹ M. Mafra, T. Belmonte, F. Poncin-Epaillard, A. S. da Silva Sobrinho, A. Maliska, *Plasma Chem. Plasma Proces.*, 28 (2008) 4, 495–509
- ³⁰ M. Mafra, T. Belmonte, A. Maliska, A. S. da Silva Sobrinho, F. Poncin-Epaillard, *Key Eng. Mater.*, 373–374 (2008), 421–425
- ³¹ U. Cvelbar, M. Mozetič, *J. Phys. D: Appl. Phys.*, 40 (2007), 2300–2303
- ³² M. Mozetič, U. Cvelbar, *Plasma Sources Sci. Technol.*, 18 (2009) 3, 034002
- ³³ U. Cvelbar, N. Krstulović, S. Milošević, M. Mozetič, *Vacuum*, 82 (2007) 2, 224–227
- ³⁴ A. Drenik, U. Cvelbar, A. Vesel, M. Mozetič, *Strojarstvo*, 48 (2006) 1/2, 17–22
- ³⁵ A. Drenik, U. Cvelbar, K. Ostrikov, M. Mozetič, *J. Phys. D: Appl. Phys.*, 41 (2008) 11, 115201
- ³⁶ M. Mozetič, A. Ricard, D. Babič, I. Poberaj, J. Levaton, V. Monna, U. Cvelbar, *J. Vac. Sci. Technol: A Vac. Surf. Films*, 21 (2003), 369–374
- ³⁷ M. Mozetič, U. Cvelbar, A. Vesel, A. Ricard, D. Babič, I. Poberaj, *J. Appl. Phys.*, 97 (2005), 103308
- ³⁸ M. Mozetič, A. Vesel, U. Cvelbar, A. Ricard, *Plasma Chem. Plasma Process*, 26 (2006), 103–117
- ³⁹ M. Mozetič, *Surf. Coat. Technol.*, 201 (2007) 9–11, 4837–4842
- ⁴⁰ A. Kreter, M. J. Baldwin, R. P. Doerner, D. Nishijima, P. Petersson, A. Pospieszczyk, M. Rubel, K. Umstadter, *Physica Scripta*, 138 (2009), 014012
- ⁴¹ P. Petersson, A. Kreter, G. Possnert, M. Rubel, *Nucl. Instrum. Meth. B*, 268 (2010), 1833–1837
- ⁴² K. N. Ostrikov, M. Y. Yu, H. Sugai, *J. Appl. Phys.*, 86 (1999) 5, 2425–2430
- ⁴³ I. B. Denysenko et al., *J. Appl. Phys.*, 95 (2004) 5, 2713–2724
- ⁴⁴ J. Westerhout, D. Borodin, S. Brezinsek, N. J. L. Cardozo, J. Rapp, D. C. Schram, G. J. van Rooij, *Nucl. Fusion*, 50 (2010), 095003
- ⁴⁵ A. Widdowson, S. Brezinsek, J. P. Coad, D. E. Hole, J. Likonen, V. Philipps, M. Rubel, M. F. Stamp, *Physica Scripta*, 138 (2009), 014005
- ⁴⁶ A. Vesel, A. Drenik, R. Zaplotnik, M. Mozetič, M. Balat-Pichelin, *Surf. Interface Anal.*, 42 (2010) 6/7, 1168–1171
- ⁴⁷ A. Drenik, A. Tomelj, M. Mozetič, A. Vesel, D. Babič, M. Balat - Pichelin, *Vacuum*, 84 (2010) 1, 90–93
- ⁴⁸ A. Vesel, A. Drenik, M. Mozetič, M. Balat - Pichelin, *Vacuum*, 84 (2010) 7, 969–974
- ⁴⁹ A. Vesel, A. Drenik, M. Mozetič, A. Zalar, M. Balat - Pichelin, M. Bele, *Vacuum*, 82 (2007) 2, 228–231
- ⁵⁰ U. Cvelbar, Z. Chen, M. K. Sunkara, *Small*, 4 (2008) 10, 1610–1614
- ⁵¹ Č. Donik, A. Kocijan, M. Jenko, A. Drenik, B. Pihlar, *Corros. Sci.*, 51 (2009) 4, 827–832
- ⁵² U. Cvelbar, M. Mozetič, A. Zalar, *Vacuum*, 71 (2003), 207–211
- ⁵³ M. Mozetič, A. Zalar, M. Drobnič, *Thin Solid Films*, 343–344 (1999), 101–104
- ⁵⁴ M. Mozetič, *Vacuum*, 61 (2000) 2/4, 367–371
- ⁵⁵ W. Jacob, B. Landkammer, C. H. Wu, *J. Nucl. Mater.*, 266–269 (1999), 552–556
- ⁵⁶ F. Poncin - Epaillard, D. Debarnot, *Inform MIDEM*, 38 (2008), 252–256
- ⁵⁷ J. Fresnais, J. P. Chapel, L. Benyahia, F. Poncin - Epaillard, *J. Adhes. Sci. Technol*, 23 (2009), 447–467
- ⁵⁸ J. Fresnais, J. P. Chapel, F. Poncin - Epaillard, *Surf. Coat. Technol.*, 200 (2006), 5296–5305
- ⁵⁹ J. Fresnais, L. Benyahia, F. Poncin - Epaillard, *Surf. Interface Anal.*, 38 (2006), 144–149
- ⁶⁰ T. Belmonte, C. D. Pintassiligo, T. Czerwicz, *Surf. Coat. Technol.*, 200 (2005) 1–4, 26–30
- ⁶¹ C. Canal et al, *Plasma Chem. Plasma Process*, 27 (2007) 4, 404–413
- ⁶² M. Mafra, T. Belmonte, F. Poncin - Epaillard, A. Maliska, U. Cvelbar, *Plasma Proces. Polym.*, 6 (2009), S198–S203
- ⁶³ G. Legeay, A. Coudreuse, F. Poncin - Epaillard, J. M. Herry, M. N. Bellon-Fontaine, *J. Adhes. Sci. Technol*, 24 (2010), 2301–2322
- ⁶⁴ N. Delorme, J. F. Bardeau, A. Bulou, F. Poncin - Epaillard, *Thin Solid Films*, 496 (2006), 612–618

LOW TEMPERATURE DESTRUCTION OF BACTERIA *BACILLUS STEAROTHERMOPHILUS* BY WEAKLY IONIZED OXYGEN PLASMA

NIZKOTEMPERATURNO UNIČEVANJE BAKTERIJ *BACILLUS* *STEAROTHERMOPHILUS* S ŠIBKO IONIZIRANO KISIKOVO PLAZMO

Miran Mozetič

Center of Excellence for Polymer Materials and Technologies, Tehnološki park 24, 1000 Ljubljana, Slovenia
miran.mozetic@guest.arnes.si

Prejem rokopisa – received: 2011-02-03; sprejem za objavo – accepted for publication: 2011-03-10

Weakly ionized plasma created in oxygen at low pressure was applied in order to destruct bacteria *Bacillus stearothermophilus*. Plasma was created in an inductively coupled radiofrequency discharge. The kinetic temperature of neutral gas was kept close to room temperature in order to prevent substantial thermal damage. Plasma parameters depended on the pressure of oxygen in the reactor. The density of charged particles was decreasing with increasing pressure while the density of neutral oxygen atoms exhibited an opposite behavior. Plate count technique as well as scanning electron microscopy was used to monitor the bacterial destruction. Experiments performed at different pressures indicate that the neutral O atoms are major reactants causing etching of organic material, while ultra violet radiation from plasma is responsible for rapid deactivation in the first few seconds of plasma treatment.

Keywords: sterilization, oxygen plasma, bacteria, *Bacillus stearothermophilus*, plate count technique, scanning electron microscopy

Nizkotlačno kisikovo plazmo smo uporabili za uničevanje bakterij *Bacillus stearothermophilus*. Plazmo smo vzbujali v induktivno sklopljeni visokofrekvenčni razelektritvi. Kinetična temperatura nevtralnega plina je bila blizu sobni, s čimer smo se izognili neželenim termičnim učinkom. Plazemski parametri so bili odvisni od tlaka kisika v reaktorju. Gostota nabitih delcev je z naraščajočim tlakom padala, medtem ko je gostota nevtralnih kisikovih atomov naraščala. Za določanje števila preživelih bakterij smo uporabili inkubacijo na krvnem agarju s štetjem kolonij, za določanje poškodb pa vrstično elektronsko mikroskopijo. Raziskave, opravljene pri različnih tlakih, so pokazale, da je jedkanje organskega materiala, ki sestavlja bakterije, predvsem posledica interakcije nevtralnih kisikovih atomov. Hiter padec števila preživelih bakterij v prvih nekaj sekundah plazemske obdelave pa smo pripisali vplivu ultravijoličnega sevanja.

Ključne besede: sterilizacija, kisikova plazma, bakterije, *Bacillus stearothermophilus*, krvni agar, vrstična elektronska mikroskopija

1 INTRODUCTION

Polymer materials applied in biology and medicine should be sterile. This is especially the case for body implants where the requirements for sterility are severe. Several techniques have been developed to assure sterility of materials and devices. They include poisonous chemical reagents, a variety of energetic beams and heat treatments. All these techniques have advantages and drawbacks. In practice, heat treatment using both dry and wet atmosphere is particularly popular since the equipment is rather inexpensive and easy to use. Samples are mounted into an appropriate chamber and heated to elevated temperatures. Dry heating usually requires higher temperatures and/or longer treatment times comparing to wet treatment. Water vapour is an excellent medium for rapid heat transfer from a boiler to the samples. The device is called an autoclave and is widely used in common practice.

A small disadvantage of heat treatment is a simple fact that many materials do not stand prolonged heating. This is especially the case for many polymers since

structural modifications may occur. Many body implants are made from or contain polymer components so the problem is pretty severe. In such cases autoclaving is not the right sterilization method and other methods should be applied. The most straight-forward method is application of poisonous liquids or gases. There are a handful of such reagents such as ethylene-oxide, fluorine and chlorine. No bacteria or spores can stand prolonged treatment with such poisonous compounds. A small problem arises from the simple fact that such reagents are also poisonous for humans. Such sterilization should be performed using strict protocols, and accidents are not uncommon. It is especially difficult to remove remains of reagents as well as death bacteria that may remain toxic.

Energetic beams are increasingly popular in sterilization of delicate materials. Energetic electrons, ions, γ -rays and hard UV radiation can be applied. The procedure is effective, but unsuitable for sterilization of objects with complex shape since the energetic beams do not always reach gaps and other small features. The sterilization of implants is therefore not a trivial task and many researchers worldwide attempt to develop more

reliable methods. One of them is application of cold weakly ionized gaseous plasma.¹⁻¹⁶ The present paper addresses plasma sterilization of materials contaminated with heat resistive bacteria *Bacillus stearothermophilus*.

2 EXPERIMENTAL

Destruction of bacteria *Bacillus stearothermophilus* was performed in a small plasma reactor which has been described in details previously.¹⁻¹¹ Plasma has been well-characterized with a Langmuir probe and a catalytic probe.¹⁷⁻²³ Plasma parameters have been measured in a wide range of pressures from 10 Pa to 200 Pa.²⁸ The density of charged particles and the density of neutral oxygen atoms at the pressures at which sterilization was performed are summarized in **Table 1**.

Table 1: Two most important plasma parameters (ion and neutral atom densities) at three selected pressures in the vacuum chamber

Tabela 1: Dva najpomembnejša plazemska parametra (gostota ionov in nevtralnih kisikovih atomov) pri treh izbranih tlakih v vakuumski posodi

Pressure	Charged particle density	Neutral O atom density
30 Pa	$2.5 \cdot 10^{16} \text{ m}^{-3}$	$1.9 \cdot 10^{21} \text{ m}^{-3}$
75 Pa	$8 \cdot 10^{15} \text{ m}^{-3}$	$3.2 \cdot 10^{21} \text{ m}^{-3}$
150 Pa	$4 \cdot 10^{15} \text{ m}^{-3}$	$4.6 \cdot 10^{21} \text{ m}^{-3}$

The samples of *Bacillus stearothermophilus* were prepared according to the standard procedure. The bacteria were first incubated and then rinsed thoroughly in order to remove traces of nutrition in the incubating suspension. The initial concentration of bacteria in suspension was determined by a standard plate count technique and was about 8×10^8 cells per ml. A drop of water containing bacteria with the volume of 100 μL was deposited onto carriers. We used standard well-polished

silicon substrates. The substrates were pre-cleaned by chemical methods and exposed to oxygen plasma for few seconds in order to remove any possible traces of impurities that may prevent an even distribution of the water drop. The substrates were dried at ambient temperature and after water evaporation a rather uniform film of bacteria was created. The number of bacteria per carrier was about 8×10^6 cells (vegetative form only).

Carriers with bacteria were exposed to plasma for various times and at three different pressures of (30, 75 and 150) Pa. The corresponding plasma parameters are presented in **Table 1**. After each treatment the bacteria were washed by distilled water, diluted and applied onto agar plates. They were incubated for about 24 h so that visible colonies appeared on the agar plate. The number of visible colonies was measured and, taking into account the dilution ratio, the number of survived bacteria on the substrates was calculated.

Selected samples were mounted into a scanning electron microscope to determine any visible changes of bacteria. We used a high resolution scanning electron microscope (SEM) with a field emission source of electrons Carl Zeiss Supra 35. The kinetic energy of primary electron beam was adjusted to 1 keV. No coating was applied onto the samples prior to SEM analyses.

3 RESULTS

Results of systematic measurements of the survival rate are summarized in **Figure 1** and **Figure 2**. **Figure 1** represents results at the oxygen pressure of 75 Pa while **Figure 2** is for two different pressures: 30 Pa and 150 Pa. A pretty sharp drop of the live bacteria is observed after plasma treatment for a short time and the concen-

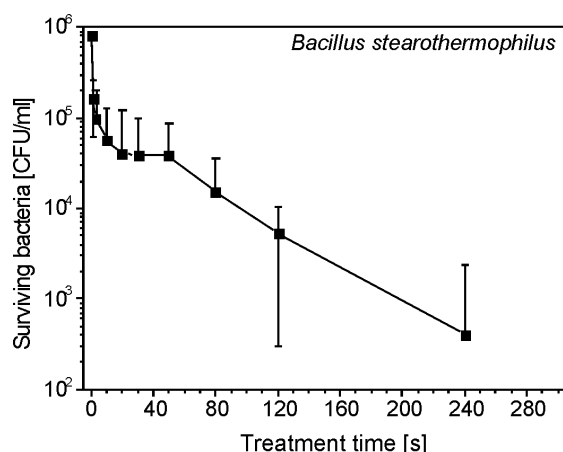


Figure 1: Survival curve of *Bacillus stearothermophilus* by PCT. The graph represents CFUs of *Bacillus stearothermophilus* versus oxygen plasma treatment time at 75 Pa.

Slika 1: Število bakterij *Bacillus stearothermophilus*, ki smo jih ugotovili z metodo nanosa na plošče krvnega agarja. Slika predstavlja prešteto število enot, ki sestavljajo kolonije, v odvisnosti od časa plazemske obdelave pri tlaku 75 Pa.

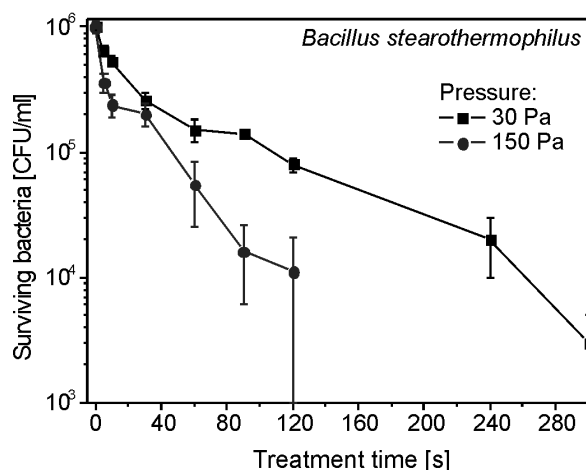


Figure 2: Survival curves of *Bacillus stearothermophilus* by PCT. The graph represents CFUs of *Bacillus stearothermophilus* vs. treatment time by oxygen plasma at pressures of 30 Pa and 150 Pa.

Slika 2: Število bakterij *Bacillus stearothermophilus*, ki smo jih ugotovili z metodo nanosa na plošče krvnega agarja. Slika predstavlja prešteto število enot, ki sestavljajo kolonije, v odvisnosti od časa plazemske obdelave pri tlakih 30 Pa in 150 Pa.

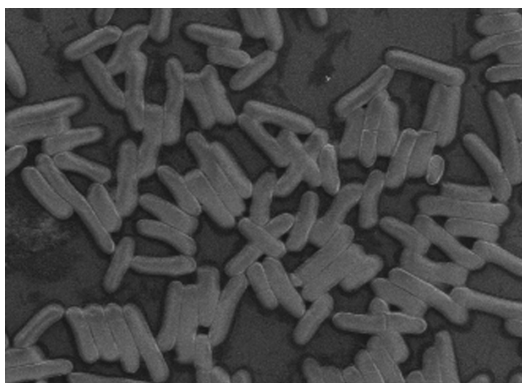


Figure 3: A SEM image of untreated bacteria
Slika 3: Posnetek neobdelanih bakterij

tration was decreasing monotonously with increasing oxygen plasma treatment time.

Selected samples were imaged by scanning electron microscopy. **Figure 3** represents a typical image of an untreated sample. The SEM image of a sample exposed to plasma for 3 s is presented in **Figure 4**. No visible changes are detected as compared to the untreated sample. **Figure 5** represents SEM image of a sample exposed to plasma for 10 s. Here, some modifications of the bacteria are observed, but the original shape is more or less preserved. The sample treated for 55 s is presented in **Figure 6**. The bacteria are now visibly damaged.

4 DISCUSSION

The results presented in **Figures 1 and 2** reveal interesting features. The initial number of survived bacteria drops significantly even for the shortest treatment time. Further on, a plateau is observed in the survival curves, and for prolonged treatment the number of survived bacteria is very small, but still measurable. The appearance of the plateau can be explained by different destruction mechanisms. Oxygen plasma is a rich source of particles that may be harmful to bacteria. The particles include excited oxygen molecules, atoms in

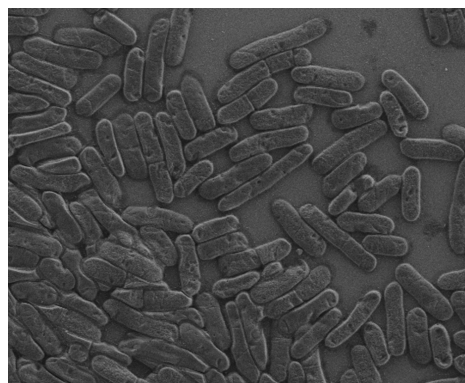


Figure 5: A SEM image of bacteria treated by oxygen plasma for 10 s
Slika 5: Posnetek bakterij, ki so bile obdelane s kisikovo plazmo 10 s

the ground state, metastable excited atoms, positively charged ions, negatively charged ions and photons emitted at relaxation of excited states by electrical dipole radiation.^{24–27} All these particles may react with bacteria. It has been shown by numerous authors that organic material is slowly etched during treatment with oxygen plasma.^{29–33} The etching has been attributed to chemical interaction between neutral oxygen atoms that abound in oxygen plasma and organic materials. The etching rate depends on plasma parameters as well as on the substrate temperature. At low temperature, the rate is often of the order of 10^{-4} .^{29–31} This value increases as the temperature is increasing.

The sharp decrease of the number of survived bacteria observed in the first few seconds of plasma treatment (**Figures 1 and 2**) can be hardly attributed to etching by neutral oxygen atoms. The sample temperature remains close to room temperature for this short period of plasma treatment so the reaction probability remains low. Also, the SEM image after 3 s of plasma treatment does not reveal any visible modification of the bacterial cell wall (**Figure 4**). The sharp drop in the number of survived bacteria in first few seconds of treatment by oxygen plasma should be therefore attributed to other mechanisms.

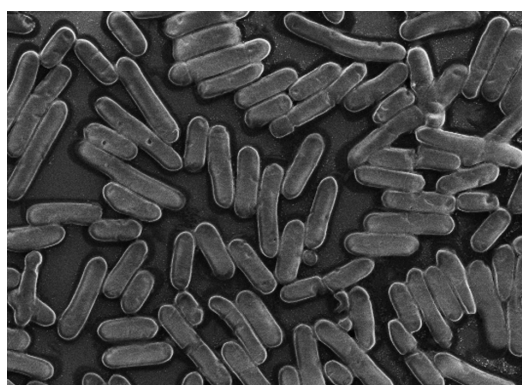


Figure 4: A SEM image of bacteria treated by oxygen plasma for 3 s
Slika 4: Posnetek bakterij, ki so bile obdelane s kisikovo plazmo 3 s

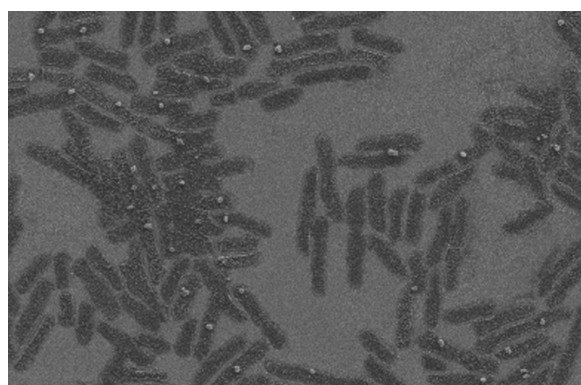


Figure 6: A SEM image of bacteria treated by oxygen plasma for 55 s
Slika 6: Posnetek bakterij, ki so bile obdelane s kisikovo plazmo 55 s

Excited oxygen atoms are definitely more aggressive against organic materials, but they cause similar damage as neutral oxygen atoms in the ground state. The same applies for metastable molecules that are expected to be present in oxygen plasma in a pretty high concentration. Negatively charged oxygen ions are unlikely to reach the surface of the samples as a thin sheath is always formed between the unperturbed plasma and the sample surface. A potential drop within this sheath repels negatively charged particles so that the flux onto the surface is negligible. Positively charged molecules and ions, on the other hand, are accelerated across the sheath and bombard the surface with the kinetic energy obtained within the sheath. The voltage drop within the sheath depends on the external biasing and could be pretty large in capacitively coupled plasma. In our case, however, we use inductively coupled plasma and the samples are not connected to an electrode. The samples are just kept at the floating potential. The difference between the plasma and floating potentials depends on electron temperature. In our case, this temperature is only a few 10 000 K, so the potential difference is of the order of 10 V. Assuming a collision-less sheath, the ions gain energy of the order of 10 eV within the sheath. The penetration depth of such ions in a solid material is only of the order of a nm, so they are unlikely to cause any damage to vital parts of bacteria. The rapid drop in the number of survived bacteria observed in **Figure 1 and 2** therefore cannot be explained by the action of ions.

The only particles left are photons. Plasma is a rich source of radiation in the range from infra-red to ultraviolet light. The radiation is best observed by optical emission spectroscopy.³⁵⁻⁴¹ The transitions between excited and ground states as well as between higher and lower excited states may occur in oxygen molecules and atoms as well as impurities that are always presented in gaseous plasma. Neutral oxygen molecules are poor light emitters since the transition by electrical dipole radiation is prohibited by laws of quantum mechanics. Charged molecules are scarce in our plasma (see **Table 1**) so the emission of light quanta is easily neglected. Atoms, on the other hand, abound in our plasma as shown in **Table 1**. Some atoms are excited to highly excited states that radiate at different wavelengths. The photons have energies either in the far UV (approximately 10 eV) or in visible range (mostly at about 2 eV). The visible light in the red part of spectrum is obviously not lethal to bacteria so they can be excluded from discussion on killing mechanisms. Hard UV radiation, on the other hand, is lethal for bacteria, but the concentration of atoms in highly excited states that produce them is pretty low (unfortunately very little work has been performed on quantitative determination of the radiation from this source). The rapid deactivation of bacteria as observed in **Figures 1 and 2** can be therefore only partly attributed to radiation from oxygen particles.

Plasma often contains impurities. The main impurity in simple vacuum systems is water vapour. Since the ultimate pressure in our system is few pascals, the concentration of water in the chamber filled with oxygen is few percent. Water molecules are quickly dissociated to OH and H radicals. Both are excellent sources of UV radiation. The Lyman series of H atoms is all in UV range, while OH molecules have rich transitions in the near UV region.⁴² The UV photons destroy the DNA of bacteria and are therefore likely to contribute significantly to deactivation of bacteria. The quick drop in the survival curves in first few seconds of plasma treatment (**Figures 1 and 2**) is therefore likely to be explained by absorption of UV radiation. UV radiation does not cause a visible damage to organic materials so this mechanism explains the preserved shape of bacteria observed in **Figure 4**.

Once many bacteria are damaged by UV radiation, the bacteria in agglomerates are only preserved. While it was difficult to observe such agglomerates they are definitely present. As long as bacteria are sheltered in agglomerates their deactivation by UV radiation is not likely to occur. They have to wait for other mechanisms to become effective. Such mechanism is chemical etching predominantly by neutral oxygen atoms. **Figure 5** represents a SEM image of bacteria after 10 s. Visible changes in morphology can be observed. The effect is even much more pronounced after 55 s of plasma treatment. The corresponding SEM image is presented in **Figure 6**. In fact, bacteria presented in **Figure 6** are really badly damaged. Only ashes are left as remains of bacteria. **Figure 6** also reveals small but perfectly visible spheres that are left after ashing process induced by oxygen plasma treatment. The origin of the spheres is unknown and any discussion on this phenomenon is beyond the scope of this paper.

There is a discrepancy between results presented in **Figures 1 and 6**. Namely, **Figure 6** reveals only ashes on the substrates while the results presented in **Figure 1** clearly show that not all bacteria are damaged lethal. A possible explanation of this discrepancy may be connected to appearance of agglomerates. Since the number of SEM images taken at these experiments was limited, we might have missed such agglomerates. Namely, the bacteria presented in **Figure 6** are definitely damaged so badly that they cannot be revitalized.

It is worth discussing the effect of pressure on the bacteria deactivation. Comparison of results presented in **Figure 2** indicates that the deactivation is much faster at high pressure. At the treatment time of 120 s, for instance, the number of survived bacteria at 30 Pa is about 80 000, while at 150 Pa it is only little more than 10 000 – almost an order of magnitude smaller. This pretty big difference may be explained taking into account different plasma parameters at different pressures as shown in **Table 1**. The density of charged particles at 30 Pa is almost an order of magnitude larger

than at 150 Pa. If bacteria were deactivated by charged particles one would expect higher deactivation at lower pressure. The results show right the opposite effect. The effect is explained by interaction of neutral oxygen atoms with bacteria. The density of oxygen atoms at 150 Pa is more than double of the value measured at 30 Pa. This result, in combination with the results presented in **Figure 2**, indicate that neutral oxygen atoms play a dominant role in deactivation of bacteria in the second phase, i.e. after destruction by UV radiation. Any quantification of the destruction probability versus the density of atoms is probably not justified for many reasons including the experimental error (both in determination of the O density and in determination of the number of survived bacteria), the unknown rate of agglomeration, and the fact that the destruction rate is not linear with the flux of neutral oxygen atoms onto the surface of bacteria. The temperature effects may not be negligible, too. While any substantial heating can be excluded for first few seconds of plasma treatment the thermal effects may not be negligible after prolonged treatment. Namely, although the neutral gas kinetic temperature is close to room temperature, exothermic reactions take place on the substrate surface due to interaction of various plasma particles with the solid material. The reactions include heterogeneous surface recombination of neutral oxygen atoms, neutralization of charged particles, weak bombardment with positive ions and de-excitation of metastable atoms and molecules. The reaction rates are, unfortunately, not known so any estimation of the bacterial temperature versus the plasma treatment time is beyond the scope of the paper. Unfortunately, the experimental system in present configuration does not allow for measuring the temperature.

Finally it is interesting that complete sterilization was not obtained even after 5 minutes of plasma treatment. This effect is difficult to explain by agglomerates since **Figure 6** shows that even after 55 s the bacteria in monolayer are ashed. The facts observed in **Figures 1 and 2** may be explained with un-careful handling of bacteria. Namely, the plate count technique applied for determination of the number of bacteria is definitely sensitive to contamination. If foreign bacteria are presented in the experimental room they would add to the measured values obtained by this technique. Plate count technique unfortunately does not distinguish between bacteria used for the experiments and foreign bacteria that might have been present in the experimental room.

5 CONCLUSION

A method for sterilization of substrates contaminated with bacteria *Bacillus stearothermophilus* was presented. The method is based on application of weakly ionized oxygen plasma. Particles created in oxygen plasma interact with bacteria causing their degradation. The

degradation was studied using the plate count technique. Rather rapid degradation was observed. The degradation mechanisms were discussed to some details. The combination of the results obtained by plate count technique and those obtained by scanning electron microscopy indicate that both destruction of bacterial DNA by absorption of UV radiation and chemical etching are responsible for deactivation or destruction of bacteria. In the first few seconds of plasma treatment the most likely mechanism is deactivation of bacterial DNK, and the chemical etching prevails thereafter. In any case it has been shown that plasma treatment is a promising technique for sterilization of delicate biomedical materials.

ACKNOWLEDGEMENT

The author acknowledges the financial support from the Ministry of Higher Education, Science and Technology of the Republic of Slovenia through the contract No. 3211-10-000057 (Center of Excellence Polymer Materials and Technologies).

6 REFERENCES

- D. Vujosevic, Z. Vratnica, A. Vesel, U. Cvelbar, M. Mozetic, A. Drenik, T. Mozetic, M. Klanjsek-Gunde, N. Hauptman, Mater. Technol., 40 (2006) 6, 227–232
- Z. Vratnica, D. Vujosevic, U. Cvelbar, M. Mozetic, IEEE Trans. Plasma Sci., 36 (2008) 4, 1300–1301
- S. Crow, J. H. Smith, Infect. Cont. Hosp. Epidemiol., 16 (1995), 483–487
- R. B. Gadri, J. Reece Roth, T. C. Montie, K. Kelly-Wintenberg, P. Tsai, D. J. Helfritch, P. Feldman, D. M. Sherman, F. Karakaya, Z. Chen, Surf. Coat. Technol., 131 (2000), 528–542
- S. Moreau, M. Moisan, M. Tabrizian, J. Barbeau, J. Pelletier, A. Ricard, L.H. Yahia, J. Appl. Phys., 88 (2000) 2, 1166–1174
- R. M. Boucher Gut, Med. Device Diagnost. Indust., 7 (1985), 51–56
- I. A. Soloshenko, V. V. Tsiolko, V. A. Khomich, A. I. Shchedrin, A. V. Ryabtsev, V. Y. Bazhenov, I. L. Mikhno, IEEE Trans. Plasma Sci., 30 (2002) 4, 1440–1444
- I. A. Soloshenko, V. V. Tsiolko, V. A. Khomich, A. I. Shchedrin, A. V. Ryabtsev, V. Y. Bazhenov, I. L. Mikhno, Plasma Phys. Rep., 26 (2000) 9, 792–800
- S. Lerouge, M. R. Wertheimer, R. Marchand, M. Tabrizian, L. H. Yahia, J. Biomed. Mater. Res., 51 (2000) 1, 128–135
- K. Kelly-Wintenberg, A. Hodge, T. C. Montie, L. Deleanu, D. Sherman, J. Reece Roth, P. Tsai, L. Wadsworth, J. Vac. Sci. Technol., A 17 (1999) 4, 1539–1544
- D. Vujosevic, M. Mozetic, U. Cvelbar, N. Krstulovic, S. Milosevic, J. Appl. Phys., 101 (2007) 10, 103305-1–103305-7
- U. Cvelbar, D. Vujosevic, Z. Vratnica, M. Mozetic, J. Phys. D: Appl. Phys., 39 (2006) 16, 3487–3493
- D. Vujosevic, Z. Vratnica, A. Vesel, U. Cvelbar, M. Mozetic, A. Drenik, T. Mozetic, M. Klanjsek-Gunde, N. Hauptman, Mater. Tehnol., 40 (2006) 6, 227–232
- K. Elersic, I. Junkar, A. Spes, N. Hauptman, M. Klanjsek Gunde, A. Vesel, Mater. Tehnol., 44 (2010) 3, 153–156
- O. Kylián, T. Sasaki, F. Rossi, Eur. Phys. J. Appl. Phys., 34 (2006) 2, 139–142
- U. Cvelbar, M. Mozetic, N. Hauptman, M. Klanjsek-Gunde, J. Appl. Phys., 106 (2009) 10, 103303-1–103303-5

- ¹⁷ M. Mozetic, U. Cvelbar, A. Vesel, A. Ricard, D. Babic, I. Poberaj, J. Appl. Phys., 97 (2005) 10, 103308-1-103308-7
- ¹⁸ M. Mozetic, A. Vesel, A. Drenik, I. Poberaj, D. Babic, J. Nucl. Mater., 363–365 (2007), 1457–1460
- ¹⁹ M. Mozetic, A. Vesel, V. Monna, A. Ricard, Vacuum, 71 (2003) 1-2, 201-205
- ²⁰ A. Vesel, M. Mozetic, Vacuum, 61 (2001) 2–4, 373–377
- ²¹ A. Drenik, U. Cvelbar, A. Vesel, M. Mozetic, Inf. MIDEEM, 35 (2005), 85–91
- ²² A. Vesel, A. Drenik, M. Mozetic, M. Balat-Pichelin, Vacuum, 84 (2010) 7, 969–974
- ²³ A. Drenik, A. Tomelj, M. Mozetic, A. Vesel, D. Babic, M. Balat-Pichelin, Vacuum, 84 (2010) 1, 90–93
- ²⁴ M. Mozetic, A. Vesel, U. Cvelbar, A. Ricard, Plasma Chem. Plasma Process., 26 (2006) 2, 103–117
- ²⁵ M. Balat-Pichelin, A. Vesel, Chem. Phys., 327 (2006) 1, 112-118
- ²⁶ A. Drenik, U. Cvelbar, A. Vesel, M. Mozetic, Strojarsstvo, 48 (2006) 1/2, 17–22
- ²⁷ A. Vesel, M. Mozetic, M. Balat-Pichelin, Vacuum, 81 (2007) 9, 1088–1093
- ²⁸ D. Vujošević, Plasma sterilization of microorganisms: doctoral dissertation, MPŠ postgraduate school, Ljubljana, 2009
- ²⁹ A. Vesel, I. Junkar, U. Cvelbar, J. Kovac, M. Mozetic, Surf. Interface Anal., 40 (2008), 11, 1444–1453
- ³⁰ A. Vesel, Surf. Coat. Technol., 205 (2010), 2, 490–497
- ³¹ M. J. Wang, Y. I. Chang, F. Poncin-Epaillard, Surf. Interface Anal., 37 (2005), 348
- ³² V. Hody, T. Belmonte, T. Czerwec, G. Henrion, J. M. Thiebaut, Thin Solid Films, 506–507 (2006), 212–216
- ³³ T. Belmonte, C. D. Pintassilgo, T. Czerwec, G. Henrion, V. Hody, J. M. Thiebaut, J. Loureiro, Surf. Coat. Technol., 200 (2005) 1–4, 26–30
- ³⁴ A. Drenik, A. Vesel, M. Mozetič, J. Nucl. Mater., 386–388 (2009), 893–895
- ³⁵ N. Krstulovic, U. Cvelbar, A. Vesel, S. Milosevic, M. Mozetic, Mater. Tehnol., 43 (2009) 5, 245–249
- ³⁶ A. Vesel, M. Mozetic, A. Hladnik, J. Dolenc, J. Zule, S. Milosevic, N. Krstulovic, M. Klanjsek-Gunde, N. Hauptman, J. Phys. D: Appl. Phys., 40 (2007) 12, 3689–3696
- ³⁷ N. Krstulovic, I. Labazan, S. Milosevic, U. Cvelbar, A. Vesel, M. Mozetic, Mater. Tehnol., 38 (2004) 1, 51–54
- ³⁸ M. Balat-Pichelin, M. Passarelli, A. Vesel, Mat. Chem. Phys., 123 (2010) 1, 40–46
- ³⁹ N. Krstulovic, I. Labazan, S. Milosevic, U. Cvelbar, A. Vesel, M. Mozetic, J. Phys. D: Appl. Phys., 39 (2006) 17, 3799–3804
- ⁴⁰ M. Mozetic, U. Cvelbar, A. Vesel, N. Krstulovic, S. Milosevic, IEEE Trans. Plasma Sci., 36 (2008), 868–869
- ⁴¹ A. Vesel, U. Cvelbar, M. Mozetic, N. Krstulovic, I. Labazan, S. Milosevic, Mater. Tehnol., 38 (2004) 3/4, 177–180
- ⁴² N. Glavan, N. Krstulović, N. Čutić, S. Milošević, U. Cvelbar, A. Vesel, A. Drenik, M. Mozetič, Vakuunist, 25 (2005), 4, 23–27

SURFACE CHARACTERIZATION OF POLYMERS BY XPS AND SIMS TECHNIQUES

ANALIZA POVRŠINE POLIMEROV Z METODAMA XPS IN SIMS

Janez Kovač

Center of Excellence for Polymer Materials and Technologies, Tehnološki park 24, 1000 Ljubljana, Slovenia.
janez.kovac@ijs.si

Prejem rokopisa – received: 2011-02-14; sprejem za objavo – accepted for publication: 2011-03-10

Polymers are very often subjects of different surface treatments. To understand and control the basic processes during surfaces modifications, analyses with advanced analytical techniques are required. We present two of such state of the art techniques, X-ray photoelectron spectroscopy – XPS and secondary ion mass spectroscopy – SIMS, often applied for characterization of polymers surfaces. In this work we give an overview of these techniques and their advantages and limitations related to polymer characterization. The combined use of these techniques is demonstrated in the application example, in which the cotton fibers were characterized before and after deposition of fluorine-based thin coating.

Keywords: X-ray photoelectron spectroscopy, XPS, TOF-SIMS, polymers, cotton

Polimerni materiali so pogosto predmet površinskih obdelav. Za razumevanje in kontrolo osnovnih procesov, ki potekajo med površinskimi modifikacijami, je potrebna uporaba naprednih analitskih tehnik. Predstavljamo dve takšni moderni tehniki: rentgensko fotoelektronsko spektroskopijo – XPS in masno spektroskopijo sekundarnih ionov – SIMS, ki se pogosto uporabljata pri karakterizaciji površin polimernih materialov. V delu predstavljamo osnove teh tehnik ter njihove prednosti in omejitve, povezane s preiskavo polimerov. Kombinirana uporaba obeh analitskih tehnik je predstavljena na primeru preiskave bombažnih vlaken pred nanosom tanke plasti na osnovi fluorovih spojin in po njem.

Ključne besede: rentgenska fotoelektronska spektroskopija, XPS, TOF-SIMS, polimeri, bombaž

1 INTRODUCTION

Polymers are widely used materials in everyday life. Their inertness, low specific weight, low production cost, variability of mechanical properties and other unique properties, make them even more attractive for future applications. Among modifications of polymers the polymer surface treatments play an important role since many surface related properties are crucial for technological applications of these materials. These applications are relevant for improvement of wettability, adhesion, surface barrier properties, biocompatibility, thin film deposition ... The reason for surface modifications is often the intrinsic property of many polymers, i.e. low surface energy, which should be changed in order to improve polymers compatibility with other materials and processes. Another reason for modification can be to introduce new functional properties at the polymer surface. The technological processes for polymer surface modifications are physical (corona, plasma, UV, laser treatments ...) and chemical (wet treatment, surface grafting ...) modifications ¹. The effect of such surface modification may be followed by different more or less sophisticated analytical tools. Surface analytical techniques with high surface sensitivity have been used to understand basic phenomena during surface modifications. Among them are X-ray photoelectron spectroscopy – XPS and secondary ion mass spectroscopy – SIMS, which were very often applied for advanced surface characterization of organic

and inorganic solid surfaces ²⁻⁵. Both of them have very high surface sensitivity combined with high elemental and molecular sensitivity. There are many other methods to analyze polymer surfaces like optical, electron and scanning probe microscopy, vibrational spectroscopies (FTIR, Raman spectroscopy), methods for surface energy measurements like contact angle measurements and others ¹.

The aim of this work is to present the main features of XPS and SIMS techniques as two state of the art analytical techniques for surface polymer characterization. Both of them have very high surface, elemental and molecular sensitivity. The main features and limitations of these two techniques are described in relation to polymer surface characterization. An application of combined use of the XPS and SIMS technique is given for cotton fabric.

2 X-RAY PHOTOELECTRON SPECTROSCOPY – XPS

XPS analyses give information on the chemical composition and chemical bonds of solid surface ^{2-4,6}. During the XPS analysis, a sample is illuminated with the monochromatic X-ray light in an XPS spectrometer and the energy of emitted photoelectrons from the sample surface is analyzed. In the photoelectron spectrum, which represents the distribution of emitted photoelectrons as a function of their binding energy,

Table 1: Comparison of main features of two surface analytical techniques XPS and SIMS**Tabela 1:** Primerjava glavnih značilnosti dveh površinsko občutljivih tehnik: XPS in SIMS

Feature	XPS	SIMS
Main information	Elemental composition and type of chemical bonds of surface atoms	Type of atoms, molecules and pendant groups at surface
Surface sensitivity	From 3–6 nm for polymers	1–2 uppermost monolayers (1 nm)
Sensitivity for elements	All, except H and He	All
Need for ultra-high vacuum ambient	Yes	Yes
Spatial resolution	1–100 μm	Less than 1 μm
In-depth information for thin films	Yes	Yes
fautoImaging	Limited	Yes with high resolution and sensitivity
3D analysis	No	Yes with high resolution and sensitivity
Quantification	Yes	Limited
Typical acquisition time for high resolution spectrum	1–3 min	5–15 min
Required expertise for data interpretation	High	High

peaks can be observed which are typical of elements present on the sample surface. The analysis area can be from some microns to mm in diameter and the signal during the XPS analysis originates from the surface layer up to 6 nm in thickness. During the analysis, two types of XPS spectra are usually recorded. Firstly, a spectrum through a wide energy range is acquired, in which the peaks of present elements are identified. Their concentration is calculated by dividing the peak intensities with the relative sensitivity factors provided by the XPS spectrometer manufacturer⁶. The attained results are normalized to 100 %. The relative error at the calculation of surface composition is approximately 20 % of reported value, while the elemental sensitivity is about 0.5 %. The XPS method does not enable the analysis of hydrogen and helium. In addition to wide energy range spectra, high-energy resolution spectra of characteristic peaks of the elements like C 1s, O 1s and others (N 1s, S 2p, Cl 2p, F 1s, Si 2p ...) are recorded through a narrow energy range. From the shape and binding energy of the peaks within these XPS spectra, the chemical bonding of surface elements can be identified with the help of data from the literature. For example in the case of organic materials one can identify from the carbon C 1s spectrum (energy range 282–297 eV) the bonding of carbon atoms like C-C/C-H, C-O, C=O, C-N, O-C-O, O=C-O, C-F and others. In addition to this other spectral features like shake-up peak in C 1s spectrum at 292 eV helps to identify aromatic pendant groups. During the analysis, the polymer samples are usually charging electrically, thus, a low-energy electron gun-neutralizer should be used. Prior to the spectra processing, spectra should be shifted, so that within the spectrum of carbon C 1s, the peak typical of the chemical bonds C-C/C-H is at the binding energy of 285.0 eV. The analysis took place in an ultra-high vacuum, which was during the analysis approximately 10^{-7} Pa or less. For precise XPS analysis of chemical bonding of surface atoms a special X-ray source should be used. In such a source X-rays are

emitted from the Al-anode with energy of 1486.6 eV and they are additionally monochromatized by special monochromator in order to reduce their energy spread to about 0.25 eV. The total recommended energy resolution during polymer analysis is 0.6 eV.

In order to get depth distribution of elements beneath the surface, ion bombardment with argon ions with energy of few keV was traditionally applied what results in a control removal of surface material. By subsequent XPS analyses one can in this way obtain XPS depth profiles presenting the concentration of elements as a function of sputtering time what can be converted into depth. In this way also polymers and thin organic films can be analyzed. Unfortunately due to local damage of chemical bonds in soft material like polymers and preferential sputtering effects very limited information on subsurface chemical bonds can be obtained by depth profiling. In last years large progress was achieved towards reducing surface damage introducing ion bombardment by cluster ion beams like C_{60}^+ .

Table 1 gives some characteristic features of the XPS technique. XPS technique was often applied for characterization of surface modifications of polymeric materials by other and also by our research group^{7–24}.

3 SECONDARY ION MASS SPECTROSCOPY – SIMS

SIMS is an analytical technique for compositional analysis of the solid surfaces and thin films^{2,5}. Due to its ability to identify the molecular structure i.e. type of molecules at the surface, SIMS technique was extensively applied in last decades just for polymer analyses^{12,15,24}. During the SIMS analysis the surface is bombarded with focused high energy (1–30 keV) ion beam what results in the ejection or sputtering of the species from the solid surface. Most of the emitted particles are neutral but small fraction of them is charged ions which are called secondary ions. They are measured

with a mass analyzer to determine the elemental composition and molecular structure of the surface. SIMS is a very surface sensitive technique because the emitted particles originate from the 1–2 top-most monolayers (1 nm). During the SIMS analysis the surface atoms are removed from the surface therefore the SIMS is locally destructive. In order to obtain chemical information of the original surface, the primary ion dose must be low enough ($<10^{13}$ cm $^{-2}$) to prevent a surface damage. This regime is so-called "static SIMS" mode and it is widely used for the characterization of polymer surfaces. If the primary ion dose is large enough it can be used to erode the surface layer in a controlled manner. In this way information on the in-depth distribution of elements can be obtained similar as it was described above for XPS depth profiling. This, so called "dynamic SIMS" mode is widely applied for depth-profiling of thin films, layer structures and dopant concentration. Layers of up to few microns thick can be depth-profiled using SIMS technique.

The sensitivity of the SIMS technique depends on the yield of secondary ion sputtering which is a function of the specimen's material (matrix effect), and the type, energy and incidence angle of the primary beam of ions. This is a reason for limited possibility for precise quantification of SIMS results in terms of surface composition. On the other hand the sensitivity of the SIMS technique is very high and is in the range of 10^{-6} . This technique allows the routine measurement of many trace elements at very low concentration, even in the ppb-range. The proper choice of primary ions is important for optimum sensitivity²⁵. For different materials different types of ion guns should be used to provide an optimum detection sensitivity for secondary ions. In general inorganic materials do not exhibit very complex structure with high mass units. Therefore for inorganic materials the SIMS spectra acquired in the low mass region (up to 100 u) can provide enough information for successful analysis. Opposite is valid for organic materials containing often ingredients with very high molecular mass. In this case it is important to get as much information as possible from the SIMS spectra in the high mass region (above 200 u) where small mass differences between similar molecular structures can be distinguished. For this purpose ion beams with high yield of surface sputtering of higher mass secondary ions is required. In last decade liquid metal ion sources (LMIG) for enhanced excitations in organic SIMS analyses were developed. They are based mainly on gold and bismuth clusters of atoms, like Au_3^+ , Bi_3^+ , Bi_5^+ . Similar characteristics are valid also for the ion beam of the C_{60}^+ clusters. Such ions sources provide enhanced increase for sputtering of high mass secondary ions and are very suitable for the analysis of organic and bio-organic systems. In the case of inorganic materials oxygen ions are usually used for analysis of electropositive elements or those with low ionization potentials, whereas electro-

positive ions like cesium atoms are better for sputtering negative ions from electronegative elements.

From the construction point of view there are three basic types of ion guns. In one, ions of gaseous elements are usually generated by electron ionization, for instance noble gases (Ar^+ , Xe^+), oxygen (O^-), or even ionized molecules such as SF_5^+ or C_{60}^+ . This type of ion gun is easy to operate and generates high current ion beams. A second source type, the surface ionization source, is one that generates Cs^+ primary ions. A third source type, the liquid metal ion source (LMIG), operates with metals or metallic alloys, which are liquid at room temperature. While a gallium source is able to operate with elemental gallium, recently developed sources for gold, indium and bismuth use cluster ions. The LMIG source provides a high focused ion beams (<60 nm) for high-resolution work with moderate intensity and is additionally able to generate short pulsed ion beams. It is therefore commonly used in static TOF-SIMS instruments. Highly focused ion beam allows chemical or molecular imaging of the surface, an analytical approach in which focused ion beam is rastered over the surface and mass spectra are collected at every pixel point. Retrospectively, for any peak in the mass spectrum, an image can be generated.

The mass analyzer may be a quadrupole mass analyzer, magnetic sector mass analyzers or time-of-flight (TOF) analyzer. They differ with respect to transmission, mass resolution, mass detection (parallel or sequential) and sensitivity. Among them the TOF-SIMS analyzers provide the highest sensitivity and mass resolution, a much greater mass range and they are preferred for static SIMS analyses of polymers. In SIMS measurements the spectra of positive and negative ions are measured. The TOF-SIMS spectra obtained from polymer surfaces can be divided into three regions. In the first low mass range (up to 300 u) ions consisting of end groups, fractions of repeat units, or side chains are detected (e.g. $C_xH_y^{+/-}$). In general the detection of these low mass fragments is sufficient for an identification of inorganic materials. In the second range (300–2000 u), typically ions consisting of multiple repeat units with and without the loss of functional groups are detected, what is important for polymer analyses. In the third high mass range (up to 10 000 u) intact oligomer ions can be observed. These quasimolecular ions are typically formed by an attachment ($M + H$) or loss of hydrogen ($M - H$) and are important for recognition of surface species. Recently developed polyatomic or cluster ions primary sources such as gold (Au_n^+), bismuth (Bi_n^+) and C_{60}^+ (buckminster fullerenes) overcome the problem of insufficient yields of these higher mass species observed under atomic primary bombardment²⁶. The use of cluster ions has also another advantage. It decreases also the residual chemical damage on the surface comparing to monoatomic ions due to larger size, shallower implantation depth and higher sputtering yields. For these

reasons cluster ions are also very suitable for molecular depth profiling of most organic and biological samples, where in-depth molecular distribution is measured.

At this point we can compare also the acquisition time between SIMS and XPS techniques. In the TOF-SIMS instruments due to the time-of-life type of measurements whole mass spectrum is acquired in parallel at very high sensitivity. This is a reason that the typical acquisition of SIMS spectrum at one point takes about 1–3 min. It depends also on the required mass region and mass resolution. This time is shorter than typical time needed for acquisition of high-energy resolution spectra of different elements in the XPS analysis. In the XPS analyses such acquisition time is typical from 5 min to 15 min.

In comparison to other surface analytical techniques the SIMS offers several advantages, namely the ability to identify all elements, including H and He and the ability to identify elements present in very low concentration levels, such as dopants in semiconductors. Some of the SIMS main features are summarized in **Table 1**.

4 APPLICATION OF XPS AND SIMS TECHNIQUES FOR COTTON FIBERS CHARACTERIZATION

In the following an example is given, which shows the combined application of XPS and SIMS techniques for surface characterization of cotton fabrics treated with fluoroalkylsilane (FAS). The cotton is an example of the natural polymer and it was often characterised by XPS and SIMS techniques^{11,12,15,16,18,20,23}. The thin fluoroalkylsilane treatment was applied in order to modify the wettability of the cotton surface towards the hydrophobic surface. Surface analyses were performed on the untreated and treated cotton fabrics. The XPS and SIMS techniques were used to follow the surface composition, chemical bonds of surface atoms, molecular structures and spatial distribution of coated material.

The XPS analysis was performed in the XPS spectrometer produced by Physical Electronics Inc., model TFA XPS. The Al monochromatized source of X-ray light with the power of 200 W was used. The energy resolution was approximately 0.7 eV and the analysis area was about 0.4 mm in diameter. **Figure 1** shows an XPS survey spectra obtained on the cotton

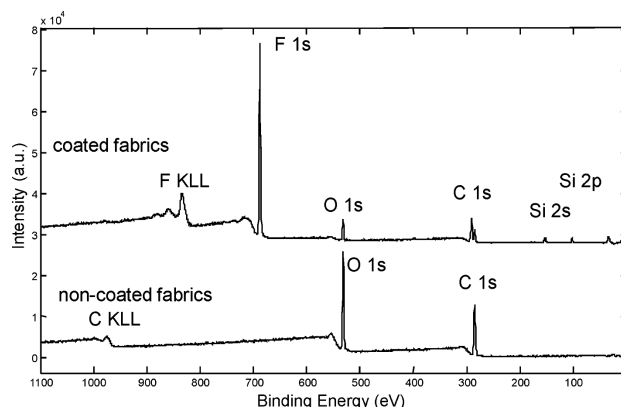


Figure 1: XPS survey spectra obtained on the surface of the non-treated cotton fabrics (lower) and on fabrics treated with fluoroalkylsilane (upper).

Slika 1: Pregledni XPS-spektri, dobljeni na površini neobdelane bombažne tkanine (spodaj), in na tkanini, obdelani s fluoroalkilsilanom (zgoraj)

fabrics and the fabrics after treatment. In the spectrum of untreated sample the peaks of C 1s and O 1s are present indicating the pure cotton surface. The surface composition deduced from this spectrum is given in **Table 2**. There is the mole fraction 61.6 % of C and 38.4 % of oxygen on the surface. This composition corresponds well to expected cotton nominal composition. As mentioned above XPS method can in addition to surface composition yield also information on bonding of surface atoms. **Figure 2a** shows high-energy resolution carbon C 1s spectrum obtained on the untreated sample. The spectrum is composed from more peaks, which were identified by de-convolution procedure. After C 1s spectrum de-convolution into different components, C1, C2, C3, we assigned them to different chemical bonds of carbon atoms. In this case a peak C1 at binding energy of 285.0 eV is assigned to C-C and C-H bonds, a peak C2 at 286.4 eV is assigned to C-O, a peak C3 at 287.8 eV is assigned to C=O and O-C-O bonds. The origin of peaks C2 and C3 is related to backbone of the cellulose molecules from the cotton matrix. The C1 component related to C-C/C-H bonds probably originates from some non-cellulosic components as waxes or pectine or from additives or surface contamination. Namely the C-C/C-H bonds are not present in cotton backbone structure. The relative concentration of C1, C2, C3 components is given in **Table 2**.

Table 2: Surface composition and relative concentration of different bonds of carbon atoms obtained by the XPS analysis of the cotton fabrics before and after treatment with fluoroalkylsilane

Tabela 2: Sestava površine in relativne koncentracije kemijskih vezi ogljikovih atomov, dobljene z XPS-analizo bombažne tkanine pred obdelavo s fluoroalkilsilanom in po njej

Sample	$x(C)/\%$	$x(O)/\%$	$x(F)/\%$	$x(Si)/\%$	C1 (%), C-C/C-H	C2 (%), C-O	C3 (%), C=O, O-C-O	C4 (%), O=C-O	C5 (%), CF ₂	C6 (%), CF ₃
Non-treated cotton fabrics	61.6	38.4	0	0	38.0	43.4	18.6	0	0	0
Treated fabrics	37.7	9.6	48.6	4.2	15.9	18.6	3.1	5.0	48.4	9.0

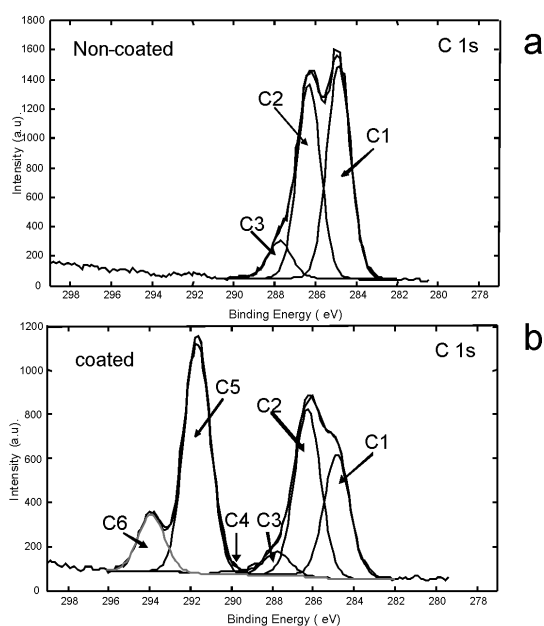


Figure 2: XPS high-energy resolution spectra C 1s obtained on the non-treated cotton fabrics (a) and fabrics treated with fluoroalkylsilane (b). The spectra are deconvoluted in the C1–C6 peaks presenting different C-atom bonds.

Slika 2: Energijsko visoko ločljivi spektri XPS C 1s, dobljeni na površini neobdelane bombažne tkanine (a), in na tkanini, obdelani s fluoroalkilsilanom (b). Spektri so bili razstavljeni na vrhove C1–C6, ki pomenijo različne vezi ogljikovih atomov.

After the treatment of the cotton fabrics with fluoroalkylsilane, the upper XPS survey spectrum present in **Figure 1** was obtained. In addition to C 1s and O 1s the peaks of F 1s, Si 2p and Si 2s appeared indicating successful deposition of functional coating. The new surface composition is also given in **Table 2**. The major element on the surface is fluorine (48.6 %) originating from the deposited coating. The deposition of

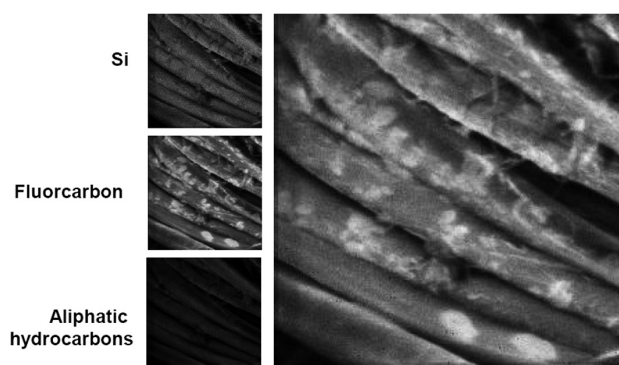


Figure 4: TOF-SIMS images obtained on the cotton fibers treated with fluoroalkylsilane. Images were taken using raster size of $(80 \times 80) \mu\text{m}$. Images on left side were obtained summarizing the signals of Si_xO_y clusters (left top), fluorocarbon (left middle) and aliphatic hydrocarbons (left down). An image on the right side is a composite image obtained from three images on the left.

Slika 4: TOF-SIMS-slike, dobljene na bombažnih vlaknih, obdelanih z fluoroalkilsilanom. Slike so bile posnete po področju $(80 \times 80) \mu\text{m}$. Slike na levi strani so bile dobljene iz signalov, značilnih za Si_xO_y spojine (levo zgoraj), fluoroogljkovih spojin (sredina levo) in alifatskih ogljikovodikovih spojin (levo spodaj). Slika na desni strani je dobljena kot vsota slik na levi strani.

functional coating can be recognized also in different chemical bonding of the surface atoms with respect to untreated cotton. Carbon C 1s spectrum from the coated cotton surface is shown in **Figure 2b**. New peaks are present in this spectrum representing new types of C-atoms bonding. The two peaks are at binding energies of 291.7 eV (C5) and 293.9 eV (C6). These energies are characteristic for CF_2 and CF_3 bonding which shows the fluorinated-carbon compound on the surface. Also the ratio between the C1 and C2 peaks changed after coating deposition (**Table 2**). Applying the XPS method we concluded on the surface composition and chemical

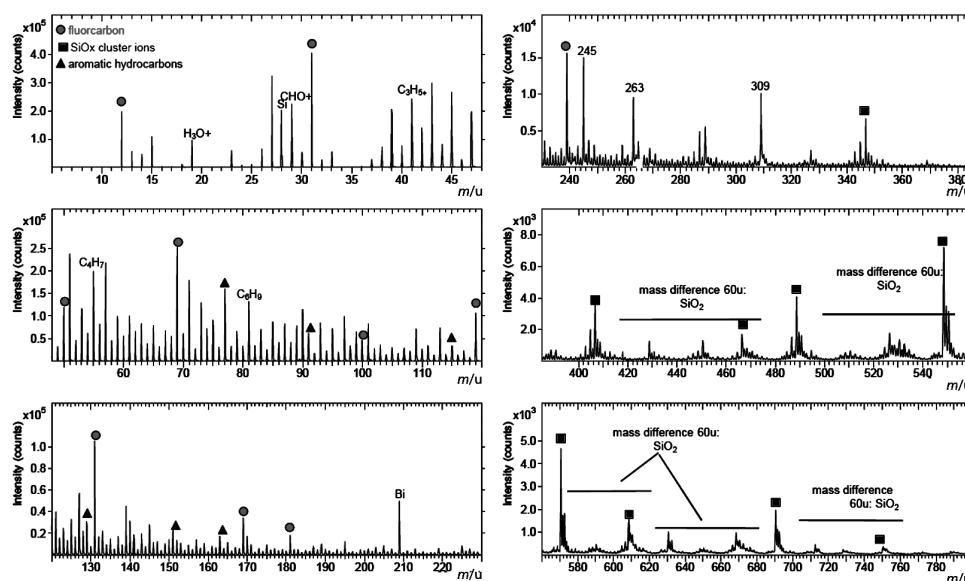


Figure 3: TOF-SIMS spectra of positive polarity obtained on the cotton fibers treated with fluoroalkylsilane
Slika 3: TOF-SIMS-spektri pozitivnih ionov, dobljeni na bombažnih vlaknih, obdelanih s fluoroalkilsilanom

bonding of elements on non-treated cotton fabrics and on the fabrics after coating deposition.

Due to the lack of spatial resolution of the XPS method there is an open question how the deposited coating is distributed over the surface. Is the coating homogeneously distributed or there are some non-treated regions. To analyse the homogeneity of the applied coating we carried out the SIMS analysis on the treated sample. The SIMS instrument with TOF mass analyzer was used. The primary ion beam of Bi-ions of energy 25 keV was produced by LMIG source. In the first step the spectroscopic analysis was performed at one point. A typical SIMS mass spectrum in the range between 5 u and 790 u obtained with positive ions from the treated fabrics is presented in **Figure 3**. The spectrum consists of great number of peaks at different masses. The peaks assignment is more complicated comparing to XPS method. Anyhow there are known groups of peaks at characteristic masses belonging to expected chemical molecules and their fragments. In the case of coated cotton the SIMS spectrum shows the main peaks at masses m/u (12, 31, 69, 131, 240), which originate from the fluorocarbon compound due to fluoroalkylsilane treatment, the peaks at (77, 116, 129) u originating from aromatic hydrocarbons and peaks at (347, 407, 488, 548) u originating from the SiO_x clusters. Beside mentioned peaks which were used to identify the molecular structure of the surface, other peaks exist in the SIMS spectrum, as for example at 18 u (H_3O^+), 28 (Si), 29 (CHO^+), 41 (C_3H_3^+), 55 (C_4H_7) ... After SIMS point analysis the SIMS images were recorded analyzing the region of (256×256) pixels and acquiring the whole mass spectra at each pixel. The characteristic peaks of fluorocarbon compound, aromatic hydrocarbons and a peak from the SiO_x clusters were used to construct the images, which help to follow the distribution of deposited coating. These SIMS images are presented in **Figure 4** as three separated images (on the left side) and as a composite image. These results show that different species are distributed in different manner. From the composite image it can be recognized that there are regions where the SiO_x -clusters and fluorocarbon compounds from the fluoroalkylsilane film are more concentrated. In this way we conclude that some inhomogeneities from the coating deposition process which can be further improved by modifying process parameters.

5 CONCLUSIONS

In this work the main features of XPS and SIMS analytical techniques were presented and discussed. Both of them are relevant for surface characterization of polymer materials. These two techniques have very high surface sensitivity. The main features of the XPS method are the ability to obtain quantitative information on chemical composition and on types of chemical bonds in particular of carbon atoms, which are the most abundant

in organic materials. On the other hand the main features of the SIMS techniques are the ability to obtain the chemical information of the type of atoms, clusters and molecules at the surface with very high lateral resolution. The combination of both methods gives the very complete information on polymer surface chemistry. The combined use of the XPS and SIMS techniques was demonstrated on the analyses of cotton fibers coated with fluorine-containing film. XPS data confirm the formation of film through the presence of fluorine and C-F bonds on the cotton surface. The spatially resolved SIMS images revealed partially nonuniform distribution of coated surface species related to the reactivity of deposited material.

ACKNOWLEDGEMENT

The author acknowledges the financial support from the Ministry of Higher Education, Science and Technology of the Republic of Slovenia through the contract No. 3211-10-000057 (Center of Excellence Polymer Materials and Technologies). The author thanks to dr. B. Simončič and B. Tomšič for sample preparation and to ION-TOF company from Münstrer, Germany, for help at SIMS measurements.

6 REFERENCES

- 1 F. Garbassi, M. Morra, E. Occhiello, *Polymer Surfaces: From Physics to Technology*, John Wiley and Sons, Chichester, UK, 2000, 233–311
- 2 John C. Vickerman, Ian S. Gilmore (editors), *Surface Analysis: The Principal Techniques*, 2nd edition, John Wiley and Sons, Chichester, UK, 2009, 47–203
- 3 G. Beamson, D. Briggs, *High Resolution XPS of Organic Polymers*, Wiley, Chichester, 1992
- 4 D. Briggs, J. T. Grant (editors), *Surface Analysis by Auger and X-Ray Photoelectron Spectroscopy*, IM Publications, Chichester and SurfaceSpectra Limited, Manchester, 2001, 1–31
- 5 J. C. Vickerman, D. Briggs (editors), *ToF-SIMS: Surface Analysis by Mass Spectrometry*, IM Publications, Chichester and SurfaceSpectra Limited, Manchester, 2001, 75–161
- 6 J.F. Moulder, W. F. Stickle, P. E. Sobol, K. D. Bomben, *Handbook of X-Ray Photoelectron Spectroscopy*, Eden Prairie, Minnesota, USA: Physical Electronics Inc., 1995
- 7 N. Vandencastele, F. Reniers, Plasma-modified polymer surfaces: Characterization using XPS, *Journal of Electron Spectroscopy and Related Phenomena*, 178–179 (2010), 394–408
- 8 A. Vesel, M. Mozetič, A. Zalar, XPS study of oxygen plasma activated PET, *Vacuum*, 82 (2008) 2, 248–251
- 9 A. Vesel, M. Mozetič, A. Zalar, XPS characterization of PTFE after treatment with RF oxygen and nitrogen plasma, *Surf. Interface Anal.*, 40 (2008) 3–4, 661–663
- 10 L. S. Johansson, J. M. Cambell, *Surf. Interface Anal.*, 36 (2004), 1018–1022
- 11 T. Topalovic, V. A. Nierstrasz, L. Bautista, D. Jocić, A. Navarro, M.C.G. Warmoeskerken, *Colloids and Surfaces A: Physicochem. Eng. Aspects*, 296 (2007), 76–85
- 12 P. Fardim, J. Gustafsson, S. Schoultz, J. Peltonen, B. Holmbom, *Colloids and Surfaces A: Physicochemical and Engineering Aspects*, 255 (2005) 1–3, 91–103

- ¹³ I. Junkar, A. Vesel, U. Cvelbar, M. Mozetič, S. Strnad, Influence of oxygen and nitrogen plasma treatment on polyethylene terephthalate (PET) polymers, *Vacuum*, 84 (2010) 1, 83–85
- ¹⁴ A. Vesel, I. Junkar, U. Cvelbar, J. Kovač, M. Mozetič, Surface modification of polyester by oxygen and nitrogen-plasma treatment, *Surf. Interface Anal.*, 40 (2008), 1444–1453
- ¹⁵ N. E. Zafeiropoulos, P.E. Vickers, C.A. Baillie, J. F. Watts, *Journal of Materials Science*, 38 (2003), 3903–3914
- ¹⁶ A. Vesel, M. Mozetič, S. Strnad, Z. Peršin, K. Stana-Kleinschek, N. Hauptman, Plasma modification of viscose textile, *Vacuum*, 84 (2010) 1, 79–82
- ¹⁷ M. Gorenšek, M. Gorjanc, V. Bukošek, J. Kovač, P. Jovančić, D. Mihailović, Functionalization of PET fabrics by corona and nano silver, *Tex. Res. J.*, 80 (2010) 3, 253–262
- ¹⁸ D. Ciolacu, J. Kovač, V. Kokol, The effect of the cellulose-binding domain from *Clostridium cellulovorans* on the supramolecular structure of cellulose fibres, *Carbohydr. Res.*, 345 (2010) 5, 621–630
- ¹⁹ E. Sarantopoulou, J. Kovač, Z. Kollia, I. Raptis, S. Kobe, A. C. Cefalas, Surface modification of polymeric thin films with vacuum ultraviolet light, *Surf. Interface Anal.*, 40 (2008) 3–4, 400–403
- ²⁰ B. Tomšič, B. Simončič, B. Orel, L. Černe, P. Forte-Tavčer, M. Zorko, I. Jerman, A. Vilčnik, J. Kovač, Sol-gel coating of cellulose fibres with antimicrobial and repellent properties, *J. sol-gel sci. technol.*, 47 (2008) 1, 44–57
- ²¹ M. Schroeder, E. Fatarella, J. Kovač, G. M. Gübitz, V. Kokol, Laccase-induced grafting on plasma-pretreated polypropylene, *Biomacromolecules*, 9 (2008) 10, 2735–2741
- ²² I. Jerman, A. Šurca Vuk, M. Koželj, B. Orel, J. Kovač, A structural and corrosion study of triethoxysilyl functionalized POSS coatings on AA 2024 alloy, *Langmuir*, 24 (2008) 9, 5029–5037
- ²³ A. Vilčnik, I. Jerman, A. Šurca Vuk, M. Koželj, B. Orel, B. Tomšič, B. Simončič, J. Kovač, Structural properties and antibacterial effects of hydrophobic and oleophobic sol-gel coatings for cotton fabrics, *Langmuir*, 25 (2009) 10, 5869–80
- ²⁴ A. Karen, N. Man, T. Shibamori, K. Takahashi, *Appl. Surf. Science* (2003) 203–204, 541–546
- ²⁵ M. P. Seah, *J. Vac. Sci. Technol.*, A 26 (2008) 4, 660
- ²⁶ J. Brison, S. Muramoto, D. G. Castner, *J. Phys.Chem., C* (2010), 5565–5573

MODIFICATION OF PET-POLYMER SURFACE BY NITROGEN PLASMA

MODIFIKACIJA POVRŠINE PET-POLIMERA Z DUŠIKOVO PLAZMO

Rok Zaplotnik¹, Metod Kolar², Aleš Doliška², Karin Stana-Kleinschek²

¹Jožef Stefan Institute, Jamova 39, 1000 Ljubljana, Slovenia

²Center of Excellence for Polymer Materials and Technologies, Tehnološki park 24, 1000 Ljubljana, Slovenia
rok.zaplotnik@ijs.si

Prejem rokopisa – received: 2011-02-09; sprejem za objavo – accepted for publication: 2011-03-05

Nizkotlačno, šibko ionizirano dušikovo plazmo smo uporabili za površinsko modifikacijo polimera polietilen tereftalat z dušikovimi funkcionalnimi skupinami. Plazmo smo vzbujali v brezelektrodni visokofrekvenčni plinski razelektritvi z generatorjem, ki deluje pri koristni moči okoli 200 W in osnovni frekvenci 27,12 MHz. Dušikove molekule, ki vstopijo v plinsko razelektritev, se vzbudijo v visoka vzbujena stanja, delno disociirajo in šibko ionizirajo. Transformacija plina v stanje plazme omogoča nastanek kemično reaktivnih delcev z veliko potencialno energijo, medtem ko ostane njihova kinetična energija blizu vrednosti, ki je značilna za plinske molekule pri sobni temperaturi. Velika kemijska reaktivnost dušikove plazme omogoča hitro funkcionalizacijo površine PET-polimera z dušikom bogatimi funkcionalnimi skupinami. Ta pojav smo spremljali z rentgensko fotoelektronsko spektroskopijo. Polimerni vzorci so postali hitro nasičeni z dušikom, iz česar je mogoče sklepati, da je funkcionalizacija omejena na zelo tanko plast prav ob površini vzorcev.

Ključne besede: poly(ethylene terephthalate), dušikova plazma, modifikacija površine, funkcionalne skupine, rentgenska fotoelektronska spektroskopija

Low pressure weakly nitrogen plasma was applied for incorporation of nitrogen-containing functional groups onto poly(ethylene terephthalate) – PET polymer. Nitrogen plasma was created in an electrode-less radiofrequency discharge at the nominal power of 200 W and the frequency of 27.12 MHz. Nitrogen molecules entered the discharge region were highly excited, partially dissociated and weakly ionized. Transformation into the state of plasma allowed for creation of chemically reactive particles with a high potential energy while the kinetic energy remained close to the value typical for room temperature. The chemical reactivity allowed for rapid functionalization with nitrogen-rich functional groups. The appearance of these groups was monitored by X-ray photoelectron spectroscopy – XPS. The polymer surface was quickly saturated with nitrogen indicating that the modification was limited to an extremely thin surface film.

Keywords: poly(ethylene terephthalate), nitrogen plasma, surface modification, functional groups, X-ray photoelectron spectroscopy

1 INTRODUCTION

Polymer materials are widely used not only in industry but also in biomedical applications. A polymer which is of particular interest in biomedical applications is poly(ethylene terephthalate) – PET. The structural formula is presented in **Figure 1**. PET is supplied in variety of forms from bulk pieces through thin foils to fabrics. Perforated foils are often used as the first layer of plasters, while artificial blood vessels are made from knitted material. The PET material has excellent chemical and mechanical properties and expresses reasonably good bio-compatibility. The latter property, however, is not always adequate since un-specific interaction with body fluids is often observed. It is therefore desirable to modify the surface properties of PET before specific applications. The modification can

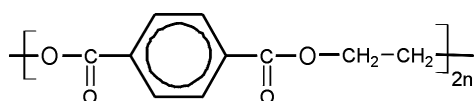


Figure 1: Structural formulae of poly(ethylene terephthalate)
Slika 1: Strukturna formula polietilen tereftalata

be performed by a variety of wet chemical treatments, but such procedure often does not yield optimal results.

A popular technology for modification of polymer surface properties is treatment by gaseous plasma.¹⁻¹⁴ The surface properties of PET polymer can be modified using oxygen plasma treatment (to make it more hydrophilic),¹⁵⁻²¹ or fluorine plasma (to obtain excellent hydrophobicity).²²⁻²³ Such treatments have been applied, but it seems that in some cases they do not allow for optimal modification of surface properties. This is especially the case when optimal interaction with proteins is required. In such cases other types of plasma should be used. In the present paper, modification of PET by nitrogen plasma is addressed.

2 NITROGEN PLASMA

Plasmas of diatomic gases are often used in order to modify surface properties of polymer and other materials. It has been shown that oxygen molecules dissociate in plasma forming highly reactive atoms.²⁴⁻²⁷ Similar effects were observed in hydrogen plasma.²⁸⁻³⁵ Nitrogen, however, behaves much different in an

electrical discharge. This is due to a particular property of excited states as well as collision phenomena. In oxygen plasma, for instance, the probability for super-elastic collisions between vibrationally excited molecules and neutral atoms is huge, while in nitrogen it is negligible. This particular phenomenon allows for extremely high vibrational temperature of molecules in nitrogen plasma.

Appearance of highly vibrationally excited molecules is not the only particularity of nitrogen plasma. Nitrogen molecules also have a variety of electronically excited states and most are metastable. Plasma, created in nitrogen, is therefore a rich source of excited nitrogen molecules that are chemically pretty reactive. Some common excited states are presented in **Figure 2**.

3 EXPERIMENTAL

Samples of PET foils were treated in nitrogen plasma. The reactor has been described to details elsewhere.^{15,36,37} Due to the completeness of the paper let us just summarize the most important features of the experimental system. The system comprises a discharge chamber, a vacuum pump, gas feeding system, radio-frequency generator and an optical spectrometer. The discharge chamber is a borosilicate glass tube (Schott 8250) with the length of 60 cm and the outer diameter of 4 cm. It is connected to kovar rings on both sides, and the rings are welded to standard FK 40 flanges. Rubber gaskets are used for vacuum seals. The discharge chamber is pumped on one side with a two stage oil rotary pump with the nominal pumping speed of 28 m³/h. The pressure is measured with an absolute vacuum gauge. Nitrogen is leaked continuously on the other side of the discharge tube through a manually adjustable needle valve. The valve is connected to a nitrogen flask via a copper tube. The vacuum system is often exposed to ambient atmosphere and never baked so the ultimate pressure is several Pa. The residual atmosphere contains mostly water vapour. Plasma is created in the discharge

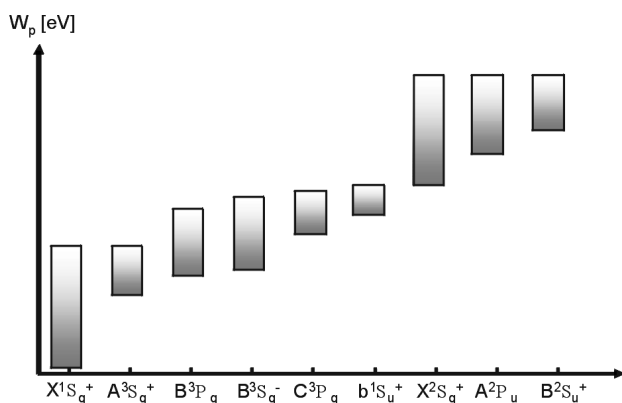


Figure 2: Some excited states of nitrogen molecule. The width of the states is due to vibrationally excitation

Slika 2: Nekatera vzbujena stanja dušikove molekule. Širok razpon po potencialni energiji je posledica vibracijskih vzbujenih stanj

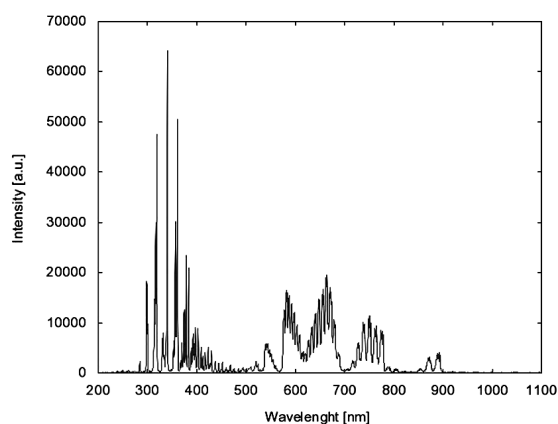


Figure 3: A typical optical spectrum of nitrogen plasma
Slika 3: Značilen optični spekter dušikove plazme

chamber by radiofrequency generator with the nominal power of 700 W and the fundamental frequency of 27.12 MHz. A coil of 14 turns is wound up the discharge chamber and connected directly to the generator. Since no matching network is applied between the generator and the coil, the matching is rather poor so it was estimated that the forward power was only about 200 W³⁸⁻⁴². Both inductive and capacitive components are present in the discharge. The glowing plasma fills the entire volume in the discharge tube at low pressure, but at high pressure it is limited to a small volume inside the coil. At the pressure of 75 Pa the plasma is at its optimal condition so the samples are usually treated at this pressure. An optical spectrometer of rather poor resolution is used to monitor the plasma radiation from about 300 nm to 1000 nm. The best sensitivity of the spectrometer is between 400 nm and 800 nm where the borosilicate glass is pretty transparent.

Commercially available PET foils were cut to small pieces and exposed to plasma for (3, 10 and 30) s. No cleaning or other pretreatments were performed prior to exposure to plasma, but handling was careful so any presence of foreign material is unlikely. Samples were

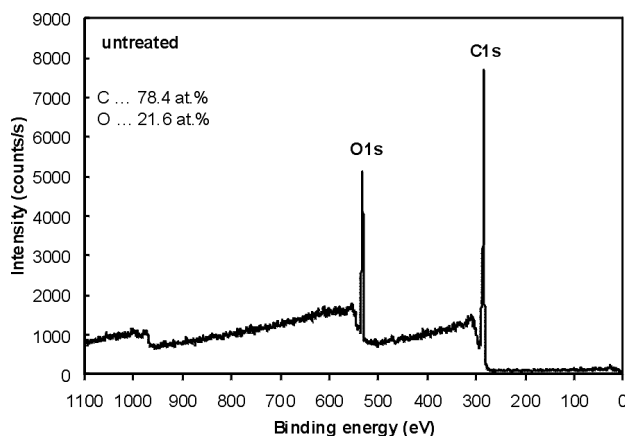


Figure 4: XPS survey spectrum of an untreated sample
Slika 4: Pregledni XPS-spekter neobdelanega vzorca

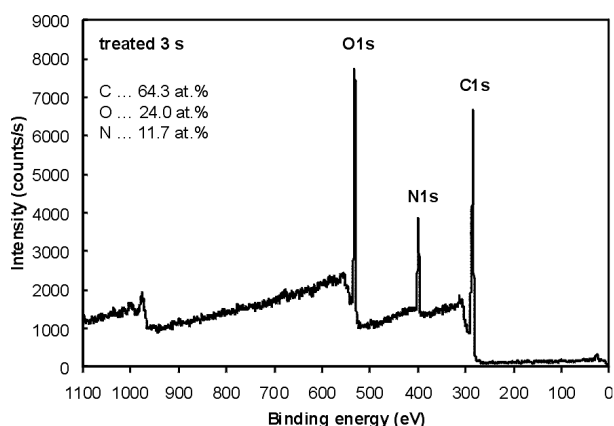


Figure 5: XPS spectrum of the sample treated with nitrogen plasma for 3 s

Slika 5: XPS-spekter vzorca, ki je bil obdelan z dušikovo plazmo 3 s

analyzed by X-ray photoelectron spectroscopy (XPS). We used our spectrometer AvaSpec 3648 from Avantes.

The surface of the plasma treated PET samples was analyzed with an XPS instrument TFA XPS Physical Electronics. The base pressure in the XPS analysis chamber was about 6×10^{-8} Pa. The samples were excited with X-rays over a 400- μm spot area with a monochromatic Al $K_{\alpha 1,2}$ radiation at 1486.6 eV. The photoelectrons were detected with a hemispherical analyzer positioned at an angle of 45° with respect to the normal to the sample surface. Survey-scan spectra were made at a pass energy of 187.85 eV a 0.4 eV energy step, while for C1s individual high-resolution spectra were taken at a pass energy of 23.5 eV and a 0.1 eV energy step. Since the samples are insulators, we used an additional electron gun to allow for surface neutralization during the measurements. The spectra were fitted using MultiPak v7.3.1 software from Physical Electronics, which was supplied with the spectrometer. The curves were fitted with symmetrical Gauss-Lorentz functions. A Shirley-type background subtraction was used. Both the

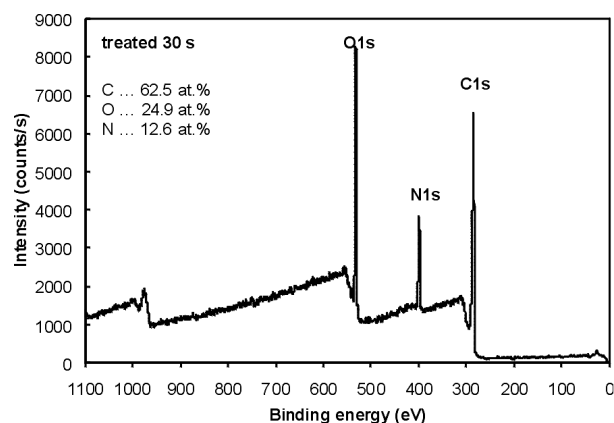


Figure 7: XPS spectrum of the sample treated with nitrogen plasma for 30 s

Slika 7: XPS-spekter vzorca, ki je bil obdelan z dušikovo plazmo 30 s

relative peak positions and the relative peak widths (FWHM) were fixed in the curve fitting process.

3 RESULTS

Optical spectra of nitrogen plasma were measured during treatment of the samples. The spectra did not change noticeably during the treatment indicating pretty poor interaction of plasma with the samples. A typical spectrum is shown in **Figure 3**.

Samples were characterized by XPS before and after plasma treatment. A typical survey spectrum for untreated sample is presented in **Figure 4**, while **Figures 5, 6 and 7** represent spectra measured for samples exposed to nitrogen plasma for (3, 10 and 30) s, respectively. The survey spectra allow for quantification of the composition in the surface layer from which photo-electrons can reach the detector. The elemental composition in atomic percent is given in boxed text placed in each spectrum presented in **Figures 3 – 7**.

4 DISCUSSION

The treatment of PET samples by nitrogen plasma caused interesting modification of the surface layer that is worth discussing. First, and most significant effect, is appearance of nitrogen. The spectrum of untreated sample, presented in **Figure 4**, is free from nitrogen. Only carbon and oxygen are presented and the concentration (79 % C and 21 % O) is close to the theoretical value for bulk poly(ethylene terephthalate). Even a 3 s long exposure to nitrogen plasma causes a pretty large concentration of nitrogen atoms at about 12 % (**Figure 5**). The appearance of nitrogen is a consequence of interaction between reactive particles generated in plasma and surface atoms. Namely, nitrogen molecules in the thermally equilibrium gas at room temperature do not interact chemically with PET. A question arises, which particles are responsible for breaking of surface chemical bonds and formation of functional groups containing

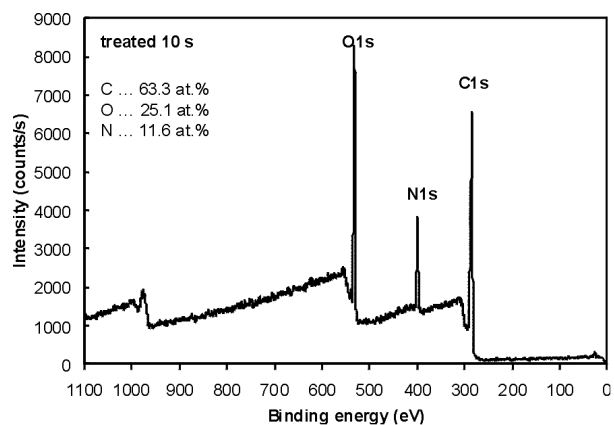


Figure 6: XPS spectrum of the sample treated with nitrogen plasma for 10 s

Slika 6: XPS-spekter vzorca, ki je bil obdelan z dušikovo plazmo 10 s

nitrogen. The list of candidates is pretty long. **Figure 2** reveals the candidates. The most reactive particles are usually those with the highest potential energy – positively charged molecules. The density of ions in plasma, however, is pretty low (the order of magnitude is solely 10^{15} m^{-3}) so they cannot cause such rapid functionalization. The list of neutral particles with potential energy around 10 eV, which are chemically very reactive, too, include a variety of molecular excited states as shown in **Figure 2**. Finally, there are also neutral atoms in the ground as well as excited states. In plasma of some other two-atom molecules such as hydrogen, the concentration of excited molecules is pretty low because the radiative life time of those states is short, and their contribution to chemical reactivity is easily neglected. Nitrogen molecules, on the other hand, have most excited states metastable meaning that the radiative decay due to electrical dipole interactions is not allowed. The concentration of such highly excited molecules is thus pretty large, definitely larger than the concentration of ions. Namely, in plasma with a rather low electron temperature the positive ions are created by step-like process and not directly by electron impact ionization of a molecule in the ground state. Since a variety of excited states is available, the interaction of nitrogen plasma with polymer materials is far from being well understood. In addition, nitrogen plasma is also rich in high vibrationally excited molecules. **Figure 4** reveals some. Unlike oxygen plasma, where the vibrational population is usually limited to few lowest excited states, molecules nitrogen plasma are found in energetic excited states with potential energy up to about 10 eV. Such molecules are chemically reactive, too, so they can also contribute to functionalization of polymer materials.

Figures 5, 6 and 7 reveal that the concentration of nitrogen does not depend on treatment time, as long as it is at least 3 s. This effect is explained by saturation of the surface layer nitrogen functional groups. As mentioned earlier, the molecules and atoms capable of chemical interaction with a polymer abound in nitrogen plasma so saturation is obtained quickly.

More surprising is enrichment of the surface film with oxygen. This effect cannot be explained by poor purity of nitrogen, since the original gas in the flask contains over 99.99% of nitrogen and since the tube connecting the flask with the needle valve is made from copper that does not represent a significant source of oxygen. Also, the vacuum system is hermetically tight as no nitrogen is detected in the residual atmosphere. The enrichment is rather explained by interaction of water molecules with the surface film. As already mentioned, the ultimate pressure is several Pa and the residual atmosphere contains practically only water vapor. The dissociation energy of water molecules is below the excitation energy of nitrogen metastables, so a collision with a nitrogen molecule found in a metastable excited state is likely to cause dissociation of water molecule to

OH and O radicals. These radicals are chemically very reactive and interact with organic materials causing formation of oxygen functional groups. In fact, a competition between oxygen and nitrogen probably appears: both functional groups can be created on a polymer surface and the exact functionalization depends on the fluxes of nitrogen and oxygen reactive particles onto the polymer surface. A study of the reaction probabilities is definitely beyond the scope of current paper but should be addressed in order to understand the functionalization of polymers with nitrogen rich functional groups in industrial environments. Finally, it is worth mentioning that many polymers absorb substantial amounts of water which is slowly released under vacuum conditions so avoiding of oxygen radicals is a hard task in real environment.

5 CONCLUSION

The functionalization of polymer surface with nitrogen was addressed. XPS results clearly showed that simple nitrogen plasma was a suitable medium for modification of FET surface with nitrogen groups. The exact mechanisms that lead to functionalization are, however, far from being well understood. This is predominantly due to the fact that numerous highly excited molecules are found in nitrogen plasma. Optical emission spectroscopy revealed that not only electronically excited, but also vibrationally excited molecules abound in our plasma. The enrichment of the surface layer with oxygen observed at current experiments reveals that functionalization with nitrogen functional groups only may be a pretty difficult task in industrial environments. The oxygen containing radicals are formed in nitrogen plasma by dissociation of water molecules. The concentration of water in a vacuum system can be minimized by intensive and/or prolonged pumping, using high vacuum compatible systems and drying of the polymer before entering the system, but all these procedures are difficult to apply in real industrial environments.

ACKNOWLEDGEMENT

The authors acknowledge the financial support from the Ministry of Higher Education, Science and Technology of the Republic of Slovenia through the contract No. 3211-10-000057 (Center of Excellence Polymer Materials and Technologies).

6 REFERENCES

- ¹ A. Asadinezhad, I. Novak I, M. Lehocky, V. Sedlarik, A. Vesel, I. Junkar, P. Saha, I. Chodak, *Plasma Processes Polym.*, **7** (2010) 6, 504–514
- ² S. Marais, M. Metayer, M. Labbe, J. M. Valleton, S. Alexandre, J. M. Saiter, F. Poncin-Epaillard, *Surf. Coat. Technol.*, **122** (1999) 2–3, 247–259

- ³ M. J. Wang, Y. I. Chang, F. Poncin-Epaillard, *Surf. Interface Anal.*, 37 (2005), 348
- ⁴ T. Belmonte, J. M. Thiebaut, D. Mezerette, *J. Phys. D: Appl. Phys.*, 35 (2002) 16, 9–1926
- ⁵ M. Sowe, I. Novak, A. Vesel, I. Junkar, M. Lehocky, P. Saha, I. Chodak, *Int. J. Polym. Anal. Ch.*, 14 (2009) 7, 641–651
- ⁶ A. Vesel, *Surf. Coat. Technol.*, 205 (2010) 2, 490–497
- ⁷ F. Gaboriau, G. Cartry, M. C. Peignon, C. Cardinaud, *J. Vac. Sci. Technol. B*, 20 (2002) 4, 1514–1521
- ⁸ U. Cvelbar, M. Mozetic, I. Junkar, A. Vesel, J. Kovac, A. Drenik, T. Vrlinic, N. Hauptman, M. Klanjek-Gunde, B. Markoli, N. Krstulovic, S. Milosevic, F. Gaboriau, T. Belmonte, *Appl. Surf. Sci.*, 253 (2007) 21, 8669–8673
- ⁹ M. Lehocky, A. Mracek, *Czechoslovak J. Phys.*, 56 (2006) 7, B1277–B1282
- ¹⁰ M. Lehocky, L. Lapcik, M. C. Neves, T. Trindade, L. Szyk-Warszynska, P. Warszynski, D. Hui, *Mat. Sci. Forum*, 426 (2003) 4, 2533–2538
- ¹¹ T. Belmonte, C. D. Pintassilgo, T. Czerwicz, G. Henrion, V. Hody, J. M. Thiebaut, J. Loureiro, *Surf. Coat. Technol.*, 200 (2005), 26–30
- ¹² T. Belmonte, T. Czerwicz, H. Michel, *Surf. Coat. Technol.*, 142 (2001), 306–313
- ¹³ A. Vesel, K. Elersic, I. Junkar, B. Malic, *Mater. Tehnol.*, 43 (2009) 6, 323–326
- ¹⁴ T. Vrlinic, A. Vesel, U. Cvelbar, M. Krajnc, M. Mozetic, *Surf. Interface Anal.*, 39 (2007) 6, 476–481
- ¹⁵ A. Vesel, I. Junkar, U. Cvelbar, J. Kovac, M. Mozetic, *Surf. Interface Anal.*, 40 (2008) 11, 1444–1453
- ¹⁶ I. Junkar, U. Cvelbar, A. Vesel, N. Hauptman, M. Mozetic, *Plasma Processes Polym.*, 6 (2009) 10, 667–675
- ¹⁷ R. Morent, N. De Geyter, C. Leys, L. Gengembre, E. Payen, *Surf. Coat. Technol.*, 201 (2007) 18, 7847–7854
- ¹⁸ C. Riccardi, R. Barni, E. Selli, G. Mazzone, M. R. Massafra, B. Marcandalli, G. Poletti, *Appl. Surf. Sci.*, 211 (2003) 1–4, 386–397 [http://dx.doi.org/10.1016/S0169-4332\(03\)00265-4](http://dx.doi.org/10.1016/S0169-4332(03)00265-4)
- ¹⁹ N. Inagaki, K. Narushim, N. Tuchida, K. Miyazaki, *J. Polym. Int. B*, 42 (2004) 20, 3727–3839
- ²⁰ N. De Geyter, R. Morent, C. Leys, L. Gengembre, E. Payen, *Surf. Coat. Technol.*, 201 (2007) 16–17, 7066–7075
- ²¹ A. Vesel, M. Mozetic, A. Zalar, *Vacuum*, 82 (2008) 2, 248–251
- ²² C.-H. Wen, M.-J. Chuang, G.-H. Hsiue, *Appl. Surf. Sci.*, 252 (2006), 3799–3805
- ²³ S. Marais, Y. Hirata, C. Cabot, S. Morin-Grognet, M. R. Garda, H. Atmani, F. Poncin-Epaillard, *Surf. Coat. Technol.*, 201 (2006) 3–4, 868–879
- ²⁴ M. Mozetic, A. Vesel, U. Cvelbar, A. Ricard, *Plasma Chem. Plasma Process.*, 26 (2006) 2, 103–117
- ²⁵ A. Drenik, U. Cvelbar, A. Vesel, M. Mozetic, *Strojarsstvo*, 48 (2006) 1–2, 17–22
- ²⁶ M. Balat-Pichelin, A. Vesel, *Chem. Phys.*, 327 (2006) 1, 112–118
- ²⁷ A. Vesel, M. Mozetic, M. Balat-Pichelin, *Vacuum*, 81 (2007) 9, 1088–1093
- ²⁸ A. Vesel, A. Drenik, M. Mozetic, M. Balat-Pichelin, *Vacuum*, 84 (2010) 7, 969–974
- ²⁹ A. Drenik, A. Tomelj, M. Mozetic, A. Vesel, D. Babic, M. Balat-Pichelin, *Vacuum*, 84 (2010) 1, 90–93
- ³⁰ M. Mozetic, M. Kveder, M. Drobnic, A. Paulin, A. Zalar, *Vacuum*, 45 (1994) 10/11, 1095–1097
- ³¹ M. Mozetic, M. Drobnic, A. Pregelj, K. Zupan, *Vacuum*, 47 (1996) 6–8, 943–945
- ³² M. Mozetic, M. Drobnic, *Vacuum*, 50 (1998) 3–4, 319–322
- ³³ M. Mozetic, A. Vesel, V. Monna, A. Ricard, *Vacuum*, 71 (2003), 201–205
- ³⁴ A. Pregelj, M. Kveder, M. Mozetic, A. Paulin, *Inf. Midem*, 23 (1993) 2, 112–116
- ³⁵ M. Mozetic, A. Vesel, A. Drenik, I. Poberaj, D. Babic, *J. Nucl. Mater.*, 363–365 (2007), 1457–1460
- ³⁶ A. Vesel, *Inf. Midem*, 38 (2009), 257–265
- ³⁷ A. Vesel, M. Mozetic, A. Hladnik, J. Dolenc, J. Zule, S. Milosevic, N. Krstulovic, M. Klanjek-Gunde, N. Hauptman, *J. Phys. D: Appl. Phys.*, 40 (2007) 12, 3689–3696
- ³⁸ D. Babič, I. Poberaj, M. Mozetič, *Rev. sci. instrum.*, 72 (2001), 4110–4114
- ³⁹ F. Breclj, M. Mozetič, *Vacuum* 40 (1990) 1/2, 177–178
- ⁴⁰ F. Breclj, M. Mozetič, K. Zupan, M. Drobnič, *Vacuum*, 44 (1993) 5–7, 459–460
- ⁴¹ M. Mozetič, *Surf. coat. technol.*, 201 (2007) 9–11, 4837–4842
- ⁴² M. Mozetič, *Vacuum*, 71 (2003), 237–240

FUNCTIONALIZATION OF AFM TIPS FOR USE IN FORCE SPECTROSCOPY BETWEEN POLYMERS AND MODEL SURFACES

FUNKCIONALIZACIJA AFM-KONIC ZA UPORABO V SPEKTROSKOPIJI SIL MED POLIMERI IN MODELNIMI POVRŠINAMI

Tina Maver^{1,2}, Karin Stana - Kleinschek^{1,2}, Zdenka Peršin^{1,2}, Uroš Maver^{3,*}

¹University of Maribor, Faculty of Mechanical Engineering, Laboratory for Characterisation and Processing of Polymers, Smetanova 17, SI-2000 Maribor, Slovenia

²Centre of Excellence for Polymer Materials and Technologies, Tehnološki park 24, SI-1000 Ljubljana, Slovenia

³National Institute of Chemistry, Laboratory for materials electrochemistry, Hajdrihova 19, SI-1000 Ljubljana, Slovenia
uros.maver@ki.si

Prejem rokopisa – received: 2011-02-12; sprejem za objavo – accepted for publication: 2011-03-03

The following work presents the use of two different methods for the attachment of different functional groups onto the AFM tip surface. Such functionalized tips then allow for further binding of molecules with different origins and natures, thus allowing for use when measuring forces, and the extent of interactions appearing between two model surfaces and in real systems. Force spectroscopy, in combination with chemical force microscopy (CFM), as used in this study, exhibits great potential for chemical sensing in the field of polymer sciences. In modern wound treatment, it is very important to know the type and ranges of interactions between different polymer materials, which are mostly crucial components of the dressings. Precise measurement of these interactions would help to choose those materials that fit together without the use of additional chemical modifications on their surfaces. Such modifications are often the cause of unpredictable complications during the course of wound healing. This same method could also be used for interaction evaluation between chosen polymer materials with biological macromolecules, which appear within the wound during the healing process. Such in vitro testing could be of great help when optimal wound dressing materials need to be chosen in order to alleviate a patient's suffering after application. Scanning electron and atomic force microscopies were used in order to prove the effectiveness and applicability of the used functionalization procedures.

Keywords: atomic force microscopy, chemical force microscopy, force spectroscopy, functionalization of AFM tips

V prispevku predstavljamo uporabo dveh različnih metod za pripravo AFM-konic z različnimi funkcionalnimi skupinami. Takšna funkcionalizacija je primerna za nadaljnje pripenjanje različnih molekul, kar je osnova za uporabo pri določanju moči in obsega interakcij med modelnimi površinami in v realnih sistemih. Spektroskopija sil v kombinaciji z mikroskopijo na kemijsko silo, ki je bila uporabljena v tem delu, ima velik potencial na področju kemijskega zaznavanja v polimerni znanosti. Pri pripravi večplastnih polimernih materialov, ki se uporabljajo pri moderni obravnavi kroničnih ran, nam natančno določanje interakcij lahko pomaga pri njihovi izbiri. Na podlagi takih meritev bi lahko izbrali materiale, ki med seboj najbolje interagirajo, in ne bi bilo treba vpeljati nobene kemijske modifikacije, ki bi lahko negativno vplivala na potek celjenja ran. Prav tako bi bilo mogoče metodo uporabiti za določanje interakcij izbranih polimernih materialov z biološkimi molekulami v rani, s čimer bi in vitro določili optimalen material za plast obliža, ki je v stiku z rano. V delu smo uspešnost in uporabnost funkcionalizacije preverjali z elektronsko mikroskopijo in mikroskopijo na atomsko silo.

Ključne besede: mikroskop na atomsko silo, mikroskop na kemijsko silo, spektroskopija sil, funkcionalizacija konic

1 INTRODUCTION

Polymers have found their way into all fields of science and industry over the last decades. Their potential applications range from binders in batteries¹ to composite materials in drug delivery.² Whilst the range of possible combinations between different monomers is endless, polymers found or based on natural polymers have recently become the subject of thorough research, once again.^{3,4} Synthetic changes to their native structure make them even more propelling; especially cellulose derivatives exhibit a lot of potential for satisfying most industrial needs.³

Although AFM has been used for more than three decades; we are still experiencing some breakthroughs for its use in several areas of science and industry. This

AFM method is particularly useful for studying those modifications obtained on surfaces of polymer materials treated with reactive non-equilibrium gaseous plasma.^{5–18}

Namely, it has been shown that even a mild plasma treatment results in important changes in surface morphology. Such changes may eventually lead to a nano-textured surface and thus to an extremely high hydrophilicity for otherwise moderately hydrophobic polymer materials.^{19–32}

From its origins in 1986,³³ this technique has evolved from a shaky method to the ultimate tool on the nanoscale.³⁴ The first years of AFM use were dedicated to pushing the resolution boundary, to some unimaginable extent,³⁵ during the last decade research has been dedicated more to force measurements,³⁶ the identifi-

cation and characterization of processes at the molecular level³⁷ and mainly by the use of force spectroscopy and chemical force microscopy (CFM).

The latter is, at the moment, the most propelling within the field of polymer examination on the nano-scale.^{38,39} CFM provides the possibility of gaining knowledge about those interactions appearing between polymer molecules or polymers, and different surfaces.⁴⁰ This additional information allows for the prediction of final material characteristics based on the examined polymers, even before their finalization. Quantitative assessment of the involved forces and their extent makes it easier to choose the correct polymers for achieving desired interactions between those materials used in several different interest fields (adhesion, adsorption, repelling etc.). Multilayer polymeric materials are, at the moment, first choice materials for the preparation of modern wound dressings. When sticking together layers of different polymeric origins, their interaction gains importance regarding the behavior of the final product. Methods enabling us to monitor this would greatly improve any success when choosing the right material and consequentially, avoid any chemical modification. Wound healing is a precisely regulated process, which can be interrupted or even worsened by even small interventions, thus making derivatives of previously proven biocompatible polymers dangerous and sometimes even toxic. The use of CFM for this aspect could decrease the need for chemical modification and thus improve the success of those polymers used for wound dressings.

Successful research using AFM is impossible without the proper tools, so choosing right tips is crucial in this regard. Many commercial tips are available at the moment, but only some exhibit characteristics that allow for easy and repeatable functionalization. Whilst the functionalization of tips may seem quite simple during the first iteration, it quickly becomes clear, that a lot of chemical skills are needed to bind the right species to the right place.⁴¹ As a careful researcher always desires to know as much as possible about each preparation step, a lot of statistical evaluation is needed in order to prove and evaluate the success of any attachment⁴². During the course of our research, we found that silicon-based tips are the most promising in regard to ease of chemical modification. Their biggest advantage proved to be the commercial availability of several different silica precursors, which are highly suitable for decorating the AFM tips with the desired functional groups. Although the literature shows some direction towards the attachment of NH_2 groups on the surface,⁴³ we attempted to widen the field of possible attachments by introducing other functional groups, such as the SH groups or certain hydrophobic ones like CH_3 . Gold-coated tips were also used additionally in order to prove their applicability for functionalization purposes.

The purpose of our study was to evaluate, test, and alter available techniques for AFM tip functionalization,

thus enabling its later use for the binding of test molecules. Different types of silica precursors were used to prepare those tips with the desired functional groups, which are known to allow further functionalization at mild conditions. These are often necessary when soft molecules, such as polymers or biological macromolecules, are the test subjects.

2 EXPERIMENTAL

2.1 Preparation of functionalized AFM tips

2.1.1 Silicon-based tips

Table 1 shows the chemical formulae and short names for the used silica precursors in this study. A known procedure was used for the attachment of NH_2 groups to the surface, which is described elsewhere.⁴³ Depending on the characteristics of the used precursors, the initial procedure was modified to suit the attachment of desired functional groups. The used parameters are written along with their chemical structures and names, in **Table 1**.

2.1.1.1 Attachment of NH_2 groups

Firstly APTES (30 μL) triethylamine-TEA (10 μL) was poured into separate Eppendorf tubes of 1 ml. These tubes were then placed inside an exiccator, which was thoroughly cleaned with acetone and ethanol, respectively and blown through using argon gas. Fresh tips (NP-S10 contact-mode tips, Veeco) were placed beside the two tubes on a flat surface and then the exiccator was again mildly blown through with argon gas and sealed. The precursors and tips were left inside the exiccator for two hours. **Figure 1** shows the scheme of the procedure.

2.1.1.2 Attachment of SH and CH_3 groups

This procedure was similar to the previous one but with slight changes regarding the used volumes and times of tip exposure to the reagents in the exiccator. Molecular weight and relative density were the only parameters taken into account when adjusting the used volume because the structural differences between the three used silica precursors appear on the same fragment of the molecule (whilst all other parts remained the

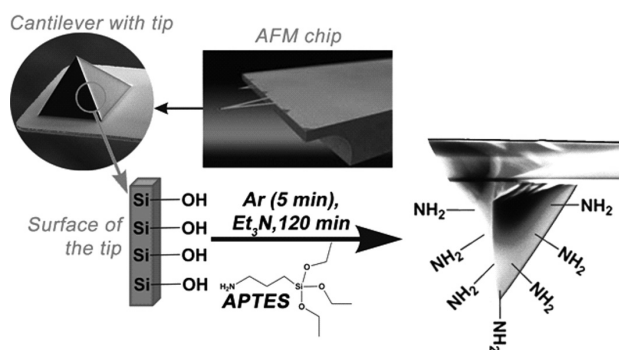
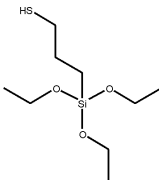
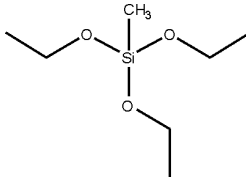
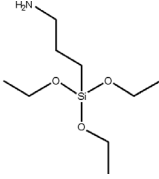


Figure 1: Preparation scheme for the amino functionalized AFM tips
Slika 1: Shema priprave AFM-konic s amino skupinami

Table 1: Used silica precursors and their physic–chemical characteristics**Tabela 1:** Uporabljeni silikatni prekurzorji in njihove fizikalno-kemijske lastnosti

SILICA PRECURSOR		STRUCTURAL FORMULA
Name	MPTES [3-mercaptopropyltriethoxysilane]	
$\rho/(\text{g}/\text{cm}^3)$	0.98	
$M_r/(\text{g}/\text{mol})$	238.42	
$T_{\text{tal.}}/^\circ\text{C}$	/	
$T_{\text{vrel.}}/^\circ\text{C}$	210	
Vapour pressure p/hPa	6.66 (at 20 °C)	
Name	MTES [methyl–triethoxysilane]	
$\rho/(\text{g}/\text{cm}^3)$	0.895	
$M_r/(\text{g}/\text{mol})$	178.30	
$T_{\text{tal.}}/^\circ\text{C}$	–40	
$T_{\text{vrel.}}/^\circ\text{C}$	142	
Vapour pressure p/hPa	6,40 (at 20 °C)	
Name	APTES [(3-aminopropyl)triethoxysilane]	
$\rho/(\text{g}/\text{cm}^3)$	0.949	
M_r	221.37	
$T_{\text{tal.}}/^\circ\text{C}$	/	
$T_{\text{vrel.}}/^\circ\text{C}$	122–123	
Vapour pressure p/hPa	13,30 (at 20 °C)	

same). Vapour pressure had, in our case, the biggest impact on the relative rate of functional group attachment to the surface and was therefore used to adjust the time of tips exposure in order to achieve the required coverage. The used volumes and times for the attachment of SH and CH₃ groups were 32 μL , 25 μL and 4 h, 4 h, respectively.

2.1.2 Gold-coated tips

Tips without coating on the reflective side were chosen for this purpose, in order to avoid any possible loss of resolution. Functionalization of the tips reflective side could cause laser refraction, resulting in signal decrease. Fresh gold-coated tips (ATEC-CONTAu-10, Nanosensors) were dipped into a mixture of MPTES (20 μL) and EtOH (2 mL). They remained in the solution for 1 h in order to achieve the desired surface coverage.⁴⁴ Immediately after removal from the mixture, tips were washed over a few stages, by combined dipping into water (millie Q) and chloroform (CF), respectively and

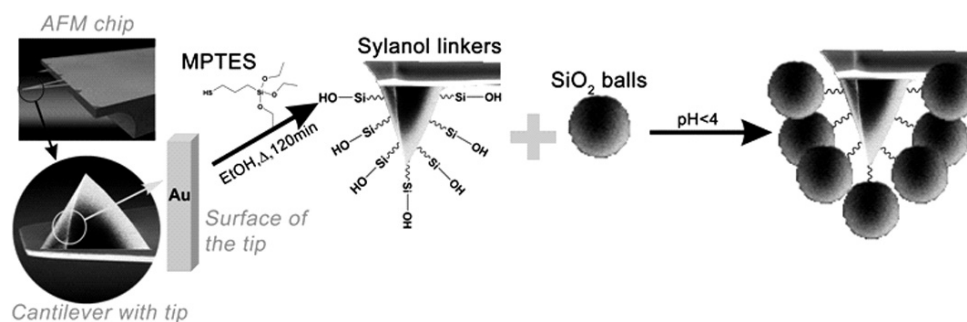
then dried using high grade nitrogen (5.0.). **Figure 2** shows a schematic depiction of this procedure.

2.2 Attachment of polymers to the tip surface

Two approaches were used to show that the functionalized tips are able to bind additional species to their decorated surface. The first enabled us to adsorb two different cellulose derivatives (amylose – AM and carboxymethyl cellulose – CMC), and the second was used to covalently bind one of them (CMC) to the tip for further use. Additionally silicon spheres were bound to the surface of the functionalized tips (as shown in **Figure 2**), which is proven to be very useful for examining the elasticity of films, biological structures, such as cells and macromolecules.⁴⁵

2.2.1 Adsorption

Solutions with 10 mmol concentrations were used for both polymers in order to achieve adsorption on the tips. Pure tips, out of the box, were gently dipped into the

**Figure 2:** Preparation scheme for gold-coated AFM tips**Slika 2:** Shema funkcionalizacije z zlatom obloženih AFM-konic

solution using freshly cleaned tweezers (they were sonicated in acetone for 30 min and dried using clean nitrogen), and left there for 2 h. Afterwards, tips were removed from the solution and carefully washed 6 times using two different solvents (water and chloroform – CF), alternately.

2.2.2 Covalent binding

The amino decorated tips, prepared as mentioned previously, were used for the covalent attachment. CMC was attached to amino-functionalized tips, via amide bond, using *N,N'*-carbonyldiimidazole (N-CDI) (CDI method). In this way, the carboxyl group of CMC was activated, which was then prone to binding to the amino species of the tips, under mild conditions. The reaction took place in a small beaker containing the solution of the activated CMC in water. Amino-functionalized tips were placed inside the beaker, and left there for 24 h. Tips were washed and dried in the same way as previously mentioned, within the section for the adsorption of polymers.

2.2.3 Attachment of silicon balls

The same procedure, as shown in **Figure 3** was used for the attachment of silicon balls. First the gold-coated tips were functionalized using MPTES, as mentioned in the section Gold-coated tips. These were then gently dipped in an extremely diluted water suspension of silicon balls with a pH below 4, which was adjusted using citric acid, and left there for 2 h to allow for attachment of the balls. Silicon balls were obtained during the same preparation, procedure as stated elsewhere.⁴⁶

All the used solvents and other chemicals (unless stated otherwise) were of analytical grade (high purity), and bought from Sigma-Aldrich.

2.3 Methods

2.3.1 Scanning electron microscopy

Dried AFM tips for scanning electron microscopy were pressed on a double-sided adhesive carbon tape (SPI Supplies, USA). Tips were imaged using field emission scanning electron microscopy (FE-SEM, Supra 35 VP, Carl Zeiss, Germany) operated at 1 keV.

2.3.2 AFM

Force spectroscopy measurements were performed using an Agilent 5500 AFM. All measurements were done in liquid medium (milli-Q water) to avoid capillary forces. 100 curves were measured during each time scale at different points on the sample's surface, and the outliers eliminated. Some of the measurements were repeated and the measurements included in the final results in order to achieve better statistics and prove the measurements were performed correctly. In all cases, a model atomically flat silicon surface was used to avoid any discrepancies due to specific surface characteristics

or various roughness at different spots where force spectroscopy was performed.

3 RESULTS

3.1 SEM imaging of the functionalized tips

Scanning electron microscopy showed that almost all functionalization attempts were successful. No clear differences could be seen between the images of those functionalized tips with different functional groups. Images also showed that the functionalization was mostly confined to the actual end of the tip and not to the surrounding chip. **Figure 3** shows representative images of the functionalized tips.

3.2 AFM measurements

These measurements were performed to show the applicability of the proposed functionalization procedures in further investigations regarding interacting polymers species to be used in materials preparation or drug delivery. All the measured force curves were analyzed and those maximal forces that the functionalized tips experienced were compared for chosen tips. Addition-

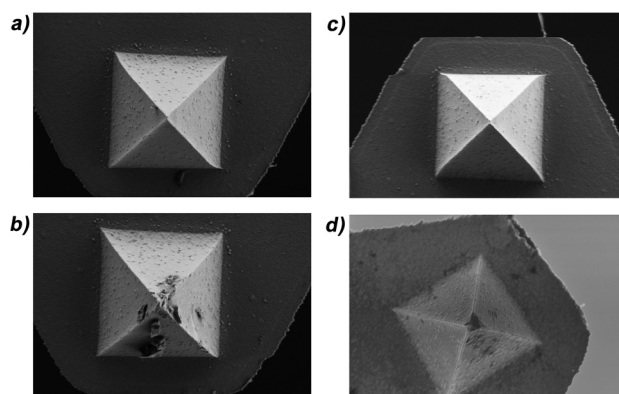


Figure 3: SEM micrographs of functionalized AFM tips: a) decorated with amino groups, b) decorated with thiol groups, c) with adsorbed amylose and d) with adsorbed carboxymethyl cellulose

Slika 3: Slike funkcionaliziranih AFM-konic, pridobljene z uporabo vrstične elektronske mikroskopije: a) s pripetimi amino skupinami, b) s pripetimi tiolnimi skupinami, c) z adsorbirano amilozo in d) z adsorbirano karboksimetil celulozo

Table 2: Results of force spectroscopy measurements

Tabela 2: Rezultati spektroskopije sil

Interaction type	Average force [nN]	Average distance [nm]
Amylose (AM)		
Adsorption on pure tips	50	150
Adsorption on hydrophobic tips	80	200
Carboxymethyl cellulose (CMC)		
Adsorption on pure tips	27	90
Covalent bond with amino functionalized tips	103	300

ally, those distances were analyzed, at which interaction with the surface disappeared. **Table 2** shows the representative data as measured and evaluated.

3.2.1 Force curve explanation

A typical force curve is shown in **Figure 4**. The explanation is as follows: when approaching the surface the cantilever is in an equilibrium position (A) and the curve is flat. As the tip approaches the surface (B), the cantilever is pushed up to the surface – being deflected upwards, which is seen as a sharp increase in the measured force. At (C) the approach half-cycle ends and the retract half-cycle begins. Once the tip starts retracting, the deflection starts to decrease and passes its equilibrium position at (D). As we start moving away from the surface the tip snaps in due to interaction with the surface, and the cantilever is deflected downwards (E). Once the tip-sample interactions are terminated due to increased distance, the tip snaps out, and returns to its equilibrium position.

Figure 5 shows representative force curves, and their comparison when appropriate. It can be seen that the covalently bound CMC exhibits far greater forces and ranges when compared to the adsorbed species. Comparison of the response for the two used polymer species also reveals that the additional carboxyl groups in CMC contribute to a greater force and range when compared to AM. The final comparison shows the differences between the measured forces and ranges for the AM bound to two differently functionalized tips, namely the slightly more hydrophobic ones (additional CH_3 groups on the surface) and the fresh tips without any functionalization. As the more hydrophobic nature of AM suggests, the interaction between AM and the slightly more hydrophobic tips (functionalized with additional CH_3 groups) is greater, which is also reflected in the increased force involved in the interaction.

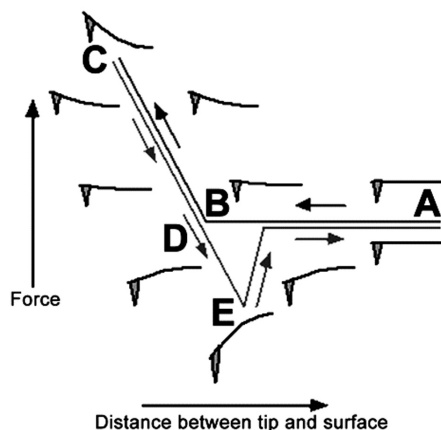


Figure 4: Example of a simple force curve. The upper is the approach curve, and the bottom the retract curve. More details regarding this characteristic feature can be found in the text

Slika 4: Primer krivulje pri spektroskopiji sil. Zgornja predstavlja krivuljo med približevanjem, medtem ko je spodnja krivulja oddaljavanja. Podrobnosti v zvezi s potekom meritve so zapisane v besedilu.

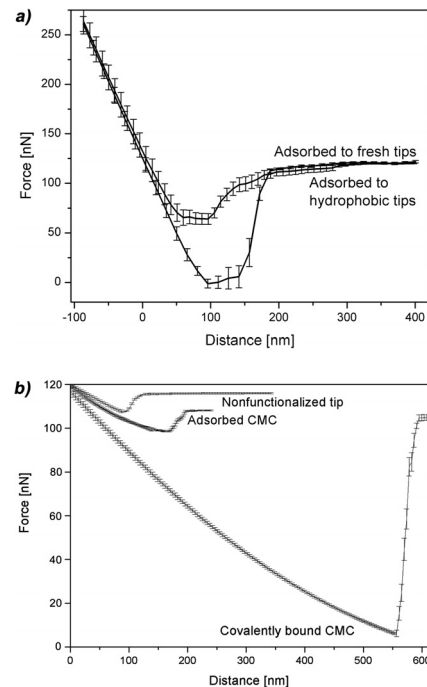


Figure 5: Representative force curves after tip functionalization. a) comparison between three different procedures for CMC attachment to the tip surface and b) comparison of force curves as measured using two types of amylose attachment. It can be clearly observed that the type of functionalization has a huge impact on any interaction between the tip and the model surface.

Slika 5: Vzorčni primeri spektroskopije sil. a) primerjava treh različnih načinov vezave CMC na površino AFM-konice in b) primerjava meritev sil med dvema načinoma pripetja amiloze. Krivulje jasno nakazujejo, da tip funkcionalizacije drastično vpliva na obseg interakcij med konico in modelno površino.

4 DISCUSSION

Chemical force microscopy can be a very powerful tool when used correctly. The most crucial part of achieving its purpose is the functionalization of the tips, thus enabling progressive sensing. Its use in polymer sciences is no exception. It seems that by employing some alterations to the known functionalization procedures, we are now able to attach different functional groups to the tip surface, thus providing numerous possibilities for the further bonding of a wide variety of different species. All used procedures proved to be successful for mainly decorating mostly the edge of tips, leaving the surroundings almost as clean as before the functionalization. In this way, there is no response by the AFM feedback system and none of the resolution is lost. SEM images confirm the latter by showing that the tip's surroundings remain almost unchanged, whilst the surface of the tip exhibits some new features when compared to the non-functionalized ones (**Figure 4**). The introduction of two different polymers to the tip's surface proves to be almost equally successful, as no increase in "chemical waste" can be examined on the surface surrounding the tip. Attached molecules seem to concentrate right at the end of the tip's pyramid, which is

therefore ready to interact with the model surface (**Figures 3c and d**).

AFM measurements revealed that, when using different bonding natures to bind the polymers to the tip, these changes alter the forces and distances at which they disappear. In the case of CMC, it can be seen that the forces involved are a couple of scales bigger when they are bound to the tip via a covalent bond, as compared to the preparation procedure, in which they are only adsorbed. Such knowledge could be of extreme importance when preparing novel polymer based materials; as such forces contribute to the materials final characteristics, such as adhesion properties, sensitivity to mechanical stress and others.

These measurements also reveal that the used preparation procedure is applicable for chemical sensing purposes. We have successfully showed that a different amount of force is exhibited when using different bond types and polymers. At the same time, we have discovered that these forces disappear at different distances when the tips are pulled away from the model's surface. This clear difference between measurements proves that our preparation procedure is applicable for chemical sensing, and can be further used during the characterization process of polymers and polymeric materials. The used method could be of great benefit to the public health because polymers are the most used materials in the preparation of wound dressings.

5 CONCLUSIONS

We have successfully prepared different functionalized AFM tips, which are not only capable of binding additional chemical species to their surfaces, but also allow for their use during chemical sensing. With further improvement and transfer to those systems found in real materials, these techniques could make a significant contribution to the characterization process of polymers in order to maximize the effectiveness of the preparation process, especially during the preparation of wound dressings.

Acknowledgement

The authors acknowledge the financial support from the Ministry of Higher Education, Science and Technology of the Republic of Slovenia through the contract No. 3211-10-000057 (Center of Excellence Polymer Materials and Technologies).

6 REFERENCES

- M. Kaneko, M. Nakayama, M. Wakihara, *Journal of Solid State Electrochemistry*, 11 (2007), 1071–1076
- N. S. Satarkar, D. Biswal, J. Z. Hilt, *Soft Matter*, 6 (2010), 2364–2371
- Z. H. Liu, Y. P. Jiao, Y. F. Wang, C. R. Zhou, Z. Y. Zhang, *Advanced Drug Delivery Reviews*, 60 (2008), 1650–1662
- S. Huang, X. Fu, *Journal of Controlled Release*, 142 (2010), 149–159
- M. Mozetič, A. Zalar, P. Panjan, M. Bele, S. Pejovnik, R. Grmek, *Thin Solid Films*, 376 (2000), 5–8
- A. Vesel, M. Mozetič, *Vacuum*, 61 (2001), 373–377
- M. Klanjšek - Gunde, M. Kunaver, M. Mozetič, P. Pelicon, J. Simčič, M. Budnar, M. Bele, *Surf. coat. int., Part B, Coat. Trans.*, 85 (2002), 115–121
- U. Cvelbar, S. Pejovnik, M. Mozetič, A. Zalar, *Appl. Surf. Sci.*, 210 (2003), 255–261
- M. Kunaver, M. Klanjšek - Gunde, M. Mozetič, A. Hrovat, *Dyes Pigm.*, 57 (2003), 235–243
- M. Mozetič, *Vacuum*, 71 (2003), 237–240
- M. Kunaver, M. Mozetič, M. Klanjšek - Gunde, *Thin Solid Films*, 459 (2004), 115–117
- U. Cvelbar, M. Mozetič, M. Klanjšek - Gunde, *IEEE Trans. Plasma Sci.*, 33 (2005), 236–237
- N. Krstulović, I. Labazan, S. Milošević, U. Cvelbar, A. Vesel, M. Mozetič, *Appl. Phys.*, 39 (2006), 3799–3804
- U. Cvelbar, M. Mozetič, I. Junkar, A. Vesel, J. Kovač, A. Drenik, T. Vrlinič, N. Hauptman, M. Klanjšek Gunde, B. Markoli, N. Krstulović, S. Milošević, F. Gaboriau, T. Belmonte, *Appl. Surf. Sci.*, 253 (2007) 19, 8669–8673
- A. Vesel, M. Mozetič, A. Hladnik, J. Dolenc, J. Zule, S. Milošević, N. Krstulović, M. Klanjšek - Gunde, N. Hauptman, Nina. Modification of ink-jet paper by oxygen-plasma treatment. *J. Phys., Appl. Phys.*, 40 (2007), 3689–2696
- T. Vrlinič, A. Vesel, U. Cvelbar, M. Krajnc, M. Mozetič, *Surf. Interface Anal.*, 39 (2007) 6, 476–481
- A. Vesel, M. Mozetič, A. Zalar, *Surf. Interface Anal.*, 40 (2008), 661–663
- A. Vesel, M. Mozetič, A. Zalar, *Vacuum*, 82 (2008) 2, 248–251
- A. Vesel, I. Junkar, U. Cvelbar, J. Kovač, M. Mozetič, *Surf. Interface Anal.*, 40 (2008) 11, 1444–1453
- A. Drenik, A. Vesel, M. Mozetič, *J. Nucl. Mater.*, 386–388 (2009), 893–895
- I. Junkar, U. Cvelbar, A. Vesel, N. Hauptman, M. Mozetič, *Plasma Processes Polym.* 6 (2009) 10, 667–675
- A. Vesel, M. Mozetič, *Inf. MIDEM*, 40 (2010) 1, 67–73
- A. Vesel, M. Mozetič, P. Panjan, N. Hauptman, M. Klanjšek - Gunde, M. Balat - Pichelin, *Surf. Coat. Technol.*, 204 (2010), 1503–1508
- M. Gorjanc, V. Bukošek, M. Gorenšek, M. Mozetič, *Tex. Res. J.*, 80 (2010) 20, 2204–2213
- A. Vesel, M. Mozetič, S. Strnad, K. Stana - Kleinschek, N. Hauptman, Z. Peršin, *Vacuum*, 84 (2010) 1, 79–82
- I. Junkar, A. Vesel, U. Cvelbar, M. Mozetič, S. Strnad, *Vacuum*, 84 (2010) 1, 83–85
- M. Mozetič, *Mater. tehnol.*, 44 (2010) 4, 165–171
- M. Gorjanc, V. Bukošek, M. Gorenšek, A. Vesel, *Tex. Res. J.*, 80 (2010) 6, 557–567
- A. Vesel, *Surf. Coat. Technol.*, 205 (2010) 2, 490–497
- A. Asadinezhad, I. Novák, M. Lehocký, V. Sedlarik, A. Vesel, I. Junkar, P. Sába, I. Chodák, I. Chodák, *Plasma Processes Polym.*, 7 (2010) 6, 504–514
- A. Asadinezhad, I. Novák, M. Lehocký, F. Bílek, A. Vesel, I. Junkar, P. Sába, A. Popelka, *Molecules (Basel)*, 15 (2010) 2, 1007–1027
- A. Asadinezhad, I. Novák, M. Lehocký, V. Sedlarik, A. Vesel, P. Sába, I. Chodák, *Biointerfaces*, 77 (2010) 2, 246–256
- G. Binnig, C. F. Quate, C. Gerber, *Physical Review Letters*, 56 (1986), 930
- G. Kada, F. Kienberger, P. Hinterdorfer, *Nano Today*, 3 (2008), 12–19
- F. Oesterhelt, D. Oesterhelt, M. Pfeiffer, A. Engel, H. E. Gaub, D. J. Müller, *Science*, 288 (2000), 143–146

- ³⁶ H.-J. Butt, B. Cappella, M. Kappl, *Surface Science Reports*, 59 (2005), 1–152
- ³⁷ Y. Sugimoto, P. Pou, M. Abe, P. Jelinek, R. Perez, S. Morita, O. Custance, *Nature*, 446 (2007), 64–67
- ³⁸ T. Ito, S. Ibrahim, I. Grabowska, *TrAC Trends in Analytical Chemistry*, 29 (2010), 225–233
- ³⁹ M. Kocun, M. Grandbois, L. A. Cuccia, *Colloids and Surfaces B: Biointerfaces*, 82 (2011), 470–476
- ⁴⁰ F. Kienberger, A. Ebner, H. J. Gruber, P. Hinterdorfer, *Accounts of Chemical Research*, 39 (2006), 29–36
- ⁴¹ A. Ebner, L. Wildling, R. Zhu, C. Rankl, T. Haselgrübler, P. Hinterdorfer, H. Gruber, in *STM and AFM Studies on (Bio)molecular Systems: Unravelling the Nanoworld*, ed. P. Samorì, Springer Berlin, Heidelberg 2008, 29–76
- ⁴² C. K. Riener, C. M. Stroh, A. Ebner, C. Klampfl, A. A. Gall, C. Romanin, Y. L. Lyubchenko, P. Hinterdorfer, H. J. Gruber, *Analytica Chimica Acta*, 479 (2003), 59–75
- ⁴³ A. P. Limansky, L. S. Shlyakhtenko, S. Schaus, E. Henderson, Y. L. Lyubchenko, *Probe Microscopy*, 2 (2002), 227–234
- ⁴⁴ A. Ulman, *Chemical Reviews*, 96 (1996), 1533–1554
- ⁴⁵ A. J. Engler, F. Rehfeldt, S. Sen, D. E. Discher, in *Methods in Cell Biology*, ed. E. D. YuLi Wang and Dennis, Academic Press, 2007, 521–545
- ⁴⁶ W. Stöber, A. Fink, E. Bohn, *Journal of Colloid and Interface Science*, 26 (1968), 62–69

A NOVEL APPROACH FOR QUALITATIVE DETERMINATION OF RESIDUAL TIN BASED CATALYST IN POLY(LACTIC ACID) BY X-RAY PHOTOELECTRON SPECTROSCOPY

NOV NAČIN KVALITATIVNE DOLOČITVE VSEBNOSTI KATALIZATORJA KOSITRA V POLILAKTIČNI KISLINI Z RENTGENSKO FOTOELEKTRONSKO SPEKTROSKOPIJO

Vladimír Sedlařík^{1,3*}, Alenka Vesel², Pavel Kucharczyk³, Pavel Urbánek³

¹Jožef Stefan Institute, Jamova cesta 39, 1000 Ljubljana, Slovenia

²Center of Excellence for Polymer Materials and Technologies, Tehnološki park 24, 1000 Ljubljana, Slovenia

³Centre of Polymer Systems, Polymer Centre, Tomas Bata University in Zlín, nám. T. G. Masaryka 5555, 760 01 Zlín, Czech Republic
sedlarik@ft.utb.cz

Prejem rokopisa – received: 2011-02-15; sprejem za objavo – accepted for publication: 2011-03-04

This work is focused on description of qualitative determination of residual tin based catalysts in poly(lactic acid) by using X-ray photoelectron spectroscopy and fluorimetry as standard technique. Three types of poly(lactic acid) were prepared by direct melt polycondensation of lactic acid by using methanesulfonic acid ($w = 0.5\%$) or various amount of stannous 2-ethylhexanoate ($w = (0.5 \text{ and } 2)\%$). The results from both methods show that the amount of observed tin in the samples correlates with the concentration of the stannous 2-ethylhexanoate used for polycondensation. X-ray photoelectron spectroscopy was proven to be suitable for detection of tin residuals in polymer matrix.

Keywords: poly(lactic acid), catalyst residuals, tin, X-ray photoelectron spectroscopy, fluorimetry

Delo je osredinjeno na opis kvalitativne določitve katalizatorjev na osnovi kositra v polilaktični kislini z uporabo rentgenske fotoelektronske spektroskopije in fluorimetrije. Tri vrste polilaktične kisline smo pripravili z neposredno polikondenzacijo laktične kisline z uporabo metansulfonske kisline ($w = 0,5\%$) ali različne količine kositrovega 2-etilheksanoata ($w = (0,5 \text{ in } 2)\%$). Rezultati obeh metod kažejo, da je vsebnost kositra v vzorcih povezana s koncentracijo kositrovega 2-etilheksanoata, ki se uporablja za polikondenzacijo. Rentgenska fotoelektronska spektroskopija se je izkazala kot primerna metoda za odkrivanje majhnih vsebnosti kositra v polimerni matrici

Ključne besede: polilaktična kislina, katalizator, kositer, rentgenska fotoelektronska spektroskopija, fluorimetrija

1 INTRODUCTION

Polymers are widely used for a variety of applications, which include packaging, adhesives, engineering materials, composites, and electronic as well as medical devices. The lastly mentioned application of polymers, production of medical devices, has gained an enormous interest in the last decades.¹⁻⁶

Bioresorbable polymer based items are one of the most developing areas in the field of medical device production, due to necessity to introduce a material with favourable chemical, biological and mechanical properties, which would also bring a comfort with respect to traditional materials (metals or ceramics). An elimination of the second surgery after healing process could be mentioned as an example of using of an implant made of bioresorbable polymers.^{7,8}

Poly(lactic acid) (PLA) is well known biodegradable polyester,⁹⁻¹³ which has been already used in biomedical applications such as implant for bone fixation and tissue engineering scaffold. The synthesis techniques and its modification have been described elsewhere. However, one can find that mostly organic tin based catalysts are

used for PLA preparations. It has been observed that the uptake of tin by human beings can cause acute effects (eye irritation, headache, stomach-ache, urination problems etc.) as well as long-term effects (depressions, liver and brain damage, chromosomal changes etc.).¹⁴ In addition, Cam et al. has reported negative influence of residual metallic compounds (including tin) in the PLA matrix on a thermal stability of the polymer during its thermoplastic processing.³ These facts must be considered during PLA based medical devices evaluation.

Tin can be analytically determined by several techniques including atomic absorption spectrometry, inductively coupled plasma atomic emission spectrometry, energy-dispersive X-ray fluorescence.¹⁵ Nevertheless, these techniques are reported for inorganic materials. On the other hand, fluorimetry has been introduced for organic samples. A disadvantage of this method is a complex procedure of sample preparation. This work is dedicated to introduction of a novel approach to tin determination in PLA matrix by using X-ray photoelectron spectroscopy, which has been already used for analysis of polymer surfaces. This approach offers fast and reliable and experimentally

undemanding way of Tin determination in polymer matrix. This method was correlated with fluorimetric measurements.

2 EXPERIMENTAL

2.1 Polymer samples preparation

Three types of PLA were used for investigation in this study. The detailed characteristics of the prepared samples are shown in **Table 1**. Generally, PLA samples were prepared by direct melt polycondensation of lactic acid. A typical procedure was as follows: 50 mL lactic acid solution (80 %, LachnerNeratovice, Czech Republic) was added into a double necked flask (250 mL) equipped with a Teflon stirrer. The flask was then placed in an oil bath heated by magnetic stirrer with heating and connected to a laboratory apparatus for distillation under reduced pressure. The dehydration step followed at 160 °C, reduced pressure 15 kPa for 4 h. After that, the reactor was disconnected from the vacuum pump and the relevant amount of the catalyst (Stannous 2-ethylhexanoate ($\text{Sn}(\text{Oct})_2$) or methanesulfonic acid (MSA) both Sigma Aldrich, Steinheim, Germany) was added dropwise under continuous stirring. The flask with dehydrated mixture was connected back to the source of vacuum (100 Pa) and the reaction continued for 24 h at the temperature 160 °C. The resulting product was allowed to cool down at room temperature and then dissolved in acetone. The polymer solution was precipitated in a mixture of chilled methanol/distilled water 1 : 1 (v/v). The obtained product was filtrated, washed with methanol and dried at 45 °C for 48 h. The average values of molecular weight were determined by gel permeation chromatography. Detailed procedure is shown in one of our previous works.⁹

Table 1: Characteristics of the PLA samples

Tabela 1: Karakteristike vzorcev PLA

Sample designation	Catalyst	Concentration of catalyst (w/%)*	$M_w/$ (g mol ⁻¹)	M_w/M_n
PLA1	MSA	0.5	17 200	1.60
PLA2	$\text{Sn}(\text{Oct})_2$	0.5	47 000	2.08
PLA3	$\text{Sn}(\text{Oct})_2$	2	67 700	2.06

*related to monomer

2.2 Characterization techniques

2.2.1 X-ray photoelectron spectroscopy (XPS)

Samples in powder form were analyzed with an XPS instrument TFA XPS Physical Electronics. The base pressure in the chamber was about 6×10^{-8} Pa. The samples were excited with X-rays over a 400- μm spot area with a monochromatic Al $K_{1,2}$ radiation at 1486.6 eV. The photoelectrons were detected with a hemispherical analyzer positioned at an angle of 45° with respect

to the normal to the sample surface. Survey-scan spectra were made at a pass energy of 187.85 eV and 0.4 eV energy step. An electron gun was used for surface neutralization. The concentration of elements was determined by using MultiPak v7.3.1 software from Physical Electronics, which was supplied with the spectrometer. On each sample two survey spectra were recorder on two different spots on the surface. The sensitivity of the method is 0.5 %.

2.2.2 Fluorimetric analysis

Fluorimeter FSL 920 Edinburg was used for fluorescence spectra and intensity measurements. The device was equipped with a xenon lamp. A quartz cell was used for the measurement (10 mm). A uniform resolution of 1 nm was kept in all cases. The procedure of samples treatment before the analyte determination is described in detail by Mazooriet al.¹⁵

3 RESULTS AND DISCUSSION

As can be noticed in **Table 1**, the expected tin concentration in the investigated samples has following trend: PLA1 < PLA2 < PLA3. Moreover, it can be expected that tin concentration is equal zero in PLA1.

A method which can be used for detecting small amounts of tin in PLA samples is XPS (X-ray photoelectron spectroscopy).^{16–28} The technique is particularly useful for characterization of polymer materials whose surface properties have been modified using non-equilibrium plasma treatments.^{29–45} Figure 1 shows XPS survey spectra of the PLA samples. The measured spectrum consists of characteristic peaks which correspond to electronic energy levels of the investigated material. Because each element has a unique set of binding energies, XPS can be used to identify and determine the concentration of the elements at the surface. XPS survey spectra shown in **Figure 1** represent characteristic peaks due to the presence of oxygen (O1s), carbon (C1s) and

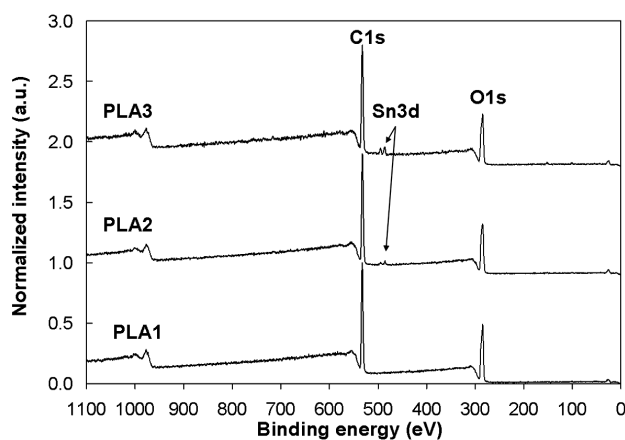


Figure 1: XPS survey spectra of PLA samples with tin additives
Slika 1: Pregledni spekter XPS površine vzorca PLA z dodatkom kositra

tin (Sn3d) elements in the examined samples. Carbon and oxygen are constituents of PLA polymer while a small peak of tin found in the samples PLA2 and PLA3 clearly shows the presence of the small amounts of catalyst.

Surface composition of the samples as determined from the XPS survey spectra (**Figure 1**) is shown in **Table 2**. Surface composition was determined from the area of the measured peaks which was correlated by taking into account special sensitivity factors, which are due to different ionization cross section. It can be noticed that no tin evidence is observed in the case of PLA1 where only carbon and oxygen was detected. On the other hand PLA2 proves a trace of tin presence in the polymer matrix. Interestingly, almost four times higher values were found for PLA3. It means that this observation directly correspond to mass of the added catalyst during PLA preparation (**Table 1**).

Table 2: Surface composition of the samples (in mole fractions, $x/\%$) as determined from the XPS survey spectra (average \pm standard deviation)

Tabela 2: Površinska sestava vzorcev (v molskih deležih, $x/\%$) določena iz preglednih spektrov XPS

Sample designation	$x(\text{C})/\%$	$x(\text{O})/\%$	$x(\text{Sn})/\%$
PLA1	62.7 ± 0.8	37.4 ± 0.8	0.00 ± 0.00
PLA2	61.0 ± 0.1	38.8 ± 0.2	0.23 ± 0.05
PLA3	61.1 ± 1.4	37.8 ± 1.8	1.09 ± 0.36

The emission spectra of PLA samples show noticeable peak at 357 nm in all cases (**Figure 2**). The maximal intensities of the observed peaks for PLA

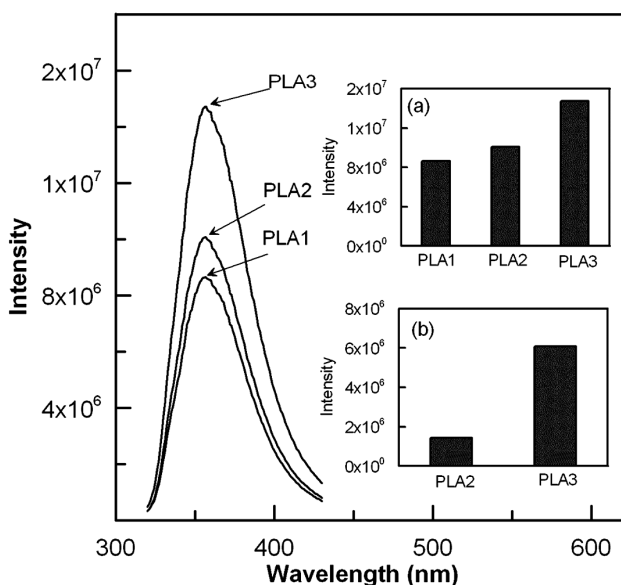


Figure 2: Fluorescence emission of PLA samples, values of maximal intensities observed for PLA samples at 257 nm (a) and intensities of polycondensates catalyzed by stannous 2-ethylhexanoate after subtraction (b)

Slika 2: Fluorescenčna emisija vzorcev PLA: vrednosti maksimalne intenzitete, določene na vzorcu PLA pri 257 nm (a) in intenziteta polikondenzatov kataliziranih s kositrovim 2-etilheksanoatom (b)

samples are presented in **Figure 2a**. It can be noticed that PLA1 emits at the given wavelength as well as tin containing samples PLA2 and PLA3. However, differences between the observed detector responses for PLA2 and PLA3 after subtraction of the signal (**Figure 2b**) of PLA1 is related with initial concentration of the catalyst used for PLA polycondensation (**Table 1**) by means of the intensities ratio PLA3/PLA2.

The results presented above reveal that both XPS and fluorimetric method show similar observations in qualitative detection of tin based compounds in PLA matrix. The former method, however, consider only surface composition of a sample. That can be a limitation of the method. Practically, it brings high requirements for samples homogeneity. On the other hand, undisputed advantage of XPS technique is low demand for sample mass, which is important in the small scale productions such as medical grade PLA synthesis.

4 CONCLUSIONS

This study introduces a novel way of residual tin based catalyst determination in poly(lactic acid) by using X-ray photoelectron spectroscopy (XPS). In addition, XPS observations were correlated with fluorimetry. The results from both methods correspond with the concentration of tin based catalyst used for polymer preparation. XPS techniques can be considered as suitable for qualitative or even semi-quantitative analysis of tin based compounds in polymer matrixes providing achieving of sufficient homogeneity of the studied material.

Acknowledgements

This research was financially supported by the Ministry of Education, Youth and Sports of the Czech Republic (project No. 2B08071) and Operational Program Research and Development for Innovations co-funded by the European Regional Development Fund (ERDF, project No. CZ.1.05/2.1.00/03.0111). The authors acknowledge the financial support from the Ministry of Higher Education, Science and Technology of the Republic of Slovenia through the contract No. 3211-10-000057 (Center of Excellence for Polymer Materials and Technologies). Furthermore, this work was also co-supported Slovenian Research Agency (ARRS) and Science and Education Foundation of the Republic of Slovenia within the "Ad futura" programme and by the Ministry of Higher Education, Science and Technology of the Republic of Slovenia through the contract No. 3211-10-000057 (Center of Excellence Polymer Materials and Technologies).

5 REFERENCES

- ¹ Y. Wan, C. Tu, J. Yang, J. Bei, S. Wang, *Biomaterials*, 27 (2006), 2699–2704
- ² L. Safinia, K. Wilson, A. Mantalaris, A. Bismarck, *J. Biomed. Mater. Res. A*, 87A (2008) 3, 632–642
- ³ D. Cam, M. Marucci, *Polymer*, 38 (1997) 8, 1879–1884
- ⁴ M. Gricar, I. Poljansek, B. Brulc, T. Smigovec, M. Zidon, E. Zagar, *Acta. Chim. Slov.*, 55 (2008) 3, 575–581
- ⁵ I. Poljansek, M. Gricar, E. Zagar, M. Zigon, *Macromolecular Symposia*, 272 (2008), 75–80
- ⁶ M. Vukomanovic, S. D. Skapin, I. Poljansek, E. Zagar, B. Kralj, N. Ignjatovic, D. Uskokovic, *Colloids. Surf., B Biointerfaces.*, 82 (2011) 2, 414–421
- ⁷ C.M. Alves et al., *J. Biomed. Res. B*, 87B (2008) 1, 59–66
- ⁸ T. A. P. Engels, S. H. M. Sontjens, T. H. Smith, L. E. Govaert, *J. Mater. Sci.: Mater. Med.* (2010) 21, 89–97
- ⁹ V. Sedlarik, P. Kucharczyk, V. Kaasarkova, J. Drbohlav, A. Salakova, P. Saha, *J. Appl. Polym. Sci.*, 116 (2010) 3, 1597–1602
- ¹⁰ V. Sedlarik, N. Saha, J. Sedlarikova, P. Saha, *Macromolecular Symposia*, 272 (2008), 100–103
- ¹¹ M. Hrabalova, A. Gregorova, R. Wimmer, V. Sedlarik, M. Machovsky, N. Mundigler, *J. Appl. Polym. Sci.*, 118 (2010) 3, 1534–1540
- ¹² A. Gregorova, M. Hrabalova, R. Wimmer, *J. Appl. Polym. Sci.*, 114 (2010) 5, 2616–2623
- ¹³ A. Gregorova, M. Hrabalova, R. Wimmer, *Abstract of papers of the American chemical society*, 235 (2008)
- ¹⁴ Tin-Sn in Lenntech periodic table, Available at: <http://www.lenntech.com/periodic/elements/sn.htm>, Cited 13. 2. 2010
- ¹⁵ J. L. Manzoori, M. Amjadi, D. Abolhasani, *J. Hazard. Mater. B137* (2006), 1631–1635
- ¹⁶ A. Vesel, M. Mozetic, J. Kovac, A. Zalar, *Appl. Surf. Sci.*, 253 (2006), 2941–2946
- ¹⁷ T. Vrlinic, A. Vesel, U. Cvelbar, M. Krajnc, M. Mozetic, *Surf. Interface Anal.*, 39 (2007) 6, 476–481
- ¹⁸ A. Vesel, M. Mozetic, A. Drenik, N. Hauptman, M. Balat-Pichelin, *Appl. Surf. Sci.*, 255 (2008) 5, 1759–1765
- ¹⁹ A. Vesel, K. Elersic, I. Junkar, B. Malic, *Mater. Tehnol.*, 43 (2009) 6, 323–326
- ²⁰ A. Asadinezhad, I. Novak, M. Lehocky, F. Bilek, A. Vesel, I. Junkar, P. Saha, A. Popelka, *Molecules*, 15 (2010) 2, 1007–1027
- ²¹ A. Asadinezhad, I. Novak, M. Lehocky, V. Sedlarik, A. Vesel, I. Junkar, P. Saha, I. Chodak, *Plasma Processes Polym.*, 7 (2010) 6, 504–514
- ²² A. Vesel, M. Mozetic, A. Zalar, *Surf. Interface Anal.*, 40 (2008) 3–4, 661–663
- ²³ A. Vesel, M. Mozetic, A. Zalar, *Vacuum*, 82 (2008) 2, 248–251
- ²⁴ A. Asadinezhad, I. Novak, M. Lehocky, V. Sedlarik, A. Vesel, P. Saha, I. Chodak, *Colloids Surf. B Biointerfaces*, 77 (2010) 2, 246–256
- ²⁵ A. Vesel, A. Drenik, R. Zaplotnik, M. Balat-Pichelin, *Surf. Interface Anal.*, 42 (2010) 1168–1171
- ²⁶ A. Vesel, M. Mozetic, P. Panjan, N. Hauptman, M. Klanjšek-Gunde, M. Balat - Pichelin, *Surf. Coat. Technol.*, 204 (2010) 9/10, 1503–1508
- ²⁷ A. Vesel, M. Mozetic, A. Hladnik, J. Dolenc, J. Zule, S. Milosevic, N. Krstulovic, M. Klanjšek - Gunde, N. Hauptman, *J. Phys. D: Appl. Phys.*, 40 (2007) 12, 3689–3696
- ²⁸ A. Vesel, M. Mozetic, S. Strnad, K. Stana-Kleinschek, N. Hauptman, Z. Persin, *Vacuum*, 84 (2010) 1, 79–82
- ²⁹ M. Mozetič, A. Zalar, P. Panjan, M. Bele, S. Pejovnik, R. Grmek, *Thin Solid Films*, 376 (2000), 5–8
- ³⁰ A. Vesel, M. Mozetič, *Vacuum*, 61 (2001), 373–377
- ³¹ M. Klanjšek Gunde, M. Kunaver, M. Mozetič, P. Pelicon, J. Simčič, M. Budnar, M. Bele, *Surf. coat. int., Part B, Coat. trans.*, 85 (2002), 115–121
- ³² M. Kunaver, M. Klanjšek Gunde, M. Mozetič, A. Hrovat, *Dyes Pigm.*, 57 (2003), 235–243
- ³³ M. Mozetič, *Vacuum*, 71 (2003), 237–240
- ³⁴ M. Kunaver, M. Mozetič, M. Klanjšek Gunde, *Thin Solid Films*, 459 (2004), 115–117
- ³⁵ U. Cvelbar, M. Mozetič, M. KlanjšekGunde, *IEEE Trans. Plasma Sci.*, 33 (2005), 236–237
- ³⁶ N. Krstulović, I. Labazan, S. Milošević, U. Cvelbar, A. Vesel, M. Mozetič, *Appl. Phys.*, 39 (2006), 3799–3804
- ³⁷ A. Drenik, A. Vesel, M. Mozetič, *J. Nucl. Mater.*, 386–388 (2009), 893–895
- ³⁸ M. Mozetič, *Mater. Tehnol.*, 44 (2010) 4, 165–171
- ³⁹ Drenik, U. Cvelbar, K. Ostrikov, M. Mozetic, *J. Phys. D: Appl. Phys.*, 41 (2008) 11, 115201-1–115201-7
- ⁴⁰ A. Ricard, M. Gaillard, V. Monna, A. Vesel, M. Mozetic, *Surf. Coat. Tech.*, 142–144 (2001), 333–336
- ⁴¹ U. Cvelbar, K. Ostrikov, A. Drenik, M. Mozetic, *Appl. Phys. Lett.*, 92 (2008) 13, 133505-1–133505-3
- ⁴² D. Babič, I. Poberaj, M. Mozetič, *Rev. Sci. Instrum.*, 72 (2001), 4110–4114
- ⁴³ I. Junkar, U. Cvelbar, A. Vesel, N. Hauptman, M. Mozetic, *Plasma Processes Polym.*, 6 (2009) 10, 667–675
- ⁴⁴ U. Cvelbar, M. Mozetic, I. Junkar, A. Vesel, J. Kovac, A. Drenik, T. Vrlinic, N. Hauptman, M. Klanjšek-Gunde, B. Markoli, N. Krstulovic, S. Milosevic, F. Gaboriau, T. Belmonte, *Appl. Surf. Sci.*, 253 (2007) 21, 8669–8673
- ⁴⁵ M. Gorjanc, V. Bukosek, M. Gorenssek, M. Mozetic, *Tex. Res. J.*, 80 (2010) 20, 2204–2213

HYDROPHOBIZATION OF POLYMER POLYSTYRENE IN FLUORINE PLASMA

HIDROFOBIZACIJA POLIMERA POLISTIREN S FLUOROVO PLAZMO

Alenka Vesel

Center of Excellence for Polymer Materials and Technologies, Tehnološki park 24, 1000 Ljubljana, Slovenia
alenka.vesel@ijs.si

Prejem rokopisa – received: 2011-02-10; sprejem za objavo – accepted for publication: 2011-03-05

Modification of surface properties of polymers by plasma fluorination was studied by X-ray Photoelectron Spectroscopy (XPS). Samples of polystyrene (PS) were exposed to weakly ionized reactive gaseous plasma created in tetrafluoromethane (CF₄) gas. Reactive plasma particles rapidly interacted with the samples forming a surface film rich with CF_x functional groups. The appearance of these groups was monitored by high-resolution XPS, while the resultant modification of surface properties was monitored by water drop contact angle technique. Survey XPS spectra showed a substantial concentration of over mole fraction 50 % of fluorine, while high resolution C1s spectra revealed the appearance of different functional groups. The CF₂ group was predominant as approximately a third of carbon atoms was found in this group. The contact angle measurement revealed simultaneous modification of the surface free energy from moderately hydrophobic original material to highly hydrophobic state, as the water contact angle increased from original 85° to 111°. Plasma fluorination is therefore a suitable method for improving of surface properties of polymers for biomedical applications.

Keywords: CF₄ plasma, fluorination, PS polymer, polystyrene, surface functionalization, hydrophobization, XPS

Z metodo rentgenske fotoelektronske spektroskopije (XPS) smo preiskovali spremembe v površinski sestavi polimerov pri plazemski fluorinaciji. Vzorci polistirena (PS) smo izpostavili šibko ionizirani reaktivni plinski plazmi, ustvarjeni v fluorometanu (CF₄). Reaktivni delci iz plazme so izredno hitro reagirali s površino vzorca, zaradi česar je nastala tanka površinska plast, bogata s CF_x-skupinami, kar je povzročilo spremembo omočljivosti vzorca. Nastanek teh skupin smo dokazali z metodo XPS, medtem ko smo spremembo omočljivosti določali s kontaktnim kotom vodne kapljice. Iz preglednih XPS spektrov je razvidna znatna koncentracija fluora na površini vzorca z molskim deležem večjim od 50 %. Iz visoko ločljivih spektrov ogljika smo določili različne fluorove funkcionalne skupine, med katerimi je največji delež, skoraj eno tretjino, zavzela skupina CF₂. Z merjenjem kontaktnega kota smo ugotovili porast hidrofobnosti površine, saj je kontaktni kot narasel iz začetnih 85° na 111°. Rezultati so pokazali, da je plazemska fluorinacija primerna metoda za izboljšanje površinskih lastnosti polimerov za biomedicinske aplikacije, kjer želimo imeti čim bolj inertno površino.

Ključne besede: CF₄-plazma, fluorinacija, PS-polimer, polistiren, površinska funkcionalizacija, hidrofobizacija, XPS

1 INTRODUCTION

Polymer materials are nowadays widely used in industry and medicine. The type of polymer suitable for particular application is chosen according to chemical, mechanical and thermal properties, as well as the production cost. The surface properties of selected polymers are often not optimal for particular application. In such cases they should be modified prior to application. Improved hydrophilicity is usually obtained by surface functionalization with polar functional groups, and better hydrophobicity is assured by incorporation of highly non-polar groups. Numerous techniques have been invented for modification of surface properties but it seems that nowadays one technique predominates. The technique is mild treatment by non-equilibrium gaseous plasma¹⁻¹¹. Namely, this technique is extremely fast, ecologically benign and rather inexpensive. Increased hydrophilicity is obtained by treatment with oxygen (and sometimes nitrogen) plasma. Numerous authors reported excellent results for several types of polymers including polyethylene terephthalate¹²⁻¹⁴, polyethersulphone¹⁵⁻¹⁶, polyphenylene sulphide¹⁷, polystyrene^{18,19}, polyvinyl-

chloride²⁰⁻²², polyethylene naphthalate²³, polymethyl methacrylate²⁴, cellulose²⁵⁻²⁹ etc. The opposite effect, i.e. increased hydrophobisation, is achieved by treatment with gases rich in fluorine such as CF₄ or C₂F₆.³⁰⁻³⁴

Hydrophobisation of polymers is required in cases where adhesion of liquids should be minimized. A classical example is medicine. The wounds are protected by plasters. Both for the medical reasons as well as patient comfort it is important that the plaster does not stick to the wounded place too strongly. Although the major part of the plaster made from cellulose to soak the liquids³⁵⁻³⁹ the uppermost layer is made from a hydrophobic polymer, typically in the form of perforated membrane, which allows for a good transport of liquids and simultaneously for poor adhesion onto the wounded place. Typical examples of currently applied membrane include PET, PES and PP. In some cases the surface properties of these materials assure a good functionality, but in many cases they fail and the plaster stick on to a wound. Obviously, a material with better properties should be applied or, alternatively, the surface of such materials should be made more hydrophobic.

As mentioned earlier, a suitable method for hydrophobization of polymer materials is application of gaseous plasma. In the present paper we address the hydrophobization of polystyrene by treatment with mild plasma created in tetrafluoromethane.

2 EXPERIMENTAL

2.1 Plasma treatment of polymer

Experiments were performed with a polystyrene (PS) foil from DuPont. The samples were treated in the experimental system which was pumped with a two-stage oil rotary pump with a pumping speed of $4.4 \cdot 10^{-3} \text{ m}^3 \text{ s}^{-1}$. The discharge chamber was a Pyrex cylinder with a length of 0.6 m and an inner diameter of 0.036 m. The plasma was created with an inductively coupled RF generator, operating at a frequency of 27.12 MHz and an output power of about 200 W. Commercially available CF_4 gas was leaked into the discharge chamber. The pressure was measured by an absolute vacuum gauge. At our experiments, the pressure was fixed at 75 Pa. The samples of PS foil were treated in CF_4 plasma for 3 s and 10 s.

Since it is known that polymer surface which was treated in plasma is not stable with time, we have performed also ageing studies. After plasma treatment one of the samples which was treated for 3 s was stored in a dry plastic box and left ageing for 4 d.

2.2 X-ray photoelectron spectroscopy (XPS) characterization

The surface of the plasma treated PET samples was analyzed with an XPS instrument TFA XPS Physical Electronics. The base pressure in the XPS analysis chamber was about $6 \times 10^{-8} \text{ Pa}$. The samples were excited with X-rays over a 400- μm spot area with a monochromatic $\text{Al } K_{\alpha 1,2}$ radiation at 1486.6 eV. The photoelectrons were detected with a hemispherical analyzer positioned at an angle of 45° with respect to the normal to the sample surface. Survey-scan spectra were made at a pass energy of 187.85 eV a 0.4 eV energy step, while for C1s individual high-resolution spectra were taken at a pass energy of 23.5 eV and a 0.1 eV energy step. Since the samples are insulators, we used an additional electron gun to allow for surface neutralization during the measurements. The spectra were fitted using MultiPak v7.3.1 software from Physical Electronics, which was supplied with the spectrometer. The curves were fitted with symmetrical Gauss-Lorentz functions. A Shirley-type background subtraction was used. Both the relative peak positions and the relative peak widths (FWHM) were fixed in the curve fitting process.

2.3 Water-contact angle measurements

Wettability was examined immediately after the plasma treatment by measuring the water contact angle with a demineralised water droplet of a volume of 3 μL .

A home made apparatus equipped with a CCD camera and a PC computer was used for taking high resolution pictures of a water drop on the sample surface. Each determination was obtained by averaging results of 5 measurements. The relative humidity (45 %) and temperature (25°C) were monitored continuously and were found not to vary significantly during the contact angle measurements. The contact angles were measured by our own software which enables fitting of the water drop on the surface in order to allow a relatively precise determination of the contact angle.

3 RESULTS AND DISCUSSION

Immediately after the plasma treatment the surface wettability of the samples was measured by water drop. The measurements showed a decrease of surface wettability since the contact angle has increased from 85° for untreated PS sample to about 110° for plasma treated sample. Such contact angle is often found on polymers treated in CF_4 plasma and was found also for PET polymer. A well pronounced increase of the contact angle is a good sign for surface hydrophobization which is due to formation of unpolar fluorine functional groups at the surface. This was proved by XPS measurements.

Figure 1 shows the XPS survey spectrum of untreated and treated PS sample. Since PS is hydrocarbon polymer we can observe only one peak due to carbon on untreated sample (hydrogen can not be detected by

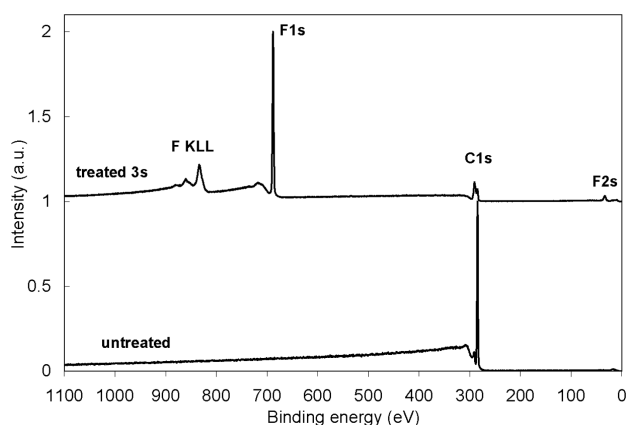


Figure 1: XPS survey spectra of untreated and plasma-treated PS showing attachment of fluorine to the surface

Slika 1: Pregledni XPS-spekter neobdelanega in plazemsko obdelanega vzorca PS

Table 1: Surface composition of the plasma treated PS samples (atom fractions, $x/\%$)

Tabela 1: Površinska sestava plazemsko obdelanih vzorcev PS (atomske deleži, $x/\%$)

Sample	C	F	O	F/C	O/C
Untreated PS	100				
Treated in CF_4 plasma for 3 s	43.0	56.5	0.5	1.31	0.012
Treated in CF_4 plasma for 10 s	43.4	56.1	0.5	1.29	0.012
Treated 3 s and aged 1 d	43.0	56.3	0.7	1.31	0.016
Treated 3 s and aged 4 d	42.6	56.0	1.4	1.31	0.033

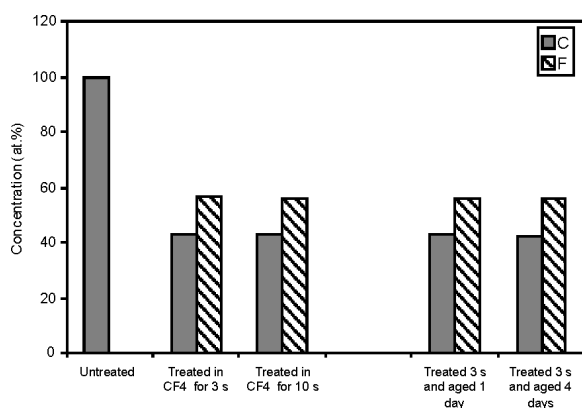


Figure 2: Comparison of surface composition of the PS samples (see also **Table 1**)

Slika 2: Primerjava površinske sestave vzorcev PS (glej tudi **tabelo 1**)

XPS). After plasma treatment a new huge peak is observed which corresponds to fluorine. Corresponding surface composition is shown in **Table 1** and **Figure 2**. The concentration of fluorine at the surface is rather high more than 50 atomic %. The surface is well saturated with fluorine atoms since there is no difference between 3 s and 10 s of treatment. Small amount of oxygen which is also detected on plasma treated surface is due to the presence of water vapour in the vacuum system. Incorporation of fluorine to the polymer surface caused formation of different functional groups, which can be deduced from high resolution spectrum of carbon. In **Figure 3** is shown a comparison of carbon peaks before and after plasma treatment. Untreated sample has only one big peak due to C-C (from aliphatic chain) and $-C=C$ bonds (from phenyl ring). Another small peak can be observed at high binding energies at about 291 eV which is a satellite peak that is typical for aromatic polymers. A huge difference is observed in the shape of the carbon peak of the treated samples indicating formation of different functional groups at the surface. Functional groups can be determined by decomposition of the measured peak into subpeaks which are shown in

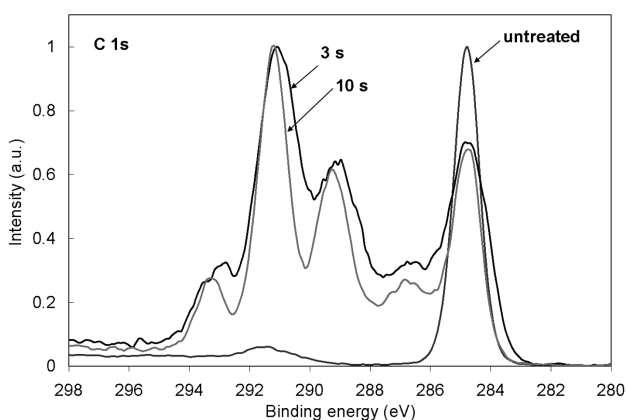


Figure 3: Comparison of carbon C1s spectra of untreated and plasma-treated PS samples

Slika 3: Primerjava spektrov ogljika C1s neobdelanega in plazemsko obdelanega vzorca PS

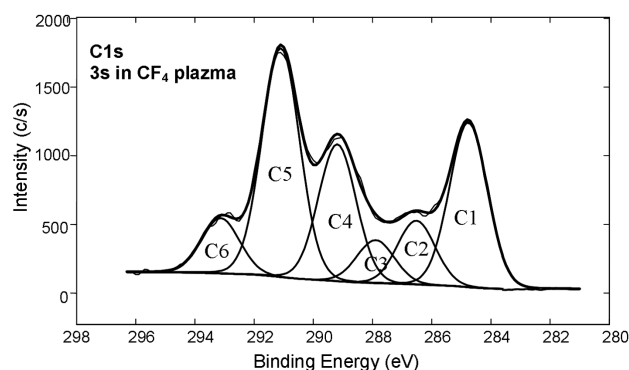


Figure 4: Example of curve fitting of C1s peak of a PS sample treated for 3 s showing formation of new peaks due to formation of different carbon-fluorine functional groups, which are presented in **Table 2**

Slika 4: Primer spektra ogljika C1s vzorca PS obdelanega 3 s, v katerem smo z metodo prilagajanja krivulj določili podvrhove, ki pripadajo različnim fluorovim funkcionalnim skupinam, nastalih med obdelavo (glej tudi **tabelo 2**)

Table 2: Chemical binding of carbon atoms of plasma treated PS samples.

Tabela 2: Vezava atomov ogljika na plazemsko obdelanih vzorcih PS

Peak assignment	C1	C2	C3	C4	C5	C6
Binding energy (eV)	284.8	286.5	287.8	289.2	291.2	293.2
Chemical binding	C-C	CH ₂ -CHF	CHF	CF	CF ₂	CF ₃
Untreated	100 %					
Treated 3 s	23.8	9.2	6.2	19.8	33.0	8.0
Treated 10 s	22.7	9.0	5.6	21.9	33.4	7.4
Treated 3 s and aged 1 d	22.9	7.6	5.7	21.6	34.3	8.0
Treated 3 s and aged 4 d	24.8	7.6	6.1	20.5	32.8	8.1

Figure 4. **Figure 4** shows that incorporation of fluorine resulted in formation of different functional groups at the surface which can be attributed to CF₃, CF₂, CF and CHF groups³⁰. The concentration of these groups is presented in **Table 2**. The majority of fluorine is found in CF₂ groups.

Here we should also mention, the fluorine-containing polymers may be sensitive to x-ray degradation during recording of spectra. In our case we did not observe any degradation (modification of the shape of carbon spectra) with time, since exposure times were low.

The ageing of the samples was studied as well. The surface composition was measured for samples aged one day and four days. As shown in **Table 1** it was not possible to observe any trend of ageing during first four days since the concentration of fluorine is stable. Normally the plasma treated samples are ageing very fast¹⁸, especially the first day because we can observe remarkable changes in water contact angle on samples treated in oxygen plasma. Here the contact angle was stable within these four days. An explanation for this is the following: polymers treated in oxygen plasma which is used to make surface hydrophilic have high surface energy, which is energetically unfavourable. Therefore such surface tends to decrease an excess of surface energy which leads to surface rearrangement and ageing.

During hydrophobization with CF_4 plasma treatment the surface energy is lowered. Surfaces having low surface energy are more stable than the one with high surface energy.

During treatment of samples in plasma we may either have substitution of fluorine atoms to the surface or deposition of C_xF_y radicals. Therefore the formation of fluorine functional groups needs further discussion. CF_4 molecules are dissociated in plasma into CF_3 , CF_2 , CF molecules and F atoms. In our case we have only substitution of fluorine atoms to the surface, because deposition is normally observed when using gas with higher carbon content and bigger molecular mass (e.g. C_2F_6 , C_3F_8). It was observed for PET (polyethylene terephthalate) polymer which was treated at the same conditions, that the mass of the sample was little lower after the treatment. This was due to etching and definitely not due to deposition.

4 CONCLUSION

The results presented in this paper clearly indicate that treatment of PS with CF_4 plasma improves the hydrophobic character of this polymer. Even a brief exposure allowed for functionalization of the surface film with fluorine rich functional groups. High resolution XPS C1s spectra revealed formation of different fluorine groups including CHF, CF, CF_2 , CF_3 . The majority of carbon atoms are bounded in the CF_2 group as in polytetrafluorethylene (PTFE), but the XPS results also revealed about 8 percent of fluorine richest CF_3 groups. All this groups allow for a stable hydrophobization of the PS polymer, since the concentration did not decrease even after prolonged ageing. The technology is therefore suitable for application in medicine for improving of the medical plaster quality.

ACKNOWLEDGEMENT

The authors acknowledge the financial support from the Ministry of Higher Education, Science and Technology of the Republic of Slovenia through the contract No. 3211-10-000057 (Center of Excellence Polymer Materials and Technologies).

5 REFERENCES

- M. Mozetič, A. Zalar, P. Panjan, M. Bele, S. Pejovnik, R. Grmek, *Thin Solid Films*, 376 (2000), 5–8
- M. Klanjšek - Gunde, M. Kunaver, M. Mozetič, P. Pelicon, J. Simčič, M. Budnar, M. Bele, *Surf. Coat. Int. B*, 85 (2002), 115–121
- M. Kunaver, M. Klanjšek - Gunde, M. Mozetič, A. Hrovat, *Dyes Pigment.*, 57 (2003), 235–243
- M. Mozetič, *Vacuum*, 71 (2003), 237–240
- M. Kunaver, M. Mozetič, M. Klanjšek - Gunde, *Thin Solid Films*, 459 (2004), 115–117
- A. Drenik, A. Vesel, M. Mozetič, *J. Nucl. Mater.*, 386–388 (2009), 893–895
- A. Vesel, M. Mozetič, *Inf. Midem*, 40 (2010) 1, 67–73
- M. Mozetič, *Mater. Tehnol.*, 44 (2010) 4, 165–171
- Drenik, U. Cvelbar, K. Ostrikov, M. Mozetic, *J. Phys. D: Appl. Phys.*, 41 (2008) 11, 115201-1–115201-7
- A. Ricard, M. Gaillard, V. Monna, A. Vesel, M. Mozetic, *Surf. Coat. Technol.*, 142–144 (2001), 333–336
- D. Babič, I. Poberaj, M. Mozetič, *Rev. Sci. Instrum.*, 72, (2001), 4110–4114
- I. Junkar, U. Cvelbar, A. Vesel, N. Hauptman, M. Mozetic, *Plasma Processes Polym.*, 6 (2009) 10, 667–675
- A. Vesel, M. Mozetic, A. Zalar, *Vacuum*, 82 (2008) 2, 248–251
- A. Vesel, I. Junkar, U. Cvelbar, J. Kovac, M. Mozetic, *Surf. Interface Anal.*, 40 (2008) 11, 1444–1453
- T. Vrlinic, A. Vesel, U. Cvelbar, M. Krajnc, M. Mozetic, *Surf. Interface Anal.*, 39 (2007) 6, 476–481
- J. Feng, G. Wen, W. Huang, E. Kang, K. G. Neoh, *Polym. Degrad. Stabil.*, 91 (2005) 1, 12–20
- U. Cvelbar, M. Mozetic, I. Junkar, A. Vesel, J. Kovac, A. Drenik, T. Vrlinic, N. Hauptman, M. Klanjšek - Gunde, B. Markoli, N. Krstulovic, S. Milosevic, F. Gaboriau, T. Belmonte, *Appl. Surf. Sci.*, 253 (2007) 21, 8669–8673
- A. Vesel, *Surf. Coat. Technol.*, 205 (2010) 2, 490–497
- M. J. Wang, Y. I. Chang, F. Poncin - Epailard, *Surf. Interface Anal.*, 37 (2005), 348
- M. Sowe, I. Novak, A. Vesel, I. Junkar, M. Lehocky, P. Saha, I. Chodak, *Int. J. Polym. Anal. Ch.*, 14 (2009) 7, 641–651
- A. Asadinezhad, I. Novak, M. Lehocky, F. Bilek, A. Vesel, I. Junkar, P. Saha, A. Popelka, *Molecules*, 15 (2010) 2, 1007–1027
- A. Asadinezhad, I. Novak, M. Lehocky, V. Sedlarik, A. Vesel, I. Junkar, P. Saha, I. Chodak, *Plasma Processes Polym.*, 7 (2010) 6, 504–514
- A. Vesel, K. Elersic, I. Junkar, B. Malic, *Mater. Tehnol.*, 43 (2009) 6, 323–326
- B. Tomcik, D. R. Popovic, I. V. Jovanovic, Z. L. J. Petrovic, *J. Polym. Res. - Taiwan*, 8 (2001) 4, 259–266
- A. Vesel, M. Mozetic, A. Hladnik, J. Dolenc, J. Zule, S. Milosevic, N. Krstulovic, M. Klanjšek - Gunde, N. Hauptman, *J. Phys. D: Appl. Phys.*, 40 (2007) 12, 3689–3696
- M. Gorjanc, V. Bukosek, M. Gorenssek, A. Vesel, *Tex. Res. J.*, 80 (2010) 6, 557–567
- N. Puač, Z. Lj. Petrović, M. Radetić, A. Djordjević, *Mat. Sci. Forum*, 494 (2005), 291–296
- P. Jovancic, D. Jovic, M. Radetic, T. Topalovic, Z. L. Petrovic, *Curr. Res. Adv. Mater. Process*, 494 (2005), 283–290
- A. Vesel, M. Mozetic, S. Strnad, K. Stana-Kleinschek, N. Hauptman, Z. Persin, *Vacuum*, 84 (2010) 1, 79–82
- N. Vandecasteele, H. Fairbrother, F. Reniers, *Plasma Process. Polym.*, 2 (2005), 493
- M. Gorjanc, V. Bukosek, M. Gorenssek, M. Mozetic, *Tex. Res. J.*, 80 (2010) 20, 2204–2213
- R. di Mundo, F. Palumbo, R. d'Agostino, *Langmuir*, 24 (2008), 5044–5051
- S. Marais, Y. Hirata, C. Cabot, S. Morin - Grognet, M. R. Garda, H. Atmani, F. Poncin - Epailard, *Surf. Coat. Technol.* 201 (2006) 3–4, 868–879
- F. Poncin-Epailard, D. Debarnot, *Inform. Midem*, 38 (2008), 252
- K. Stana - Kleinschek, T. Kreže, L. Fras Zemljič, V. Ribitsch, *Mater. Res. Innov.*, 6 (2001) 1, 13–18
- Z. Peršin, K. Stana - Kleinschek, M. Sfiligoj - Smole, T. Kreže, *Tex. Res. J.*, 74 (2004), 55–62
- T. Kreže, K. Stana - Kleinschek, V. Ribitsch, Z. Peršin, M. Sfiligoj - Smole, *Mater. Res. Innov.*, 9 (2005) 1, 108–129
- L. Fras Zemljič, L. Johansson, P. Stenius, J. Laine, K. Stana - Kleinschek, V. Ribitsch, *Colloids Surf. A*, 260 (2005), 101–108
- Z. Peršin, K. Stana - Kleinschek, T. Kreže, *Croat. Chem. Acta*, 75 (2002), 271–280

PLASMA TREATMENT OF BIOMEDICAL MATERIALS

PLAZEMSKA OBDELAVA BIOMEDICINSKIH MATERIALOV

Ita Junkar¹, Uroš Cvelbar², Marian Lehocky³

¹Odsek za tehnologijo površin in optoelektroniko, Institut "Jožef Stefan", Jamova cesta 39, 1000 Ljubljana, Slovenija

²Center of Excellence for Polymer Materials and Technologies, Tehnološki park 24, 1000 Ljubljana, Slovenia.

³Medical Materials Research Centre, Technology Park, Tomas Bata University, Nad Ovcirnou 3685, Zlín, Czech Republic
ita.junkar@ijs.si

Prejem rokopisa – received: 2011-02-15; sprejem za objavo – accepted for publication: 201103-06

Surface plasma treatment techniques for modification of biomedical polymeric materials are presented. The emphasis is on the use of non-equilibrium radiofrequency (RF) oxygen and nitrogen plasma. By variation of discharge parameters (power, discharge frequency, type of gas) and plasma parameters (density of neutrals and ions, kinetic energy of electrons, gas temperature) it is possible to produce polymer surfaces with different surface properties. Already after short plasma treatment time the surface of polymeric material becomes hydrophilic. Formation of nitrogen and oxygen functional groups is observed immediately after plasma treatment. By optimisation of plasma treatment time the number of newly formed functional groups can be increased. Plasma treatment also produces morphological changes of the surface; nanohills of different shapes and height can be formed on PET surface depending on the treatment time and type of gas. Evidently the change in surface morphology affects the change in surface roughness, which increases with longer plasma treatment time. Plasma treatment influences also on the biological response, as all plasma treated surfaces exhibit improved proliferation of fibroblast and endothelia cells. The number of adherent platelets practically does not change after nitrogen plasma treatment, however much lower number of adherent platelets is observed on oxygen plasma treated surfaces.

Key words: plasma treatment, biocompatibility, polymer, vascular grafts, endothelia cells, platelets

Predstavljene so tehnike plazemske obdelave površin, s katerimi lahko modificiramo površine biomedicinskih polimernih materialov. Poudarek je na uporabi neravnovesne radiofrekvenčne (RF) plazme dušika in kisika. S spreminjanjem razelektrivnih (moč, razelektrivna frekvenca, vrsta plina) in plazemskih parametrov (gostota nevtralnih delcev, ionov, kinetične energije elektronov, temperatura plina) je mogoče pripraviti površine polimerov z različnimi lastnostmi. Že po kratkih časih izpostavitve polimernih površin dušikovi ali kisikovi plazmi le-ta postane hidrofilna. Takoj po obdelavi je na površini mogoče opaziti novonastale dušikove oziroma kisikove funkcionalne skupine. Z optimizacijo časa izpostavitve plazmi je mogoče koncentracijo le-teh še nekoliko povečati. Plazemska obdelava vpliva tudi na spremembe v morfoloških lastnostih površine, tako je mogoče na plazemsko obdelanih površinah opaziti nanostrukture, katerih oblika in velikost je odvisna od časa izpostavitve plazmi, kot tudi od vrste plina uporabljenega za plazmo. Morfološke spremembe vplivajo tudi na spremembe v hrapavosti površine, ki se poveča s časom plazemske obdelave. Modifikacija površine vpliva na biološki odziv, saj se po plazemski obdelavi proliferacija endotelijskih in fibroblastnih celic na površini poveča. Število adheriranih trombocitov na površinah, obdelanih z dušikovo plazmo, se bistveno ne spremeni, medtem ko se njihovo število bistveno zmanjša na površinah, obdelanih s kisikovo plazmo.

Ključne besede: plazemska obdelava, biokompatibilnost, polimer, umetne žile, endotelijske celice, trombociti

1 INTRODUCTION

Surface properties of biomaterials play a major role in determining biocompatibility; they have a significant influence on biological response and also determine the long term performance *in vivo*. The main goal in designing biomaterials is therefore to ensure that they exhibit appropriate surface properties as well as desired physical and mechanical characteristics, which would enable them to function properly in the biological environment. It is hard to satisfy all of these characteristics; this is why surface treatment techniques are commonly employed in order to improve surface properties. It is still a highly challenging task to modify surface properties in order to produce hemocompatible surfaces, and many controversial results are reported in the literature.

Biological response to biomaterials is very complex and still not fully understood. As the surface of the biomaterial is responsible for initiating the primary interaction with body fluids it is of vital importance to

ensure that the surface is suitably conditioned to ensure an appropriate biological response (biocompatibility). It was thought for many years that the surface of the biomaterial should be inert. However, nowadays it has been found that the contact of biomaterials with blood enables integration with the body, prevents infections, inflammatory reactions, blood coagulation and other correlated reactions. It is of primary importance that the surfaces of hemocompatible materials exhibit anti-thrombogenic properties, as this prevents thrombosis. Thrombosis is initiated with the adsorption of blood plasma proteins on the surface of the biomaterial and is strongly influenced by its physical and chemical properties.

Surface properties of implants are usually described with wettability, chemistry, surface charge and texture (roughness). These factors all influence the sequence of protein adsorption and subsequent platelet adhesion/thrombus formation. Although the mechanism of occlusion and dysfunction of artificial prostheses is

multifactorial, all the studies performed suggest that fibrinogen and platelet deposition play a predominant role.^{1,2} It also seems that the outermost atomic layer of the surface of an alloplastic implant is a decisive factor for determining biocompatibility.³ One possible method to alter surface characteristics, such as wettability, chemistry, charge and morphology to improve biocompatibility of implant devices⁴ is by treatment of the surface with different gaseous plasma, like glow discharge created in different gases and by variation of discharge parameters (discharge power, pressure, etc.),⁵ which in turn influence plasma parameters (density of atoms, energy of plasma particles, etc.). Plasma modification has been used recently to enhance biocompatibility of implant devices made from stainless steel, titanium and various polymers.⁶⁻¹⁴ The unique advantage of plasma modification of implant devices is that the surface can be modified without altering the bulk properties of the material.¹⁵ It is thus possible to obtain desired mechanical and physical properties of implant material and at the same time also improve its surface properties to accomplish biocompatibility.

2 SURFACE MODIFICATION BY PLASMA TREATMENT

Combined surface treatments incorporating photons, ions and electrons and some other excited particles, are found in gas-electric discharges, often denominated plasmas. Ionised gas is usually called plasma when it is electrically neutral (i.e., electron density is balanced by that of positive ions) and contains a significant number of electrically charged particles, which is sufficient to affect its electrical properties and behaviour.¹⁶ Therefore plasma is composed of highly excited atomic, molecular, ionic, and other native radical species. It is typically obtained when gases are excited into energetic states by radio-frequency (RF), microwave, or electrons from a hot filament discharge. To produce plasma, electron separation from atoms or molecules in gas state, or ionization is required. When an atom or a molecule gains enough energy from an outside excitation source or via interaction (collisions) with one another, ionization occurs.¹⁷

Plasmas are divided into thermodynamically balanced and unbalanced. Plasma characteristics are dependent upon the electrical discharge type, the type of gas or gaseous mixture, and the pressure. Thermodynamically balanced plasmas are characterized by very high temperatures of heavy particles (often about 10 000 K). These types of plasmas are not suitable for the treatment of polymeric materials, as the gas temperature is so high as to cause their thermal degradation. While in thermodynamically unbalanced plasma the gas temperature is significantly lower, as they are composed of low temperature heavy particles (charged and neutral molecular and atomic species) and very high temperature electrons

(often about 50 000K). This type of plasmas are suited for the treatment of delicate polymeric products¹⁸⁻³² such as PET, PDMS or PTFE, which are used for biomedical applications.

Clark and Hutton³³ showed that with hydrogen plasma they can rapidly defluorinate fluoropolymers to a depth of 2 nm. On the other hand it was reported that plasma treatment with oxygen increased endothelial cell attachment on vascular grafts made of PTFE.³⁴ Comparison of plasma treatment with oxygen, nitrogen and gas mixture of nitrogen and oxygen, where conducted by M. Chen et al., where it has been shown that the mixture of gases uniquely modifies PTFE surfaces and reduces levels of inflammatory cells.⁵ Surfaces having incorporated nitrogen were more effective than those of oxygen containing functional groups in promoting cell adhesion.³⁵ Though, appropriate surface modification is not only a function of working gas, but also of other discharge parameters, such as pressure, type of gas, power etc. Chevallier et. al. showed that nitrogen plasma treatment of PTFE at low-power (10 W) experimental conditions exhibits more alkene and less amino groups formed on the surface than a higher-power plasma treatment (20 W). Consequently, surface chemistry could be modulated through appropriate selection of discharge parameters.³⁶

In our investigation surface properties of polymeric biomedical implants have been tailored by RF oxygen and nitrogen plasma treatment. The PET polymeric implants were treated in the experimental system shown in **Figure 1**. The plasma was created with an inductively coupled RF generator, operating at a frequency of 27.12 MHz and an output power of about 200 W. The plasma parameters were measured with a double Langmuir probe and a catalytic probe³⁶⁻⁴⁴. In our experiments, the pressure was fixed at 75 Pa, as at this pressure the highest degree of dissociation of molecules, as measured by the catalytic probes, was obtained. At these discharge parameters, plasma with an ion density of about $2 \cdot 10^{15}$

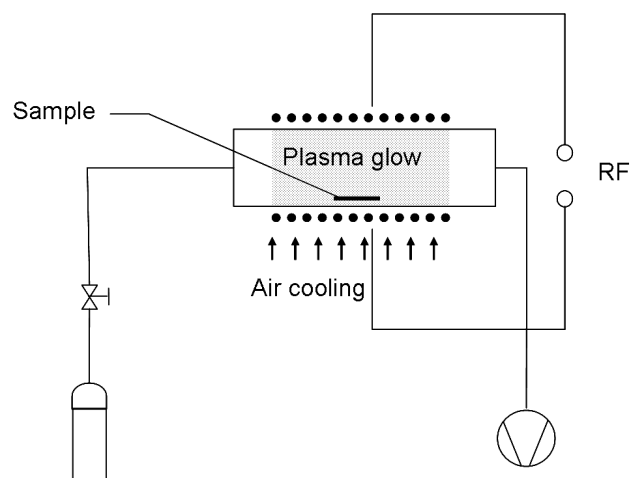


Figure 1: The RF plasma reactor chamber with the sample in position
Slika 1: Cev RF plazemskega reaktorja z vzorcem

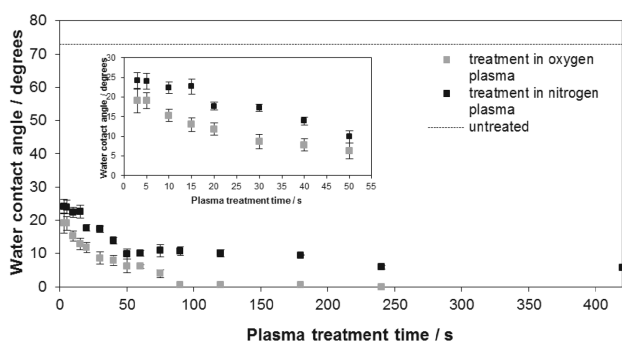


Figure 2: Water contact angle measured on the PET polymer as a function of treatment time and plasma gas, (■) oxygen plasma treatment, (●) nitrogen plasma treatment

Slika 2: Kontaktni kot vodne kapljice, izmerjen na površini PET polimera, v odvisnosti od časa obdelave in vrste plina. (■) obdelava v kisikovi plazmi, (●) obdelava v dušikovi plazmi

m^{-3} , an electron temperature of 4 eV, and neutral atoms density of about $4 \cdot 10^{21} m^{-3}$ for oxygen plasma and about $1 \cdot 10^{21} m^{-3}$ for nitrogen plasma was obtained. After plasma treatment surface chemistry, wettability and topography was altered.

Change in chemical composition was determined from (x-ray photoelectron spectroscopy) XPS. It has been shown that newly formed oxygen, or nitrogen functional groups are formed on the surface, depending on the type of gas used for modification. Already after short exposure to oxygen plasma the increase in oxygen concentration from initial mole fraction 21 % to 39 % was observed. With prolonged exposure to oxygen plasma the concentration slowly increased, and at 90 s it reached 44 %. On nitrogen plasma treated samples nitrogen concentration increased from 0 % to 12 % after 3 s of treatment time, and after 90 s of treatment it reached about 14 %. During nitrogen plasma treatment a small increase in oxygen concentration was also observed.

Wettability was examined immediately after the plasma treatment by measuring the water contact angle with a demineralised water droplet of a volume of 3 μ L. The relative humidity (45 %) and temperature (25 °C) were monitored continuously and were found not to vary significantly during the contact angle measurements. Contact angle measurements show a decrease in contact angles after oxygen and nitrogen plasma treatment **Figure 2**, corresponding to a higher hydrophilicity of the polymer surface. During the water contact angle measurements room temperature was 21 °C and The oxygen plasma treated samples exhibit lower values of contact angles, and thus demonstrating that this treatment provides a higher hydrophilic character. Even after short exposure times the surfaces show an increased hydrophilicity, regardless of the type of gas used. The treatment with nitrogen plasma, however, seems to be less efficient in reaching high hydrophilicity. However the high hydrophilicity of oxygen plasma treated surfaces could be attributed to degradation products, which

are formed on the surface after longer treatment times and could cause a lower contact angle, due to surface roughening.

The morphology of untreated and plasma treated surfaces was analyzed by atomic force microscopy (AFM) and scanning electron microscopy (SEM). In both cases change in surface morphology was observed. In **Figure 3** phase AFM images are shown. In **Figure 3 a** a surface of untreated sample is shown, while in **Figure 3 b** and **c** change in surface morphology after treatment in nitrogen and oxygen plasma can be observed, respectively. Untreated sample has smooth surface, without any particular features on the surface, while treated samples exhibit small nanostructures on its surface. The diffe-

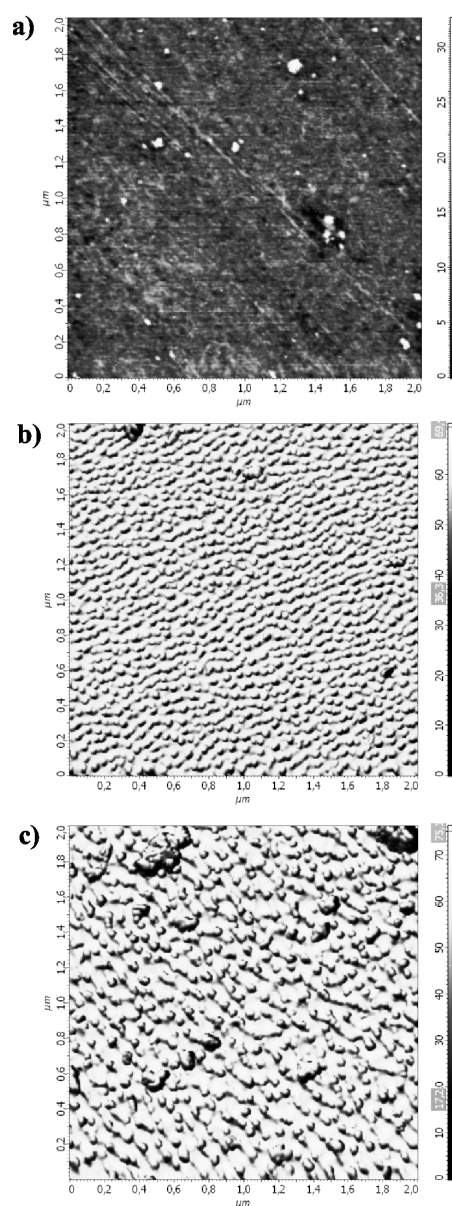


Figure 3: Phase AFM images of PET polymer; a) untreated, b) treated for 90 s in nitrogen plasma and c) treated for 90 s in oxygen plasma

Slika 3: Fazne AFM-slike PET polimera; a) neobdelanega, b) obdelanega 90 s v dušikovi plazmi in c) obdelanega 90 s v kisikovi plazmi

rence between the samples treated with oxygen (**Figure 3 a**) and nitrogen (**Figure 3 b**) plasma is noticeable: the samples treated by oxygen plasma have structures which are higher and further apart, than those treated with nitrogen plasma. This could be attributed to highly oxidative nature of oxygen plasma. However the height of these nanostructures is not only dependent on the type of gas employed for treatment, but also on the treatment time. By longer treatment time the height of these nanostructures can be increased, especially for the case of oxygen plasma treatment. Due to growth of nanostructures, surface roughness is increased on these surfaces as well.

3 BIOLOGICAL RESPONSE

To achieve a desired biological response, the attachment of cells to the surface of biomaterials is of primary importance. When a biomaterial is exposed to a living organism many extremely complex reactions may occur at the cell-biomaterial surface. These reactions include coagulation, healing, inflammation, mutagenicity, and carcinogenicity and play an important role in the successful implementation of the implemented material or device⁴⁵⁻⁴⁸. Surface parameters, such as surface chemistry, wettability, surface topography and surface roughness influence protein adsorption, and the adsorbed protein layer further dictates subsequent cellular reactions. Thus, by carefully tailoring surface properties by plasma treatment one could engineer the surface for a specific protein adsorption which would lead to a desired cellular response.

Gas plasma treatment is one of the strategies for enhancing surface properties by enriching the surface with new functional groups known to enhance cell proliferation – such as oxygen or nitrogen.^{49,50} One of the strategies to improve biocompatibility/hemocompatibility of the surface is to introduce new functional groups, such as hydroxyl (-OH), amine (-NH_x), methyl (-CH₃) sulphate (-SO₄) or carboxylic (-COOH).⁵¹⁻⁵⁴ This is either employed to tailor the biological response (improve cell proliferation, reduce platelet adhesion etc.) or to enable immobilisation of biomolecules (enzymes, proteins etc.). The effects of functional groups on hemocompatibility have been extensively studied, but again results are not always consistent. The study by Wilson et. al. has shown that treatment of polymer (polyethyetherurethane- PEU) surface with RF ammonia and nitrogen plasma (incorporation of nitrogen groups) significantly reduces contact activation⁵⁴. However, no changes in thrombogenicity, as compared to the untreated surface, were observed after oxygen and argon plasma (incorporation of oxygen groups). Similar results were obtained for RF plasma treatment of polydimethylsiloxane (PDMS) by Williams.⁵⁵

On the other hand surface wettability is also believed to be one of the important parameters which affect

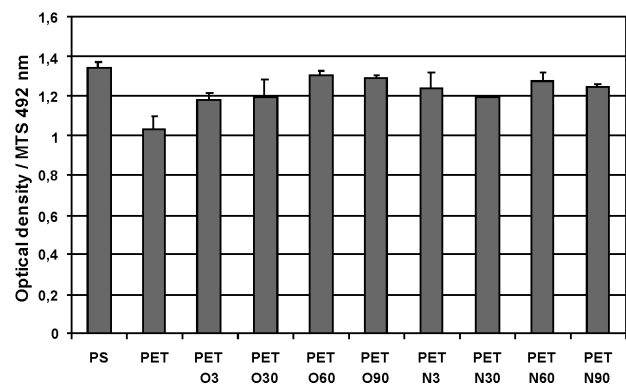


Figure 4: Viability of endothelial cells (HUVEC) cultured on surfaces treated by oxygen and nitrogen plasma for different treatment times

Slika 4: Viabilnost endotelijskih celic (HUVEC) na površinah, obdelanih s kisikovo in dušikovo plazmo pri različnih časih obdelave

biological response to a biomaterial. It is established that protein adsorption is the first event that takes place on the surface of a biomaterial with biological fluids,⁵²⁻⁵⁴ and that the biological response is controlled by the nature and confirmation of the proteins adsorbed to the surface. Thus, wettability is believed to play an important role in the amount and conformational changes of adsorbed proteins⁵⁹ platelet adhesion/activation, blood coagulation⁶⁰ and adhesion of cells.^{61,62}

Generally hydrophobic surfaces are considered to be more protein-adsorbent than hydrophilic surfaces, due to strong hydrophobic interactions occurring at these surfaces.⁶³⁻⁶⁵

Nevertheless surface morphology should also be taken in account when talking about biological response to biomaterials. Surface morphology is important in protein adsorption and subsequent cell response. Reidel and colleagues showed that adsorption of albumin dramatically increased due to presence of nanoislands.⁶⁶ While Vertegel et. al. showed that the adsorption of lysozyme to silica nanoparticles decreased with decreasing nanoparticle size⁶⁷. Surface topography plays an important role in providing three-dimensionality of cells⁶⁸. For instance the topography of the collagen fibres, with repeated 66 nm binding, has shown to affect cell shape.⁶⁹

It has been shown that RF oxygen and nitrogen plasma treatment improve proliferation of fibroblast as well as endothelial cells. **Figure 4** shows the measured absorbance, which is directly proportional to viability of endothelial cells, cultured on different samples. These results show that proliferation of endothelial cells is improved on all plasma treated surfaces, which is in accordance with the results published in the literature.^{5, 70} Improved proliferation of cells can be attributed to newly formed functional groups (oxygen and nitrogen) introduced after short plasma treatment time (3 s), as well as to higher hydrophilicity of the surface, surface morphology etc. It seems that longer treatment time (longer than 30 s) by oxygen plasma is more effective in promoting endothelial cell attachment than nitrogen plasma.

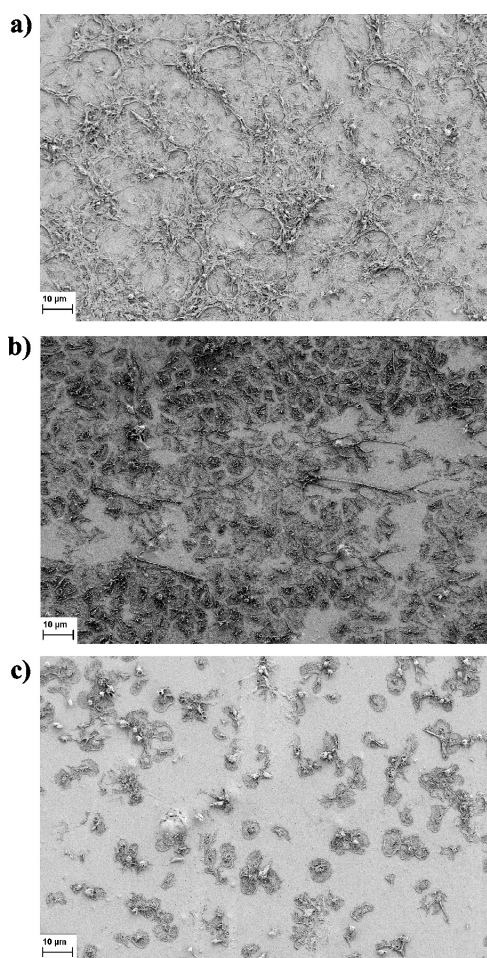


Figure 5: SEM images of platelets interacting with: a) untreated, b) 3 s nitrogen plasma treated (PET N3), c) 3 s oxygen plasma treated (PET O3) surface of PET foils

Slika 5: SEM-slike trombocitov v kontaktu s PET polimerom; a) ne-obdelanim, b) obdelanim 3 s v dušiku in c) obdelanim 3 s v kisiku

Endothelia cell seeding is a common approach to improving hemocompatibility of vascular grafts, as endothelia cells are thought to be an ideal hemocompatible surface. However adhesion of platelets is not desired for hemocompatible surfaces. Thus lower or practically no adhesion of platelets would be desired. Interestingly our study showed significant differences in adhesion of platelets to oxygen and nitrogen plasma treated surfaces. Observable differences in the number of adherent platelets and their shape can be seen in **Figure 5**. The number of adherent platelets decreased dramatically on oxygen plasma treated surfaces; as can be seen from **Figure 5 c** after only 3 s of oxygen plasma treatment, a lower number of platelets was observed. Those that did adhere seemed to be in a more round form, which is thought to be attributed to low platelet activity. On the contrary there were many aggregated platelets on untreated (**Figure 5 a**) and nitrogen plasma treated surfaces (**Figure 5 b**). Fibrin formation was also observed on these surfaces, especially on the untreated surface.

The platelets on the untreated polymer surface are mostly in well spread form and start to aggregate.

4 CONCLUSIONS

It has been shown that plasma treatment techniques enable surface modification of biomedical materials and thus enable desired biological response of the surface. Therefore many biomedical materials have been treated by plasma in order to improve their surface properties to accomplish biocompatibility. By fine tuning the discharge and plasma parameters the surface can be appropriately modified.

Our study showed that by oxygen and nitrogen plasma treatment surface chemistry, wettability and morphology can be altered. Furthermore plasma treatment enables improved proliferation of fibroblast and endothelia cells and influences on adhesion properties of platelets. Interestingly adhesion of platelets was noticeably reduced on oxygen plasma treated surfaces, while adhesion on nitrogen plasma treated surfaces was similar to the untreated ones. It has been shown that oxygen plasma treatment is a promising way to improve hemocompatible properties of PET surface, as surfaces modified in this manner exhibit improved proliferation of endothelia cells and reduced platelet adhesion.

ACKNOWLEDGEMENT

The authors acknowledge the financial support from the Ministry of Higher Education, Science and Technology of the Republic of Slovenia through the contract No. 3211-10-000057 (Center of Excellence Polymer Materials and Technologies).

5 REFERENCES

- J. H. Joist, P. D. Cennington, *Transactions-American Society for Artificial Internal Organs*, 33 (1987), 341
- L. Vroman, *Bulletin of the New York Academy of Medicine*, 64 (1988), 352
- T. Chandu, G. S. Das, R. F. Wilson, G. H. R. Rao, *Biomaterials*, 21 (2000), 699
- J. H. Lee, G. Khang, J. W. Lee, *Journal of Colloid and Interface Science*, 205 (1998), 323
- M. Chen, P. O. Zamora, P. Som, L. A. Pena, S. Osaki, *J. Biomater. Sci. Polymer Edn* 14 (2003) 9, 917–935
- A. Asadinezhad, I. Novak, M. Lehocky, V. Sedlarik, A. Vesel, I. Junkar, P. Saha, I. Chodak, *Irgasan coating, Plasma Processes and Polymers*, 7 (2010) 6, 504–514
- M. Lehocký, P. F. F. Amaral, P. S'ahel, A. M. Z. Coelho, A. M. Barros-Timmons, J. A. P. Coutinho, *Surface Engineering*, 24 (2008), 23–27
- M. Lehocký, L. Lapčík, R. Dlabaja, L. Rachunek, J. Stoch, *Czechoslovak Journal of Physics*, 54 (2004), 533–538
- U. Cvelbar, M. Mozetic, I. Junkar, A. Vesel, J. Kovac, A. Drenik, T. Vrlinic, N. Hauptman, M. Klanjsek-Gunde, B. Markoli, N. Krstulovic, S. Milosevic, F. Gaboriau, T. Belmonte, *Appl. Surf. Sci.*, 253 (2007) 21, 8669–8673

- ¹⁰ A. Vesel, M. Mozetic, A. Hladnik, J. Dolenc, J. Zule, S. Milosevic, N. Krstulovic, M. Klanjek-Gunde, N. Hauptman, *J. Phys. D: Appl. Phys.*, 40 (2007) 12, 3689–3696
- ¹¹ M. Lehocký, H. Drnovská, B. Lapčíková, A.M. Barros – Timmons, T. Trindade, M. Zembala, L. Lapčík, *Physicochemical and Engineering Aspects*, 222 (2003), 125–131
- ¹² A. Vesel, M. Mozetic, A. Zalar, *Surf. Interface Anal.*, 40 (2008) 3–4, 661–663
- ¹³ M. Sowe, I. Novak, A. Vesel, I. Junkar, M. Lehocky, P. Saha, I. Chodak, *Int. J. Polym. Anal. Ch.*, 14 (2009) 7, 641–651
- ¹⁴ M. Aouinti, P. Bertrand, F. Poncin-Epaillard, *Plasmas Polym.*, 8 (2003) 4, 225–236
- ¹⁵ A. Vesel, M. Mozetic, S. Strnad, K. Stana-Kleinschek, N. Hauptman, Z. Persin, *Vacuum*, 84 (2010) 1, 79–82
- ¹⁶ J. G. Terlingen, L. M. Brenneisen, H. T. Super, A. P. Pijpers, A. S. Hoffman, J. Feijen, *Journal of Biomaterials Science*, 3 (1993), 165
- ¹⁷ A. Fridman, *Plasma Chemistry*, Cambridge University Press, New York, 2008
- ¹⁸ M. Venugopalan, *Reaction under cold plasma conditions*, Wiley/Interscience, New York, 1971
- ¹⁹ T. Vrlinic, A. Vesel, U. Cvelbar, M. Krajnc, M. Mozetic, *Surf. Interface Anal.*, 39 (2007) 6, 476–481
- ²⁰ A. Vesel, M. Mozetic, A. Zalar, *Surf. Interface Anal.*, 40 (2008) 3–4, 661–663
- ²¹ A. Vesel, I. Junkar, U. Cvelbar, J. Kovac, M. Mozetic, *Surf. Interface Anal.*, 40 (2008) 11, 1444–1453
- ²² A. Vesel, M. Mozetic, A. Zalar, *Vacuum*, 82 (2008) 2, 248–251
- ²³ M. Sowe, I. Novak, A. Vesel, I. Junkar, M. Lehocky, P. Saha, I. Chodak, *Int. J. Polym. Anal. Ch.*, 14 (2009) 7, 641–651
- ²⁴ I. Junkar, U. Cvelbar, A. Vesel, N. Hauptman, M. Mozetic, *Plasma Processes Polym.*, 6 (2009) 10, 667–675
- ²⁵ M. Gorjanc, V. Bukosek, M. Gorenssek, A. Vesel, *Tex. Res. J.*, (2009), 1–11, doi:10.1177/0040517509348330
- ²⁶ A. Vesel, M. Mozetic, S. Strnad, K. Stana - Kleinschek, N. Hauptman, Z. Persin, *Vacuum*, 84 (2010) 1, 79–82
- ²⁷ I. Junkar, A. Vesel, U. Cvelbar, M. Mozetic, S. Strnad, *Vacuum*, 84 (2010) 1, 83–85
- ²⁸ A. Asadinezhad, I. Novák, M. Lehocký, V. Sedlařík, A. Vesel, I. Junkar, P. Sáha, I. Chodák, *Irgasan Coating, Plasma Processes and Polymers*, 7 (2010), 504–514
- ²⁹ J. López García, A. Asadinezhad, J. Pacherník, M. Lehocký, I. Junkar, P. Humpolíček, P. Sáha, P. Valášek, *Molecules*, 15 (2010), 2845–2856
- ³⁰ A. Asadinezhad, I. Novák, M. Lehocký, V. Sedlařík, A. Vesel, I. Junkar, P. Sáha, I. Chodák, *Colloids and Surfaces B: Biointerfaces*, 77 (2010), 246–256
- ³¹ A. Asadinezhad, I. Novák, M. Lehocký, F. Bilek, A. Vesel, I. Junkar, P. Sáha, A. Popelka, *Molecules*, 15 (2010), 1007–1027
- ³² M. Lehocký, P. Šťáhel, M. Koutný, J. Čech, J. Institoris, A. Mráček, *Journal of Materials Processing Technology*, 209 (2009), 2871–2875
- ³³ D.T. Clark, D.R. Hutton, *J. Polym. Sci.*, A25 (1987), 2643
- ³⁴ D. L. Mooradian, Trescony P, Keeney K, Furcht LT, *J. Surg. Res.*, 53 (1992) 74
- ³⁵ J. G. Steele, G. Johnson, C. McFarland, B. A. Dalton, T. R. Gengenbach, R. C. Chatelier, R. A. Underwood, H. J. Griesser, *J. Biomaterial. Sci. Polymer*, 6 (1994), 511
- ³⁶ P. Chevallier, M. Castonguay, S. Turgeon, N. Dubrulle, D. Mantovani, P. H. McBreen, J. C. Wittmann, G. Laroche, *J. Phys. Chem.*, B105 (2001), 12490–12497
- ³⁷ I. Poberaj, M. Mozetic, D. Babic, *Journal of Vacuum Science and Technology*, A20 (2002), 189
- ³⁸ D. Babic, I. Poberaj, M. Mozetic, *Review of Scientific Instruments*, 72 (2001), 4110
- ³⁹ M. Mozetic, U. Cvelbar, A. Vesel, A. Ricard, D. Babic, I. Poberaj, *Journal of Applied Physics* 97 (2005), 103308
- ⁴⁰ M. Mozetič, A. Vesel, U. Cvelbar, A. Ricard, *Plasma Chemistry and Plasma Processing* 26 (2006), 103
- ⁴¹ M. Mozetič *Vacuum* 71 (2003), 237–240
- ⁴² M. Mozetič B. Praček, *Inf. MIDEM*, 28 (1998), 171–174
- ⁴³ M. Mozetič. *Inf. MIDEM* 28 (1998), 175–179
- ⁴⁴ M. Drobnič, M. Mozetic, M. Gams, A. Zalar *Vacuum* 50 (1998), 50, 277–280
- ⁴⁵ B. D. Ratner, A. Hoffman, F.J. Schoen, J.E. Lemons, *Biomaterials Science*, Academic Press, San Diego, 1996
- ⁴⁶ D. Shi, *Biomaterials and Tissue Engineering*, Springer-Verlag, Berlin, 2004
- ⁴⁷ V. Sedlarik, T. Galya, J. Sedlarikova, P. Valasek, P. Saha, *Journal of Biomaterials Science-Polymer Edition*, 21 (2010), 1421–1440
- ⁴⁸ V. Sedlarik, T. Galya, J. Sedlarikova, P. Valasek, P. Saha, *Journal of Biomaterials Science-Polymer Edition*, 21 (2010), 1421–1440
- ⁴⁹ Y. J. Kim, I. Kang, M.W. Huh, S. Yoon, *Biomaterials* 21 (2000), 121
- ⁵⁰ M. C. Coen, R. Lehmann, P. Groening, L. Schlapbach, *Applied Surface Science* 207 (2003), 276
- ⁵¹ R. Tzoneva, B. Seifert, W. Albrecht, K. Richau, T. Groth, A. Lendlein, *Journal of Material Science*, 19 (2008), 3203
- ⁵² C. Sperling, R.B. Schweiss, U. Streller, C. Werner, *Biomaterials*, 26 (2005), 6547
- ⁵³ B. Seifert, G. Mihanetzis, T. Groth, W. Albrecht, K. Richa, Y. Missirlis, D. Paul, G. Sengbusch, *Artificial Organs*, 26 (2002), 189
- ⁵⁴ D. J. Wilson, R. L. Williams, R. C Pond, *Surface Interface Analysis* 31 (2001), 385
- ⁵⁵ D. F. Williams, *Advances in biomaterials*, Elsevier, Amsterdam, 1988
- ⁵⁶ T. A. Horbett, *Cardiovascular Pathology*, 2 (1993), 37
- ⁵⁷ B. Montargent, D. Letourneur, *Infection Control and Hospital Epidemiology*, 21 (2000), 404
- ⁵⁸ P. Roach, D. Farrar, C. C. Perry, *Journal of the American Chemical Society*, 127 (2005), 8168
- ⁵⁹ L. Vroman, *Bulletin of the New York Academy of Medicine*, 64 (1988), 352
- ⁶⁰ J. H. Lee, H. B. Lee, *Journal of Biomedical Material Research*, 41 (1998), 304
- ⁶¹ J. H. Choe, S. J. Lee, Y. M. Rhee, H. B. Lee, G. Khang, *Journal of Applied Polymer Science*, 92 (2004), 599
- ⁶² N. Fauchaux, R. Schweiss, K. Lutzow, C. Werner, T. Groth, *Biomaterials*, 25 (2004), 2721
- ⁶³ K. C. Dee, D. A. Puelo, R. Bizius, *An introduction to tissue-biomaterial interactions*, Hoboken, John Wiley & Sons, New Jersey, 2002
- ⁶⁴ A. Kongde, T. Bechtold, L. Teufel, *Journal Applied Polymer Scienc*, 96 (2005), 1421
- ⁶⁵ L. C. Xu, C. Siedlecki, A. Christopher, *Biomaterials*, 28 (2007), 3273
- ⁶⁶ M. Reidel, B. Muller, E. Wintermantel, *Biomaterials*, 22 (2001), 2307
- ⁶⁷ A. A. Vertegel, R. W. Siegel, J. S. Dordick, *Langmuir*, 20 (2004), 6800
- ⁶⁸ M. J. Dalby, M. O. Riehle, H. Johnstone, S. Affrossman, A. S. G. Curtis, *Biomaterials*, 23 (2002), 2945
- ⁶⁹ A. Curtis, C. Wilkinson, *Biochemical Society Symposia*, 65 (1999), 15
- ⁷⁰ P. A. Ramires, L. Mirengi, A. R. Romano, F. Palumbo, G. Nicolardi, *Journal of Biomedical Material Research*, 51 (2000), 535

RADIOFREQUENCY INDUCED PLASMA IN LARGE-SCALE PLASMA REACTOR

RADIOFREKVENČNO INDUCIRANA PLAZMA V REAKTORJU VELIKIH DIMENZIJ

Rok Zaplotnik¹, Alenka Vesel²

¹Jožef Stefan Institute, Department F4, Jamova 39, 1000 Ljubljana, Slovenia

²Center of Excellence for Polymer Materials and Technologies, Tehnološki park 24, 1000 Ljubljana, Slovenia
rokzaplotnik@yahoo.com

Prejem rokopisa – received: 2011-02-05; sprejem za objavo – accepted for publication: 2011-03-05

In this contribution we describe the characteristics of an electrical discharge in rarified gas created by dual-excitation coil. By using two parallel and overlapping excitation coils we can achieve a better transfer of the electromagnetic power from the radiofrequency (RF) generator to gaseous plasma. Dual-excitation coil is connected via a matching unit and a high frequency cable to the RF generator. Such special assembly (coupling of plasma with RF generator) has several advantages in comparison with normally used set-up. These advantages are the following: power transfer to plasma is increased, plasma is more homogeneous, the voltage necessary for generating plasma is lower, and many side-effects which are due to capacitive coupling of the plasma system are reduced.

Keywords: radiofrequency discharge, gaseous plasma, large plasma reactor, matching network

V prispevku opisujemo meritve karakteristik plinske razelektivitve, inducirane z dvojno vzbujevalno tuljavo. Z uporabo dveh vzporedno vezanih prekrivajočih se in zamaknjenih vzbujevalnih tuljav dosežemo boljši prenos elektromagnetne moči od radiofrekvenčnega generatorja v plinsko plazmo. Tuljavi sta vezani zaporedno v sklopu: tuljava-uskladitveni člen-visokofrekvenčni kabel-generator. Tovrstna vezava tuljav ima pred doslej opisanimi sklopi več prednosti, med drugim naslednje: izkoristek moči generatorja se poveča, plazma v razelektivitveni posodi je bolj homogena, napetost na generatorju, ki je potrebna za generiranje plazme, je manjša, obenem pa so bistveno zmanjšani stranski pojavi, ki so posledica kapacitivnih sklopitvev v plazemskem sistemu.

Ključne besede: radiofrekvenčna razelektivitve, plinska plazma, sklopitveni člen, veliki plazemski reaktorji

1 INTRODUCTION

In last few decades, plasma has become an important medium for treatment of materials in many modern technologies like surface cleaning,¹⁻⁴ sterilization,⁵⁻⁶ surface functionalization,⁷⁻¹⁶ selective etching¹⁷⁻²⁰ and surface (nano)modification.²¹⁻²⁵ Plasma can be divided to thermodynamically thermal and nonthermal plasma. Thermal plasma, where the gas particles are in thermodynamic equilibrium, is used for plasma cutting and welding, for synthesis of ceramics, for the degradation of hazardous chemical waste, for the plasma spraying etc.²⁶⁻²⁸ A request for ecologically suitable technologies has led to the development of new types of technologies like thermodynamically nonequilibrium plasma for processing of materials. Examples of application are: vacuum deposition of thin films, laser industry, microelectronics, macroelectronics (e.g. plasma displays), silicon micromachining (e.g. production of silicon pressure sensors) etc.²⁹ Numerous examples have been used in the automotive, optical and military industry and in biomedicine.

For processing of materials we can use different types of thermodynamic nonequilibrium plasmas, which are excited in different gases. Plasma can be created by passing the gas through an electric field. Such gas is

partially ionized, which means that it contains not just neutral particles but also free electrons and ions. Free electrons are accelerated in the electric field and make collision with the atoms or molecules. At collisions atoms and molecules are excited from the ground state into different excited states.

Electrical discharges are further divided according to the frequency of the electric field needed for excitation of plasma to: DC discharge, corona discharge 50–450 kHz, radiofrequency (RF) discharge 5–100 MHz, microwave (MW) discharge 2.45 GHz and ECR (electron cyclotron resonance) discharge 2.45 GHz with magnetic field.³⁰⁻³¹

Radiofrequency (RF) plasma usually works at two different frequencies 27.12 MHz or 13.56 MHz. RF plasma can be divided into capacitive and inductive coupled plasma, depending on the method used for creation of electric field. In the case of capacitive coupling the electric field is established between two electrodes (i.e. a capacitor) while for inductive coupling we need an excitation coil or a spiral.³⁰⁻³¹

Inductively coupled plasma is not perfectly inductive but we can also have a contribution of capacitive component. Therefore, inductively coupled plasma can operate in two different operating modes: E- and H-mode.³²⁻³⁸ At low RF powers the inductively coupled

plasma is characterized by weak light emission intensity, low electrons density and relatively high electron temperature. This mode is called E-mode and here capacitive coupling prevails. With increasing RF power we can observe a transition to H-mode which is characterized by sudden increase of light intensity and electron density, while electron temperature is slightly reduced. In this mode, the inductive component prevails and plasma is concentrated in a small volume inside the excitation coil or in the vicinity of the excitation coil.

H-mode is fairly easy to create in a small plasma reactor,³⁹⁻⁴⁹ but on the other hand it can be a big problem in large-scale plasma reactors. In large plasma reactor it is very difficult to create uniform inductive plasma in H-mode. In this paper we present characteristics of large plasma reactor, where plasma is excited with special dual-excitation coil, which is connected to RF generator via a special matching unit. Electrical characteristics and light emission was measured and compared to plasma created by normal excitation coil.

2 EXPERIMENTAL

2.1 Construction of plasma reactor

Schematic of the plasma system is shown in **Figure 1**. Plasma was created in a large quartz discharge tube with a length of 200 cm and a diameter of 20 cm. The discharge tube was pumped by rotary pump with a nominal pumping speed of $15 \text{ m}^3 \text{ h}^{-1}$. The pressure was measured with an absolute vacuum gauge. The base pressure in the system was about 1 Pa. Oxygen was leaked into the discharge chamber through a precise leak valve and was set to two different pressures: 10 Pa and 40 Pa.

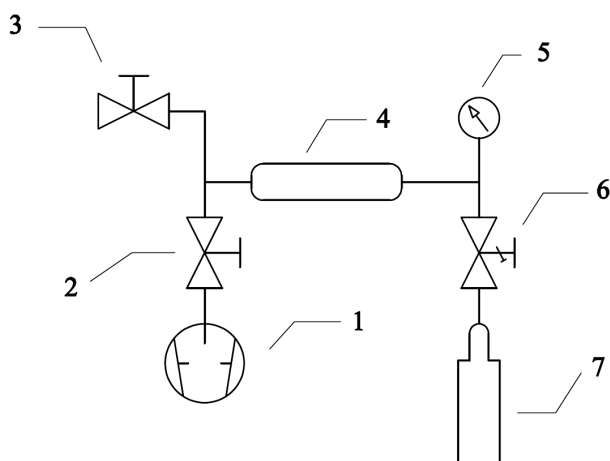


Figure 1: Schematic of the vacuum system: 1 – vacuum pump, 2 – valve, 3 – air-inlet valve, 4 – quartz discharge tube, 5 – absolute vacuum gauge, 6 – leak valve, 7 – gas

Slika 1: Shema vakuumskega sistema: 1 – vakuumska črpalka, 2 – ventil, 3 – ventil za vpust zraka, 4 – razelektrivna kremenova cev, 5 – merilnik absolutnega tlaka, 6 – precizni dozirni ventil in 7 – plinska jeklenka

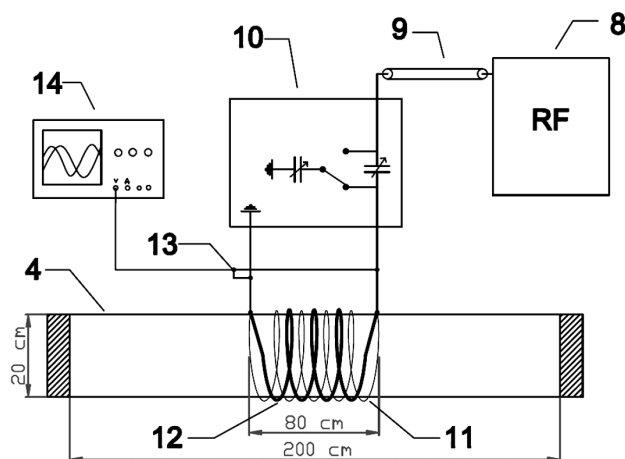


Figure 2: Excitation coil and matching network of plasma system: 8 – RF generator (8 kW), 9 – high frequency cable, 10 – matching unit, 11, 12 – normal or dual-excitation coil, 13 – high-voltage probe, 14 – oscilloscope

Slika 2: Vzbujevalni in sklopitveni člen vakuumskega sistema: 8 – RF generator, 9 – visokofrekvenčni kabel, 10 – uskladitveni člen, 11, 12 – navadna ali dvojna vzbujevalna tuljava, 13 – visokonapetostna sonda, 14 – osciloskop

For plasma excitation special dual-excitation coil was constructed. This coil was connected to the RF generator via a special matching unit (**Figure 2**). The RF generator is working at a frequency of 27.12 MHz and a maximum nominal power of 8 kW. Matching unit consist of two high-frequency, high voltage, vacuum variable capacitors, whose capacitance can be adjusted with the servo motors that are controlled by the RF generator. This matching unit is used to match the output impedance of the power supply and the impedance of the plasma system (load) to maximize the power transfer to plasma.³¹

2.2 Electrical characterization

Voltage on the excitation coils was measured with high voltage probe Tektronix P6015a connected to oscilloscope Tektronix TDS3024B. We measured root mean square-RMS voltage. Forwarded power measurement of the radiofrequency generator was taken from the generator display.

2.3 Plasma characterization

Optical emission spectroscopy (OES) was applied as a method for measuring the difference in light emission intensity of normal and dual-excitation coil. Spectra were measured in the range from 200 nm to 1100 nm by an optical spectrometer (Avantes AvaSpec-3648-USB2). Spectral resolution was about 1 nm. Integration time was 100–200 ms.

3 RESULTS AND DISCUSSION

The matching unit is attached to a dual excitation coil, which consists of two parallel overlapping exci-

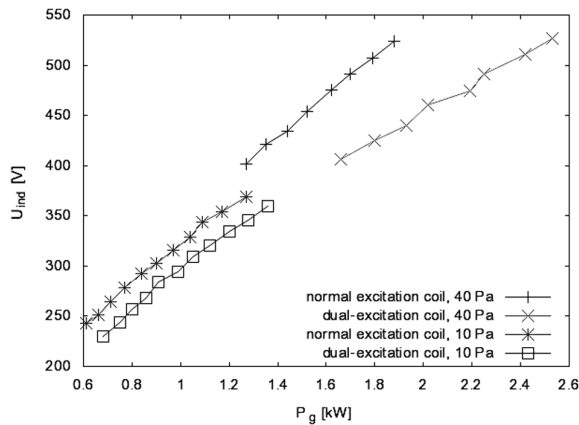


Figure 3: Voltage measured on normal excitation coil and dual-excitation coil versus RF power

Slika 3: Meritve napetosti na navadni vzbujevalni tuljavi in dvojni vzbujevalni tuljavi v odvisnosti od moči generatorja

tation coils. Excitation coils, which are of the same diameter, are overlapping in such a way that they have the same axis and are fixed together only at the beginning and the end, where they are linked to the matching unit. First excitation coils is shifted along the axis in comparison to the second excitation coil in such a way that turns of the second excitation coil are wound in the middle of the turns of the first excitation coil (**Figure 2**). Furthermore, both excitation coils are wound in the same direction, so that turns of the first excitation coils run parallel with the turns of the second excitation coil. Dual-excitation coil is made of 25 mm wide copper band with a thickness of 0.4 mm. The first excitation coil has five turns, while the second one has four turns. The entire length of the dual-excitation coil is 800 mm.

Comparison of measurements made in oxygen plasma generated by a normal excitation coil and measurements made with a dual-excitation coil is shown in **Figures 3–6**. Here we should also note that a length of

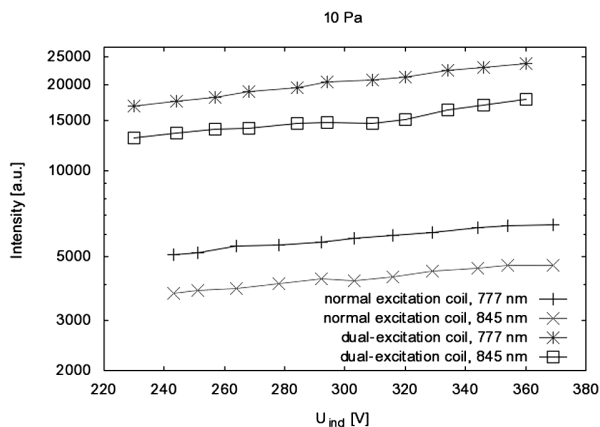


Figure 4: Light intensity measured in the centre of normal excitation coil and dual-excitation coil versus the applied voltage to the coil. The pressure was 10 Pa.

Slika 4: Meritve intenzitete izsevane svetlobe na sredini navadne vzbujevalne tuljave in dvojne vzbujevalne tuljave v odvisnosti od napetosti na vzbujevalni tuljavi pri tlaku 10 Pa

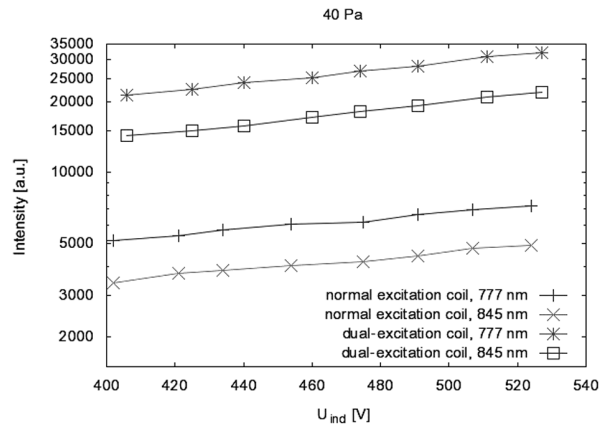


Figure 5: Light intensity measured in the centre of normal excitation coil and dual-excitation coil versus the applied voltage to the coil. The pressure was 40 Pa.

Slika 5: Meritve intenzitete izsevane svetlobe na sredini navadne vzbujevalne tuljave in dvojne vzbujevalne tuljave v odvisnosti od napetosti na vzbujevalni tuljavi pri tlaku 40 Pa

the normal excitation coil is the same as a length of dual-excitation coil and has five turns. **Figure 3** shows the measured voltage of normal excitation coil and dual-excitation coil as a function of power of RF generator. From **Figure 3** we can conclude that in the case of dual-excitation coil lower voltage is required for the same power transfer than in the case of normal excitation coil. By using dual-excitation coil the applied voltage is reduced in comparison with the normal excitation coil and this is from the technological point of view very useful.

The emission intensity of oxygen plasma measured in the middle of the excitation coil as a function of voltage or RF power shows that the plasma generated in a dual-excitation coil is much more intense than plasma, generated in the normal excitation coil (**Figures 4 and 5**). **Figure 4** presents the results of measurements of the intensity of oxygen emission lines 777 nm and 845 nm (transition $O(3p^5P \rightarrow 3s^5S)$ and $O(3p^3P \rightarrow 3s^3S)$)^{50–52} in a

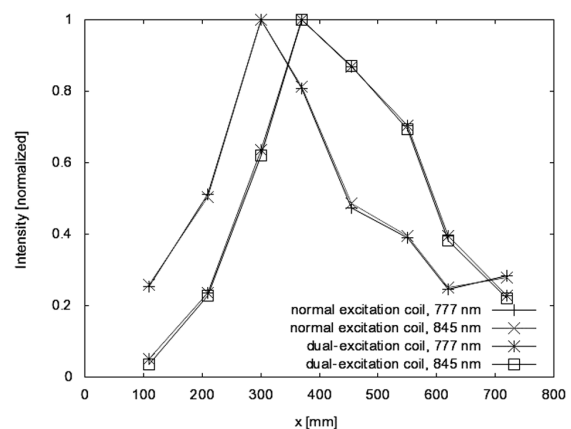


Figure 6: Light emission intensity of oxygen plasma measured along normal excitation coil and dual-excitation coil

Slika 6: Meritve intenzitete izsevane svetlobe vzdolž navadne vzbujevalne tuljave in dvojne vzbujevalne tuljave

plasma at a pressure of 10 Pa. The integration time was 200 ms. We can see that the intensity of light in plasma generated in a normal excitation coil, is about three times lower than in the case of dual-excitation coil. In **Figure 5** are presented the same results for the pressure of 40 Pa. In this case the spectrometer integration time was 100 ms. The difference is even more evident than at a pressure of 10 Pa. The light emission intensity in a dual-excitation coil is at the same applied voltage up to 4-times bigger than in the case of normal excitation coil.

With OES method we have measured also the difference in homogeneity of the plasma in H-mode (**Figure 6**) for both coils (normal and dual). This was done by measuring the plasma emission in the range between 200 nm and 1100 nm at eight different points along the coil. **Figure 6** shows the normalized intensity of oxygen 777 nm and 845 nm emission lines as a function of position of spectrometer along the excitation coil. First position (point at $x = 100$ mm in **Figure 6**) of the spectrometer was at the beginning of the excitation coil. The graph shows that the intensity of oxygen lines in the case of dual-excitation coil is at four measured points higher than a half of the maximum intensity, while in the case of normal excitation coil the intensity is higher at only two points. Furthermore, the width of the measured curve at half of the maximum intensity is for a factor of two wider for the case of a dual-excitation coil in comparison to the normal one. It can be concluded that the length of plasma column in H-mode is larger when we used dual-excitation coil, while in the case of normal excitation coil it is shorter.

At the end we should also mention, that instead of dual-excitation coil we can also use triple-excitation coil (or even multiple coils). The only limitation is that turns of individual excitation coil may not overlap turns of another excitation coil. So this means that another excitation coil must be shifted along the discharge tube in such a way that turns of the second (third ...) coil run between turns of the first coil. From practical point of view, if we have dense coil windings around the discharge tube, we have limit space for further wrapping of additional coils between the turns of the first coil. So this means that too many coils are not useful.

4 CONCLUSION

In this paper we present characteristics of a large plasma reactor, where plasma is excited with a special dual-excitation coil, which is connected to RF generator via a matching unit. By this special set-up plasma is run in inductive mode without capacitive coupling. We have shown that in such configuration power transfer to plasma is optimized and plasma is homogenous. Measurements of voltage on the excitation coil show that in the case of dual-excitation coil lower voltage is required for the same transfer of power than in the case of normal excitation coil. Comparison of normal and

dual-excitation coils which run at the same voltage shows that plasma is much more intense if it is generated in dual-excitation coil.

ACKNOWLEDGEMENT

The authors acknowledge the financial support from the Ministry of Higher Education, Science and Technology of the Republic of Slovenia through the contract No. 3211-10-000057 (Center of Excellence Polymer Materials and Technologies) and Slovenian Technology agency – TIA for a grant for young researcher. Operation also part financed by the European Union, European Social Fund.

5 REFERENCES

- ¹ A. Vesel, M. Mozetic, A. Drenik, S. Milošević, N. Krstulovic, M. Balat - Pichelin, I. Poberaj, D. Babic, *Plasma Chem. Plasma P.*, 26 (2006) 6, 577–584
- ² T. Belmonte, J. M. Thiebaut, D. Mezerette, *J. Phys. D Appl. Phys.*, 35 (2002), 1919–1926
- ³ P. Kruger, R. Knes, J. Friedrich, *Surf. Coat. Technol.*, 112 (1999), 240–244
- ⁴ M. Mozetic, A. Zalar, *Vacuum*, 71 (2003), 233–236
- ⁵ D. Vujosevic, Z. Vratnica, A. Vesel, U. Cvelbar, M. Mozetic, A. Drenik, T. Mozetic, M. Klanjsek - Gunde, N. Hauptman, *Mater. Tehnol.*, 40 (2006) 6, 227–232
- ⁶ K. Elersic, I. Junkar, A. Spes, N. Hauptman, M. Klanjsek - Gunde, A. Vesel, *Mater. Tehnol.*, 44 (2010) 3, 153–156
- ⁷ M-J. Wang, Y-I. Chang, F. Poncin - Epailard, *Surf. Interface Anal.*, 37 (2005), 348–355
- ⁸ N. Médard, J-C. Soutif, F. Poncin - Epailard, *Langmuir*, 18 (2002), 2246–2253
- ⁹ C. Canal, F. Gaboriau, A. Vilchez, P. Erra, M. J. Garcia - Celma, *J. Esquena, Plasma Processes Polym.* 6 (2009), 686–692
- ¹⁰ T. Belmonte, C. D. Pintassilgo, T. Czerwiec, G. Henrion, V. Hody, J. M. Thiebaut, J. Loureiro, *Surf. Coat. Technol.*, 200 (2005), 26–30
- ¹¹ T. Belmonte, T. Czerwiec, H. Michel, *Surf. Coat. Technol.*, 142 (2001), 306–313
- ¹² M. Sowe, I. Novak, A. Vesel, I. Junkar, M. Lehocky, P. Saha, I. Chodak, *Int. J. Polym. Anal. Ch.*, 14 (2009) 7, 641–651
- ¹³ A. Asadinezhad, I. Novak, M. Lehocky, F. Bilek, A. Vesel, I. Junkar, P. Saha, A. Popelka, *Molecules*, 15 (2010) 2, 1007–1027
- ¹⁴ A. Asadinezhad, I. Novak, M. Lehocky, V. Sedlarik, A. Vesel, I. Junkar, P. Saha, I. Chodak, *Plasma Processes Polym.*, 7 (2010) 6, 504–514
- ¹⁵ N. Puač, Z. Lj. Petrović, M. Radetić, A. Djordjević, *Mat. Sci. Forum*, 494 (2005), 291–296
- ¹⁶ P. Jovancic, D. Jovic, M. Radetic, T. Topalovic, Z. L. Petrovic, *Curr. Res. Adv. Mater. Process*, 494 (2005), 283–290
- ¹⁷ M. Klanjsek - Gunde, M. Kunaver, M. Mozetic, P. Pelicon, J. Simcic, M. Budnar, M. Bele, *Surf. Coat. Int. B.*, 85 (2002), 115
- ¹⁸ M. Kunaver, M. Klanjsek - Gunde, M. Mozetic, A. Hrovat, *Dyes Pigm.*, 57 (2003), 235–243
- ¹⁹ P. Eiselt, *Inform. Midem*, 37 (2007), 123–131
- ²⁰ M. Kunaver, M. Mozetic, M. Klanjsek - Gunde, *Thin Solid Films*, 459 (2004), 115–117
- ²¹ A. Vesel, M. Mozetic, A. Drenik, N. Hauptman, M. Balat - Pichelin, *Appl. Surf. Sci.*, 255 (2008) 5, 1759–1765
- ²² A. Hassanien, M. Tokumoto, P. Umek, D. Vrbanic, M. Mozetic, D. Mihailovic, P. Venturini, N. Pejovnik, *Nanotechnology*, 16 (2005), 278–281

- ²³ A. Drenik, U. Cvelbar, K. Ostrikov, M. Mozetic, *J. Phys. D Appl. Phys.*, 41 (2008), 115201-1
- ²⁴ D. Mariotti, K. Ostrikov, *J. Phys. D: Appl. Phys.*, 42 (2009) 9, 092002-1–092002-4
- ²⁵ I. Levchenko, U. Cvelbar, K. Ostrikov, *Appl. Phys. Lett.*, 95 (2009) 2, 021502-1–021502-3
- ²⁶ M. Mihovsky, *Journal of the University of Chemical Technology and Metallurgy*, 45 (2010) 1, 3–18
- ²⁷ E. Bouyer, M. Müller, R.H. Henne, G. Schiller, *J. Nanoparticle Research*, 3 (2001), 373–378
- ²⁸ J. Heberlein, A. B. Murphy, *J. Phys. D: Appl. Phys.*, 41 (2008), 053001
- ²⁹ J. R. Roth, *Industrial plasma engineering. Vol.2: Applications to nonthermal plasma processing*, Institute of Physics Publishing, Bristol, 2001
- ³⁰ A. Fridman, *Plasma Chemistry*, Cambridge University Press, New York, 2008
- ³¹ R. d'Agostino, P. Favia, Y. Kawai, H. Ikegami, N. Sato, F. Arefi-Khonsari, *Advanced Plasma Technology*, Wiley, Weinheim, 2008
- ³² A. M. Daltrini, S. A. Moshkalev, T. J. Morgan, R. B. Piejak, W. G. Graham, *Appl. Phys. Lett.*, 92 (2008), 061504
- ³³ M. Abdel-Rahman, V. Schulz-von der Gathen, T. Gans, *J. Phys. D* 40 (2007), 1678
- ³⁴ S. V. Singh, *J. Appl. Phys.*, 103 (2008), 083303
- ³⁵ Q. Xuelian, R. Chunsheng, Z. Jian, M. Tengcai, *Plasma Sci. Technol.*, 9 (2007), 578
- ³⁶ S. Xu and K. N. Ostrikov, *J. Vac. Sci. Technol.*, A 18 (2000) 5, 2185
- ³⁷ S. V. Singh, P. Kempkes, H. Soltwisch, *Appl. Phys. Lett.*, 89 (2006), 161501
- ³⁸ P. Kempkes, S. V. Singh, C. Pargmann, and H. Soltwisch, *Plasma Sources Sci. Technol.*, 15 (2006), 378
- ³⁹ D. Babič, I. Poberaj, M. Mozetič, *Rev. sci. instrum.*, 72 (2001), 4110–4114
- ⁴⁰ F. Brecej, M. Mozetič, *Vacuum* 40 (1990) 1/2, 177–178
- ⁴¹ F. Brecej, M. Mozetič, K. Zupan, M. Drobnič, *Vacuum* 44 (1993) 5–7, 459–460
- ⁴² M. Mozetič, *Surf. coat. technol.*, 201 (2007) 9–11, 4837–4842
- ⁴³ M. Mozetič, *Vacuum*, 71 (2003), 237–240
- ⁴⁴ M. Mozetič, A. Zalar, U. Cvelbar, D. Babič, *Surf. interface anal.*, 36 (2004), 986–988
- ⁴⁵ A. Drenik, U. Cvelbar, A. Vesel, M. Mozetič, *Inf. MIDEM*, 35 (2005), 85–91
- ⁴⁶ U. Cvelbar, M. Mozetič, I. Poberaj, D. Babič, A. Ricard, *Thin Solid Films*, 475 (2005), 12–16
- ⁴⁷ I. Arčon, M. Mozetič, A. Kodre, *Vacuum*, 80 (2005), 178–183
- ⁴⁸ M. Mozetič, A. Vesel, A. Drenik, I. Poberaj, D. Babič, *Vacuum*, 80 (2005), 178–183
- ⁴⁹ D. Vujošević, M. Mozetič, U. Cvelbar, N. Krstulović, S. Milošević, *J. appl. phys.*, 101 (2007) 10, 103305-1–103305-7
- ⁵⁰ N. Krstulovic, I. Labazan, S. Milosevic, U. Cvelbar, A. Vesel, M. Mozetic, *Mater. Tehnol.* 38 (2004) 1–2, 51–54
- ⁵¹ N. Krstulovic, U. Cvelbar, A. Vesel, S. Milosevic, M. Mozetic, *Mater. Tehnol.* 43 (2009) 5, 245–249
- ⁵² Z. Kregar, N. Krstulovic, N. Glavan Vukelic, S. Milošević, *J. Phys. D: Appl. Phys.* 42 (2009), 145201

MODIFICATION OF SURFACE MORPHOLOGY OF GRAPHITE BY OXYGEN PLASMA TREATMENT

SPREMEMBA MORFOLOGIJE GRAFITA MED OBDELAVO S KISIKOVO PLAZMO

Kristina Eleršič¹, Ita Junkar¹, Martina Modic¹, Rok Zaplotnik¹, Alenka Vesel², Uroš Cvelbar²

¹Institut "Jožef Stefan", Jamova cesta 39, 1000 Ljubljana, Slovenia

²Center of Excellence for Polymer Materials and Technologies, Tehnološki park 24, 1000 Ljubljana, Slovenia
kristina.egersic@ijs.si

Prejem rokopisa – received: 2011-02-13; sprejem za objavo – accepted for publication: 2011-030

Samples of highly oriented pyrolytic graphite (HOPG) were exposed to fully dissociated oxygen plasma created by a radiofrequency discharge in pure oxygen. The discharge was powered with a radiofrequency generator operating at the standard industrial frequency of 13.56 MHz and the output power of 1000 W. Samples of pyrolytic graphite were in pieces with dimensions of 10 mm × 10 mm × (≈1.7) mm in high and exposed to plasma for different periods up to 90 s. The morphology of originally perfectly flat samples was monitored with a high resolution scanning electron microscope (SEM). Oxygen plasma caused non-homogeneous etching of samples. The first visible effect of plasma treatment was an appearance of rather spherical features of sub-micrometer dimensions as well as randomly oriented channel - like structures. Increasing the treatment time caused transformation of the spherical features into cones. The size of cones increased until about 40 s of plasma treatment. Large cones of few micrometers in size were observed at spots with surface dust particles. Prolonged treatment caused destruction of the cones and formation of sub-micrometer large holes. The effects were explained by interaction of highly excited oxygen Particles with surface carbon atoms.

Keywords: graphite, oxygen plasma, scanning electron microscopy, morphology, nanocones

Vzorci visoko orientiranega pirolitskega grafita smo izpostavili delovanju popolnoma disociirane kisikove plazme, ki smo jo vzbujali z radiofrekvenčnim generatorjem. Generator deluje pri industrijski frekvenci 13,56 MHz in izhodni moči 1000 W. Grafitne vzorce, narezane na kose z merami 10 mm × 10 mm × (≈1,7) mm v višino in jih obdelovali s plazmo v različnem času do 90 s. Morfologijo prvotno povsem ravnih vzorcev smo opazovali z vrstičnim elektronskim mikroskopom visoke ločljivosti. Opazili smo, da plazemska obdelava vodi k nehomogenemu jedkanju. Sprva se na površini grafita tvorijo kroglasti skupki dimenzije pod 1 μm, ki kaj kmalu prerastejo v stožce. Velikost stožcev narašča s časom plazemske obdelave do okoli 40 s, z nadaljnjo obdelavo pa postopoma izginjajo. Po dolgem času obdelave stožci povsem izginejo, namesto njih pa nastanejo okrogle vdolbine. Pri krajših časih obdelave smo opazili tudi nepravilno orientirane kanale. Na mestih, kjer so se nahajali prašni drobcji, smo opazili tudi večje stožce dimenzije več mikrometrov. Opažene pojave smo razložili z interakcijo visoko vzbujenih kisikovih delcev s površinskimi atomi ogljika.

Gljučne besede: grafit, kisikova plazma, vrstični elektronski mikroskop, morfologija, nanodelci

1 INTRODUCTION

Treatment of materials by oxygen plasma is a popular technique for modification of surface morphology. The development of high resolution scanning electron microscopes allow for monitoring the surface features at almost nanometer scale. It has been found that oxygen plasma treatment causes oxidation of metals.¹⁻⁶ The oxidation is never uniform, but interesting nanostructures appear on the surface of samples exposed to plasma with right parameters.^{3,7,8} Interaction of aggressive plasma with polymer materials usually results in burning of samples. Mild oxygen plasma treatment, however, causes both functionalization of polymers with polar functional groups⁹⁻¹¹ and modification of surface morphology. Quite often it happens that extremely rough surface is obtained with well-defined and dense nanocones and similar structures on the surface of polymer exposed to highly reactive but cold oxygen plasma.^{12,13} Quite interesting as well, plasma treatment also causes modification of organic cells and tissues and represents an

interesting method for modification of bacterial cell wall during plasma sterilization of delicate materials.¹⁴⁻¹⁶ Plasma treatment of different materials therefore results in modification of surface properties of practically all materials.¹⁷

Different discharges were applied for generation of oxygen plasma but it seems that the majority of authors like high frequency electrode-less discharges such as radiofrequency¹⁸⁻²¹ and microwave one.²²⁻²⁴ The properties of plasma created in such discharges vary enormously and depend on the size of the discharge chamber, the type of materials facing plasma, the discharge power, frequency and coupling, the pressure and flow of oxygen through a vacuum system, the concentration of impurities in the discharge vessel, and (usually neglected but often very important) the properties of samples treated by plasma. The major reactants in such plasma are neutral oxygen atoms in the ground state,²⁵⁻²⁹ although other excited particles may play a certain role in modification of materials as well. The density of oxygen

atoms depends on many discharge parameters including the discharge power, but in highly concentrated plasma the dissociation fraction is practically 100 % as long as the materials facing plasma exhibit a low coefficient for heterogeneous surface recombination. Although graphite samples have been exposed to oxygen plasma by several authors,³⁰⁻³⁴ the evolution of surface morphology during plasma treatment is still far from being well understood. The current paper presents recent results obtained in our laboratories using extremely aggressive oxygen plasma for treatment of highly oriented pyrolytic graphite samples.

2 EXPERIMENTAL

Commercially available graphite samples were used. Samples were supplied by NT-MDT, HOPG marked as ZYH, with piece thickness of 1,7 mm. Samples have special properties as they are prepared layer by layer. After exposure to plasma we can renew upper working layer with simply removing it with scotch tape. Graphite molecular layers have a spalling angle in relation to the surface layer, at which the layers are easily removed and the sample can be exposed to plasma modification more than once.

Samples were exposed to extremely reactive oxygen plasma created in a discharge chamber of a vacuum system. The system was pumped with a two stage rotary pump with a pumping speed of $80 \text{ m}^3 \text{ h}^{-1}$ and commercially available oxygen was leaked into the chamber during continuous pumping. The pressure of oxygen inside the chamber was 75 Pa. Plasma was generated with a radiofrequency generator operating at the standard industrial frequency of 13.56 MHz and the output power of 1000 W. The plasma volume was pretty small (less than 1 L) so plasma was pretty energetic. Any attempt to measure plasma parameters by an electrical or a catalytic probe resulted in a rapid melting of the probe so we were unable to obtain a meaningful result. Only optical emission spectroscopy was used for estimation of plasma parameters. The measurements showed that oxygen molecules are almost fully dissociated. Taking into account the measured pressure in the system before turning on the discharge it was possible to calculate the density of oxygen atoms using the standard vacuum equation

$$p = n_M k T \quad (1)$$

where p is the measured pressure, n the density of molecules, k Boltzmann constant and T the absolute gas temperature before turning on the discharge. Assuming 100 % dissociation as suggested by optical emission spectroscopy measurements, the density of O atoms in plasma is twice the density of molecules before turning on the discharge, i.e.

$$n_A = 2 p / (k T) \quad (2)$$

Taking into account numerical values the density of oxygen atoms in our plasma is $3.7 \times 10^{22} \text{ m}^{-3}$.

The morphology of samples was monitored by scanning electron microscopy. We used the high-resolution scanning electron microscopy FEG-SEM7600F from JEOL. Images were taken by angle of 45° and magnitudes of 1 000-times and 10 000-times at low accelerating voltage 2 kV. Lower secondary electron images (LEI) are presented in this paper.

3 RESULTS

Samples of pyrolytic graphite were cut to pieces with dimensions of (10×10) mm with thickness of working layer (1.7 ± 0.2) mm and exposed to plasma for different periods up to 90 s. After the plasma treatment they were mounted in the electron microscope and imaged at different magnifications. In this paper we present only results obtained at two different magnifications: 1 000-times and 10 000-times. The surface of an untreated sample was almost perfectly flat so we do not show a corresponding SEM image. Interesting modification of surface morphology starts after about 15 s of plasma treatment. **Figure 1** represents a couple of SEM images of the samples exposed to oxygen plasma for 18 s. The original image is obtained at magnification of 1 000-times, while the insert was obtained 10 000-times. The same applies for all other Figures. The SEM image pre-

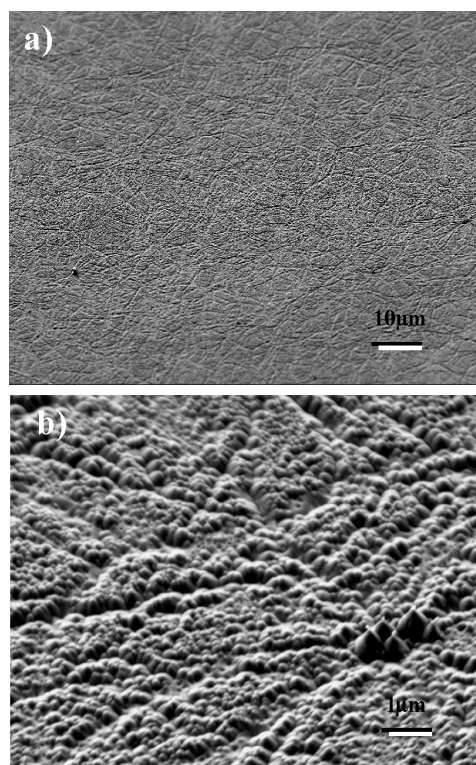


Figure 1: SEM image of a sample exposed to plasma for 18 s; a) at magnification of 1 000-times, b) at magnification of 10 000 times

Slika 1: Površina vzorca po obdelavi s kisikovo plazmo za 18 s; a) pri povečavi 1 000-krat, b) pri povečavi 10 000-krat

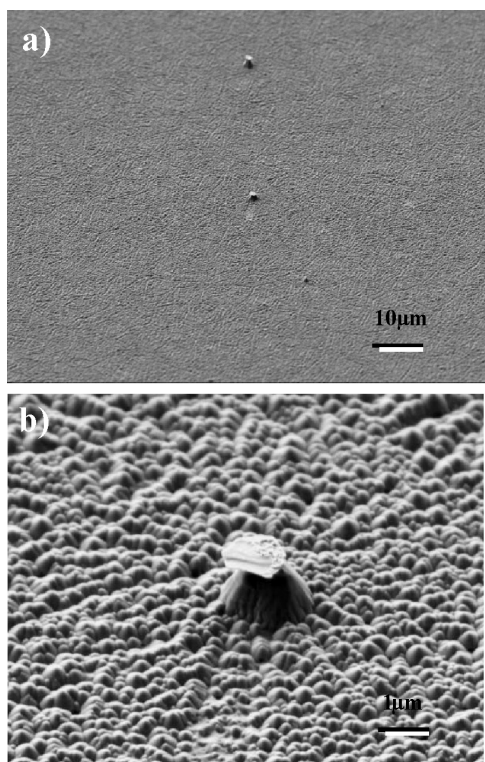


Figure 2: SEM image of a sample exposed to plasma for 20 s; a) at magnification of 1 000-times, b) at magnification of 10 000-times

Slika 2: Površina vzorca po obdelavi s kisikovo plazmo za 20 s; a) pri povečavi 1 000-krat, b) pri povečavi 10 000-krat

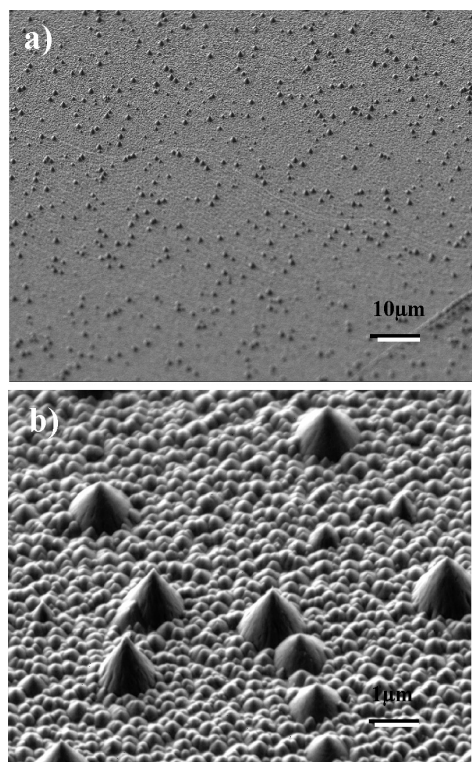


Figure 4: SEM image of a sample exposed to plasma for 31 s; a) at magnification of 1 000-times, b) at magnification of 10 000-times

Slika 4: Površina vzorca po obdelavi s kisikovo plazmo za 31 s; a) pri povečavi 1 000-krat, b) pri povečavi 10 000-krat

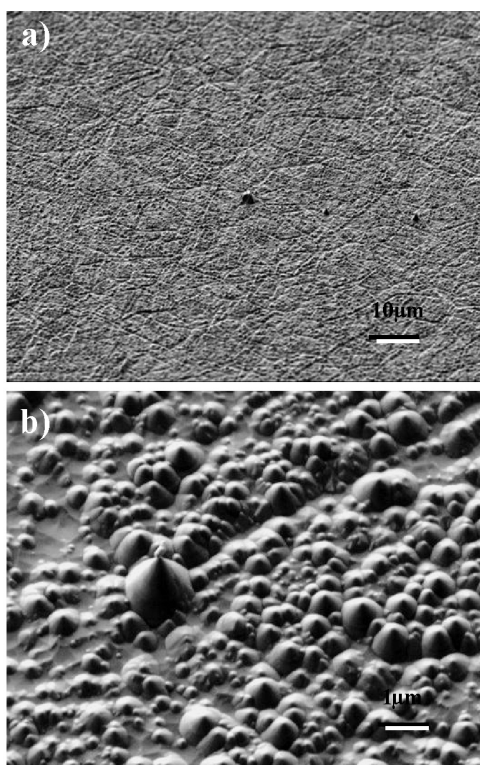


Figure 3: SEM image of a sample exposed to plasma for 25 s; a) at magnification of 1 000-times, b) at magnification of 10 000-times

Slika 3: Površina vzorca po obdelavi s kisikovo plazmo za 25 s; a) pri povečavi 1 000-krat, b) pri povečavi 10 000-krat

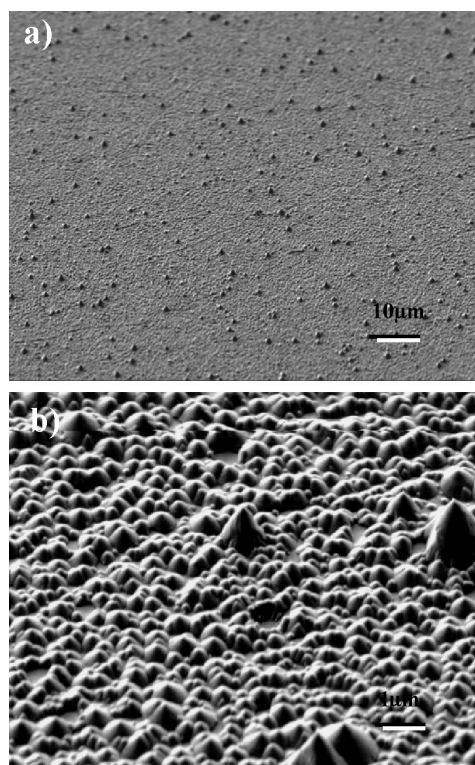


Figure 5: SEM image of a sample exposed to plasma for 35 s; a) at magnification of 1 000-times, b) at magnification of 10 000-times

Slika 5: Površina vzorca po obdelavi s kisikovo plazmo za 35 s; a) pri povečavi 1 000-krat, b) pri povečavi 10 000-krat

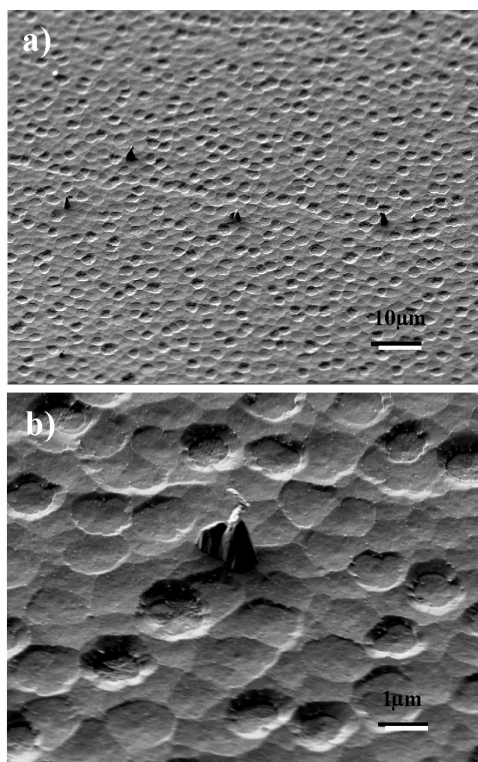


Figure 6: SEM image of a sample exposed to plasma for 52 s; a) at magnification of 1 000-times, b) at magnification of 10 000-times

Slika 6: Površina vzorca po obdelavi s kisikovo plazmo za 52 s; a) pri povečavi 1 000-krat, b) pri povečavi 10 000-krat

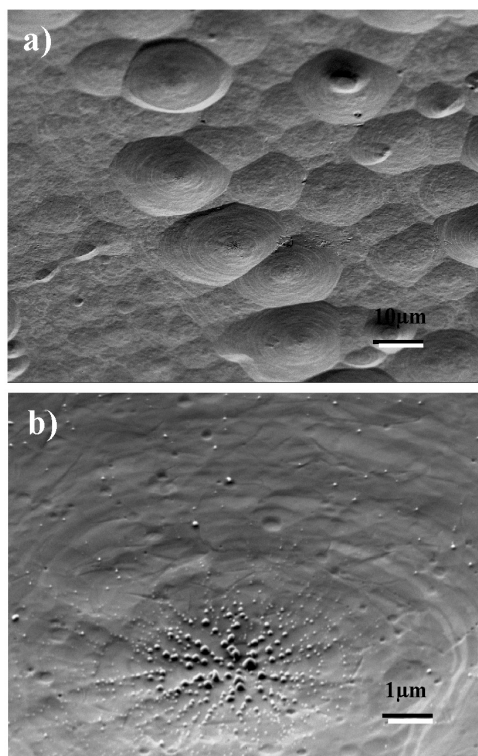


Figure 7: SEM image of a sample exposed to plasma for 90 s; a) at magnification of 1 000-times, b) at magnification of 10 000-times

Slika 7: Površina vzorca po obdelavi s kisikovo plazmo za 90 s; a) pri povečavi 1 000-krat, b) pri povečavi 10 000-krat

sented in **Figure 1** shows interesting surface morphology. Randomly oriented channels are observed already at 1 000-times, but the 10 000-times magnification reveals spherical features on the surface of (as mentioned above) originally flat surface. The features are transformed quickly to cone – like structures as shown in **Figure 2** which is the image after 20s of plasma treatment. The features become somewhat bigger since they may be visible even at the small magnification. **Figure 3** presents a couple of images obtained after 25 s of plasma treatment. Numerous small cones with randomly distributed large cones are observed in **Figure 4** which represents the images obtained after 31 s. The features remain rather unchanged for 35 s (**Figure 5**). After 52 s of plasma treatment, however, they almost vanished as demonstrated in **Figure 6**. Also, small craters become visible. Further increase of treatment time causes an important increase of the crater diameters and disappearance of all surface cones. **Figure 7** represents the SEM images after 90 s. It is interesting that small cones are observed at the bottom of craters as revealed from **Figure 7**.

4 DISCUSSION

The SEM images presented in **Figures 1–7** are attractive if not all that un-expected and definitely deserve a discussion. As mentioned in Introduction, exposure of almost any material to oxygen plasma causes increased roughness. In the case of materials that form rather stable oxides, exposure to oxygen plasma leads to formation of a thin oxide film. The oxide film created at exposure of a metal to non-equilibrium oxygen plasma, however, may have different morphology than an oxide film obtained by thermal oxidation performed close to thermal equilibrium conditions. For instance, bundles of nanowires with an extremely favorite aspect ratio may grow on the surface of some metals. The first report on this phenomenon appeared in 1995,³⁵ but until recently, no solid hypothesis that would explain the phenomenon appeared. Much work has been performed on oxidation of iron and an appropriate hypothesis appeared recently.³⁶ The hypothesis may explain interaction of oxygen plasma with metals, but is inappropriate for the case of carbon containing materials. Namely, carbon does not form stable oxides but the interaction between reactive oxygen particles results in formation of CO radicals and perhaps also CO₂ molecules that desorb from the surface even at room temperature. Exposure of carbon containing materials to oxygen plasma therefore results in etching. Surprisingly enough, etching is far from being homogeneous. Numerous authors showed that exposure of many polymers to oxygen plasma yields to formation of cone – like structures. While no internationally accepted theory appeared, an appropriate hypothesis was launched recently by Junkar et al.¹² The authors proposed a hypothesis that the extremely non-homo-

geneous etching was due to non-homogeneity of the sample. Namely, polymers are often semi-crystalline and a hypothesis was that the crystalline part of polymer is etched at lower rate than the amorphous component. Unfortunately, the authors of that paper presented no solid confirmation in terms of the size of polymer crystallites. In any case, the hypothesis of Junkar is not applicable to the case of highly oriented graphite since it is almost mono-crystalline. The results observed in **Figures 1–7** therefore cannot be explained by inhomogeneity of the original material.

One possible explanation that seems obvious when monitoring **Figure 2** is an existence of surface dust particles. Namely, the insert in **Figure 2** reveals a dust particle above the large cone. The dust particle prevents reactive oxygen particles that abound in our plasma reaching the surface of graphite. The result is a side erosion of material. Such effects are known to exist in natural formations on a meter-scale practically in all cases where the uppermost layer of material is eroded at lower rate than the material beneath. This hypothesis therefore explains formation of large cones such as the one observed in **Figure 2**. The hypothesis, however, cannot explain formation of numerous small features observed in **Figures 1–5**.

The lack of appropriate hypothesis may lead to a speculation that an extremely thin, by SEM not visible film of impurities is presented on the surface of the graphite. The film may shrink to small islets upon plasma treatment either due to electrostatic forces (assuming the impurities are not conductive), or due to thermodynamic forces (heating of materials often leads to formation of droplets, or both). The speculation may be justified by careful examination of cone peaks, for instance the largest cone in the insert of **Figure 3**. It seems that this cone as well as many others is peaked with a foreign material. The EDX analysis, however, did not reveal any impurities so the speculation is questionable. Still, appearance of quite a few cones scattered randomly on the surface of the sample best observed in **Figure 4** keeps this speculation appropriate.

Scientists familiar with materials etching by ion beams would quickly find an explanation for appearance of the cones. Namely, it is well known that etching of organic as well as some other materials by ion beams (for instance in Auger electron depth profiling) leads to formation of nanostructured surface. The explanation, however, fails in our case since the samples are not exposed to ions with any kinetic energy worth speaking about. Namely, the samples were kept at floating potential during plasma treatment. The floating potential depends on the electron temperature in plasma as well as on the mass of ions. As mentioned earlier, the electron temperature has not been measured but it can be estimated to few electron volts. The ion mass is known since we have only two ions: O_2^+ and O^+ . The concentration of other gases in the system is negligible. The

voltage across the sheath between unperturbed plasma and the sample can be estimated to about 10 V so the ions gain kinetic energy of only 10 eV. This energy is definitely too low for any decent discussion of ballistic effects caused on the surface of samples due to exposure to oxygen ions.

The formation of the features observed in **Figures 1–5** therefore remains an unresolved problem. Instead of presenting any other speculation let us point to another observation – this one is rather unexpected. **Figure 6** reveals a disappearance of the nano-cones after prolonged plasma treatment. The Figure clearly indicates that only largest cones are visible if not preserved as those shown in **Figures 2–5**. Obviously, the mechanism that is responsible for formation of cones becomes less important than a destruction mechanism. Also, well defined holes appear on the surface of the graphite sample. While the destruction may be explained by thermal effects (very high temperature of features stretching away from the surface) the explanation of the hole formation is a difficult task. The hole size increases with further treatment as shown in **Figure 7**. This Figure represents SEM images obtained after plasma treatment for 90 s. The size and depth of the holes vary but it is clear that the size of holes increases with increasing plasma treatment time. Any speculation on the observed fact that at least some holes contain small features at the bottom is beyond the scope of this paper.

The fact that molecules in our oxygen plasma are fully dissociate allows for estimation of the oxygen atom flux onto the surface and speculations of the effects they may cause on the graphite surface. The density of atoms in plasma was calculated using equation (2). The flux of atoms onto the surface is calculated using the standard equation

$$j = \frac{1}{4} n v \quad (3)$$

where v is the average thermal velocity of oxygen atoms. This value is not known since the gas kinetic temperature could not be measured. Still, the order of magnitude is 1000 K so the velocity in equation (3) is of the order of 1 000 m/s. The resultant flux is then of the order of $10^{25} \text{ m}^{-2} \text{ s}^{-1}$. This is a really huge flux. Taking into account the recombination probability of the order of 10^{-2} – 10^{-3} the sample is heated due to heterogeneous surface recombination at the rate of

$$P = \frac{1}{2} j \gamma W A \quad (4)$$

Here, γ is the probability for surface recombination, W the dissociation energy of an oxygen molecule and A the total surface of the sample. Taking into account numerical values, the power is of the order of 1 W. The power is pretty low and definitely does not suggest extensive heating of the graphite sample. Obviously, if thermal effects are important for disappearance of cones on the surface of graphite samples after prolonged plasma treatment, they should be due to other effects. Such effects may include neutralization of charged

particles and relaxation of metastables. Unfortunately, any attempt for a decent characterization of plasma failed so any discussion of the heating mechanisms is beyond the scope of the paper.

5 CONCLUSION

Exposure of highly oriented pyrolytic graphite samples to aggressive oxygen plasma revealed formation of nanocones on the surface. The appearance of nanocones was explained by non-homogeneous etching of material upon exposure to reactive oxygen particles created in plasma. The nanocones were of similar size of few 100 nm apart from few that were several micrometers large. The formation of such large cones was explained by presence of dust particles on the sample surface. The dust particles prevented reactive oxygen atoms from reaching the surface so side erosion prevailed. At prolonged treatment of samples the cones disappeared and were slowly but gradually replaced by holes whose dimensions increased with increasing plasma treatment time. Several speculations about the observed phenomena were presented and discussed but the results did not allow for presenting a decent hypothesis. The results, however, are interesting and represent just another example of un-usual modification of a material upon exposure to non-equilibrium oxygen plasma.

ACKNOWLEDGEMENT

The authors acknowledge the financial support from the Ministry of Higher Education, Science and Technology of the Republic of Slovenia through the contract No. 3211-10-000057 (Center of Excellence Polymer Materials and Technologies).

6 REFERENCES

- ¹ N. M. D. Brown, N. Cui, A. McKinley, *Applied Surface Science*, 134 (1998), 11
- ² G. Arnoult, R. P. Cardoso, T. Belmonte, G. Henrion *Appl. Phys. Lett.* 93 (2008), 191507
- ³ I. Denysenko, K. Ostrikov, U. Cvelbar, M. Mozetic, N. A. Azarenkov, *Journal of Applied Physics* 108 (2010), 74901
- ⁴ H-X. You, N. Brown, K. F. Al-Assadi, *Surface Science*, 284 (1993), 263
- ⁵ J. I. Paredes, A. Martínez-Alonso, P. X. Hou, T. Kyotani, T. J. M. D. Tascón, *Carbon*, 44 (2006), 2469
- ⁶ M. Mozetic, A. Zalar, M. Kveder, M. Drobnic, *Vacuum*, 45 (1994), 1017
- ⁷ U. Cvelbar, K. Ostrikov, I. Levchenko, M. Mozetic, M. K. Sunkara, *Appl. Phys. Lett.* , 94 (2009), 211502
- ⁸ U. Cvelbar, K. Ken Ostrikov, M. Mozetic, *Nanotechnology* 19 (2008), 405605
- ⁹ A. Vesel, M. Mozetič, *J. Phys.: Conf. Ser.*, 100 (2008), 012027
- ¹⁰ A. Vesel, M. Mozetič, *J. Phys.: Conf. Ser.*, 162 (2009), 012015
- ¹¹ U. Cvelbar, M. Mozetič, I. Junkar, A. Vesel, J. Kovac, A. Drenik, T. Vrlic, N. Hauptman, M. Klanjšek - Gunde, B. Markoli, N. Krstulovic, S. Milosevic, F. Gaboriau, T. Belmonte, *Applied Surface Science*, 253 (2007), 8669
- ¹² I. Junkar, A. Vesel, U. Cvelbar, M. Mozetic, S. Strnad *Vacuum*, (2009) 84, 83.
- ¹³ M. Mozetic, *Vacuum*, (2003) 71, 237.
- ¹⁴ K. Lee, K.-H. Paek, W-T Ju, Y. Lee, *J Microbiol.* ,44 (2006), 269
- ¹⁵ U. Cvelbar, D. Vujošević, Z. Vratnica, M. Mozetič, *J. Phys. D: Appl. Phys.*, 39 (2006), 487
- ¹⁶ C. Canal, F. Gaboriau, S. Villeger, U. Cvelbar, A. Ricard, *International Journal of Pharmaceutics*, 367 (2009), 155
- ¹⁷ A. Vesel, M. Mozetič, S. Strnad, Z. Persin, K. Stana-Kleinschek, N. Hauptman, *Vacuum*, 84 (2009), 79
- ¹⁸ A. Brockhaus, G. F. Leu, V. Selenin, K. Tarnev, *J. Engemann Plasma Sources Sci. Technol.*, 15 (2006), 171
- ¹⁹ Z. Shpilman, I. Gouzman, G. Lempert, E. Grossman, A. Hoffman *Review of Scientific Instruments*, 79 (2008), 025106
- ²⁰ Z. Kregar, N. Krstulović, N. Glavan Vukelić, S. Milošević, *J. Phys. D: Appl. Phys.*, 42 (2009), 145201
- ²¹ M. Goujon, T. Belmonte, G. Henrion, , *Thin Solid Films*, 475 (2005), 118
- ²² B. W. Muir, H. Thissen, G. P. Simon, P. J. Murphy, H. J. Griesser, *Thin Solid Films*, 500 (2006), 34
- ²³ R. P. Cardoso, T. Belmonte, G. Henrion, N. Sadeghi, *J. Phys. D: Appl. Phys.*, 39 (2006), 4178
- ²⁴ A. Vesel, M. Mozetic, M. Balat - Pichelin, *Vacuum*, 81(2007), 1088
- ²⁵ N. Krstulović, I. Levchenko, S. Milošević, U. Cvelbar, A. Vesel, M. Mozetič, *J. Phys. D: Appl. Phys.*, 39 (2006),799
- ²⁶ Č. Donik, A. K., D. Mandrino, I. Paulin, M. Jenko, B. Pihlar, *Applied Surface Science*, 255 (2009), 7056
- ²⁷ I. Arcon, M. Mozetič, A. Kodre, *Vacuum*, 80 (2005), 178
- ²⁸ M. Mozetic, *Surface and Coatings Technology*, 201 (2007), 4837
- ²⁹ M. Mozetic, A. Vesel, V. Monna, A. Ricard, *Vacuum*, 71 (2003), 201
- ³⁰ E. Bourelle, H. Konno, M. Inagaki, *Carbon*, 37 (1999), 2041
- ³¹ H. Fredriksson, D. Chakarov, B. Kasemo, *Carbon*, 47 (2009), 1335
- ³² J. I. Paredes, A. Martínez-Alonso, J. M. D. Tascón, *Carbon*, 38 (2000), 1183
- ³³ U. Cvelbar, B. Markoli, I. Poberaj, A. Zalar, L. Kosec, S. Spai, *Applied Surface Science*, 253 (2006) 1861
- ³⁴ M. Mozetič, A. Zalar, *Materials Science Forum* 437–438 (online 2003), 81
- ³⁵ K. (Ken) Ostrikov, I. Levchenko, U. Cvelbar, M. Sunkara, M. Mozetic, *Nanoscale* 5 (2010) 2012
- ³⁶ M. Mozetic, A. Zalar, P. Panjan, M. Bele, S. Pejovnik, R. Grmek, *Thin Solid Films*, 376 (2000), 5
- ³⁷ A. Drenik, A. Vesel, A. Kreter, M. Mozetič, *Applied Surface Science*, (2011) In Press, Accepted Manuscript
- ³⁸ M. Wolter, I. Levchenko, H. Kersten, S. Kumar, K. Ostrikov, *Journal of Applied Physics*, 108 (2010), 053302
- ³⁹ S. Xu, I. Levchenko, S. Y. Huang, K. Ostrikov, *Applied Physics Letters*, 95 (2009), 111505
- ⁴⁰ R. P. Cardoso, T. Belmonte, C. Noël, F. Kosior, G. Henrion, *Journal of Applied Physics*,105 (2009), 93306
- ⁴¹ R. P. Cardoso, T. Belmonte, G. Henrion, T. Gries, E. Tikhon, *Journal of Applied Physics* 107 (2010), 24909
- ⁴² A. Vesel, M. Mozetič, P. Panjan, N. Hauptman, M. Klanjšek - Gunde, M. Balat - Pichelin, *Surface and Coatings Technology*, 204 (2010), 1503
- ⁴³ J. A. Ferreira, F. L. Tabares, *Plasma Sources Science and Technology*, 18 (2009) 3, 034019
- ⁴⁴ A. Drenik, M. Mozetič, A. Vesel, U. Cvelbar, *Journal of Physics: Conference Series*, 207 (2010), 012009
- ⁴⁵ S. Kumar, I. Levchenko, M. Keidar, K. Ostrikov, *Appl. Phys. Lett.*, 97 (2010), 151503
- ⁴⁶ S. Y. Huang, Q. J. Cheng, S. Xu, K. Ostrikov, *Appl. Phys. Lett.*, 97 (2010), 213103

- ⁴⁷ A. Drenik, A. Vesel, M. Mozetič, *Journal of Nuclear Materials*, 386–388 (2009), 893
- ⁴⁸ M. Inagaki, E. Bouelle, V. Vignal, H. Konno, A. W. Morawski, *Synthetic Metals*, 125 (2001), 231
- ⁴⁹ A. Böttcher, M. Heil, N. Stürzl, S. S. Jester, S. Malik, F. Pérez-Willard, P. Brenner, M. M. Kappes, *Nanotechnology*, 17 (2006), 5889
- ⁵⁰ V. Chirila, G. Marginean, W. Brandl, *Surface and Coatings Technology*, 200 (2005), 548
- ⁵¹ C-K. Liu, M.-W. Huang, H. C. Shih, *Diamond and Related Materials*, 19 (2010), 981
- ⁵² I. Levchenko, K. Ostrikov, D. Mariotti, V. Švrček, *Carbon*, 47 (2009), 2379
- ⁵³ Z. Lj. Petrović, S. Dujko, D. Marić, G. Malović, Ž. Nikitović, O. Šašić, J. Jovanović, M. Radmilović-Radenović *Journal of Physics D: Applied Physics*, 42 (2009), 194002
- ⁵⁴ C. Canal, F. Gaboriau, S. Villeger, U. Cvelbar, A. Ricard, S. Villeger, S. Cousty, B. Rouffet, J-P. Sarrette, P. Erra, A. Ricard, *Applied Surface Science*, 254 (2008), 5959
- ⁵⁵ D. Mariotti, R. Mohan Sankaran, *Journal of Physics D: Applied Physics*, 43 (2010), 23001
- ⁵⁶ I. Levchenko, O. Volotskova, A. Shashurin, Y. Raitses, K. Ostrikov, M. Keidar, *Carbon*, 48 (2010), 4570
- ⁵⁷ G. Gottardi, N. Laidani, R. Bartali, V. Micheli, M. Anderle, *Thin Solid Films*, 516 (2008), 3910
- ⁵⁸ A. Vesel, A. Drenik, M. Mozetic, M. Balat-Pichelin, *Vacuum*, 84 (2010), 969
- ⁵⁹ A. Ricard, F. Gaboriau, C. Canal *Surface and Coatings Technology*, 202 (2008), 5220

PROPERTIES OF PARTICLEBOARDS MADE BY USING AN ADHESIVE WITH ADDED LIQUEFIED WOOD

LASTNOSTI IVERNIH PLOŠČ, IZDELANIH Z UPORABO LEPILA Z DODANIM UTEKOČINJENIM LESOM

Nataša Čuk^{1,2}, Matjaž Kunaver^{1,2}, Sergej Medved³

¹National Institute of Chemistry, Hajdrihova 19, SI-1000 Ljubljana, Slovenia

²Center of Excellence for Polymer Materials and Technologies, Tehnološki Park 24, SI-1000 Ljubljana, Slovenia

³Biotechnical Faculty, Department of Wood Science and Technology, Rožna dolina, Cesta VIII/34, 1000 Ljubljana, Slovenia
nataša.cuk@ki.si

Prejem rokopisa – received: 2011-02-10; sprejem za objavo – accepted for publication: 2011-03-28

In this study, three-layer particleboards were produced using liquefied wood in an adhesive mixture. The influence of two different formaldehyde resins: melamine-formaldehyde and melamine-urea-formaldehyde resin and two various catalysts: ammonium sulfate and ammonium formate on the particleboard properties was investigated. There were also two pressing parameters examined: temperature and time. The following physical and mechanical properties of particleboards were measured: board thickness, density, moisture content, bending strength and modulus of elasticity, internal bonding strength, surface soundness, thickness swelling and formaldehyde content. The results showed that properties of produced particleboards were better when melamine-formaldehyde resin and ammonium formate as a catalyst were used in combination with liquefied wood in the adhesive mixture. Also, mechanical properties were improved as the press time and press temperature increased. The optimal mechanical properties of particleboards made with the utilization of the liquefied wood in the adhesive mixture were achieved at 3 min press time and 180 °C press temperature using melamine-formaldehyde resin and 3 % of ammonium formate as a catalyst. A very important characteristic is the low formaldehyde content and that is extremely important in the provision of better quality of life. With the liquefaction of wood and the application of liquefied wood in the particleboard production wood biomass exploitation could be significantly increased. We are able to produce new materials from renewable resources that can be a great alternative to the raw materials, originating from crude oil.

Keywords: liquefied wood, renewable resources, particleboards, mechanical properties

Izdelali smo trislojne iverne plošče, kjer smo za pripravo lepila uporabili utekočinjen les. Ugotavljali smo, kako v kombinaciji z utekočinjenim lesom na lastnosti ivernih plošč vplivata dve različni formaldehidni smoli: melamin-formaldehidna in melamin-urea-formaldehidna smola, ter dva različna katalizatorja: amonijev sulfat in amonijev formiat. Ugotavljali smo tudi vpliv dveh parametrov stiskanja, in sicer temperature stiskanja in časa stiskanja. Fizikalne in mehanske lastnosti, ki smo jih ivernim ploščam določili, so bile: debelina plošče, gostota, vsebnost vlage, upogibna trdnost in modul elastičnosti, razslojna trdnost, čvrstost površine, debelinski nabrek in vsebnost prostega formaldehida. Rezultati so pokazali, da smo izboljšali lastnosti ivernih plošč, ko smo v kombinaciji z utekočinjenim lesom uporabili melamin-formaldehidno smolo in amonijev formiat kot katalizator. Ugotovili smo tudi, da so se lastnosti izdelanih ivernih plošč s časom in temperaturo stiskanja izboljšale. Optimalne lastnosti ivernih plošč, pri katerih smo lepilni mešanici dodali utekočinjen les, smo dosegli pri času stiskanja 3 min in temperaturi stiskanja 180 °C, pri uporabi melamin-formaldehidne smole in 3 % amonijevega formiata kot katalizatorja. Zelo pomembna pri izdelanih ivernih ploščah je tudi majhna vsebnost prostega formaldehida, kar močno vpliva na izboljšanje kvalitete bivanja. Z utekočinjanjem lesa in njegovo uporabo pri izdelavi ivernih plošč povečamo izrabo lesne biomase. Iz obnovljivih virov tako lahko sintetiziramo nove materiale, ki so odlična alternativa materialom, ki jih sicer pridobivamo iz surove nafte.

Ključne besede: utekočinjen les, obnovljivi viri, iverne plošče, mehanske lastnosti

1 INTRODUCTION

Wood is recyclable, renewable, biodegradable and one of the most abundant natural polymers. It can be used for many different purposes and converted to many useful industrial chemicals. Nowadays, it can also be liquefied using different polyhydric alcohols and acid catalysts. Cellulose, hemicellulose and lignin are the main wood components and during liquefaction these components are decomposed – depolymerized. The final product has lots of free hydroxyl groups and can therefore be used to prepare an adhesive for gluing the wood and wood composites. Particleboards for which we use 10–15 % of adhesive (based on the weight of particles) represent almost 60 % of the wood composites production.

To produce particleboards wood is broken down into particles of various size and glued together. Wood particles are bonded using synthetic adhesives and pressed into boards at high temperature and high pressure. The pressing operation provides increased density and strength.¹

The properties of particleboards are engineered in a manner to meet many service requirements. Particleboards can be made in large panel sizes, with a full range of thicknesses. With the introduction of continuous presses, endless boards emerge and are subsequently cut into any length desired.² There are many factors affecting the properties of the particleboards and the most important are:

- species of wood, fiber structure, density, hardness, compressibility;

- form and size of raw wood;
- share of bark;
- non-wood lignocellulose materials;
- type and size of particles;
- method of particle drying;
- particle screening and separating, particle size distribution;
- type and amount of binding agents;
- method of mat formation, structure of particleboard;
- moistening of particles prior to pressing, final moisture content of board, conditioning;
- curing conditions;
- thickness of board;
- sand content of particleboard;
- surface quality;
- primings, coats of varnish or lacquer;
- laminating, veneering, overlaying.³

Over the years many different lignocellulosic materials beside wood were used in particleboard production: coconut chips,⁴ paper sludge,⁵ waste tea leaves,⁶ castor stalks,⁷ wheat straw,⁸ flax shiv,⁹ kenaf stalks,¹⁰ needle litter,¹¹ waste grass clippings,¹² bagasse,¹³ saline creeping wild rye,¹⁴ peanut hull,¹⁵ cotton carpel,¹⁶ vine prunings,¹⁷ kiwi prunings,¹⁸ waste tissue paper and corn peel,¹⁹ almond shell²⁰ and others.

Next to the commonly used urea-formaldehyde resin for particleboard manufacturing, there were also other adhesives applied: melamine-modified urea-formaldehyde resin,²¹ phenol-formaldehyde resin and melamine-urea-phenol-formaldehyde resin,²² PTP resin,²³ soy-protein adhesive,^{8, 24} cement,²⁵ rice bran adhesive,²⁶ EMDI isocyanate resin,⁴ MDI resin.⁸

Lee and Liu prepared resol resin based on liquefied bark and used it for particleboard production.²⁷ Particleboard made from liquefied Taiwan acacia bark, using H₂SO₄ as a liquefaction catalyst, had the best properties in bending strength, internal bonding strength and thickness swelling. Liquefied wood was also used in preparation of phenol-formaldehyde resin,²⁸ polyurethane resin,²⁹ isocyanate adhesive³⁰ and epoxy resin.³¹

Since we have already proved in our previous research that liquefied wood can be used in the adhesive mixture for particleboard production,³² the aim of this research was to evaluate the influence of some factors on the properties of particleboards made from liquefied wood. We investigated the impact of two different formaldehyde resins and two various catalysts used in combination with liquefied wood in the adhesive mixture on the properties of particleboards. We also examined the influence of two pressing conditions: temperature and time. Other parameters such as liquified wood loading, resin content and press pressure were held constant.

2 EXPERIMENTAL

2.1 Wood liquefaction

Sawdust of spruce wood (*Picea abies* (L.) Karst.) was liquefied using the mixture of glycerol and diethylene glycol (mass ratio 80/20,) as a liquefying reagent and p-toluenesulphonic acid as a catalyst. The mass ratio of wood sawdust to glycols was 1 : 3 and the amount of p-toluenesulphonic acid was 3 % based on the mass of glycols.

The mixture of glycols and acid was charged into three neck glass reactor equipped with mechanical stirrer, thermometer, condenser and external heating. When the mixture in the reactor reached temperature 160 °C wood sawdust was added. After all the wood sawdust was added the temperature was elevated to 180 °C and maintained for 90 min to carry out the liquefaction reaction. After the liquefaction the liquefied product was cooled down.

2.2 Adhesive preparation

The adhesive was prepared with the addition of liquefied wood (LW) to the melamine-formaldehyde (MF) or the melamine-urea-formaldehyde (MUF) resin. Both resins, MF and MUF, were received from Melamin Kočevje where they also measured the properties. The properties of MF and MUF resin are presented in **Table 1**. The liquefied wood loading was 30 % based on the mass of adhesive needed (dry content based), other 70 % was either MF or MUF resin. The mixture was thoroughly blended, then water and catalyst were added. The catalyst was only added into the adhesive mixture for the core layer. Catalysts used were 20 % solution of ammonium sulfate ((NH₄)₂SO₄) and 10 % solution of ammonium formate (NH₄HCO₂). The catalyst content was 3 % based on the weight of the adhesive mixture, except when the influence of catalyst on the properties of particleboards was investigated. The whole resin mixture was blended for a few minutes before use.

Table 1: Characteristics of MF and MUF resin
Preglednica 1: Karakteristike MF in MUF smole

Properties	MF	MUF
Solid content	(58 ± 1) %	(63 ± 2) %
Viscosity*	18–22 s	80–200 s
Free formaldehyde content	below 0.2 %	max. 0.5 %
pH value	9–10	9.2–9.5
Stability (at 20 °C)	20 d	2 months

*viscosity was determined according to the standard DIN EN ISO 2431. $\phi = 4$ mm, 20 °C

2.3 Particleboard production

Three-layer particleboards of 500 mm by 500 mm in size, 16 mm of thickness and 0.600 g/cm³ of target density were produced in laboratory conditions. The

resin content was 10.50 % in the surface layer and 6.50 % in the core layer. The resin content was calculated based on the dry weight of wood particles.

Wood particles mixture composed from 75 % of spruce wood (*Picea abies* (L.) Karst.) and 25 % of beech wood (*Fagus sylvatica* L.) was first dried at 70 °C to obtain the moisture content approximately 4 %, then the resin was added. After blending for several minutes the glued wood particles were hand-formed into a mat using wood mold. For the determination of resin and catalyst type impact on the particleboard properties, the wood mat was hot-pressed for 3 min at temperature 180 °C. Later the press times were (2, 2.5, 3 and 3.5) min at the press temperature 180 °C and the press temperatures were 140 °C, 160 °C, 180 °C and 200 °C at the press time of 3 min. Before testing, all particleboards were conditioned for 4–5 d at temperature 20 °C and relative humidity 65 %.

2.4 Particleboard testing

The physical and mechanical properties of produced particleboards were tested according to the European standards: the board thickness EN 324, the density EN 323, the moisture content EN 322, the bending strength and the modulus of elasticity EN 310, the internal bonding strength EN 319, the surface soundness EN 311, the thickness swelling EN 317 and the formaldehyde content EN 120.

3 RESULTS AND DISCUSSION

The results of the physical and mechanical properties of laboratory made particleboards bonded with LW combined with the MF and the MUF resin are presented in **Table 2**. The results indicate that mechanical properties of particleboards were up to 25 % better when MF resin was used. The reason may be that the resin containing more melamin is more reactive. Also, the cyclic structure of the melamine imparts greater stability to the resulting linkages. The three amine groups assure a three-dimensional, cross-linked molecular structure when fully cured.³³ Consequently, mechanical properties of particleboards using LW and MF resin were better in comparison to the particleboards where LW and melamine enhanced UF (MUF) resin was used. Nevertheless, in both cases, the properties satisfied the standard requirements. There was no major difference in thickness swelling with regard to the resin type used.

From previous research we have already found out that the addition of LW in the adhesive mixture reduces the content of formaldehyde in the boards.³² In this research we have again obtained low formaldehyde content. We observed that formaldehyde content was lower when MF resin was used. Lower formaldehyde content at use of MF resin, compared to formaldehyde content at use of MUF is related to the nature of reaction between formaldehyde and melamine or formaldehyde

and melamine-urea, as it was reported by Eom et al.³⁴ Such boards can easily be used in dry conditions for general and interior purposes.

Table 2: Properties of particleboards produced by using an adhesive mixture made of LW combined with MF or MUF resin

Preglednica 2: Lastnosti ivernih plošč, izdelanih iz utekočinjenega lesa v kombinaciji z MF in MUF smolo v lepilni mešanici

Particleboard properties	LW-MF	LW-MUF
Board thickness (mm)	15.71	16.18
Density (g/cm ³)	0.627	0.610
Moisture content (%)	7.98	7.70
Bending strength (N/mm ²)	13.42	11.06
Modulus of elasticity (N/mm ²)	2322	1823
Internal bonding strength (N/mm ²)	0.47	0.45
Surface soundness (N/mm ²)	1.28	1.18
Thickness swelling (%)	19.51	19.97
Formaldehyde content (mg/100 g of dry board)	1.40	2.55

Table 3: Properties of particleboards produced by using an adhesive with added LW and ammonium formate or ammonium sulfate as a catalyst

Preglednica 3: Lastnosti ivernih plošč, izdelanih iz utekočinjenega lesa, dodanega lepilni mešanici pri uporabi amonijevega formiata in amonijevega sulfata kot katalizatorja

Particleboard properties	NH ₄ HCO ₂				(NH ₄) ₂ SO ₄			
	1 %	2 %	3 %	4 %	1 %	2 %	3 %	4 %
Catalyst content (%)	1 %	2 %	3 %	4 %	1 %	2 %	3 %	4 %
Board thickness (mm)	15.58	15.70	15.71	15.69	16.04	15.83	15.53	15.71
Density (g/cm ³)	0.658	0.643	0.627	0.660	0.637	0.642	0.659	0.651
Moisture content (%)	7.80	7.55	7.98	8.27	8.23	7.49	7.18	7.08
Bending strength (N/mm ²)	12.37	12.71	13.42	12.70	10.48	11.96	12.98	11.71
Modulus of elasticity (N/mm ²)	2286	2327	2322	2240	2091	2193	2404	2321
Internal bonding strength (N/mm ²)	0.40	0.54	0.47	0.47	0.34	0.40	0.46	0.39
Surface soundness (N/mm ²)	1.22	1.22	1.28	1.18	1.01	1.09	1.14	1.24
Thickness swelling (%)	20.82	18.77	19.51	18.20	21.62	20.74	21.33	22.00
Formaldehyde content (mg/100 g of dry board)	2.51	2.06	1.40	1.22	3.44	2.85	2.71	2.25

We also investigated the impact of type and amount of catalyst on the particleboard properties. We used two different ammonium salts: ammonium formate (NH₄HCO₂) and ammonium sulfate ((NH₄)₂SO₄). The results of particleboard testing are shown in **Table 3**. It can be seen that the properties of particleboards were better when ammonium formate was used. We also varied the quantity of the catalyst from 1 % to 4 %. The properties of particleboards were the best when the 3 % loading of each catalyst was applied. When comparing the efficiency of both catalysts and the influence of the amount of the catalyst the difference in thickness swelling is not very distinctive. Nevertheless, there are some differences in formaldehyde content. With higher amount of catalyst the formaldehyde content was lower

for the both catalysts. Furthermore, the formaldehyde content was higher when ammonium sulfate was used.

Further on, we evaluated the influence of pressing conditions, i.e. time and temperature, on the properties of particleboards made by using an adhesive with added liquefied wood. The results of testing particleboards pressed at different times are presented in **Table 4**. The prolongation of the press time resulted in an improvement of mechanical properties. The best properties were achieved at press time of 3 min. The time of pressing can be shorten to 2.5 min and consequently, the energy could be saved significantly. Namely, the reduction of press time means greater level of production, i.e. increased output, and consequently, the reduction of the unit production costs. Of course, press time reduction must be carefully watched because of the impact on the board quality. The press time had no larger effect on the thickness swelling and the formaldehyde content.

Table 4: Properties of particleboards produced by using an adhesive with added LW pressed at different times

Preglednica 4: Lastnosti ivernih plošč, izdelanih iz utekočinjenega lesa, dodanega lepilni mešanici pri različnih časih stiskanja

Particleboard properties	2 min	2,5 min	3 min	3,5 min
Board thickness (mm)	16.35	16.15	16.12	15.85
Density (g/cm ³)	0.614	0.595	0.596	0.624
Moisture content (%)	6.18	5.97	5.43	5.53
Bending strength (N/mm ²)	8.53	9.53	10.62	9.65
Modulus of elasticity (N/mm ²)	1872	1806	2106	1904
Internal bonding strength (N/mm ²)	0.37	0.52	0.46	0.48
Surface soundness (N/mm ²)	0.95	0.94	1.03	0.93
Thickness swelling (%)	19.58	19.59	19.75	17.82
Formaldehyde content (mg/100 g of dry board)	3.49	2.94	2.83	3.02

Table 5: Properties of particleboards produced by using an adhesive with added LW pressed at different temperatures

Preglednica 5: Lastnosti ivernih plošč, izdelanih iz utekočinjenega lesa, dodanega lepilni mešanici pri različnih temperaturah stiskanja

Particleboard properties	140 °C	160 °C	180 °C	200 °C
Board thickness (mm)	17.51	16.47	16.12	16.27
Density (g/cm ³)	0.592	0.629	0.596	0.628
Moisture content (%)	6.03	5.63	5.43	4.77
Bending strength (N/mm ²)	8.10	9.34	10.62	10.99
Modulus of elasticity (N/mm ²)	1655	1974	2106	2037
Internal bonding strength (N/mm ²)	0.26	0.44	0.46	0.43
Surface soundness (N/mm ²)	0.94	0.99	1.03	0.96
Thickness swelling (%)	19.86	20.56	19.75	20.44
Formaldehyde content (mg/100 g of dry board)	2.74	2.76	2.83	2.71

The results of testing of particleboards which were pressed at various temperatures are presented in **Table 5**. When the press temperature was elevated, the properties of particleboards were improved. The optimal properties were obtained at press temperature of 180 °C, while the

temperature of 140 °C was too low to achieve required strength and the temperature of 200 °C did not provide better quality of the board than of the 180 °C. The press temperature can be lowered to 160 °C and the properties would still satisfy the European standards requirements. The press temperature did not have much effect on both the thickness swelling and the formaldehyde content, what was also observed when evaluating the influence of the press time.

4 CONCLUSIONS

The three-layer particleboards were successfully produced using adhesive with the addition of 30 % of liquefied wood. The physical and mechanical properties of produced particleboards met the European standard requirements and were better when using melamine-formaldehyde resin and 3 % of ammonium formate. The optimal properties of particleboards were achieved at the press time of 3 min and the press temperature 180°C. By shortening the press time to 2.5 min or by decreasing the press temperature to 160°C reduction of the energy costs could be achieved. Nevertheless, the additional research will be needed to confirm these findings. Particleboards made with the adhesive with added liquefied wood have low formaldehyde content, and that is of special importance when using particleboards for interior applications. With the liquefaction of wood and application of liquefied wood in particleboard production the wood biomass exploitation can be increased. That would enable efficient lignocellulosic waste recycling, increase renewable resources usage and reduce the crude oil consumption.

ACKNOWLEDGEMENTS

The authors wish to thank for the support to Ministry of Higher Education, Science and Technology of the Republic of Slovenia within the contract No. 3211-10-000057 (Center of Excellence for Polymer Materials and Technologies), GG Postojna for their financial and material support, Melamin Kočevje for their material support and Janez Renko for his technical help.

5 REFERENCES

- Rowell R. M., Handbook of wood chemistry and wood composites, CRC Press, Boca Raton 2005, 284, 293
- Moslemi A. A., Particleboard, Volume 1: Materials, Southern Illinois University Press Carbondale and Edwardsville 1974, 6
- Kollmann F. F. P., Kuenzi E. W., Stamm A. J., Principles of wood science and technology, Volume II: Wood based materials, Springer-Verlag, Berlin, Heidelberg, New York 1975, 463
- Papadopoulos A. N., Traboulay E. A., Hill C. A. S., One layer experimental particleboard from coconut chips – (*Cocos nucifera* L.), Holz als Roh- und Werkstoff, 60 (2002), 394–396

- ⁵Taramian A., Doosthoseini K., Mirshokraii S.A., Faezipour M., Particleboard manufacturing: an innovative way to recycle paper sludge, *Waste Management*, 27 (2007), 1739–1746
- ⁶Yalinkilic M. K., Imamura Y., Takahashi M., Kalaycioglu H., Nemli G., Demirci Z., Ozdemir T., Biological, physical and mechanical properties of particleboard manufactured from waste tea leaves, *International Biodeterioration & Biodegradation*, 41 (1998), 75–84
- ⁷Grigoriou A. H., Ntalos G. A., The potential use of *Ricinus Communis* L. (Castor) stalks as a lignocellulosic resource for particleboards, *Industrial Crops and Products*, 13 (2001), 209–218
- ⁸Mo X., Cheng E., Wang D., Sun X. S., Physical properties of medium-density wheat straw particleboard using different adhesives, *Industrial Crops and Products*, 18 (2003), 47–53
- ⁹Papadopoulou A.N., Hague J.R.B., The potential for using flax (*Linum usitatissimum* L.) shiv as a lignocellulosic raw material for particleboard, *Industrial Crops and Products*, 17 (2003), 143–147
- ¹⁰Kalaycioglu H., Nemli G., Producing composite particleboard from kenaf (*Hibiscus cannabinus* L.) stalks, *Industrial Crops and Products*, 24 (2006), 177–180
- ¹¹Nemli G., Yildiz S., Gezer E. D., The potential for using the needle litter of Scotch pine (*Pinus sylvestris* L.) as a raw material for particleboard manufacturing, *Bioresource Technology*, 99 (2008), 6054–6058
- ¹²Nemli G., Demirel S., Gümüşkaya E., Aslan M., Acar C., Feasibility of incorporating waste grass clippings (*Lolium perenne* L.) in particleboard composites, *Waste Management*, 29 (2009), 1129–1131
- ¹³Xu X., Yao F., Wu Q., Zhou D., The influence of wax-sizing on dimension stability and mechanical properties of bagasse particleboard, *Industrial Crops and Products*, 29 (2009), 80–85
- ¹⁴Li B., Zheng Y., Pan Z., Hartsough B., Improved properties of medium-density particleboard manufactured from saline creeping wild rye and HDPE plastic, *Industrial Crops and Products*, 30 (2009), 65–71
- ¹⁵Guler C., Copur Y., Tascioglu C., The manufacture of particleboard using mixture of peanut hull (*Arachis hypoqaea* L.) and European Black pine (*Pinus nigra* Arnold) wood chips, *Bioresource Technology*, 99 (2008), 2893–2897
- ¹⁶Alma M. H., Kalaycioglu H., Bektas I., Tutus A., Properties of cotton carpel-based particleboards, *Industrial Crops and Products*, 22 (2005), 141–149
- ¹⁷Ntalos G. A., Grigoriou A. H., Characterization and utilisation of vine prunings as a wood substitute for particleboard production, *Industrial Crops and Products*, 16 (2002), 59–68
- ¹⁸Nemli G., Kirci H., Serdar B., Ay N., Suitability of kiwi (*Actinidia sinensis* Planch.) prunings for particleboard manufacturing, *Industrial Crops and Products*, 17 (2003), 39–46
- ¹⁹Lertsutthiwong P., Khunthon S., Siralertmukul K., Noomun K., Chandkrachang S., New insulating particleboards prepared from mixture of solid wastes from tissues paper manufacturing and corn peel, *Bioresource Technology*, 99 (2008), 4841–4845
- ²⁰Gürü M., Tekeli S., Bilici I., Manufacturing of urea-formaldehyde-based composite particleboard from almond shell, *Materials & Design*, 27 (2006), 1148–1151
- ²¹Hse C.-Y., Fu F., Pan H., Melamine-modified urea-formaldehyde resin for bonding particleboard. *Forest Products Journal*, 58 (2008), 56–61
- ²²Wagner D., Schwarzinger C., Leidl M., Schmidt H., Endesfelder A., Particleboards from acetylated wood flakes, *Monatshefte für Chemie*, 138 (2007), 321–325
- ²³Boquillon N., Elbez G., Schönfeld U., Properties of wheat straw particleboards bonded with different types of resin, *Journal of Wood Science*, 50 (2004), 230–235
- ²⁴Wang D., Sun X. S., Low density particleboard from wheat straw and corn pith, *Industrial Crops and Products*, 15 (2002), 43–50
- ²⁵Erakhrumen A. A., Areghan S. E., Ogunleye M. B., Larinde S. L., Odeyale O. O., Selected physico-mechanical properties of cement-bonded particleboard made from pine (*Pinus caribaea* M.) sawdust-coir (*Cocos nucifera* L.) mixture, *Scientific Research and Essay*, 3 (2008), 197–203
- ²⁶Pan Z., Cathcart A., Wang D., Properties of particleboard bond with rice bran and polymeric methylene diphenyl diisocyanate adhesives, *Industrial Crops and Products*, 23 (2006), 40–45
- ²⁷Lee W.-J., Liu C.-T., Preparation of liquefied bark-based resol resin and its application to particleboard, *Journal of Applied Polymer Science*, 87 (2003), 1837–1841
- ²⁸Lee W.-J., Chen Y.-C., Novolak PF resins prepared from phenol liquefied *Cryptomeria japonica* and used in manufacturing moldings, *Bioresource Technology*, 99 (2008), 7247–7254
- ²⁹Wei Y., Cheng F., Li H., Yu J., Synthesis and properties of polyurethane resins based on liquefied wood, *Journal of Applied Polymer Science*, 92 (2004), 351–356
- ³⁰Tohmura S.-I., Li G.-Y., Qin T.-F., Preparation and characterization of wood polyalcohol-based isocyanate adhesives, *Journal of Applied Polymer Science*, 98 (2005), 791–795
- ³¹Kishi H., Fujita A., Miyazaki H., Matsuda S., Murakami A., Synthesis of wood-based epoxy resins and their mechanical and adhesive properties, *Journal of Applied Polymer Science*, 102 (2006), 2285–2292
- ³²Kunaver M., Medved S., Čuk N., Jasiukaitytė E., Poljanšek I., Strnad T., Application of liquefied wood as a new particle board adhesive system, *Bioresource Technology*, 101 (2010), 1361–1368
- ³³Marra A. M., Technology of wood bonding, *Principles in Practice*, Van Nostrand Reinhold, New York 1992, 89
- ³⁴Eom Y. G., Kim, S., Baek I.-C., Kim, H.-J. Comparison of Formaldehyde Emission of Wood-Based Panels With Different Adhesive-hardener Combinations by Gas Chromatography and Standard Methods, *Mokchae Konghak*, 33 (2005), 29–39

POLY(STYRENE-CO-DIVINYLBENZENE-CO-2-ETHYLHEXYL)ACRYLATE MEMBRANES WITH INTERCONNECTED MACROPOROUS STRUCTURE

POLI(STIREN-KO-DIVINILBENZEN-KO-2-ETILHEKSIL)AKRILATNE MEMBRANE S POVEZANO POROZNO STRUKTURO

Urška Sevšek¹, Silvo Seifried¹, Črtomir Stropnik¹, Irena Pulko^{2,3}, Peter Krajnc^{1,3}

¹University of Maribor, Faculty of Chemistry and Chemical Engineering, Smetanova 17, Maribor, Slovenia

²Polymer Technology College, Pod gradom 4, Slovenj Gradec, Slovenia

³Centre of Excellence PoliMaT, Tehnološki park 24, Ljubljana, Slovenia
peter.krajnc@uni-mb.si

Prejem rokopisa – received: 2011-02-15; sprejem za objavo – accepted for publication: 2011-03-28

A combination of doctor blading and emulsion templating was used to prepare macroporous poly(styrene-co-divinylbenzene-co-2-ethylhexylacrylate) and poly(styrene-co-divinylbenzene) membranes with an interconnected porous structure. Water in oil high internal phase emulsions including monomers in the oil phase were cast onto a glass plate and polymerised at elevated temperature. After purification porous polyHIPE membranes were obtained. The volume ratio of aqueous phase (75 % or 85 %) and the molar ratio of divinylbenzene (2 % or 4 %) were varied, while the addition of chlorobenzene to the oil phase influenced the viscosity of the emulsions. A comonomer, 2-ethylhexylacrylate substantially improved the flexibility of the membranes. All yielding membranes were characterized by measuring their cast thicknesses and flow densities for deionised water. Scanning electron microscopy was used to study the morphological features of the membranes.

Keywords: membranes, porous polymers, polyHIPE, emulsions

Za pripravo makroporoznih poli(stiren-ko-divinilbenzen-ko-2-etilheksil)akrilatnih in poli(stiren-ko-divinil)benzenskih membran z odprto porozno strukturo smo uporabili kombinacijo nanosa z nožem in emulzij. Emulzije tipa voda v olju z visokim deležem notranje faze, z monomeri v oljni fazi smo nanесли na stekleno ploščo in polimerizirali pri povišani temperaturi. Po čiščenju smo pridobili porozne poliHIPE-membrane. Variirali smo volumski delež vodne faze (75 % ali 85 %) in molski delež divinilbenzena (2 % ali 4 %), medtem ko je dodajanje klorobenzena v oljno fazo vplivalo na viskoznost emulzije. Z dodatkom komonomera, 2-etilheksil akrilata so se elastične lastnosti membran bistveno izboljšale. Dobljene membrane smo okarakterizirali z merjenjem njihove končne debeline in merjenjem njihove pretočnosti za deionizirano vodo. Elektronsko vrstično mikroskopijo smo uporabili za studij morfoloških lastnosti membran.

Ključne besede: membrane, porozni polimeri, poliHIPE, emulzije

1 INTRODUCTION

Macroporous polymers with interconnected porous structure can be prepared by polymerising the continuous phase of a high internal phase emulsion. The most common definition of a high internal phase emulsion describes it as an emulsion where the volume fraction of the internal phase is very high, normally higher than 74 % (figure representing the maximum occupiable space by uniform spheres).¹ Polymers of this type are referred to as polyHIPEs.² Typically, hierarchically porous structure is obtained, with larger pores (referred to as cavities or voids) as the result of internal phase droplets and smaller connecting pores as a result of polymer shrinkage during the polymerisation. The most studied polyHIPE system is the styrene/divinylbenzene class material. Hydrophilic polyHIPE materials can also be prepared from HIPE emulsions.^{3,4} Cooper *et. al* described the preparation of a number of polyHIPE materials using supercritical CO₂ in water (C/W) HIPE emulsions.⁵ Other polyHIPE materials that have been investigated include those prepared from urea and

formaldehyde.⁶ Monolithic polyHIPE materials from glycidyl methacrylate have also been described.^{7,8} PolyHIPE material is suitable for a variety of applications, such as solid phase organic synthesis, separation of biomacromolecules, biocatalyst supports, water purification, sensors material, filtration, etc.⁹ Due to relative simplicity of high internal phase emulsion preparation (although the issue of stability is frequently problematic) and its liquid form, a wide range of shapes and sizes of these porous materials can be prepared. It has been found that the nature of the mould substrate against which the polyHIPE material is prepared has a profound influence on its surface morphology and the degree of adhesion to the mould.¹⁰ The influence of the substrate on the morphology of polyHIPE material is significant but not yet completely understood.^{10,11} Problems with HIPE stability were encountered when using PVC as a mould substrate, which could be due to leaching of plasticizer. Even samples that did form tended to adhere to the substrate. Polypropylene did not result in adhesion, however, the surfaces polymerised against the substrate were largely of a closed-cell structure. This is probably

due to the presence of a surface film of monomer, caused by localised HIPE collapse at the HIPE-substrate interface. Different applications of polyHIPE materials require different materials properties, such as physical, mechanical, thermal, etc. Therefore good control over properties is desirable. One of these properties is elasticity. In order to increase flexibility, hydrophobic monomers, that produce low T_g polymers, such as 2-ethylhexylacrylate (EHA) and *n*-butyl acrylate (BA) are normally used.¹² In the case of using 2-ethylhexylacrylate, the lowering of T_g is the result of integration of the flexible 2-ethylhexylacrylate units into the polymer structure. The hydrophobicity of the plasticizing monomer ensures that emulsion stability is not compromised. Another very important characteristic of porous polyHIPE materials is their pore size. The average pore size can vary from about 1 μm to over 100 μm . It was noticed that increasing the DVB content in a styrene/DVB polyHIPE, from 0 % to 100 % DVB, caused a significant decrease in average void diameter from 15 μm to 5 μm .¹³

Most polyHIPE materials are prepared in a monolithic form following the shape of the mould. Thin films can be advantageous for numerous applications and in the case of polyHIPE membranes flexible mechanical properties are especially important. Furthermore, surface morphology is crucial for the performance of polyHIPE membranes.

In this paper, the preparation of styrene/divinylbenzene/ethylhexyl acrylate based polyHIPE membranes and the influence of monomer mixture, film thickness and added porogenic solvent on the morphology, is described.

2 EXPERIMENTAL

2.1 Materials and methods

Styrene (Merck), divinylbenzene (DVB, 80 %, tech.; Aldrich), 2-ethylhexylacrylate (EHA; Aldrich, 98 %) were purified by passing through basic alumina (Al_2O_3 ; Aldrich) to remove the inhibitors. Sorbitan monooleate (Span 80; Aldrich), chlorobenzene (CB; Aldrich), calcium chloride hexahydrate ($\text{CaCl}_2 \times 6\text{H}_2\text{O}$; Merck), potassium persulphate (KPS; Fluka) were used as received.

Thicknesses of membranes were measured with MINIMER HD1 (Seltron), which is used for measurement of nonmagnetic coatings with accuracy 1 μm . Fluidity was measured with an ultrafiltration test cell AMICON, model 8400. Scanning electron micrographs were recorded on a Philips FEI XL30 ESEM.

2.2 Preparation of high internal phase emulsions and membranes

In a typical experiment, styrene, divinylbenzene and Span 80, 2-ethylhexylacrylate or chlorobenzene were placed in a 250 mL 3-neck round bottomed flask, and the mixture was stirred at 300 r/min with a glass stirring rod

fitted with a D-shaped polytetrafluoroethylene paddle, connected to an overhead stirrer motor. The aqueous phase was then added dropwise to the organic solution with continuous stirring. Once all the aqueous solution had been added, stirring was continued for further 30 min at 300 r/min to yield HIPEs. Both phases were degassed prior to use.

To prepare membranes, a doctor blade (slit 500 μm or 600 μm) was used to spread the HIPE emulsion onto a polished glass substrate ((300 \times 300 \times 15) mm). The spread of the emulsion was carefully covered with another glass plate ((300 \times 280 \times 3) mm) and heated to 60 $^\circ\text{C}$ for 24 h. After polymerisation, membranes were carefully retrieved from glass substrate, washed with deionised water and ethanol (both for 24 h) and then dried.

3 RESULTS AND DISCUSSION

Various methods can be used for the preparation of thin films of emulsions. With regards to polyHIPE membrane applications, the preparation method should be efficient and should offer the control of film thickness. Casting the emulsion onto a substrate using a doctor blade has already been demonstrated as an appropriate preparation procedure.¹⁴ Doctor blades with different slits can be used to obtain films with various thicknesses.

Precursor emulsions with volume ratio of internal phase to continuous phase 7.5 to 2.5 and 8.5 to 1.5 were stabilised by sorbitan monooleate (Span 80, hydrophilicity lipophilicity balance number 4.3). Span 80 is a standard surfactant used for numerous water in oil high internal phase emulsions where hydrophobic monomers are used in the continuous phase and the amount of surfactant necessary for obtaining open porous structure is around mass fraction 20 % with regards to the continuous phase.¹⁵ Emulsions A1, A2, A3 and A4 (**Table 1**) were prepared in that way, using mole fractions 2 % or 4 % of divinylbenzene in the continuous phase for cross-linking the styrenic chains. In our previous work, we have shown that higher degree of crosslinking reduces the flexibility of polymerised films to a degree that wrapping of membranes around a centimeter tube was not possible.¹² The casting of emulsions was done using a doctor blade on a polished glass substrate and it was found that a second glass plate was needed for retaining the emulsion stability until polymerisation. Generally, when preparing membranes from solution using doctor blading and subsequent polymer precipitation^{16,17}, the thickness of the resulting polymer membrane was close to the slit opening of the doctor blade used. In our work this was not the case and the resulting membranes were substantially thinner than the slit of the blade (**Table 2**). The explanation for this phenomenon lies probably in the viscous nature of the high internal phase emulsions. Since the shrinkage of polyHIPE with regards to precur-

Table 1: Preparation data for polyHIPE membranes

Tabela 1: Podatki za pripravo poliHIPE-membran

Membrane	$PV^a/\%$	$X_{DVB}^b/\%$	$X_{EHA}^c/\%$	$\phi(\text{porogen})/\%$	$V(\text{AP})^d/$	$V(\text{OP})^e/$	$V(\text{STY})/$	$V(\text{DVB})/$	$V(\text{EHA})/$	$V(\text{CB})/$
					mL	mL	mL	mL	mL	mL
A1	75	2	0	0	12.1	4.87	3.91	0.13	0	0
A2	85	2	0	0	22.86	4.87	3.91	0.13	0	0
A3	75	4	0	0	12.18	4.81	3.81	0.25	0	0
A4	85	4	0	0	23	4.81	3.81	0.25	0	0
B1	75	2	10	0	13.08	5.16	3.51	0.13	0.73	0
B2	85	2	10	0	24.71	5.16	3.51	0.13	0.73	0
B3	75	4	10	0	13.16	5.19	3.41	0.25	0.73	0
B4	75	2	20	0	14.06	5.54	3.11	0.13	1.45	0
B5	85	2	20	0	26.56	5.54	3.11	0.13	1.45	0
B6	75	4	20	0	14.14	5.57	3.01	0.25	1.45	0
B7	75	2	30	0	15.04	5.93	2.71	0.13	2.18	0
B8	75	4	30	0	15.11	5.96	2.61	0.25	2.18	0
B9	85	2	30	0	28.41	5.93	2.71	0.13	2.18	0
C1	75	2	0	5	12.1	4.98	3.91	0.13	0	0.2
C2	75	4	0	15	12.18	5.42	3.81	0.25	0	0.61
C3	85	2	0	40	22.86	6.39	3.91	0.13	0	1.61
C4	85	4	0	50	23	6.84	3.81	0.25	0	2.03

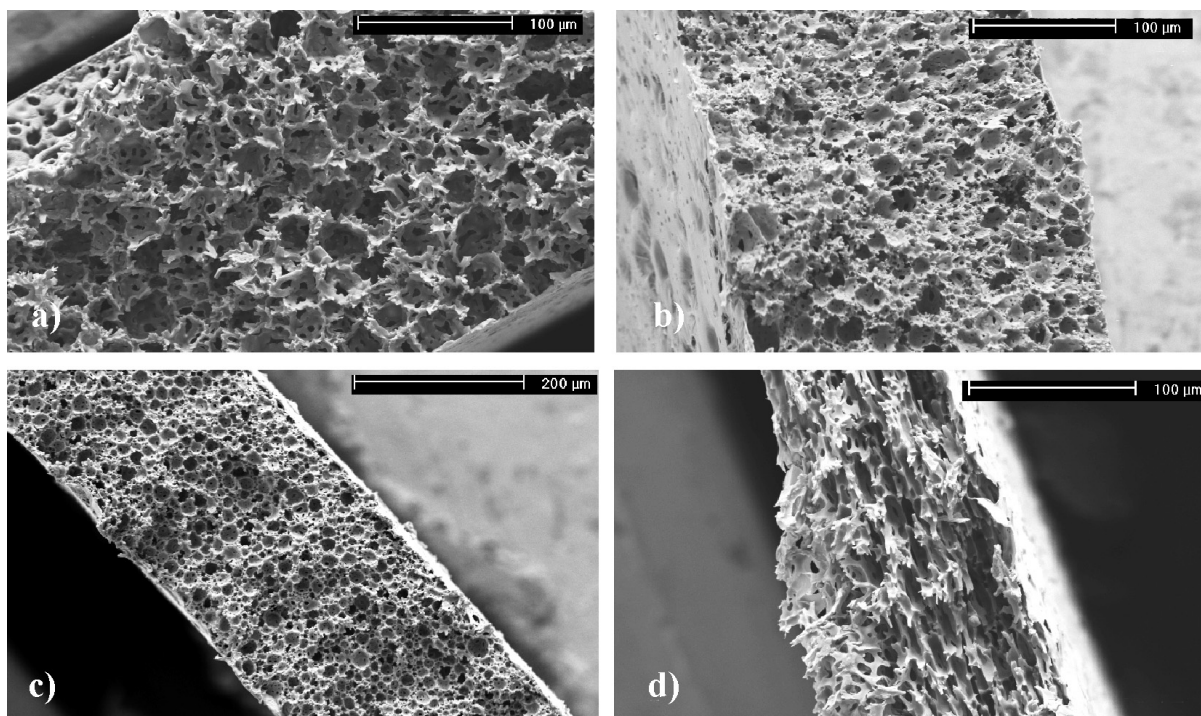
^a pore volume (volume fraction of internal phase), ^b % mol of DVB, ^c % mol of 2-ethylhexylacrylate, ^d aqueous phase, ^e oil phase

Table 2: Thicknesses of membranes

Tabela 2: Debeline membran

Sample	A1	A2	A3	A4	B1	B2	B3	B4	B5	B6	B7	B8	B9	C1	C2	C3	C4
$D^a/\mu\text{m}$	500	500	500	500	600	600	600	600	600	600	600	600	600	500	500	500	500
$\bar{d}^b/\mu\text{m}$	231.5	253.6	174.7	286	380	397	344	305	407	403	223	251	115	78.3	162.2	174.4	340

^a slit opening on doctor blade, ^b average thickness of membrane


Figure 1: SEM images of the membranes A1 (a), B4 (b), B7 (c) and C1 (d)

Slika 1: SEM-posnetki membran A1 (a), B4 (b), B7 (c) in C1 (d)

sor emulsion is usually less than 10% (established from our work on monolithic polyHIPEs), we believe that the lower thicknesses of the resulting membranes are due to the thickness of the spread itself rather than subsequent shrinkage. However, a slight influence of emulsion composition on the final membrane thickness was also observed. Membranes A1 and A2 (same monomer composition, A1 with 75 % internal phase, A2 with 85 % internal phase) show a trend of increasing thickness with increasing pore volume. The same is true for membranes A3 and A4 and for the membranes including ethylhexyl acrylate (B1-B9). The reason again might be in different viscosity of emulsions with different phase volume ratios. Further experiments will however be needed to clarify this trend.

With regards to producing membranes with increased elasticity in order to meet the criteria of flexible films, a plasticizing comonomer, ethylhexyl acrylate (membranes B1-B9) was added to the oil phase of the emulsions. Visually, the emulsion stability was not compromised, using the same surfactant type and amount. The same can be concluded from SEM images (**Figure 1, b and c**). Together with a lower amount of crosslinking, the inclusion of EHA resulted in elastic membranes that could be easily wrapped around a one centimeter diame-

ter tube. However, permeability results have shown that a high degree of EHA content increases back pressure of the membranes so a compromise in mechanical and permeable characteristics needs to be reached with a specific application in mind.

Scanning electron microscopy inspection of cross sections of membranes (**Figure 1**) revealed open porous structure in all cases. Larger pores, in diameter ranging from 18 μm (B4) to 32 μm (A1), are connected by a series of interconnecting smaller pores. The size of the bigger pores reflects the emulsion preparation and kinetic stability since the creation of large pores is the consequence of non monomer containing droplet phase and the size of the droplets guides the pore size. As we can see from **Table 3**, membrane B7 with the highest share of 2-ethylhexylacrylate has the least opened structure. We believe the reason for this is the stabilizing effect of this hydrophobic monomer on the emulsion. FTIR spectroscopy of membranes (typical examples shown in **Figure 2**) confirm the inclusion of 2-ethylhexylacrylate in the polymer matrix in the case of B samples. The signal at 1729 cm^{-1} represents the carbonyl group of acrylate ester and this signal is not present in the spectra of samples A and C which do not include 2-ethylhexylacrylate.

When comparing polyHIPE membranes to polyHIPE monoliths, more attention in the case of membranes has to be devoted to the surface since there is no possibility of removing a layer prior to application. The importance of casting substrate for open surface of polyHIPE membranes has already been demonstrated.⁸ Images of membrane surfaces, in most cases, show the open

Table 3: Pore size data

Tabela 3: Velikosti por

	A1	B4	B7	C1
$\overline{D}^a/\mu\text{m}$	31.6	18.3	21.1	22.0
$\overline{d}^b/\mu\text{m}$	9.6	7.0	5.2	7.7
$(\overline{d}/\overline{D})$	0.30	0.38	0.24	0.34

^a average pore diameter, ^b average interconnecting pore diameter; both determined from SEM images

Table 4: Permeability of the membranes for deionised water

Tabela 4: Propustnosti membran za deionizirano vodo

sample	p/bar	J ($\text{kg}/\text{m}^2 \text{ h}$)	sample	p/bar	J ($\text{kg}/\text{m}^2 \text{ h}$)
A1	0.5	36.9	B4	0.5	2.9
	1	54.7		1	2.9
	2	64.1		2	5.7
A2	0.5	25.25	B6	0.5	0.8
	1	30.00		1	1.0
	2	48.87		2	1.9
A4	0.5	87.1	B7	0.5	4.75
	1	66.8		1	6.79
	2	95.7		2	7.74
B1	0.5	32.6	B8	0.5	0.8
	1	468		1	0.8
	2	550		2	0.8
B2	0.5	36.2	B9	0.5	-
	1	48.2		1	4.8
	2	64.2		2	6.8
B3	0.5	3.8	C4	0.5	117.4
	1	4.9		1	127.9
	2	16.7		2	138.2

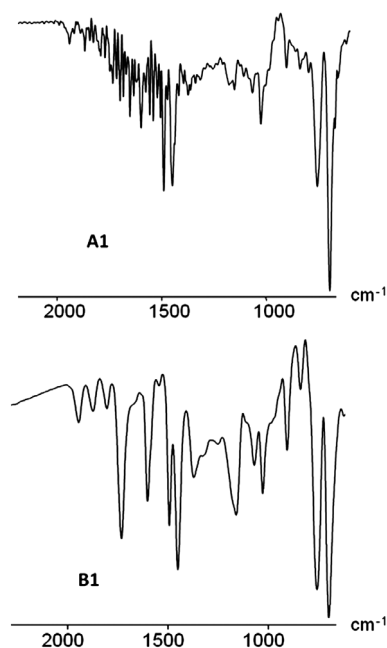


Figure 2: FTIR spectra of membranes A1 (no 2-ethylhexylacrylate) and B1 (10% 2-ethylhexylacrylate)

Slika 2: FTIR-spektra membran A1 (brez 2-etilheksil akrilata) in B1 (10 % 2-etilheksil akrilata)

polyHIPE morphology also on the surface of the membranes. This finding is important especially for applications where convective mass transfer is preferred. The high viscosity of the emulsions was occasionally causing inhomogeneous cast on the substrate. In order to address this issue, we attempted to reduce the viscosity by the addition of an organic solvent, namely chlorobenzene (CB). Improved homogeneity of the spread was observed, especially when the share of the solvent as high as the volume fraction of 40 % (in relation to oil phase) had been used.

To characterize the permeability properties of polyHIPE membranes, the flux of deionised water through the membranes at a given pressure was measured (see **Table 4**). Membranes including ethylhexyl acrylate (B1-B9) have a lower flow density than the basic membranes (no 2-ethylhexylacrylate) and, generally, their flow density decreases with the increasing share of 2-ethylhexylacrylate. The results of flow properties are not in evident relation to pore sizes as measured from SEM images. However, the actual flow characteristics were measured from membranes immersed in water while SEM images were taken from dry samples and real "wet" morphology can differ from what is evident from SEM.

4 CONCLUSIONS

Results of this work have shown that high internal phase emulsions with internal phase volume ratio up to 85 % including styrene, divinylbenzene and ethylhexyl acrylate in the continuous phase, can be used for templating the porosity in thin polymer films. Addition of a plasticizing monomer enabled the tailoring of flexibility and did not compromise the precursor emulsion stability. Resulting membranes were between 80 μm and 407 μm thick and had an open porous

structure which enabled the flow through applications; furthermore, by changing the monomer composition, the flow could be substantially affected.

Acknowledgement

The authors acknowledge the financial support from the Ministry of Higher Education, Science and Technology of the Republic of Slovenia through the contract No. 3211-10-000057 (Centre of Excellence Polymer Materials and Technologies).

5 REFERENCES

- ¹ K. J. Lissant (ed.), *Emulsions and Emulsion Technology*, Part 1, New York 1974, Chap. 1
- ² D. Barby, Z. Haq, Eur Pat 0060138, 1982
- ³ P. Krajnc, D. Štefanec, I. Pulko, *Macromol. Rapid. Comm.*, 26 (2005), 1289–1293
- ⁴ S. Kovačič, D. Štefanec, P. Krajnc, *Macromolecules*, 40 (2007), 8056–8060
- ⁵ A. I. Cooper, *Adv. Mater.*, 15 (2003) 13, 1049–1059
- ⁶ A. R. Elmes, K. Hammond, D. C. Sherrington, Eur Pat 289238, 1988
- ⁷ P. Krajnc, N. Leber, D. Štefanec, S. Kontrec, A. Podgornik, *J. Chromatogr. A*, 1065 (2005), 1, 69–73
- ⁸ D. Cummins, P. Wyman, C. J. Duxbury, J. Thies, C. E. Koning, A. Heise, *Chem. Mater.* 19 (2007), 5285–5292
- ⁹ H. F. Zhang, A. I. Cooper, *Soft Matter*, (2005) 1, 107–113
- ¹⁰ Z. Bhungara, *Filtr. Separat.*, 32 (1995) 3, 245–251
- ¹¹ I. Pulko, P. Krajnc, *Chem. Commun.*, (2008), 4481–4483
- ¹² C. J. C. Edwards, D. P. Gregory, M. Sharples, Eur Pat 239360, 1987
- ¹³ J. M. Williams, A. J. Gray, M. H. Wilkerson, *Langmuir*, 6 (1990), 437
- ¹⁴ I. Pulko, V. Smrekar, A. Podgornik, P. Krajnc, *J. Chromatogr. A*, (2010), doi:10.1016/j.croma.2010.11.069
- ¹⁵ J. M. Williams, D. A. Wroblewski, *Langmuir*, 4 (1988), 656
- ¹⁶ N. Vogrin, Č. Stropnik, V. Musil, M. Brumen, *J. Membr. Sci.*, 207 (2002) 1, 139–141
- ¹⁷ V. Kaiser, Č. Stropnik, *Mater. Tehnol.*, 34 (2000) 3/4, 151–155

MODIFICATION OF NON-WOVEN CELLULOSE FOR MEDICAL APPLICATIONS USING NON-EQUILIBRIUM GASSIOUS PLASMA

MODIFIKACIJA CELULOZNIH KOPREN, UPORABNIH V MEDICINSKE NAMENE, Z NERAVNOVESNO PLINSKO PLAZMO

Karin Stana - Kleinschek¹, Zdenka Peršin², Tina Maver²

¹University of Maribor, Faculty of Mechanical Engineering, Laboratory for Characterisation and Processing of Polymers, Smetanova 17, SI-2000 Maribor, Slovenia

²Centre of Excellence for Polymer Materials and Technologies, Tehnološki park 24, SI-1000 Ljubljana, Slovenia
karin.stana@uni-mb.si

Prejem rokopisa – received: 2011-02-09; sprejem za objavo – accepted for publication: 2011-03-04

This paper presents the use of a non-equilibrium gaseous plasma technique for the activation of regenerated non-woven cellulose, as used in the preparation of wound-dressing materials. Plasma technology provides surface modification according to the required quality in terms of speed, homogeneity, process stability, and efficiency.

In this study the non-woven cellulose was exposed to oxygen plasma (O₂) in order to acquire the natural polymer's super-hydrophilicity which, among others, defines the materials' usability for wound-dressing. The influence of the plasma parameters on the material's hydrophilicity was studied; and the optimal plasma conditions defined. Combinations of different experimental techniques (contact angle, water retention value, and moisture content) were studied and correlated with the mechanical properties, as a function of plasma modification.

The specific adsorption capacity of the non-woven cellulose using oxygen plasma treatment was achieved. In the next step, this material with increased hydrophilicity and improved mechanical properties will be used in the preparation of multilayered wound-dressing materials for specific functionalities (incorporation of drugs, specific functional properties).

Keywords: plasma, oxygen, regenerated non-woven cellulose, super-hydrophilicity, mechanical properties

V prispevku je predstavljena uporaba neravnovesne plinske plazemske tehnike za obdelavo regeneriranih celuloznih vlaken v obliki netkanih kopren, ki se uporabljajo v materialih za oskrbo površinskih ran. Le-ta omogoča modifikacijo/funkcionalizacijo površine polimerov oz. vlaken in poleg ekološke neoporečnosti zagotavlja še zeleno kakovost tako glede hitrosti, homogenosti, stabilnosti kot tudi učinkovitosti obdelave.

Za doseganja visoke stopnje hidrofilnosti, ki med drugim določa uporabnost materialov za oskrbo ran, smo celulozne koprene obdelovali s kisikovo (O₂) plazmo ter določili njene optimalne pogoje obdelave.

Hidrofilnost oz. interakcijsko sposobnost plazemsko modificiranih kopren smo analizirali z različnimi eksperimentalnimi metodami, kot so: določanje stičnih kotov, študij navzemanja vlage ter zadrževanja vode. Analizirane so bile spremembe mehanskih lastnosti plazemsko obdelanih kopren.

Kisikova plazemska obdelava je signifikantno vplivala na povečanje hidrofilnosti oz. spremembo adsorpcijske kapacitete celuloznih kopren ob sočasnih dobrih oz. izboljšanih mehanskih lastnostih. Tako modificirani celulozni materiali se bodo v naslednji stopnji uporabili za izdelavo večslojnih visoko funkcionalnih materialov za oskrbo ran (inkorporacija učinkovin, specifičnih funkcionalnih lastnosti).

Ključne besede: plazma, kisik, regenerirana celulozna koprena, superhidrofilnost, mehanske lastnosti

1 INTRODUCTION

Several different materials are used for medicinal products in wound-treatment and healing. By considering their composition and purpose, we can divide them roughly into three groups. The first comprises materials and products for the prevention of secondary infections¹⁻⁴, materials assuring restoration and regulation of suitable micro- and macro- environments for wound-healing are considered to be in the second group,⁵⁻⁷ whilst all materials used for the mitigation of patient trauma due to the acquired surface wounds or their healing, belong the third group.⁸⁻¹³

Cellulose and its derivatives are very often used as a functional part of different wound-dressing materials (in different forms i.e. fibres, non-woven materials, hydro-

gels ...). Cellulose fibres' crystalline/amorphous microfibrillar structure (two-phase model) control the accessibility of the surface, as well as those bulk polar groups responsible for fibres' hydrophilicity, an important material characteristic which, amongst others, influences the wound-healing process.

Wound-healing is a physiologic process involving a series of stages: hemostasis, inflammation, proliferation with repair and remodelling. The warm, moist micro-environment created within the wound is essential for further stages of healing.¹⁴ In the stage of re-epithelisation, new keratinocytes must migrate onto the repair site. Migration requires a fluid environment and this is why the hydrophilicity of the material, as used in the wound-dressing, is one of the more important agents.¹⁵

Characteristically different chemical approaches, i.e. bleaching, treatment with alkali, are used for achieving this.¹⁶ Thermodynamically non-equilibrium physical processes, such as the use of gaseous plasma, promise the most,⁷⁻²¹ as alternative to the usual chemical reactions. The advantages of gaseous plasma such as its ecological integrity and homogenous surface treatment far outweigh the minor negative influences on the materials' mechanical properties. It has a vast variety of possibly acquired final applications,²²⁻²³ the more often used being cleaning or etching,²⁴⁻²⁶ sterilization,²⁷⁻²⁸ functionalization,²⁹⁻³⁸ and polymerization.³⁹⁻⁴⁰

This paper studies the effects of non-equilibrium oxygen plasma for the modification of regenerated non-woven cellulose. The desired final characteristics are super-hydrophilicity, specific interaction along with non-altered mechanical properties.

2 EXPERIMENTAL PART

2.1 Materials

Regenerated cellulose fibre was studied in its non-woven form, i.e. viscose (CV), as produced by KEMEX, The Netherlands. The surface mass of the fabrics was 175 g/m². Some construction parameters, important for the sorption capacity, were studied, and are presented in **Table 1**.

Table 1: Construction parameters of the non-woven cellulose sample
Tabela 1: Konstrukcijski parametri celuloznih netkanih kopren

Sample	air permeability* (L/m ² s)	thickness ** (mm)
Viscose	650	1.7

*DIN53 887 **SIST ISO 5084

2.2 Treatment procedures

The samples were vacuum dried (vacuum oven type VS-50SC Kambič; $T = 20$ °C, $P = 100$ mbar, $t = 24$ h) before plasma treatment. Then the samples were exposed to gaseous plasma within a discharge chamber. The discharge chamber was a spherical cylinder with an inner diameter of 36 cm, and positioned as an integral part of a vacuum system pumped using two-stage oil rotary pump. The plasma was excited with a radiofrequency generator

operating at 27.12 MHz, and a power of about 1 kW. The plasma created by such a generator is a source of excited particles including neutral oxygen atoms in the ground state, excited oxygen atoms and molecules, as well as positively and negatively-charged ions. Such particles are determined by various techniques including electrical and catalytic probes, titration, laser absorption fluorescence, and mass spectrometry.⁴¹⁻⁵¹

In order to find the best/optimal conditions for the plasma modification process, several discharge parameters were varied: sample shape and dimension (fibres, fabric; spherical, square), generator power of the plasma system (between 100 W and 1000 W), frequency of the plasma system (12.56 or 27.12 MHz, DC), gas flow and pressure, and the activation time (1 s to 15 min).

The optimal conditions used for the regenerated cellulose samples' treatment using plasma modification, are summarised in **Table 2**.

2.3 Methods

Hydrophilic/hydrophobic properties determination

a) Water contact angle

The hydrophilic/hydrophobic character was studied by contact angle measurements between polymer material samples and water. The powder contact angle method was used as developed for determining the wetting properties of porous materials. The samples were cut into (2 × 5) cm rectangular pieces and suspended in a special sample holder of a Krüss K12 processor Tensiometer. Immediately before measurement, the container with the liquid (n-heptane; water) was raised until the sample edge touched the liquid surface.

The samples' mass (m) changes, as a function of time (t) during the water adsorption phase, was monitored. The initial slope of the function $m^2 = f(t)$ is known as the capillary velocity, from which the contact angle between the solid (polymer sample) and the water was calculated using a modified Washburn equation:⁵²

$$\cos \theta = \frac{m^2}{t} \frac{\eta}{\rho^2 \cdot \gamma \cdot c} \quad (1)$$

where θ is the contact angle between the solid and liquid phases, m^2/t is the capillary velocity, η is the liquid

Table 2: Optimal oxygen plasma conditions used for the modification of non-woven cellulose. ν – frequency of RF plasma generator; p – oxygen pressure; n_i – density of ions; n_a – density of neutral atoms; T_e – electron temperature, t – activation time

Tabela 2: Optimalni parametri plazemske obdelave celuloznih netkanih kopren. ν – frekvenca RF plazemskega generatorja; p – tlak dovedenega kisika; n_i – gostota ionov; n_a – gostota nevtralnih atomov; T_e – temperatura elektronov; t – čas obdelave

Sample		Plasma treatment Oxygen gas			
Shape	Dimension	Power	Frequency	Plasma parameters	Activation time
non-woven	(22 × 22) cm	500 W	N = 27.12 MHz	$p = 75$ Pa $n_i = 10^{15}$ m ⁻³ $n_a = 10^{21}$ m ⁻³ $T_e = 3$ eV	$t = 10$ min

viscosity, ρ is the liquid density, γ is the surface tension of the liquid, and c is a material constant.

The constant c was determined for each sample from contact angle measurements using n-heptane, for which the contact angle on the non-woven was zero and $\eta = 0.4$ mPa s, $\rho = 0.6836$ g/cm³, $\gamma = 20.4$ mN/m. The results were statistically processed (a set of parallel measurements until the standard deviation was less than 2°) and represent the average value of ten measurements of the water contact angle.

For more detailed description of this experimental procedure, see Persin et al.⁵³ and Fras Zemljic et al.⁵⁴⁻⁵⁵

b) Water retention value

The water retention value of the porous polymer material was determined according to standard DIN 53 814. This method is based on determining the quantity of water that the sample can absorb and retain, under strictly controlled conditions. This property is expressed as a ratio between the mass of water retained in the sample after soaking (2 h) and centrifuging (20 min), and the mass of an absolute dry sample ($T = 105$ °C, $t = 4$ h).

c) Moisture content

The moisture content of the porous polymer material was analysed using a Halogen Moisture Analyser. This was done using the thermo gravimetric principle: the samples' weight was measured before and after heating.

Mechanical properties' determination

The tensile properties of fabrics were determined according to standard SIST ISO 13934-1.

The maximum force and elongation at maximum force i.e. at the moment of the samples' tear, was determined, using the strip method.

3 RESULTS

Hydrophilic/hydrophobic properties

Figure 1 presents the square of the adsorbed mass versus time for non-treated and oxygen plasma treated

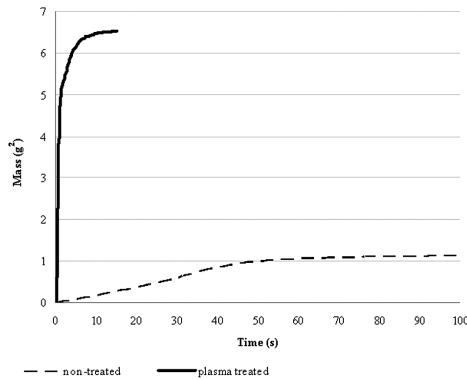


Figure 1: Capillary velocities of non-treated and oxygen plasma treated regenerated non-woven cellulose sample

Slika 1: Kapilarne hitrosti neobdelanih in s kisikovo plazmo obdelanih celuloznih netkanjih kopren

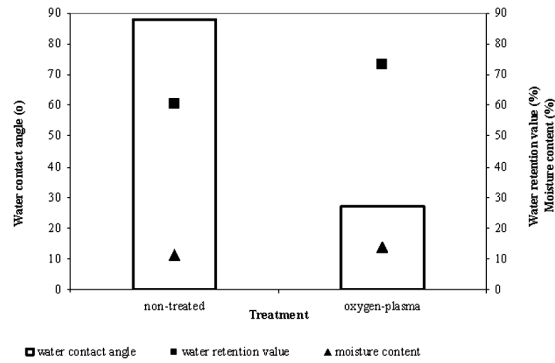


Figure 2: Hydrophilic/hydrophobic properties of a non-treated and oxygen plasma treated regenerated non-woven cellulose sample

Slika 2: Hidrofilno/hidrofobne lastnosti neobdelanih in s kisikovo plazmo obdelanih celuloznih netkanjih kopren

samples. The slopes of these capillary velocities curves characterise the rate of water sorption.

The non-treated material adsorbed the water very slow. The slope even in 100 s did not reach the plateau, respectively the non-treated material was not completely wetted by the water. Within 100 s, the non-treated sample was able to absorb 1.1 g of water. The capillary velocity by the plasma treated samples was faster. After 15 s the sample was complete wetted and was able to adsorb 2.6 g of water.

Water contact angles were calculated using equation (1). The average results for the water contact angles, water retention values, and moisture content on the non-treated and oxygen plasma treated regenerated cellulose sample, are given in **Figure 2**.

The significant effect of oxygen plasma modification resulted in enhanced non-woven wettability. The water contact angle decrease by 69 % followed by simultaneous increase in water retention value (21 % improvement) and an increase in moisture content (22 %).

Mechanical properties

The tensile properties determined as breaking force and elongations, are given in **Table 3**.

Table 3: Breaking force and elongation of non-treated and oxygen plasma treated non-woven cellulose

Tabela 3: Pretržna sila in raztezek neobdelanih in s kisikovo plazmo obdelanih celuloznih netkanjih kopren

Sample treatment	Mechanical properties			
	Breaking force (N)		Elongation (%)	
	horizontal	longitudinal	horizontal	longitudinal
non-treated	54.8 ±6.5	117.6 ±4.7	41 ±2.5	62.2 ±1.2
plasma treated	87.4 ±11.4	204.9 ±25.0	22.2 ±1.1	48.1 ±0.6

Plasma treatment also affects the samples' tensile properties. The breaking force, as measured in both directions, significantly increased (by 50 % horizontally and by 74 % longitudinally). Elongation in both direc-

tions decreased but the effect was smaller (i.e. by 46 % horizontally and 23 % longitudinally).

4 DISCUSSION

Applied oxygen plasma treatment significantly improved the non-woven cellulose sorption capacity – wettability. Surface modification resulted in the removal or oxidation of contaminants on the surface,⁵⁵ and increased the amount of surface polar carboxyl groups.^{56–58} Thus, the plasma treatment resulted in a significantly water contact angle decrease (see **Figure 1**). Longer activation time (i.e. 10 min; see **Table 2**) also caused some morphological changes in the bulk. Therefore, the modified samples were able to retain larger amounts of water, which remained in the porous structures even after the applied mechanical stress. These changes are also responsible for moisture content increase.

Oxygen plasma treatment also improved the tensile properties. The significant increase in the breaking force after plasma treatment was caused by the decreased elongation. Low-temperature O₂ treatment caused etching and ablation action on the surface substrate, resulting in a roughening effect on the fabric surface. The rougher surface may have imparted more contact points within the non-woven fibres, resulting in enhanced fibre friction. The increased friction produces a great cohesive force between the fibres. The used plasma treatment reduced the elongation of the material. This can be explained by the increased interaction between fibres in the non-woven, after plasma treatment. This caused a reduction in the effective gap between the fibres placed in longitudinal and horizontal directions, at their crossover points, and the lateral-compressional abilities of the fibres in the non-woven, leading to a reduction in the extensibility.

5 CONCLUSION

Used optimised oxygen plasma treatment proved to be an excellent tool for the surface, as well as for the bulk modification, of regenerated non-woven cellulose material. The wettability of the non-woven was drastically improved (decreased water contact angle by simultaneously increased water adsorption capacity). The changes in morphology were, besides the improvement in wettability, responsible for the better mechanical bonding in the used non-woven. In this way the cellulose material had been functionalised without changes in their mechanical properties.

We have shown that the oxygen plasma modification of regenerated cellulose samples in non-woven form, potentially offers a flexible and environmentally friendly activation process in order to obtain super-hydrophilic matrices. Such functionalised super – hydrophilic regenerated non-woven cellulose could be used as a functional layer in wound-dressing materials and could,

among others, contribute to a better surface wound-healing process.

Acknowledgement

The authors acknowledge the financial support from the Ministry of Higher Education, Science and Technology of the Republic of Slovenia through the contract No. 3211-10-000057 (Center of Excellence Polymer Materials and Technologies).

6 REFERENCES

- J. Bikowski, *Journal of Emergency Medicine*, 17 (1999), 197–206
- L. J. Eron, *Journal of Emergency Medicine*, 17 (1999), 189–195
- A. Ferguson, *Accident and Emergency Nursing*, 1 (1993), 79–86
- P. W. Greenwald, D. D. Schaible, J. V. Ruzich, S. J. Prince, A. J. Birnbaum, P. E. Bijur, *Journal of Emergency Medicine*, 23 (2002), 333–335
- D. R. Knighton, V. D. Fiegel, G. D. Phillips, *Clinical Materials*, 8 (1991), 229–241
- P. Bao, A. Kodra, M. Tomic–Canic, M. S. Golinko, H. P. Ehrlich, H. Brem, *Journal of Surgical Research*, 153 (2009), 347–358
- D. G. Greenhalgh, *The International Journal of Biochemistry & Cell Biology*, 30 (1998), 1019–1030
- N. C. Belloq, D. W. Kang, X. Wang, G. S. Jensen, S. H. Pun, T. Schlupe, M. L. Zepeda, M. E. Davis, *Bioconjugate Chemistry*, 15 (2004), 1201–1211
- M. Caldorera–Mooreand, N. A. Peppas, *Advanced Drug Delivery Reviews*, 61 (2009), 1391–1401
- J. J. Elsnerand, M. Zilberman, *Acta Biomaterialia*, 5 (2009), 2872–2883
- K. E. Fischer, B. J. Alemán, S. L. Tao, R. H. Daniels, E. M. Li, M. D. Bünger, G. Nagaraj, P. Singh, A. Zettl, T. A. Desai, *Nano Letters*, 9 (2009), 716–720
- E. M. Martín del Valle, M. A. Gala'n, R. G. Carbonell, *Industrial & Engineering Chemistry Research*, 48 (2009), 2475–2486
- H. Ueno, T. Mori, T. Fujinaga, *Advanced Drug Delivery Reviews*, 52 (2001), 105–115
- F. Strodbeck, *Newborn and Infant Nursing Reviews*, 1 (2001) 1, 43–52
- M. D. Kerstein, *Adv Wound Care*, 10 (1997), 30–36
- M. Lewin, S. B. Sello, *Chemical processing of fibres and fabrics: Fundamentals and preparation*, Part B, Marcel Dekker Inc., New York 1983, pp. 91–256
- A. Vesel, M. Mozetic, A. Hladnik, J. Dolenc, J. Zule, S. Milosevic, N. Krstulovic, M. Klanjssek–Gunde, N. Hauptman, *J. Phys. D: Appl. Phys.*, 40 (2007) 12, 3689–3696
- A. Vesel, *Surf. Coat. Technol.*, 205 (2010) 2, 490–497
- I. Junkar, U. Cvelbar, A. Vesel, N. Hauptman, M. Mozetic, *Plasma Processes Polym.*, 6 (2009) 10, 667–675
- A. Asadinezhad, I. Novak, M. Lehocky, V. Sedlarik, A. Vesel, I. Junkar, P. Saha, I. Chodak, *Plasma Processes Polym.*, 7 (2010) 6, 504–514
- N. Krstulovic, I. Labazan, S. Milosevic, U. Cvelbar, A. Vesel, M. Mozetic, *J. Phys. D: Appl. Phys.*, 39 (2006) 17, 3799–3804
- A. Holländer, J. Thome, M. Keusgen, I. Degener, W. Klein, *Applied Surface Science*, 235 (2004), 145–150
- M. C. Coen, R. Lehmann, P. Groening, L. Schlapbach, *Applied Surface Science* 207 (2003), 276–286
- R. Kulcar, M. Friskovec, N. Hauptman, A. Vesel, M. Klanjssek – Gunde, *Dyes Pigm.*, 86 (2010) 3, 271–277

- ²⁵ A. Drenik, A. Vesel, M. Mozetič, J. Nucl. Mater., 386–388 (2009), 893–895
- ²⁶ A. Vesel, M. Mozetic, A. Drenik, S. Milosevic, N. Krstulovic, M. Balat-Pichelin, I. Poberaj, D. Babic, Plasma Chem. Plasma P., 26 (2006), 577–584
- ²⁷ D. Vujosevic, Z. Vratnica, A. Vesel, U. Cvelbar, M. Mozetic, A. Drenik, T. Mozetic, M. Klanjsek-Gunde, N. Hauptman, Mater. Tehnol., 40 (2006) 6, 227–232
- ²⁸ K. Elersic, I. Junkar, A. Spes, N. Hauptman, M. Klanjsek Gunde, A. Vesel, Mater. Tehnol., 44 (2010) 3, 153–156
- ²⁹ U. Cvelbar, M. Mozetic, I. Junkar, A. Vesel, J. Kovac, A. Drenik, T. Vrlinic, N. Hauptman, M. Klanjsek-Gunde, B. Markoli, N. Krstulovic, S. Milosevic, F. Gaboriau, T. Belmonte, Appl. Surf. Sci., 253 (2007) 21, 8669–8673
- ³⁰ T. Vrlinic, A. Vesel, U. Cvelbar, M. Krajnc, M. Mozetic, Surf. Interface Anal., 39 (2007) 6, 476–481
- ³¹ A. Vesel, M. Mozetic, A. Zalar, Surf. Interface Anal., 40 (2008) 3–4, 661–663
- ³² A. Vesel, I. Junkar, U. Cvelbar, J. Kovac, M. Mozetic, Surf. Interface Anal., 40 (2008) 11, 1444–1453
- ³³ A. Vesel, M. Mozetic, A. Zalar, Vacuum, 82 (2008) 2, 248–251
- ³⁴ M. Sowe, I. Novak, A. Vesel, I. Junkar, M. Lehocky, P. Saha, I. Chodak, Int. J. Polym. Anal. Ch., 14 (2009) 7, 641–651
- ³⁵ A. Vesel, Inf. MIDEM, 38 (2009), 257–265
- ³⁶ A. Asadinezhad, I. Novak, M. Lehocky, F. Bilek, A. Vesel, I. Junkar, P. Saha, A. Popelka, Molecules, 15 (2010), 2, 1007–1027
- ³⁷ A. Vesel, K. Elersic, I. Junkar, B. Malic, Mater. Tehnol., 43 (2009) 6, 323–326.
- ³⁸ A. Asadinezhad, I. Novak, M. Lehocky, V. Sedlarik, A. Vesel, P. Saha, I. Chodak, Colloids Surf. B Biointerfaces, 77 (2010) 2, 246–256
- ³⁹ A. Bogaerts, E. Neyts, R. Gijbels, J. van der Mullen, Spectrochimica Acta Part B, 57 (2002), 609–658
- ⁴⁰ R. Shishoo, Plasma technologies for textiles, Woodhead publishing limited, Cambridge England, 2007, p. 129, 202
- ⁴¹ F. Breclj, M. Mozetič, K. Zupan, M. Drobnic, Vacuum, 44 (1993), 459–460
- ⁴² M. Mozetič, A. Zalar, Appl. Surf. Sci., 158 (2000), 263–267
- ⁴³ D. Babič, I. Poberaj, M. Mozetič, Rev. Sci. Instrum., 72 (2001), 4110–4114
- ⁴⁴ A. Ricard, A. Vesel, M. Mozetič, Surf. Coat. Technol., 142 (2001), 333–336
- ⁴⁵ A. Vesel, M. Mozetič, Vacuum, 61 (2001), 373–377
- ⁴⁶ I. Poberaj, M. Mozetič, D. Babič, Vac. Surf. Films, 20 (2002), 189–193
- ⁴⁷ M. Mozetič, A. Ricard, D. Babič, I. Poberaj, J. Levaton, V. Monna, U. Cvelbar, Vac. Surf. Films, 21 (2003), 369–374
- ⁴⁸ M. Mozetič, Vacuum, 71 (2003), 237–240
- ⁴⁹ M. Mozetič, A. Zalar, Vacuum, 71 (2003), 233–236
- ⁵⁰ N. Krstulović, I. Labazan, S. Milošević, U. Cvelbar, A. Vesel, M. Mozetič, Mater. tehnol., 38 (2004), 51–54
- ⁵¹ M. Mozetič, Surf. Coat. Technol., 201 (2007), 4837–4842
- ⁵² H. J. Jakobasch, K. Grundke, E. Mäder, K. H. Freitag, U. Panzer, Application of the surface free energy concept in polymer processing, in K. L. Mittal (ed): Contact angle, wettability & adhesion, Zeist 2003, p. 921–936
- ⁵³ Z. Peršin, K. Stana-Kleinschek, M. Sfiligoj-Smole, T. Kreže, V. Ribitsch, Textile Res J, 74 (2004), 55–62
- ⁵⁴ L. Fras-Zemljč, Z. Peršin, P. Stenius, K. Stana-Kleinschek, Cellulose, 15 (2008), 681–690
- ⁵⁵ L. Fras-Zemljč, Z. Peršin, P. Stenius, Biomacromolecules, 10 (2009), 1181–1187
- ⁵⁶ G. Carlsson, G. Ström, Langmuir, 7 (1991), 2492–2497
- ⁵⁷ M. Gorjanc, V. Bukosek, M. Gorenssek, A. Vesel, Tex. Res. J., 80/6 (2010), 557–567
- ⁵⁸ A. Vesel, M. Mozetic, S. Strnad, K. Stana-Kleinschek, N. Hauptman, Z. Persin, Vacuum, 84 (2010) 1, 79–82

USE OF AFM FORCE SPECTROSCOPY FOR ASSESSMENT OF POLYMER RESPONSE TO CONDITIONS SIMILAR TO THE WOUND, DURING HEALING

UPORABA AFM-SPEKTROSKOPIJE SIL ZA SPREMLJANJE ODZIVA POLIMERNIH MOLEKUL NA V RANI PODOBNA OKOLJA MED CELJENJEM

Uroš Maver¹, Tina Maver^{2,3}, Andrej Žnidaršič¹, Zdenka Peršin^{2,3}, Miran Gaberšček¹, Karin Stana-Kleinschek^{2,3}

¹ National Institute of Chemistry, Laboratory for materials electrochemistry, Hajdrihova 19, SI-1000 Ljubljana, Slovenia

² Centre of Excellence for Polymer Materials and Technologies, Tehnološki park 24, SI-1000 Ljubljana, Slovenia

³ University of Maribor, Faculty of Mechanical Engineering, Laboratory for Characterisation and Processing of Polymers, Smetanova 17, SI-2000 Maribor, Slovenia
tina.maver@uni-mb.si

Prejem rokopisa – received: 2011-02-10; sprejem za objavo – accepted for publication: 2011-02-28

Force spectroscopy is a very promising technique for the evaluation of interactions within different environments. Knowledge about them is especially important during the design and preparation of those modern wound dressings in contact with a changing wound-environment over a prolonged time. Such exposure can cause a drastic decrease in the material's mechanical performance, and can lead to degradation, thus lowering the success of any healing process. Our study tries to establish a model system, which would enable us to assess the applicability of the mentioned technique for the evaluation of any interaction changes between polymer molecules and a chosen surface, after exposure to different environments. Our proposed experimental setup consists of two representative polymers, a model silicon surface, and two solutions of various pHs and ionic strengths, respectively. Within the chosen range of parameters, we are confident that we can prove the usefulness of force spectroscopy for further research into polymer suitability, for the development of novel wound dressings.

Keywords: force spectroscopy, AFM, wound dressings, polymer materials, model system

Spektroskopija sil je zelo obetavna tehnika za uporabo pri določanju interakcij v številnih različnih okoljih. Poznanje le-teh je še posebej pomembno pri načrtovanju in pripravi novodobnih obližev, ki morajo biti v stiku z rano dalj časa in so tako izpostavljeni spreminjajočemu se okolju. To lahko na samem materialu povzroči drastične spremembe in vodi v otežen potek celjenja. V tem delu smo želeli pripraviti modelni sistem, s katerim bi preverjali možnost uporabe omenjene tehnike za ugotavljanje sprememb interakcij med polimernimi molekulami ter izbrano površino po izpostavitvi različnim okoljem. Eksperimentalni sistem je vseboval dva vzorčna polimera, modelno silicijevo površino ter po dve raztopini z različnimi pH in ionskimi močmi. S takim naborom parametrov smo zajeli dovolj možnosti za ugotovitev uporabnosti tehnike za nadaljnje raziskave primernosti polimernih materialov za nove obliže.

Ključne besede: spektroskopija sil, mikroskopija na atomsko silo, obliži, polimerni materiali, modelni sistem

1 INTRODUCTION

Using atomic force microscopy (AFM), a tip attached to a flexible cantilever will move across the sample surface to measure surface morphology on the atomic scale. The force between the tip and the sample is measured during scanning, by monitoring the deflection of the cantilever.¹ This force is a function of tip sample separation and the material properties of the tip and the sample. Further interactions arising between tip and sample, can be used to investigate other characteristics of the sample, the tip, or the medium inbetween.² Such measurements are usually known as force measurements. The basics of a AFM force measurement is as follows: the tip attached to a cantilever spring is moved towards the sample in a normal direction, during this movement, the vertical position of the tip and the deflection of the cantilever are recorded and converted to force-versus-distance curves, briefly called force curves.²

In addition to evaluating interaction forces between the tip and model surfaces, AFM can also produce two-dimensional chemical affinity maps by modifying the cantilever tip with specific molecules. In this way, it is possible to characterize differently responding regions on the material's surface, resulting in a better understanding and, consequently, application of the examined materials.³⁻⁶

Mapping chemical functional groups and examining their interactions with different materials is of significant importance for problems ranging from lubrication and adhesion, to the recognition of biological systems wide spectrum of fields.⁷ A chemical force microscope has been extensively used to monitor changes in the interactions between different functional groups and surfaces, whilst changing measurement conditions such as pH and ionic strength.^{8,9} This technique is particularly useful when applied in combination with electron spectroscopy techniques for the determination of surface functional

groups, such as X-ray photoelectron spectroscopy (XPS).^{10–28}

Additionally, some research has already been performed in the field of monitoring the variations of pull-off forces between differently functionalized tips and surfaces.²⁹ This method's main advantage is that it almost always allows for measurement under those conditions present in the system in which the sample will be later used.

The ultimate use of AFM is for single-molecule recognition, which can be achieved by applying force spectroscopy. This technique was introduced many years ago, but has only recently achieved most of its scientific acclaim and is now one of the more used AFM modes. Clausen-Schaumann et al. were the first to introduce some of the possibilities, which enabled all the other researchers to gain a thorough understanding of single-molecule recognition measurements using AFM.³⁰ Additional weight to the measurements was introduced by Kienberger et al., whilst introducing additional blocking experiments to prove the specificity and effectiveness of the measurements.³¹

Within the field of polymer sciences, AFM has been used to quantify the entropic elasticity of single polymer chains,³² the elastic moduli of nanowires,³³ single polymer chain elongation³⁴, molecular stiffness of hyperbranched macromolecules,³⁵ friction of single polymers on surfaces,³⁶ influence of temperature on the stability of single chain conformation,³⁷ and surface glass transition temperature.³⁸ It has also been used to perform stretching experiments on single carboxymethylated amylase,³⁹ and to differentiate between sugar isomers.⁴⁰

This work focuses on the AFM as a polymer characterization method. It attempts to simulate those conditions arising from changes in the solvent, the pH and ionic strength, and possibility to use AFM force spectroscopy to assess their influence on polymer behaviour in such media. Such information would be really crucial in the preparation of wound-dressings, which are mostly polymer-based and are exposed to drastically-changing environments in the wound during the healing process.

2 EXPERIMENTAL

2.1 Preparation of functionalized AFM tips

Firstly AFM tips were decorated in order to show the possibility of using them for force spectroscopy measurements. Two different cellulose derivatives (amylose-AM and carboxymethyl cellulose-CMC) were chosen for adsorption onto the tip.

2.1.1 Adsorption of polymers to the tip surface

In order to achieve adsorption onto the tips, solutions with 10 mmol concentrations were used for both polymers (AM and CMC). Pure tips, out of the box, (NP-S10 contact-mode tips, Veeco) were gently dipped into the solution using freshly-cleaned tweezers (they were sonicated in acetone for 30 min and dried using clean nitrogen), then left in the solution for 2 h. Afterwards tips were removed from the solution and washed carefully 6 times using two different solvents (water and chloroform – CF), alternately.

All used solvents and other chemicals (when not stated otherwise) were of analytical grade (high purity) and bought from Sigma-Aldrich.

The preparation procedure is schematically depicted in **Figure 1**.

2.2 Methods

2.2.1 AFM

We performed force spectroscopy measurements using Agilent 5500 AFM. All measurements were done in liquid medium (milli-Q water) to avoid capillary forces, and to simulate different conditions. We measured 100 curves over each time-scale at different points on the sample's surface and eliminated the outliers. In order to achieve better statistics and prove the measurements were performed correctly, some of the measurements were repeated and included in the final results. In all cases an atomically flat silicon surface was used to avoid any discrepancies due to specific surface characteristics or different roughness at different spots where the force spectroscopy was performed. Two sets of measurements were performed for each medium type. Two different pHs and two different ionic strengths

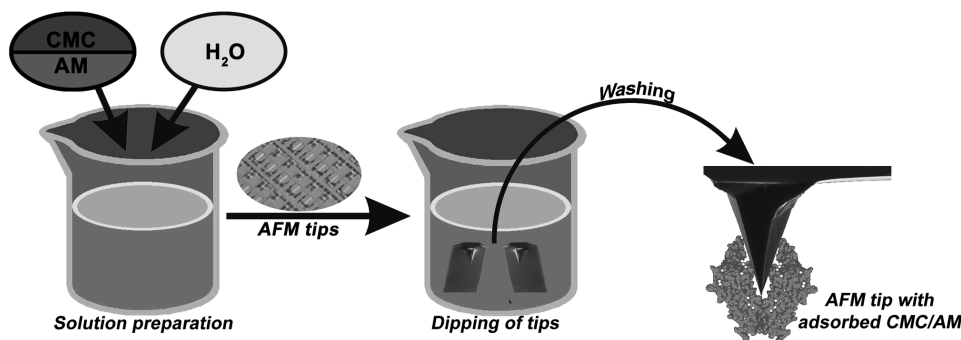


Figure 1: Preparation scheme for the attachment of polymer molecules to the AFM tip.

Slika 1: Shema pripenjanja polimernih molekul na AFM-konico

were used, in order to achieve a representative range of measurement conditions. In order to achieve desired pHs, citric acid (CA) was used as the sole reagent to lower the pH, whilst KCl was used to alter the ionic strengths. pHs were 3, 6, and ionic strengths were 5 mmol, 100 mmol, respectively.

Although measurements were also performed during other than the mentioned time-scales, only determined force using two especially representative durations were used for further discussion. The first of them was used to simulate the interactions involved in the first contact of the polymer with the environment and the second, simulating conditions after the polymer's prolonged exposure to the wound-environment.

3 RESULTS

3.1 AFM measurements

These measurements were performed to show their possible use and assessment for the best scenario, predict the behaviour of those polymer materials used for the preparation of several modern wound dressings, after their exposure to any changing environment within the healing-wound.

In our attempt to prepare the right methodology to tackle such a tough and complex problem, an attempt was made to keep the experimental setup as simple as

possible. This would allow us to apply such methodology to more complex and by far more realistic systems.

3.1.1 pH variation

Force spectroscopy was performed during the first set of measurements whilst varying the pH. As mentioned in the Experimental section, two different polymers were used for the measurements, which are, in rough approximation, representatives of possible polymers for wound-dressing preparation. One of them is the simple amylose, undissociable under the measured conditions but can, as all other cellulose derivatives, form intra- and inter-molecular H-bonds. The second is carboxymethyl cellulose which is, on the other hand, able to dissociate in alkaline solution due to its additional carboxyl groups. Two different measurement durations were used additionally one to show the forces and ranges involved upon first contact with the media, and the second to show how this changes after prolonged exposure. **Figure 2** shows the measured data for this set of force spectroscopy.

The results show that, with prolonged exposure, interactions increased for both polymers. Also it was observed that polymer nature plays a crucial role when the pH changes, as in this study. Lowering pH causes a decrease in the number of dissociated functional groups in CMC molecules, which clearly lowers the interaction. This effect is less pronounced with AM, which does not possess such groups.

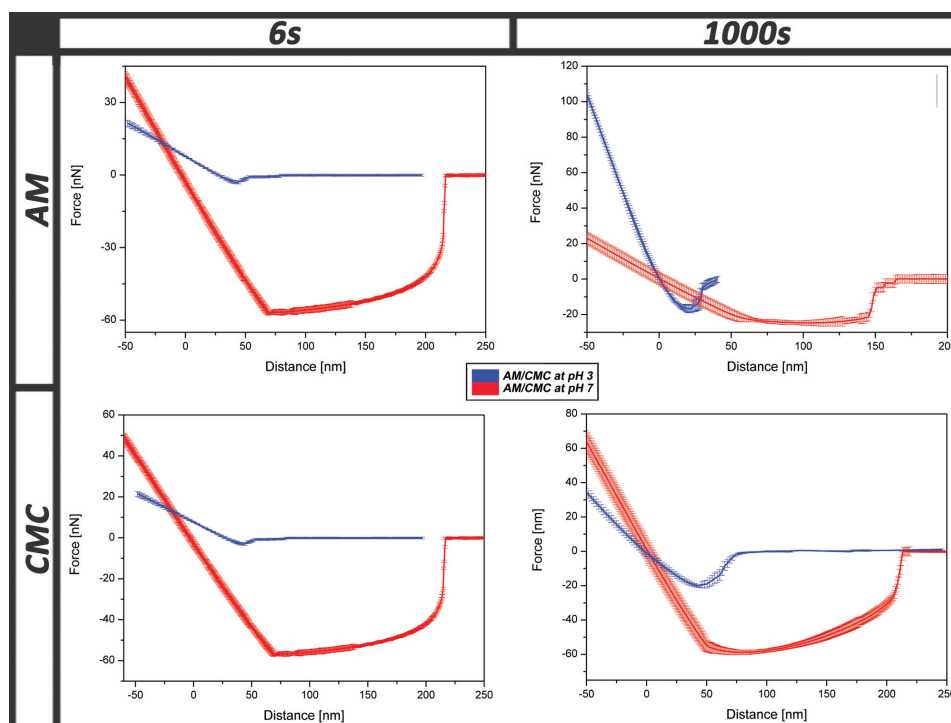


Figure 2: Force spectroscopy results for the measurements in two solutions with different pHs. TOP: retract force curves for amylose at two different measurement durations with two pHs, BOTTOM: retract force curves for carboxymethyl cellulose at two different measurement durations with two pHs.

Slika 2: Rezultati spektroskopije sil za meritve v raztopinah z dvema različnima pH. ZGORAJ: krivulje oddaljevanja pri uporabi amiloze; meritve so bile izvedene na dveh časovnih skalah in v dveh raztopinah različnih pH, SPODAJ: krivulje oddaljevanja za meritve pri uporabi karboksimetil celuloze; meritve so bile izvedene na dveh časovnih skalah in v dveh raztopinah različnih pH.

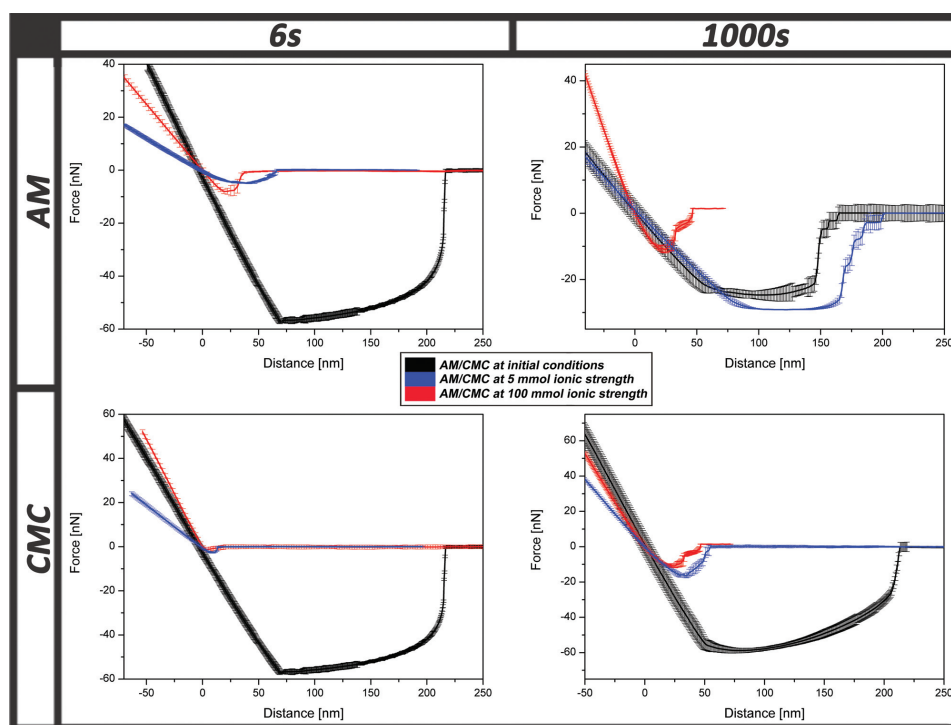


Figure 3: Force spectroscopy results for the measurements in two solutions with different ionic strengths. TOP: retract force curves for amylose at two different measurement durations in two solutions with different ionic strengths, BOTTOM: retract force curves for carboxymethyl cellulose at two different measurement durations in two solutions with different ionic strengths.

Slika 3: Rezultati spektroskopije sil za meritve v raztopinah z različnima ionskima močema. ZGORAJ: krivulje oddaljevanja za meritve pri uporabi amiloze; meritve so bile izvedene na dveh časovnih skalah in v dveh raztopinah različnih ionskih moči. SPODAJ: krivulje oddaljevanja pri uporabi karboksimitil celuloze; meritve so bile izvedene na dveh časovnih skalah in v dveh raztopinah različnih ionskih moči.

3.1.2 Ionic strength variation

In the second set of measurements, an attempt was made to assess the influence of another important and changing parameter during healing, namely the ionic strength. Again the same two polymers were used and the time was varied in order to gain some insight into the effect of prolonged polymer exposure to the changed environment over time. The results for this set of measurement are shown in **Figure 3**.

The results show that ionic strength changes influence the modified cellulose derivate, CMC more rigorously. Its carboxyl groups are clearly more sensitive to these changes, which lead to lower interactions. This effect loses some of its magnitude, with increased exposure, but the interactions stay lower when compared to AM, which does not seem to be influenced by any change in ionic strength.

4 DISCUSSION

Force spectroscopy, when used correctly, is a perfect method for assessing any interactions over a wide range of environmental conditions, especially in liquid media, which allows for the exclusion of capillary forces capable of hiding smaller interaction contributions. When using them for the first time in any research area or a new system, it is crucial that proof is found that the prepared experimental setup works and yields correct

results. For this, our experiments had to be kept as simple as possible to avoid any unexplainable discrepancies from the expected results. This presented study tried to do precisely that. By simplifying the setup to only two changing-parameters separately, it was possible to show that our proposed technique could serve as a good platform for assessing any changing wound-environment during healing.

The experiments were performed over two sets of experiments. The first used two different pHs to follow any changes in the interaction force and range between the polymer molecule and the model surface. After comparing the two used polymers, it can be said that the main difference in behaviour of CMC and AM arises due to the acidic COOH group on the glucose rings. This caused the appearance of negative charges on the chain. Repulsion of the negative charges stretched the polymer chain. When using the solution with pH 3, the H^+ concentration was sufficiently high to prevent deprotonation of COOH groups, and the formation of charges. These enabled dense packing of CMC. Due to this effect, CMC experienced lower forces (less functional groups to interact with the surface), when put into the solution of an acidic pH, This effect is far less significant for AM interactions with the model surface, because it has no such groups in its structure. Prolonged exposure times lead to an increase in interaction for the used pHs.

A similar structure-related explanation can be used to explain the results of the second experimental set, in which force spectroscopy was performed in two solutions with different ionic strengths. Again it started with the acidic carboxyl groups of CMC, which gave rise to negative charges on the CMC polymer chain. The stretching of a negatively-charged molecule is inevitable due to electrostatic repulsion. But increased ionic strength shields charged and, hence, decreased electrostatic repulsion, leading to closer packing of glucose groups. The influence of increasing ionic strength on amylose was, as expected, less drastic as no charges appeared on the amylose chain. The results to a great extent fit such an explanation. Lastly it could again be seen that an increase in interactions took place during the exposure to the medium.

5 CONCLUSIONS

We were able to design a simple test for an evaluation regarding the possible use of force spectroscopy in the assessment of polymer behaviour upon exposure to different liquid environments. Such knowledge would be of great use, as polymers are the main constituents of most modern wound-dressings, which have to stay intact upon contact with the changing environment within a healing wound. Force spectroscopy proved to be the right method for following such changes in our model system consisting of two polymers and a model surface. The results proved that such an approach is very promising for future testing in order to find the correct combination of materials for wound-dressing design regarding specific wounds.

Acknowledgement

The authors acknowledge the financial support from the Ministry of Higher Education, Science and Technology of the Republic of Slovenia through the contract No. 3211-10-000057 (Center of Excellence Polymer Materials and Technologies).

6 REFERENCES

- G. Binnig, C. F. Quate, C. Gerber, *Physical Review Letters*, 56 (1986), 930
- H. J. Butt, B. Cappella, M. Kappl, *Surface Science Reports*, 59 (2005), 1–152
- A. J. Engler, F. Rehfeldt, S. Sen, D. E. Discher, in *Methods in Cell Biology*, ed. E. D. YuLi Wang and Dennis, Academic Press, 2007, p. 521–545
- J. Preiner, H. Janovjak, C. Rankl, H. Knaus, D. A. Cisneros, A. Kedrov, F. Kienberger, D. J. Muller, P. Hinterdorfer, *Biophysical Journal*, 93 (2007), 930–937
- F. Kienberger, A. Ebner, H. J. Gruber, P. Hinterdorfer, *Accounts of Chemical Research*, 39 (2006), 29–36
- D. P. Allison, P. Hinterdorfer, W. H. Han, *Current Opinion in Biotechnology*, 13 (2002), 47–51
- C. D. Frisbie, L. F. Rzsnyai, A. Noy, M. S. Wrighton, C. M. Lieber, *Science*, 265 (1994), 2071–2074
- D. V. Vezenov, A. Noy, L. F. Rzsnyai, C. M. Lieber, *J. Am. Chem. Soc.*, 119 (1997), 2006–2015
- D. V. Vezenov, A. V. Zhuk, G. M. Whitesides, C. M. Lieber, *J. Am. Chem. Soc.*, 124 (2002), 10578–10588
- U. Cvelbar, M. Mozetič, I. Junkar, A. Vesel, J. Kovač, A. Drenik, T. Vrlinič, N. Hauptman, M. Klanjšek Gunde, B. Markoli, N. Krstulović, S. Milošević, F. Gaboriau, T. Belmonte, *Appl. Surf. Sci.*, 253 (2007) 19, 8669–8673
- A. Vesel, M. Mozetič, A. Hladnik, J. Dolenc, J. Zule, S. Milošević, N. Krstulović, M. Klanjšek - Gunde, N. Hauptman. *J. phys. D, Appl. Phys.*, 40 (2007), 3689–2696
- T. Vrlinič, A. Vesel, U. Cvelbar, M. Krajnc, M. Mozetič, *Surf. Interface Anal.*, 39 (2007) 6, 476–481
- A. Vesel, M. Mozetič, A. Zalar, *Surf. Interface Anal.*, 40 (2008), 661–663
- A. Vesel, M. Mozetič, A. Zalar, *Vacuum*, 82 (2008) 2, 248–251
- A. Vesel, I. Junkar, U. Cvelbar, J. Kovač, M. Mozetič, *Surf. Interface Anal.*, 40 (2008) 11, 1444–1453
- A. Drenik, A. Vesel, M. Mozetič, *J. Nucl. Mater.*, 386–388 (2009), 893–895
- I. Junkar, U. Cvelbar, A. Vesel, N. Hauptman, M. Mozetič, *Plasma Processes Polym.* 6 (2009) 10, 667–675
- A. Vesel, M. Mozetič, *Inf. MIDEM*, 40 (2010) 1, 67–73
- A. Vesel, M. Mozetič, P. Panjan, N. Hauptman, M. Klanjšek - Gunde, M. Balat -Pichelin, *Surf. Coat. Technol.*, 204 (2010), 1503–1508
- M. Gorjanc, V. Bukošek, M. Gorenšek, M. Mozetič, *Tex. Rs. J.*, 80 (2010) 20, 2204–2213
- A. Vesel, M. Mozetič, S. Strnad, K. Stana - Kleinschek, N. Hauptman, Z. Peršin, *Vacuum*, 84 (2010) 1, 79–82
- I. Junkar, A. Vesel, U. Cvelbar, M. Mozetič, S. Strnad, *Vacuum*, 84 (2010) 1, 83–85
- M. Mozetič, *Mater. Tehnol.*, 44 (2010) 4, 165–171
- M. Gorjanc, V. Bukošek, M. Gorenšek, A. Vesel, *Tex. Res. J.*, 80 (2010) 6, 557–567
- A. Vesel, *Surf. coat. technol.*, 205 (2010) 2, 490–497
- A. Asadinezhad, I. Novák, M. Lehocký, V. Sedlarik, A. Vesel, I. Junkar, P. Sáha, I. Chodák, I. Chodák, *Plasma Processes Polym.*, 7 (2010) 6, 504–514
- A. Asadinezhad, I. Novák, M. Lehocký, F. Bílek, A. Vesel, I. Junkar, P. Sáha, A. Popelka, *Molecules (Basel)*, 15 (2010) 2, 1007–1027
- A. Asadinezhad, I. Novák, M. Lehocký, V. Sedlarik, A. Vesel, P. Sáha, I. Chodák, *Biointerfaces*, 77 (2010) 2, 246–256
- H. Schönherr, V. Chechik, C. J. M. Stirling, G. J. Vancso, *J. Am. Chem. Soc.*, 122 (2000), 3679–3687
- H. Clausen- Schumann, M. Seitz, R. Krautbauer, H. E. Gaub, *Curr. Op. Chem. Bio.*, 4 (2000), 524–530
- F. Kienberger, A. Ebner, H. J. Gruber, P. Hinterdorfer, *Acc. Chem. Res.*, 39 (2006), 29–36
- C. Ortiz, G. Hadziioannou, *Macromolecules*, 32 (1999), 780–787
- S. Shanmugham, J. Jeong, A. Alkhatib, D. E. Aston, *Langmuir*, 21 (2005), 10214–10218
- J. E. Bemis, B. A. Akhremitev, G. C. Walker, *Langmuir*, 15 (1999), 2799–2805
- H. Shulha, X. Zhai, V. V. Tsukruk, *Macromolecules*, 36 (2003), 2825–2831
- F. Kühner, M. Erdmann, L. Sonnenberg, A. Serr, J. Morfill, H.E. Gaub, *Langmuir*, 22 (2006), 11180–11186
- M. I. Giannotti, M. Rinaudo, G. J. Vancso, *Biomacromolecules*, 8 (2007), 2648–2652
- V. N. Bliznyuk, H. E. Assender, G. A. D. Briggs, *Macromolecules*, 35 (2002), 6613–6622
- Z. Lu, W. Nowak, G. Lee, P. E. Marszalek, W. Yang, *Journal of American Chemical Society*, 126 (2004), 9033–9041
- Q. Zhang, P. E. Marszalek, *Journal of American Chemical Society*, 128 (2006), 5596–5597

BIODEGRADABLE POLYMERS FROM RENEWABLE RESOURCES: EFFECT OF PROTEINIC IMPURITY ON POLYCONDENSATION PRODUCTS OF 2-HYDROXYPROPANOIC ACID

BIORAZGRADLJIVI POLIMERI IZ OBNOVLJIVIH VIROV: VPLIV PROTEINSKIH NEČISTOT NA PRODUKTE POLIKONDENZACIJE 2-HIDROKSIPROPANOJSKE KISLINE

**Ida Poljanšek^{1, 2}, Pavel Kucharczyk³, Vladimír Sedlářik^{3, 4*}, Věra Kašpárková⁵,
Alexandra Šalaková⁶, Jan Drbohlav⁶**

¹Center of Excellence for Polymer Materials and Technologies, Tehnološki park 24, SI-1000 Ljubljana, Slovenia

²Biotechnical Faculty, Department of Wood Technology, University of Ljubljana, Jamnikarjeva ul. 101, SI-1000 Ljubljana, Slovenia

³Centre of Polymer Systems, Polymer Centre, Tomas Bata University in Zlin, nam. T. G. Masaryka 5555, 760 01 Zlin, Czech Republic

⁴Jožef Stefan Institute, Jamova cesta 39, 1000 Ljubljana, Slovenia

⁵Department of Fat, Tenside and Cosmetics Technology, Faculty of Technology, Tomas Bata University in Zlin, nam. T. G. Masaryka 275, 76272 Zlin, Czech Republic

⁶Dairy Research Institute, Milcom a.s. Ke Dvoru 12a, 16000 Prague, Czech Republic
sedlarik@ft.utb.cz

Prejem rokopisa – received: 2011-02-13; sprejem za objavo – accepted for publication: 2011-03-05

The goal of the presented work is to describe the proteinic impurity (as possible residual component from biotechnological lactic acid production from whey) in the reaction mixture with 2-hydroxypropanoic acid (lactic acid) for its direct polycondensation into poly(lactic acid). The impurity presence study was carried out in the range from mass fractions 0 % up to 2 %. For an evaluation of the impurity effect on the values of molecular weight, melting and glass transition temperatures the measurements of intrinsic viscosity, gel permeation chromatography and differential scanning calorimetry were used. Results show slight reduction of molecular weight and increase in polydispersity with rising amount of the impurity. The thermal properties investigation shows noticeable reduction of melting temperature and moderate decrease in glass transition temperature. The results reveal considerable role of lactose on formation of structural irregularities in lactic acid polycondensates.

Keywords: poly(lactic acid), whey protein, polycondensation, impurity effect

V prispevku je predstavljena študija vpliva proteinskih nečistot, ki so v reakcijski mešanici, na polikondenzacijo 2-hidroksipropanojske kisline (mlečne kisline) do polimlečne kisline. Koncentracijsko območje nečistot (komponente, ki ostanejo pri biotehnoški pridelavi mlečne kisline iz sirotke) je bilo od 0 % do 2 % glede na monomer. Z meritvami lastne viskoznosti in z gelsko prepustnostno kromatografijo ter diferenčno dinamično kalorimetrijo smo preučevali vpliv nečistot na povprečno molsko maso, na temperaturo tališča in na temperaturo steklastega prehoda nastalih polimerov. Z naraščajočo koncentracijo nečistot vrednost povprečnih molskih mas pada, narašča pa indeks polidisperznosti polimernih molekul. Rezultati raziskave termičnih lastnosti kažejo znižanje temperature tališča in tudi zmerno znižanje temperature steklastega prehoda z naraščajočo koncentracijo nečistot. Iz rezultatov študije je razvidna pomembna vloga laktoze na tvorbo strukturnih nepravilnosti pri polikondenzaciji mlečne kisline.

Ključne besede: polimlečna kislina, protein sirotke, polikondenzacija, vpliv nečistot

1 INTRODUCTION

Biodegradable and biocompatible polymers have attracted increasing interest over the past two decades both in the fundamental research and also in practical use.¹⁻³ Among them, the polymers from renewable resources are paid a special attention due to environmental concerns as well as sustainability factors. Poly(lactic acid) (PLA) is of the polymers, which is considered as biodegradable and obtainable form the not petroleum based raw materials. PLA belongs in a group of biodegradable polyesters and it represents its applicability in packaging technology but also in highly complex medical field as materials for drug delivery, orthopaedics, sutures and scaffolds due to its biocompatible properties.³⁻¹⁸

Production of the monomer for PLA preparation, 2-hydroxypropanoic acid, (known under trivial name lactic acid) can be carried out through both synthetic and biotechnological route. The latter way mostly includes microbial fermentation of saccharidic substrates into lactic acid and its subsequent polymerization. One of the promising renewable resources for lactic acid production is by-product of dairy industry – whey. Liquid whey appears in large quantities and its annual production rises continuously. Despite of its using in several applications (e.g. food supplements), a lot of whey is still wasted. Consequently, there is significant interest in finding new utilization methods for that.^{19,20}

The polymerization step represents the most difficult part of PLA preparation process due to necessity of high

monomer purity. However, biotechnologically prepared lactic acid contains various impurities (co-products, residual lactose, protein and inorganic components)^{21–25}. Purification of lactic acid represents additional economical loads, which reduce a competitiveness of this polymer with petroleum based plastics. In spite of extended research in the field of PLA synthesis, the effect of impurities has not been studied.

This work is focused on investigation of the effects of a residual proteinic impurity in lactic acid as monomer for PLA production via direct polycondensation reaction. This factor was quantified by observation of the changes in molecular weight distribution, thermal properties of the resulting product of the polycondensates.

2 EXPERIMENTAL PART

2.1 Materials

L-lactic acid (LA) C₃H₆O₃, 80 % water solution, optical rotation $\alpha = 10.6^\circ$ (measured by the polarimeter Optech P1000 at 22 °C, concentration of 10 %) was purchased from Lachner Neratovice, Czech Republic. Stannous 2-ethylhexanoate (Sn(Oct)₂) (≈ 95 %) was supplied by Sigma Aldrich, Steinheim Germany. The solvents acetone C₃H₆O, chloroform CHCl₃ and methanol CH₄O (all analytical grade) were bought from IPL Lukes, Uhersky Brod, Czech Republic. Whey protein concentrate (PROT) with a certified composition with mass fractions of 75 % protein, 17.5 % lactose and 7.5 % minerals was provided by Milcom a. s. Prague, Czech Republic.

2.2 Polycondensation

A typical procedure was as follows: relevant portions of LA and PROT (0, 0.25, 0.5, 0.75, 1.5 and 2) % – related to LA. Samples are designed as PLAPROT X/%, where X represents concentration of the PROT in the reaction mixture) were added into a double necked flask (250 mL) equipped with a Teflon stirrer. Total mass of the mixture at the beginning of reaction was 50 g (water is not included). The flask was then placed in an oil bath heated by magnetic stirrer with heating and connected to a laboratory apparatus for distillation under reduced pressure. The dehydration step followed at 160 °C, reduced pressure 15 kPa for 4 h. After that, the reactor was disconnected from the vacuum pump and the relevant amount (0.5 %, related to initial mass of the reactants) of the catalyst (Sn(Oct)₂) was added dropwise under continuous stirring. The flask with dehydrated LA/PROT/catalyst mixture was connected back to the source of vacuum (100 Pa) and the reaction continued for 24 h at the temperature 160 °C. The resulting product was allowed to cool down at room temperature and then dissolved in acetone. The polymer solution was precipitated in a mixture of chilled methanol/distilled water 1 : 1 (volume fraction) The obtained product was filtrated, washed with methanol and dried at 45 °C for 48 h. The dissolving-precipitation procedure was repeated three times.

2.3 Characterization methods

2.3.1 Intrinsic viscosity determination

Viscosity measurements were performed in chloroform at 30 °C in an Ubbelohde viscometer with capillary 0a. The intrinsic viscosity η was calculated using the equation (1):

$$[\eta] = \lim_{c \rightarrow 0} \frac{\eta_{\text{rel}} - 1}{c} \quad (1)$$

where η_{rel} is the relative viscosity, which is equal to the ratio of polymer solution and pure solvent viscosities and c is the concentration of the polymer solution (0.4, 0.8 and 1.2) %.

2.3.2 Determination of molecular weight by gel permeation chromatography (GPC)

GPC analyses were performed using a chromatographic system Breeze (Waters) equipped with a PLgel Mixed-D column ((300 × 7.8) mm, 5 μm) (Polymer Laboratories Ltd). For detection, a Waters 2487 Dual absorbance detector at 239 nm was employed. Analyses were carried out at room temperature with a flow rate of 1.0 mL min⁻¹ in chloroform. The column was calibrated using narrow molecular weight polystyrene standards with molar mass ranging from 580 g mol⁻¹ to 480 000 g mol⁻¹ (Polymer Laboratories Ltd). A 100 μL injection loop was used for all measurements. The sample concentration ranged from 1.6 mg mL⁻¹ to 2.2 mg mL⁻¹. Data processing was carried out using the Waters Breeze GPC Software (Waters). The weight average molar mass M_w , number average molar mass M_n and polydispersity (M_w/M_n) of the tested samples were determined.

2.3.3 Differential scanning calorimetry (DSC)

For the determination of glass transition temperature T_g , melting point T_m and crystallinity χ_c of the polycondensates the differential scanning calorimetry was used. Approximately 8 mg of the sample were placed in an aluminium pan, sealed and analyzed on NETZSCH DSC 200 F3, calibrated in terms of temperature and heat flow, using indium. The experiments were performed under nitrogen atmosphere (60 mL min⁻¹) in two scans in the temperature range of (0–180) °C and at the heating rate of 10 °C min⁻¹.

3 RESULTS AND DISCUSSION

The basic characteristics of the samples prepared by melt polycondensation of LA and PROT are shown in **Figures 1 and 2**. The value of η decreases with increasing impurity content. While pure PLA shows η 0.47 dL g⁻¹, PLAPROT 0.25 % proves almost 45 % reduction (0.26 dL g⁻¹). Interestingly, η of PLAPROT 0.5 % and 0.75 % fluctuates around that value. Further addition of the PROT into the reaction mixture does not influence η significantly and only slight decrease of η can be noticed (**Figure 1**). It corresponds to results from GPC analysis. The pure PLA sample has M_w 47.0 kg

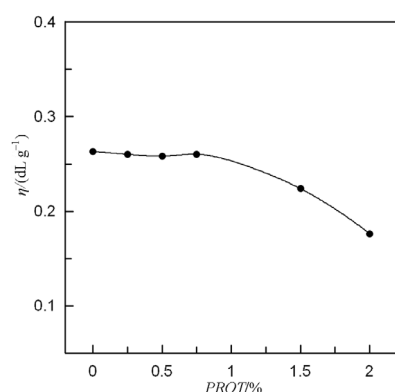


Figure 1: Dependence of intrinsic viscosity on PROT impurity concentration

Slika 1: Odvisnost lastne viskoznosti od koncentracije PROT-nečistot

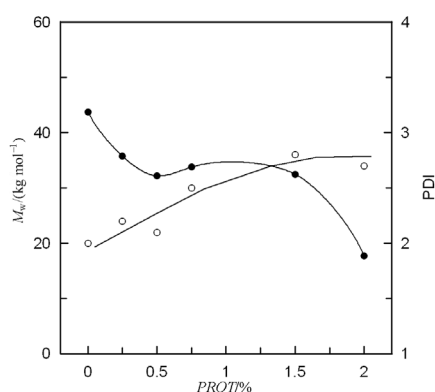


Figure 2: PROT concentration versus M_w (filled symbols) and PDI (empty symbols)

Slika 2: Odvisnost masnega povprečja molskih mas M_w , (polni simboli) in indeksa polidisperznosti, PDI, (prazni simboli) od koncentracije PROT-nečistot

mol⁻¹ and polydispersity index ($PDI = M_w/M_n$) 2.08. The presence of PROT impurity is attended by slight M_w reduction and rising PDI. The sample designated PLAPROT 2 % ($M_w = 23.4$ kg mol⁻¹, $PDI = 3.0$) can be still considered as polycondensates (Figure 2). The yield of the all polycondensates was over 60 % in all cases. However, it should be mentioned that it represents pure yield of the polycondensation products after purification process described in the experimental part above. These facts reveal that the presence of proteinic components do not disturb the polycondensation reaction as significantly as, for instance, other simple organic acids as we reported in our previous works.^{26,27} The reason could be found in, firstly, lactose presence and secondly proteins denature at temperatures higher than 40 °C. The polycondensation was carried out at 160 °C. It means that all proteinic ingredients had denatured even before polycondensation reaction started. The question is how the low molecular products of protein denaturation influences (if even) the polycondensation reaction.

The effect of PROT on thermal properties is presented in **Figure 3**. Pure PLA has a melting temperature, T_m , positioned at 151.2 °C and glass transition temperature T_g at 53.8 °C (**Figure 3**). Increasing content of

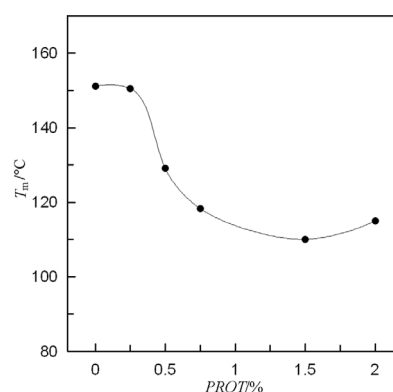


Figure 3: Dependence of melting temperature of PLA and PLAPROT samples on concentration of the impurity

Slika 3: Odvisnost temperature tališča PLA- in PLAPROT-vzorcev od koncentracije nečistot

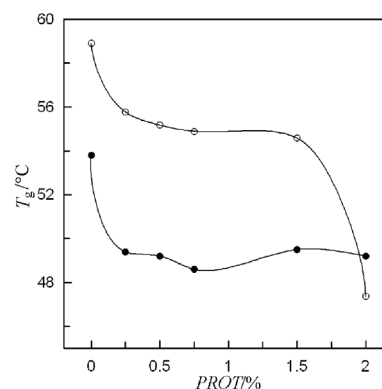


Figure 4: Glass transition temperature versus PROT concentration, full symbols represents experimental data, empty symbols represents Fox-Flory prediction of glass transition temperature ($T_g^\infty = 58$ °C and $K = 5.5 \cdot 10^4$)¹⁷

Slika 4: Odvisnost temperature steklastega prehoda od koncentracije PROT-nečistot; polni simboli pomenijo eksperimentalno pridobljene vrednosti, prazni simboli pa vrednosti, izračunane s Fox-Floryjeve enačbo za napoved temperatur steklastega prehoda ($T_g^\infty = 58$ °C in $K = 5,5 \cdot 10^4$)¹⁷

PROT in the reaction mixture leads to reduction of both T_m and T_g . The sample with the highest impurity content, PLAPROT 2 %, shows T_m lower about almost 23 °C. Reduction in T_g is about 4.6 °C, which is not as significant as in case of T_m . It means that the impurity presence effects mostly ability of the polycondensates chains to organize into highly uniform structures. It can be the result of molecular weight reduction.²⁸ However, the structural changes cannot be excluded due to low difference between T_m values of pure PLA and PLAPROT 0.25 % whose M_w varies noticeably (**Figure 2**). The same assumption can be done on the basis of T_g measurements, where Fox-Flory ($T_g^\infty = 58$ °C and $K = 5.5 \cdot 10^4$)²⁹ for theoretical prediction of T_g from M_n fails (**Figure 4**).

These facts can lead to an assumption that the impurity presence causes a non-selective branching of the PLA chain as well as inhibition of the PLA chain growth. On the basis of the fact that proteins are supposed to undergo denaturation at high temperatures,

the lactose can play important role here. This is supported by our preliminary results when the effect of pure lactose was studied^{30,31}.

4 CONCLUSIONS

The aim of this work was to investigate the effect of the proteinic impurities in the reaction mixture on resulting properties of the lactic acid polycondensates. The protein concentrate originating from the real biotechnological production was used as a source of impurities. The obtained results indicates that protein components potentially presented in the reaction mixture as residuals (up to the mass fraction 2 % related to lactic acid) from biotechnological lactic acid production do not effect polycondensation reaction significantly by means of molecular weight reduction. However, slight decrease was observed. On the other hand, noticeable decreases were observed in melting temperatures of the samples. Glass transition temperatures were reduced moderately with increasing content of the whey protein concentrate. It reveals possible structural modification of polycondensates chains (random branching). The presence of disaccharide seems to play important role here. Detailed studies of this factor will be accomplished in our future work.

Acknowledgements

This research was financially supported by the Ministry of Education, Youth and Sports of the Czech Republic (project No. 2B08071) and Operational Program Research and Development for Innovations co-funded by the European Regional Development Fund (ERDF, project No. CZ.1.05/2.1.00/03.0111). The authors acknowledge the financial support from the Ministry of Higher Education, Science and Technology of the Republic of Slovenia through the contract No. 3211-10-000057 (Center of Excellence for Polymer Materials and Technologies). Furthermore, this work was also co-supported by the Ministry of Higher Education, Science and Technology of the Republic of Slovenia (programme P4-0015) and Slovenian Research Agency (ARRS) and Science and Education Foundation of the Republic of Slovenia within the "Ad futura" programme.

5 REFERENCES

- S. Jacobsen, P. H. Degee, H. G. Fritz, P. H. Dubois, R. Jerome, *Polym Eng Sci*, 39 (1999), 1311–1319
- H. R. Kricheldorf, *Chemosphere*, 43 (2001), 49–54
- I. Junkar, A. Vesel, U. Cvelbar, M. Mozetic, S. Strnad, *Vacuum*, 84 (2009) 1, 83–85
- U. Cvelbar, M. Mozetic, I. Junkar, A. Vesel, J. Kovac, A. Drenik, T. Vrlnic, N. Hauptman, M. Klanjsek Gunde, B. Markoli, N. Krstulovic, S. Milosevic, F. Gaboriau, T. Belmonte, *Appl. Surf. Sci.* 257 (2007) 19, 8669–8673
- I. Junkar, N. Hauptman, K. Renner-Sitar, M. Klanjsek Gunde, U. Cvelbar, *Inf. MIDEM*, 38 (2008) 4, 266–271
- A. Vesel, I. Junkar, U. Cvelbar, J. Kovac, M. Mozetic, *Surf. Interface Anal.*, 40 (2008) 11, 1444–1453
- M. Sowe, I. Novak, A. Vesel, I. Junkar, M. Lehocky, P. Saha, I. Chodak, *Int. J. Polym. Anal. Charact.*, 14 (2009) 7, 641–651
- A. Vesel, K. Elersic, I. Junkar, B. Malic, *Mater. Tehnol.*, 43 (2009) 6, 323–326
- I. Junkar, V. Sustar, M. Frank, V. Jansa, A. Bedina Zavec, B. Rozman, M. Mozetic, H. Hägerstrand, V. Kralj - Igljic, *The Open Autoimmunity Journal*, 1, (2009) 50–58, doi: 10.2174/1876894600901010050
- I. Junkar, U. Cvelbar, A. Vesel, N. Hauptman, M. Mozetic, *Plasma Processes Polym.*, 6 (2009) 10, 667–675
- K. Elersic, I. Junkar, A. Spes, N. Hauptman, M. Klanjsek Gunde, A. Vesel, *Mater. Tehnol.*, 44 (2010) 3, 153–156
- A. Asadinezhad, I. Novak, M. Lehocky, F. Bilek, A. Vesel, P. Saha, A. Popelka, *Molecules*, 15 (2010) 2, 1007–10027
- J. Lopez-Garcia, A. Asadibezhad, J. Pracherník, M. Lehocky, I. Junkar, P. Humpolicek, P. Saha, O. Valasek, *Molecules*, 15(2010) 4, 2845–2856,
- A. Asadinezhad, I. Novak, M. Lehocky, V. Sedlarik, A. Vesel, I. Junkar, I. Chodak, *Plasma Processes Polym.*, 7,(2010) 6, 504–514
- A. Vesel, M. Mozetic, A. Zalar, *Surf. Interface Anal.*, 40 (2008) 3–4, 661–663
- A. Asadinezhad, I. Novak, M. Lehocky, V. Sedlarik, A. Vesel, I. Junkar, P. Saha, I. Chodak, *Colloids and Surfaces B–Biointerfaces*, 77 (2010) 2, 246–256
- V. Sedlarik, P. Kucharczyk, V. Kasparkova, J. Drbohlav, A. Salakova, P. Saha, *J Appl Polym Sci*, 116 (2010) 2, 1597–1602
- R. Auras, B. Harte, S. Selke, *Macromol BioSci.*, 4 (2009) 9, 835–864
- A. Gregorova, M. Hrabalova, R. Wimmer, B. Saake, C. Altaner, *J Appl Polym Sci*, 114 (2009) 5, 2616–2623
- V. Sedlarik, N. Saha, J. Sedlarikova, P. Saha, *Macromolecular Symposia*, 272 (2008), 100–103
- I. Olabarrieta, D. Fosstrom, U.W. Gesce, M.S. Hedenquist, *Polymer*, 42 (2001) 9, 4401–4408
- V. Sedlarik, N. Saha, I. Kuritka, P. Saha, *J Appl Polym Sci*, 106 (2007) 3, 1869–1879
- V. Sedlarik, N. Saha, I. Kuritka, I. Emri, P. Saha, *Plast Rubber Compos*, 35 (2006) 9, 355–359
- V. Sedlarik, N. Saha, P. Saha, *Polym Degrad Stabil*, 91 (2006) 9, 2039–2045
- V. Sedlarik, N. Saha, I. Kuritka, P. Saha, *Int J Polym Anal Ch*, 11 (2006), 4, 253–270
- V. Sedlarik, N. Saha, I. Kuritka, P. Saha, *Polym Composite*, 27 (2006) 2, 147–152
- P. Kucharczyk, I. Poljansek, V. Sedlarik, V. Kasparkova, A. Salakova, J. Drbohlav, U. Cvelbar, *Functionalization of polylactic acid through direct melt polycondensation in presence of tricarboxylic acid.*, *J Appl Polym Sci.*, accepted for publication (2011)
- P. Kucharczyk, V. Sedlarik, V. Kasparkova, I. Poljansek, A. Salakova, J. Drbohlav, I. Junkar, P. Saha, *Lactic acid polycondensation in presence of citric acid: Effect of concentration and catalysts on resulting products.*, *PLASTKO conference (2010)*, ISBN 978–80–7318–909–9
- J. G. Fatou, L. Mandelkern, *The Journal of Physical Chemistry*, 69 (1965) 2, 417–428
- K. Jamshidi, S. H. Hyon, Y. Ikada, *Polymer*, 29 (1988) 12, 2229–2234
- P. Kucharczyk, *The effect of impurities on the properties of the lactic acid polycondensates*, Master thesis, Tomas Bata University in Zlin, Czech Republic (2010)

SUBMIKROMETERSKI IN NANO ZnO KOT POLNILO V PMMA-MATERIALIH

SUB MICROMETER AND NANO ZnO AS FILLER IN PMMA MATERIALS

Alojz Anžlovar, Zorica Crnjak Orel, Majda Žigon

Center of Excellence for Polymer Materials and Technologies, Tehnološki park 24, SI-1000 Ljubljana, Slovenia
alojz.anzlovar@ki.si

Prejem rokopisa – received: 2011-02-14; sprejem za objavo – accepted for publication: 2011-03-10

Podan je pregled sintetskih načinov za pripravo cinkovega(II) oksida – ZnO z različnimi velikostmi delcev, oblikami, morfologijo in s površinsko modifikacijo in tudi pregled postopkov priprave nanokompozitov ZnO/poli(metil metakrilat) – ZnO/PMMA. Nanostrukture ZnO so sintetizirali iz različnih prekurzorjev, medijev in z uporabo različnih katalizatorjev. Istočasno so potekale intenzivne aktivnosti pri pripravi ZnO/PMMA nanokompozitov. Homogene nanokompozite tega tipa so pripravili po različnih postopkih z uporabo ZnO, modificiranega z različnimi površinsko aktivnimi sredstvi in tudi z uporabo nemodificiranega ZnO. V našem laboratoriju smo sintetizirali ZnO nano- in submikrometerske delce z organofilno površino v različnih diolih in pripravili homogene nanokompozite ZnO/PMMA z radikalsko verižno polimerizacijo MMA v masi. Pripravljeni nanokompoziti absorbirajo UV-svetlobo in prepuščajo vidno ter imajo izboljšano termično stabilnost. Takšni materiali so potencialno uporabni kot UV stabilizirani PMMA-materiali za zunanjo uporabo pri veliki izpostavljenosti sončni svetlobi.

Ključne besede: nano ZnO, ZnO kvantne točke, PMMA, nanokompoziti, NMR-spektroskopija, STEM-mikroskopija, TGA-analiza, fotoluminiscenčna spektroskopija

A review of synthetic approaches towards zinc(II) oxide – ZnO of various particle sizes, shapes, morphology and surface modifications is given as well as a review of preparation procedures for ZnO/poly(methyl methacrylate) – ZnO/PMMA nanocomposites. ZnO nanostructures were prepared from various precursors, media and catalysts and homogeneous nanocomposites were prepared by various preparation procedures using ZnO, modified by various surface active agents and also unmodified ZnO. In our lab, ZnO nano and sub micrometer particles with organophilic surface were prepared in various diols. Homogeneous ZnO/PMMA nanocomposites were formed by the radical chain polymerization of methyl methacrylate – MMA in bulk by optimizing the preparation method. Resulting nanocomposite materials showed high UV absorption and high transparency for visible light as well as enhanced thermal stability. Such materials have high potential as UV stabilized PMMA materials for various outdoor applications with high sun light loads.

Key words: nano ZnO, ZnO quantum dots, PMMA, nanocomposites, NMR spectroscopy, STEM microscopy, TGA analysis, photoluminescence spectroscopy

1 INTRODUCTION

Nano and micro structured materials are one of the fastest growing fields in modern materials science, especially the preparation of semiconductor materials. Zinc oxide is very promising semiconductor due to unique properties in near-UV region, electric conductivity and optical transparency and has drawn a considerable attention of scientists in last few years.¹ ZnO has large direct band gap and high exciton binding energy and it shows potential applications in catalysis, optoelectronic devices, sensors, and photovoltaic. ZnO can be synthesized in various shapes and particle sizes²⁻⁶ and also by various synthetic approaches.⁷ ZnO is also an environmentally friendly material, at least in the micrometer particle size range. Because of all this, it has attracted high attention in various fields of science.

2 SUBMICROMETER AND NANO ZnO

The solution phase approach to the preparation of nano-to-sub micrometer ZnO particles presents the low

cost preparation method and recently attracted a lot of interest due to the low temperature particle growth temperature (85–95 °C). It is much more favorable for large-scale synthesis, especially nowadays, since the consumption of energy is very low. ZnO nanoparticles with controllable morphology have been prepared with chemical precipitation method via a solution route. Unfortunately, with this method either much different morphology was obtained or the distribution range of diameter is wide. From that reason the preparation of ZnO nanostructures under low and moderate temperature conditions still presents a great challenge. Below, we list some representative routes of the preparation of ZnO nanostructures.

Zinc oxide nanocrystals were prepared by homogeneous precipitation method using urea and zinc nitrate as raw materials. The orientation/adhesion of nanocrystallites was discussed by the growth unit model of anionic coordination polyhedrons. It was shown that zinc oxide nanocrystal growth was more easily to occur along c-axis, which was primarily formed by the connection of positive hexagonal cone faces $p(1\ 0\ 1\ 1)$ and negative

hexagonal cone faces $p(1\ 0\ 1\ 1)$, secondly by the positive polar faces $c(0\ 0\ 0\ 1)$ and negative polar faces $c(0\ 0\ 0\ 1)$.⁸ Not only does the microwave irradiation of solutions of $Zn(NO_3)_2$ and urea yield ZnO micro particles much more rapidly than conventional heating methods, it also produces ZnO with a quite different well-defined needle-like morphology based on an unusual and unexpected a-axis.³

The large-scale synthesis of uniform-sized hexagonal pyramid-shaped ZnO nanocrystals can be performed by the thermolysis of Zn-oleate complex, which was prepared from the reaction of inexpensive and environmentally friendly reagents such as zinc chloride and sodium oleate.⁹ ZnO microspheres and hexagonal micro rods with sheet like and plate like nanostructures were prepared by the hydrothermal synthesis approach by using trisodium citrate which plays a key role in directing the formation of these microstructures. By increasing the reaction time, these microspheres gradually dissolved to form short hexagonal micro rods with stacked nanoplate or nanosheet structure.¹⁰ The disk-like, flower-like and nanorod flower-like ZnO nanostructures have been controllably fabricated by citric acid assisted hydrothermal process.^{11,12} Different shapes of ZnO micro crystals have been controllably prepared by a capping-molecule-assisted hydrothermal process. The flowerlike, disk-like, and dumbbell-like ZnO micro crystals of hexagonal phase have been obtained respectively using ammonia, citric acid, and poly(vinyl alcohol) as the capping molecules.¹³ A unique method was developed to produce ZnO by kinetically controlled catalytic hydrolysis of a molecular precursor (Zn nitrate) at low temperature, operating in conjunction with the vectorial control of crystal growth. Nucleation and growth of ZnO was controlled by the local variation in the chemical potential of Zn^{2+} resulting from accumulation of OH groups at the gas-liquid interface.¹⁴ Anionic surfactant sodium bis(2-ethylhexyl)sulfosuccinate – NaAOT can be made to form micelles with diverse shapes by adjusting experimental parameters. The self-assembled AOT-layers at the interface of water and oil could act as template for growing ZnO.¹⁵

ZnO nanostructures of different morphologies (nanoparticles, nanorods, and flowerlike ZnO structures) could be synthesized by controlling the content of ethylenediamine, hexamethylenetetramine and triethanolamine (soft surfactant) and the pH of the reaction mixture.^{16,17} Possible mechanisms for the variation of morphology with synthesis parameters have been discussed.¹⁸ With maleic anhydride-modified polystyrene (m-PS) microspheres as a template (core) and zinc nitrate and diethanolamine (DEA) as the starting materials the m-PS/ZnO core-shell structure was synthesized by a wet chemical route; the preferential growth of ZnO nuclei resulted in a cup-shape shell around the m-PS core.¹⁹ Polymer-assisted control of particle morphology and particle size of zinc oxide is another important synthetic

route to prepare ZnO nanostructures.²⁰ For example, water-soluble poly(ethylene oxide-block-methacrylic acid) (P(EO-b-MAA) and poly(ethylene oxide-block-styrene sulphonic acid) (P(EO-b-SSH)) diblock copolymers,^{21,22} polyacrylamide,²³ poly(vinyl alcohol),²⁴ acrylates,²⁵ PVP²⁶ or even gelatin²⁷ were used. In the latest time dendritic²⁸ and hyperbranched²⁹ polymer structures or mixed ligand coordination polymer³⁰ were also used in the controlled synthesis of nano ZnO. A highly important ZnO structures are ZnO quantum dots which are synthesized in various media such as alcohols^{31,32} or other solvents.³³

Over the past years polyol method was used for synthesis of different inorganic compounds as well as pure metals.^{34–37} In case of less electropositive metal such as cobalt, nickel copper and silver the reduction reaction takes place and metallic nanoparticles are obtained while the addition of water causes the hydrolysis reaction resulting in the formation of oxides or hydroxides.³⁵ Polyol acts simultaneously as solvent, reducing and stabilizing agent, and medium for preventing particle growth.³⁷ Due to the mild reducing power, polyols are unable to reduce a cation of an electropositive metal such as zinc. Reaction of hydrolysis takes place in these systems resulting in formation of ZnO. Using polyol method nano ZnO was synthesized in various diols from various precursors but DEG appears to be most suitable medium and Zn(II) acetate most suitable precursor for the preparation of ZnO with particle size between 50 nm

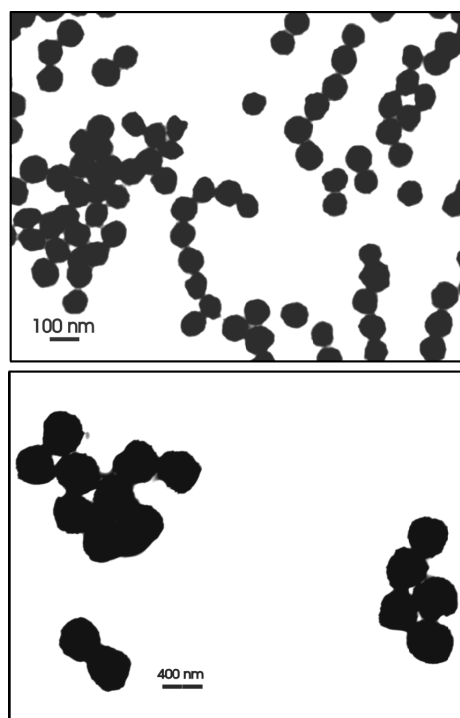


Figure 1: STEM micrographs ZnO nanoparticles synthesized by the polyol method in: a) DEG b) TEG

Slika 1: STEM-mikrografije ZnO-nanodelcev, sintetiziranih po polioli metodi v: a) DEG, b) TEG

and 100 nm.^{34,38} Besides the choice of medium, heating rate is crucial parameter which mostly determines the particle size.

In our study, ZnO sub micrometer and nanoparticles were synthesized in polyol media (di(ethylene glycol) – DEG and tetra(ethylene glycol) – TEG) using zinc(II) acetate as a precursor³⁹. STEM micrographs of ZnO particles, synthesized in DEG and TEG without p-TSA, are given in **Figure 1**. Micrographs show that 75 nm ZnO particles formed in DEG, while those formed in TEG have average particle size of 340 nm. Both ZnO particles are actually agglomerates of smaller (10–30 nm) crystallites.³⁹ Particle sizes and morphologies are similar to the reported results.^{34,38} In other diols no particulate ZnO was obtained and resulting agglomerates were unsuitable for the preparation of nanocomposites. IR spectra showed characteristic absorption band of ZnO in the range of 430–470 cm⁻¹ and weak absorption bands of oxoacetate reaction intermediates at (1590, 1415 and 1340) cm⁻¹. XRD diffractograms of the ZnO, synthesized in TEG, shows characteristic diffraction pattern of crystalline ZnO with hexagonal wurtzite structure (**Figure 2**). Wide diffraction maxima indicate small size of crystallites (18 nm – DEG, 25 nm – TEG) confirming the observations from electron micrographs.³⁹

3 ZnO/PMMA NANOCOMPOSITES

For organic-inorganic composites it is known that they possess improved properties in comparison to pure polymers such as better optical properties, thermal stability, chemical resistance, mechanical properties as well as flame-retardancy. The preferences in using ZnO in the preparation of polymeric nanocomposites, are in high transparency of the polymeric matrix in visible spectral region as well as its UV-protection. Development of simple procedures for the production of transparent UV-protective coatings or the preparation of transparent plates still represents a great scientific challenge since complete compatibility of ZnO nano-

to-sub micrometer particles with the polymeric matrix has not been achieved yet. Simply mixing nanoparticles with most polymers leads to aggregation in most cases. Small particles typically aggregate, thus nullifying any benefits of nanoscopic dimensions. The particles are frequently surface-modified or compounded in the polymer in presence of surfactants although few authors also report preparation of stable nano ZnO dispersions without any surface modification^{40,41}. To obtain miscibility of the inorganic particles and polymers usually hydrophobic ligands are used such as: alkyl silanes, oligomeric alkyl silicones, alkylphosphonic acid, hydroxy propyl methyl cellulose, fatty acids, amphiphilic statistical copolymer or block copolymers (diblock copolymers, double-hydrophilic block and grafted copolymers)⁴²⁻⁴⁹. Frequently used method of ZnO/poly(methyl methacrylate) (ZnO/PMMA) nanocomposite preparation is surface modification of ZnO nanoparticle using one of the mentioned ligands followed by the subsequent grafting of methyl methacrylate or mixtures of acrylic monomers on the modified surface of particles.⁵⁰⁻⁵⁵ Possible route towards ZnO/PMMA nanocomposites is by coating the ZnO particles with PMMA polymerized by gamma or electron radiation.⁵⁶ ZnO/PMMA nanocomposites were prepared also by the sol-gel synthesis of nano ZnO in the presence of PMMA.⁵⁷ Transparent ZnO/PMMA with high concentration of nano ZnO (up to 10 %) nanocomposites

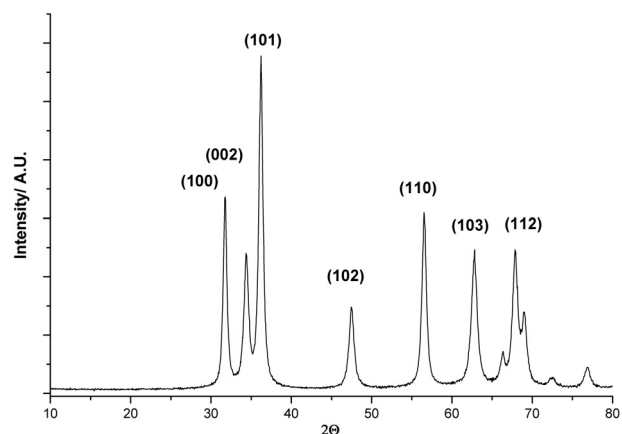


Figure 2: XRD diffractogram of nano ZnO synthesized in TEG
Slika 2: XRD-difraktogram nano ZnO, sintetiziranega v TEG

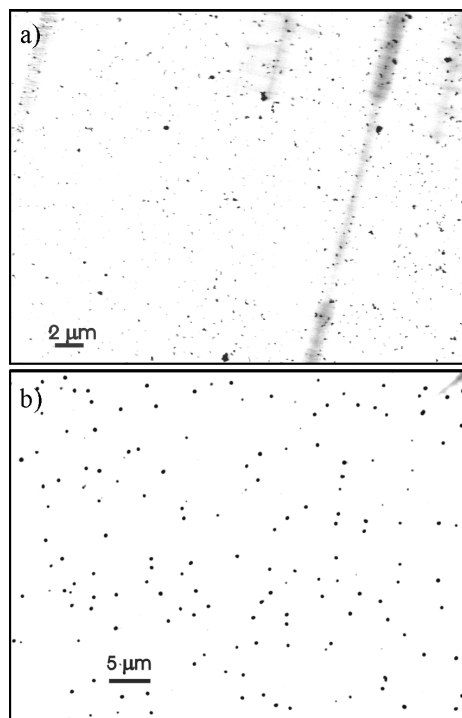


Figure 3: STEM micrographs of ultra microtome sections of ZnO/PMMA nanocomposites using ZnO synthesized in: a) DEG (part. size = 75 nm), b) TEG (part. size = 340 nm)

Slika 3: STEM-mikrografije ultramikrotomskih rezin ZnO/PMMA-nanokompozitov, pripravljenih z ZnO, sintetiziranim v: a) DEG (vel. delcev = 75 nm), b) TEG (vel. delcev = 340 nm)

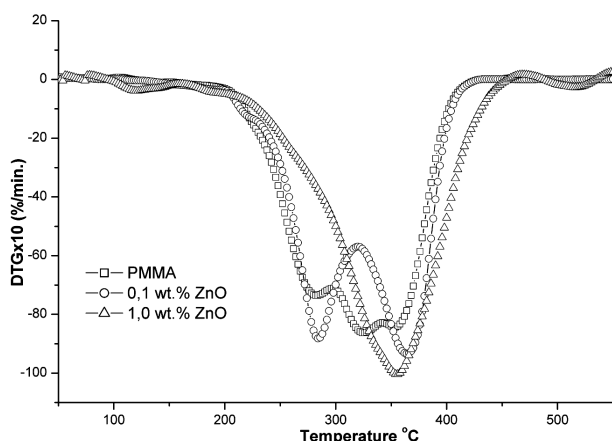


Figure 4: DTG curves of ZnO/PMMA nanocomposite using nano ZnO, synthesized in TEG (part. size = 86 nm), in dependence of ZnO concentration

Slika 4: DTG-krivulje ZnO/PMMA-nanokompozitov na osnovi nano ZnO, sintetiziranega v TEG (vel. delcev = 86 nm), v odvisnosti od koncentracije ZnO

have been also prepared by in-situ bulk polymerization in the presence of the prepared nanoparticles, which gives improved dispersion of nanoparticles compared to simple mixing.^{58–60} Bulk polymerization is the only synthetic method of PMMA which gives material with excellent optical properties (plexi glass) and is a widely used industrial process giving this method a very high potential in large scale production of ZnO/PMMA nanocomposite materials. Alternative method of ZnO/PMMA preparation is simultaneous formation of ZnO nanoparticles and PMMA polymerization³¹ or ATRP polymerization of MMA initiated from the surface of the ZnO.⁶¹ In the latest time homogeneous ZnO QDs nanocomposites were prepared by simply casting from solution^{41,62–64} or even by melt processing.⁶⁵

In our research work we focused on preparation of nanocomposites using synthesized nano ZnO particles with organophilic surface, synthesized by the polyol method. ZnO/PMMA nanocomposites were prepared by dispersing the unmodified ZnO nanoparticles in methyl methacrylate and by the subsequent in-situ chain polymerization of MMA. ZnO nanoparticles were dispersed in MMA by mixing and sonication. The dispersion was subsequently transferred into a glass mold and MMA was polymerized in a temperature controlled water bath for 20 h. The ZnO particle size, surface modification and concentration were varied.

The prepared nanocomposites were characterized by the thermo gravimetric analysis – TGA, TEM microscopy, UV-VIS spectroscopy and PLS – photoluminescence spectroscopy. STEM electron micrographs confirmed that nano ZnO is uniformly distributed in the PMMA matrix. (Figure 3).³⁹ Thermal stability of ZnO/PMMA nanocomposites was studied by the TGA. Results showed that thermal stability is enhanced at ZnO concentrations of 1 % and more (Figure 4). Enhanced thermal stability was explained by the influence of nano

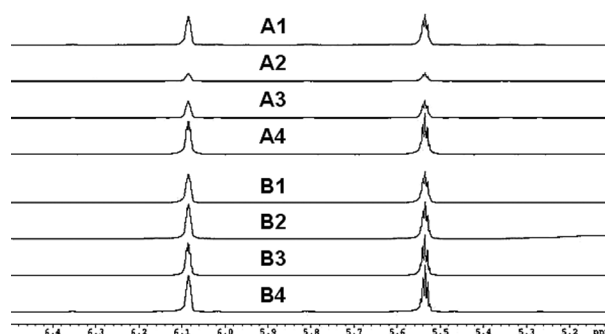


Figure 5: The intensity of vinylidene proton peaks in ¹H NMR spectra of PMMA in dependence of the ZnO concentration and size: A-ZnO (75nm); A1) 0 %, A2) 1 %, A3) 0.1 %, A4) 0.01 % and B-ZnO (340 nm); B1) 0 %, B2) 1 %, B3) 0.1 %, B4) 0.01 %

Slika 5: Intenziteta signalov vinilidenskih protonov v ¹H NMR-spektrih PMMA v odvisnosti od ZnO-koncentracije in velikosti delcev: A-ZnO (75 nm); A1) 0 %, A2) 1 %, A3) 0,1 %, A4) 0,01 % and B-ZnO (340 nm); B1) 0 %, B2) 1 %, B3) 0,1 %, B4) 0,01 %

ZnO on the termination mechanism of MMA radical polymerization causing reduced content vinylidene double bonds in PMMA chains as confirmed by ¹H NMR spectroscopy (Figure 5).³⁹ Double bonds are weak points of MMA chains where decomposition starts and reducing their content causes enhanced thermal stability. UV-VIS spectroscopic measurements confirmed that nano ZnO is extremely efficient UV absorber since 3 mm thick plates containing the mass fraction of ZnO 0.01 % absorb more than 90 % of the incident UV light (Figure 6). At the same time more than 70–80 % of the visible light is transmitted through the material when material is prepared by the prepolymer procedure. Our results are different to those reported in the literature;^{61,62} concentrations of nano ZnO filler were much lower; mainly because we used unmodified ZnO while in reported nanocomposites ZnO, modified with t-butyl phosphonic acid, was used. Nevertheless, changes in thermal stability and UV-VIS absorption are similar to the reported ones. Due to the absence of surface modification our ZnO

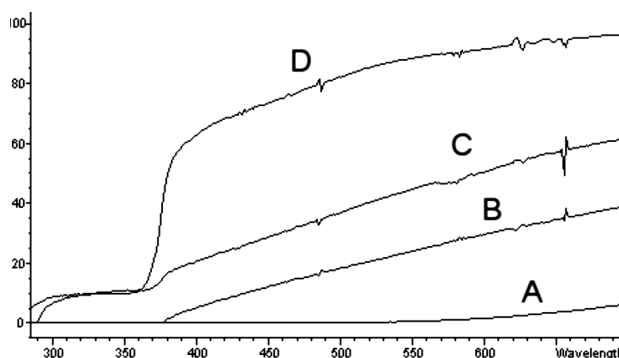


Figure 6: UV-VIS spectra of ZnO/PMMA nanocomposites using ZnO prepared in DEG in dependence of ZnO concentration: A) 1.0 %, B) 0.1 %, C) 0.01 %, D) 0.01 % – prepolymer procedure

Slika 6: UV-VIS-spektri ZnO/PMMA-nanokompozitov na osnovi ZnO, pripravljenega v DEG, v odvisnosti od masne koncentracije ZnO: A) 1.0 %, B) 0.1 %, C) 0.01 %, D) 0.01 % – postopek preko predpolimera

nanofiller is, due to lower production costs, more price competitive. Despite rather low ZnO concentration, there is a substantial effect on UV absorption as well as on the thermal stability of the prepared nanocomposites. Comparison with ZnO/PMMA nanocomposites, prepared by other procedures, is rather difficult because those nanocomposites are mostly in the form of powder or thin films while our materials are 3.5 mm thick plates.^{52–59} Prepared ZnO/PMMA nanocomposites have, due to high UV absorption, potential application as UV stabilized PMMA materials for various outdoor applications.

4 CONCLUSIONS

Syntheses of sub micrometer and nano ZnO structures as well as processing methods towards homogeneous ZnO/PMMA nanocomposites have been reviewed. ZnO nanostructures were synthesized by various hydrothermal and solvothermal synthetic routes, using various precursors, media and catalysts, and we showed that nano ZnO with organophilic surface can be successfully prepared in gram quantities in various diol media. Homogeneous ZnO/PMMA nanocomposites were prepared by different synthetic strategies using surface modified and unmodified nano ZnO. In our study, homogeneous ZnO/PMMA nanocomposites were prepared, using unmodified nano ZnO, by the radical chain polymerization of MMA in bulk and by optimizing the preparation procedure. Prepared nanocomposites showed enhanced thermal stability, when the concentration of ZnO is at least 1 %. Enhanced thermal stability, when ZnO is added in concentration of 1 % and higher, was explained, using ¹H NMR spectroscopy, as a consequence of reduced concentration of vinylidene double bonds in PMMA chains. Resulting nanocomposite materials absorbed from 80–98 % of the incident UV light by adding only the mass fraction of nano ZnO filler 0.01 %. Such materials have potential as UV stabilized PMMA materials for various outdoor applications with high sun light loads.

Acknowledgement

The authors acknowledge the financial support from the Ministry of Higher Education, Science and Technology of the Republic of Slovenia through the contract No. 3211-10-000057 (Center of Excellence for Polymer Materials and Technologies).

5 REFERENCES

- H. Yu, Z. Zhang, M. Han, X. Hao and F. Zhu, *J. Am. Chem. Soc.*, 127 (2005), 2378–2379
- M. H. Huang, S. Mao, H. Feick, H. Yan, Y. Wu, H. Kind, E. Weber, R. Russo, P. Yang, *Science*, 292 (2001), 1897–1899
- D. Ledwith, S.C. Pillai, G.W. Watson, J.M. Kelly, *Chem. Comm.*, 20 (2004), 2294–2295
- J. Zhang, L. Sun, C. Liao, C. Yan, *Chem. Comm.*, 3 (2002), 262–263
- Z. R. Tian, J. A. Voigt, J. Liu, B. Mckenzie, M. J. McDermott, *J. Am. Chem. Soc.*, 124 (2002), 12954–12955
- X. Y. Kong, Z. L. Wang, *Nano Lett.*, 3 (2003), 1625–1631
- M. M. Demir, R. M. Espi, I. Lieberwirth, G. Wegner, *J. Mat. Chem.*, 16 (2006), 2940–2947
- Y. Liu, J. Zhou, A. Larbot, M. Persin, *J. Mater. Proc. Technol.*, 189 (2007), 379–383
- S. Choi, E. Kim, J. Park, K. An, N. Lee, S. Kim, and T. Hyeon, *J. Phys. Chem. B*, 109 (2005), 14792–14794
- C-L Kuo, T-J. Kuo, M. H. Huang, *J. Phys. Chem. B*, 109 (2005), 20115–20121
- H. Zhang, D. Yang, S. Li, X. Ma, Y. Ji, J. Xu, D. Que, *Mater. Lett.*, 59 (2005), 1696–1700
- Z. Yang, Q. H. Liu, L. Yang, *Mater. Res. Bull.*, 42 (2007), 221–227
- H. Zhang, D. Yang, D. Li, X. Ma, S. Li, D. Que, *Cryst. Growth Des.*, 5 (2005), 547–550
- D. Kisailus, B. Schwenzer, J. Gomm, J. C. Weaver, D.E. Morse, *J. Am. Chem. Soc.*, 128 (2006), 10276–10280
- F. Li, Y. Ding, P. Gao, X. Xin, Z. L. Wang, *Angew. Chem. Int. Ed.*, 43 (2004), 5238–5242
- R. C. Wang, H. Y. Lin, *Mater. Chem. Phys.*, 125 (2011), 263–266
- K. Singh, *Adv. Powder Technol.*, 21 (2010), 609–613
- U. Pal, P. Santiago, *J. Phys. Chem. B*, 109 (2005), 15317–15321
- Y-S Fu, X. W. Du, J. Sun, Y. F. Song, J. Liu, *J. Phys. Chem. C*, 111 (2007), 3863–3867
- R. Shenhar, T. B. Norsten, V. C. Rotello, *Adv. Mater.*, 17 (2005), 657–669
- A. Taubert, D. Palms, O. Weiss, M. Piccini, D. N. Batchelder, *Chem. Mater.*, 14 (2002), 2594–2601
- A. Taubert, G. Glasser, D. Palms, *Langmuir*, 18 (2002), 4488–4494
- Y. Peng, An-Wu Xu, B. Deng, M. Antonietti, H. Coelfen, *J. Phys. Chem. B*, 110 (2006), 2988–2993
- H. Zhang, D. Yang, X. Ma, N. Du, J. Wu, D. Que, *J. Phys. Chem. B*, 110 (2006), 827–830
- H. C. Lin, M. D. Jiang, L. Y. Wang, W. H. Chen, S. F. Chen, C. N. Mo, *J. Chinese Inst. Engineers*, 33 (2010), 1069–1074
- R. Jetson, K. Yin, K. Donovan, Z. T. Zhu, *Mater. Chem. Phys.*, 124 (2010), 417–421
- A. K. Zak, W. H. Abd Majid, M. Darroudi, R. Yousefi, *Mater. Lett.*, 65 (2011), 70–73
- J. F. Grischwitz, R. Marczak, F. Werner, N. N. Lang, N. Jux, D. M. Guldi, W. Penkert, A. Hirsch, *J. Am. Chem. Soc.*, 132 (2010), 1624–1629
- S. Saliba, C.V. Serrano, J. Keilitz, M. L. Kahn, C. Mingotaud, R. Haag, J. D. Marty, *Chem. Mater.*, 22 (2010), 6301–6309
- Z. R. Ranjbar, A. Morsali, *Ultrason. Sonochem.*, 18 (2011), 644–651
- S. Li, M.S. Toprak, Y.S. Jo, J. Dobson, D.K. Kim, M. Muhammed, *Adv. Mater.*, 19 (2007), 4347–4352
- S. Paniraghi, A. Bera, D. Basak, *J. Coll. Interf. Sci.*, 353 (2011), 30–38
- F. J. Wang, J. Liu, Z. J. Wang, A. J. Lin, H. Luo, X. B. Yu, *J. Electrochem. Soc.*, 158 (2011), H30–H34
- D. Jezequel, J. Guenot, N. Jouini, G. Fievet, *J. Mater. Res.*, 10 (1995), 77–83
- L. Poul, S. Ammar, N. Jouini, E. Fievet F. Villain, *J. Sol–Gel Sci. Technol.*, 26 (2003), 261–265
- A. Anžlovar, Z. Crnjak Orel, M. Žigon, *J. Eur. Ceram. Soc.*, 27 (2007), 987–991
- A. Anžlovar, Z. Crnjak Orel, M. Žigon, *J. Nanosci. Nanotechnol.*, 8 (2008), 3516–3525
- C. Li, Y. Zhao, L. Wang, G. Li, Z. Shi, S. Feng, *Eur. J. Inorg. Chem.*, (2010), 217–220
- A. Anžlovar, Z. Crnjak Orel, M. Žigon, *Eur. Polym. J.*, 46 (2010), 1216–1224

- ⁴⁰ Y. Ding, Z. Gui, J. Zhu, Z. Wang, Y. Hu, L. Song, *J. Mater. Res.*, 22 (2007), 3316–3323
- ⁴¹ D. Sun, N. Miyatake, H. J. Sue, *Nanotechnology*, 18 (2007), Art. No. 215606
- ⁴² A. C. Balasz, T. Emrick, T. P. Russell, *Science*, 314 (2006), 1107–1110
- ⁴³ W. Y. Wang, J. Liu, X. B. Yu, G. Q. Yang, *J. Nanosci. Nanotechnol.*, 10 (2010), 5196–5201
- ⁴⁴ R. Munoz – Espi, G. Jeschke, I. Lieberwirth, C. M. Gomez, G. Wegner, *J. Phys. Chem. B*, 111 (2007), 697–707
- ⁴⁵ D. S. Golovko, R. Munoz – Espi, G. Wegner, *Langmuir*, 23 (2007), 3566–3569
- ⁴⁶ G. Kickelbick, *Prog. Polym. Sci.*, 28 (2003), 83–114
- ⁴⁷ V. Khrenov, M. Klapper, K. Muellen, *Macromol. Chem. Phys.*, 206 (2005), 95–101
- ⁴⁸ V. Khrenov, F. Schwager, M. Klapper, M. Koch, K. Muellen, *Polym. Bull.*, 58 (2007), 799–807
- ⁴⁹ X. K. Ma, Q. L. Tang, B. Zhou, Y. P. Xiao, H. Lei, Z. C. Wang, *E-Polymer*, (2010), art.no. 046
- ⁵⁰ R. Y. Hong, J. Z. Quian, J. X. Cao, *Powder Technol.*, 163 (2006), 160–168
- ⁵¹ E. J. Tang, G. X. Cheung, X. L. Ma, *Powder Technol.*, 161 (2006), 209–214
- ⁵² E. J. Tang, G. X. Chung, X. S. Pang, X. L. Ma, F. B. Xing, *Coll. Polym. Sci.*, 284 (2006), 422–428
- ⁵³ P. Liu, Z. X. Su, *J. Macromol. Sci.–Phys.*, B45 (2006), 131–138
- ⁵⁴ H. Y. Yu, J. Du, J. S. Gu, M. Y. Guan, Z. C. Wu, Q. Ling, Y. M. Sun, *Spectr. Spectral Anal.*, 24 (2004), 177–179
- ⁵⁵ J.W. Shim, J. W. Kim, S. H. Han, I. S. Chang, H. K. Kim, H. H. Kang, O. S. Lee, K. D. Suh, *Coll. Surf.A–Physicochem. Engin. Aspects* 207 (2002), 105–111
- ⁵⁶ Z. G. Wang, X. T. Zu, S. Zhu, X. Xiang, L. M. Fang, L. M. Wang, *Phys. Lett. A*, 350 (2006), 252–257
- ⁵⁷ W. Du, Y. S. Fu, J. Sun, X. Han, J. Liu, *Semicond. Sci. Techn.*, 21 (2006), 1202–1206
- ⁵⁸ M. M. Demir, M. Memesa, P. Castignolles, G. Wegner, *Macromol. Rapid Comm.*, 27 (2006), 763–770
- ⁵⁹ M. M. Demir, K. Koynov, Ü. Akbey, C. Bubeck, I. Park, I. Lieberwirth, G. Wegner, *Macromolecules*, 40 (2007), 1089–1100
- ⁶⁰ M. M. Demir, P. Castignolles, Ü. Akbey, G. Wegner, *Macromolecules*, 40 (2007), 4190–4198
- ⁶¹ M. Sato, A. Kawata, S. Morito, Y. Sato, I. Yamaguchi, *Eur. Polym. J.*, 44 (2008), 3430–3438
- ⁶² M. Agrawal, S. Gupta, N.E. Zafeiropoulos, U. Oertel, R. Hassler, M. Stamm, *Macromol. Chem. Phys.*, 211 (2010), 1925–1932
- ⁶³ D. Sun, H. J. Sue, *Appl. Phys. Lett.*, 94 (2009), art.no. 253106
- ⁶⁴ J. L. Ge, X. F. Zeng, X. Tao, X. Li, Z. G. Shen, J. Yun, J. F. Chen, *J. Appl. Polym. Sci.*, 118 (2010), 1507–1512
- ⁶⁵ M. H. Wong, R. Tsuji, S. Natt, H. J. Sue, *Soft Matter*, 6 (2010), 4482–4490

TUNING OF POLY(ETHYLENE TEREPHTHALATE) (PET) SURFACE PROPERTIES BY OXYGEN PLASMA TREATMENT

PRILAGODITEV LASTNOSTI POVRŠINE POLIETILEN TEREFTALATA (PET) Z OBELAVO V KISIKOVI PLAZMI

Aleš Doliška,^{1,2} Metod Kolar¹

¹Center of excellence for polymer materials and technologies (PoliMaT), Tehnološki park 24, SI-1000 Ljubljana, Slovenia

²University of Maribor, Faculty of Mechanical Engineering, Laboratory for Characterization and Processing of Polymers, Maribor, Slovenia
ales.doliska@uni-mb.si

Prejem rokopisa – received: 2011-02-10; sprejem za objavo – accepted for publication: 2011-03-25

Modification of surface properties of poly(ethyleneterephthalate) (PET) thin films by treatment with weakly ionized oxygen plasma was studied by contact angles of water and diiodomethane (DIM) drops. Samples were exposed to oxygen plasma with the ion density of $5 \cdot 10^{15}/\text{m}^3$ and the neutral oxygen atom density of $3 \cdot 10^{21}/\text{m}^3$. Just after the treatment they were characterized by contact angle measurements. Results showed a quick decrease of the water contact angle in the first few seconds of plasma treatment, while prolonged treatment did not cause any substantiated modification. The contact angles of DIM, on the other hand, remained rather constant for the first several seconds of plasma treatment, and increased after prolonged treatment. It was found that the dispersion component of the surface free energy decreased with increasing treatment time, while the polar component increased with treatment time. The results were explained by surface functionalization as well as by roughness effects.

Keywords: poly(ethylene terephthalate), PET, oxygen plasma, contact angle, hydrophilic, functionalization

Površinske lastnosti polimera polietilentereftalata (PET) smo prilagodili specifičnim zahtevam po visoki hidrofilnosti z obdelavo v kisikovi plazmi. Stopnjo hidrofilnosti smo določali iz meritev stičnih kotov dveh kapljev, in sicer vode in diiodometana. Vzorce smo obdelovali v kisikovi plazmi z gostoto ionov $5 \cdot 10^{15}/\text{m}^3$ in gostoto nevtralnih kisikovih atomov $3 \cdot 10^{21}/\text{m}^3$. Meritve stičnih kotov kapljic smo opravili takoj po plazemski obdelavi. Rezultati so pokazali hiter padec stičnega kota vodnih kapljic že v prvih sekundah plazemske obdelave. Podaljšan čas obdelave ni prinesel bistvenih sprememb. Stični koti diiodometana so ostali praktično nespremenjeni po prvih nekaj sekundah, z nadaljnjo obdelavo pa so začeli padati. Ugotovili smo, da disperzijska komponenta površinske energije počasi pada s plazemsko obdelavo, medtem ko polarna komponenta raste. Rezultate smo pojasnili s površinsko funkcionalizacijo polimera in povečano hrapavostjo površine.

Ključne besede: polietilentereftalat, PET, kisikova plazma, stični kot, hidrofilnost, funkcionalizacija

1 INTRODUCTION

Polymer materials are nowadays widely used in biology and medicine. They belong to organic materials and often express fairly good biocompatibility. The biocompatibility, however, is never optimal due to the required chemical and mechanical properties of polymers used for specific applications. In order to achieve improved biocompatibility, the surface properties should be modified. The most popular method for modification of surface properties of any material is application of non-equilibrium gaseous plasma treatment. The method is nowadays widely used for the modification of surface properties of bulk materials.¹⁻¹⁸ Plasma of particular interest is created in pure oxygen or oxygen-containing gasses. Non-equilibrium plasma has the great advantage over other techniques and the main one is the ability for the modification of surface properties while leaving the bulk properties intact. This ability is due to the fact that plasma is found at room temperature while chemical reactivity is extremely high. The chemical reactivity of plasma depends on plasma parameters but is typically as reactive as gas in thermal equilibrium would be at the

temperature of several 1000 °C. Extremely high chemical reactivity is due to the presence of gaseous particles with a high potential energy.

2 EXPERIMENTAL PROCEDURES

Experiments were performed with model PET films with a thickness of about 50 nm that were prepared as follows. Foils of commercially available PET were Mylar® foil, with a thickness of 175 µm. Mylar® foil was used as a facsimile for PET used in medical devices such as knitted or woven vascular grafts and PET angioplasty balloons. The foil was dissolved in 1,1,2,2-tetrachloroethane. PET films were deposited onto silicon wafers of rectangular shape with dimensions 1.5 cm × 3 cm × 0.20 cm. In order to achieve a uniform coating the crystals were mounted into a spin coater rotating at a maximum of 2000 r/min for 60 s. After this procedure the crystals were dried in an oven at 105 °C for 1 h. The surface free energy (SFE) of the samples was calculated from measured contact angles of water and diiodomethane drops according to OWRK (Owens, Wendt, Rabel, Kaelble) approach. For contact angles

(CA) measurements we used a professional device OCA 35 from Dataphysics (Germany). The device comprises a high speed camera that allows for pretty accurate determination of contact angles for different liquid drops. OWRK approach is one of the most common methods for calculation of the SFE of polymer materials. This model is based on assumption that the interfacial energy can be split to disperse and polar interactions equation (1). If liquid and solid surfaces come into contact there would be an interaction between polar parts as well as disperse parts of both phases at the interphase, but not between polar and disperse parts.^{19–23} Therefore, one can determine the polar and disperse part of surface free energy by measuring contact angle between a solid and liquids with different polarity.

$$\gamma_{sl} = \gamma_s + \gamma_l - 2(\sqrt{\gamma_s^d \cdot \gamma_l^d} + \sqrt{\gamma_s^p \cdot \gamma_l^p}) \quad (1)$$

Where γ_{sl} is solid liquid interface free energy, γ_s is solid free energy and γ_l is surface tension of liquid, d and p in superscript correspond to polar and dispersive part of free energies. On the basis of Young equation, the work of adhesion can be calculated from the measured contact angle of a liquid on a solid.^{19–23} With rearranging equation (1), the form as shown in equation (2) is obtained and the solid surface free energy is determined from measurement of the contact angle for water and diiodomethane with accurately known polar and dispersive components of their surface tension (**Table 1**). In the work approach, the contact angles of liquids with known values of γ_l , γ_l^d and γ_l^p are measured after which data are fitted to straight line equation (3).

$$\frac{\gamma_l(1 + \cos \theta)}{\sqrt{\gamma_l^d}} = \sqrt{\gamma_s^p} \left(\frac{\gamma_l^p}{\gamma_l^d} \right) + \sqrt{\gamma_s^d} \quad (2)$$

$$y = k \cdot x + b \quad (3)$$

The equation (2) is the linear function, where the slope of line, k ($k = \sqrt{\gamma_s^p}$) is the polar component and intercept of resulting line, b ($b = \sqrt{\gamma_s^d}$) is dispersive component of the solid's surface free energy (**Figure 5**). The surface free energy calculations were performed using the software SCA 21, supplied with the measuring device (Dataphysics, Germany).

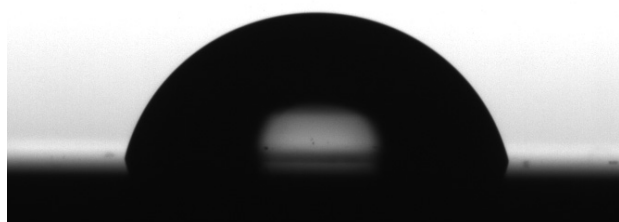


Figure 1: A photography of the water drop on untreated PET sample
Slika 1: Fotografija vodne kapljice na neobdelanem PET-vzorcu

At present experiments the volume of all drops were fixed to 3 μ L. Measurements were performed at room temperature with at least 5 repetitions and with an experimental error within ± 2 %.

Table 1: Surface tensions of test liquids for SFE determination

Tabela 1: Površinske napetosti preizkusnih raztopin za določanje površinske proste energije

	γ_l /(mN/m)	γ_l^p /(mN/m)	γ_l^d /(mN/m)
Water	72.8	51.0	21.8
Diiodomethane	50.8	0	50.8

Samples were exposed to oxygen plasma in a plasma reactor which has been described previously.^{24–26} The plasma reactor is pumped with a two stage rotary pump and never baked, so the ultimate pressure was 6 Pa. Experiments were performed at the pressure of 50 Pa. The density of charge particles and neutral oxygen atom density were measured with an electrical and a catalytic probe.^{26–34} The density of charge particles was $5 \cdot 10^{15}/\text{m}^3$, while the density of neutral oxygen atoms was $3 \cdot 10^{21}/\text{m}^3$.

3 RESULTS

The contact angles of water and DIM drops were measured at different treatment times up to 24 s. The photography of a water drop on an untreated sample is presented in **Figure 1**. The contact angle is rather high at 77° , indicating reasonable hydrophobic character of PET. A photo of a DIM drop is presented in **Figure 2**. The contact angle of this liquid is much lower at about 23° . Even a short exposure of a sample to oxygen plasma causes a huge change of the water drop contact angle. **Figure 3** represents a photo of a water drop after exposure to oxygen plasma for 1.5 s. On the other hand, the contact angle of DIM drop remains practically the same. **Figure 4** is a photo of drop after 1.5 s of plasma treatment. The contact angles have been measured at various treatment times and the results are summarized in **Figure 6**.

The contact angle of the water drops quickly decreased from initial 77° to about 17° . This quick drop happened in about 1 second of plasma treatment. With

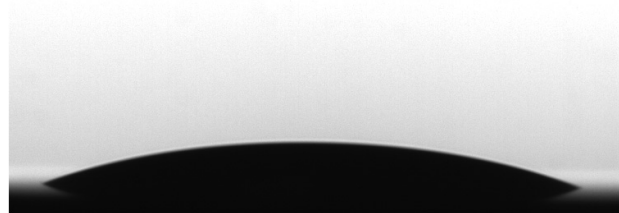


Figure 2: A photography of the diiodomethane drop on untreated PET sample

Slika 2: Fotografija kapljice diiodometana na neobdelanem PET-vzorcu

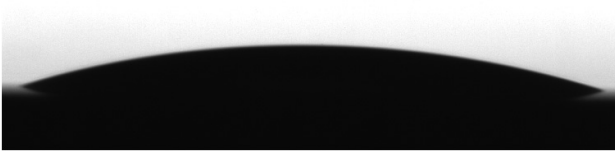


Figure 3: A photography of the water drop on oxygen plasma treated PET sample for 1.5 s

Slika 3: Fotografija vodne kapljice na PET-vzorcu, ki je bil obdelan s kisikovo plazmo 1,5 s

further treatment only small, but continuous decrease of water drop contact angle is observed. The behavior the DIM is completely different. The initial contact angle is about 23° and it remains practically unchanged for the first 6 s of plasma treatment. The contact angle increases up to about 33° for prolonged treatments. The results summarized in **Figure 6** allow for calculation of the surface free energy (SFE) according to the procedure described above. The total SFE versus the plasma treatment time is plotted in **Figure 7**. The measurements performed by two different liquids, i.e. water with the surface tension of 72.8 mN/m and DIM with the surface tension of 50.8 mN/m, allow for the determination of the dispersion and polar components of the PET surface energy. The polar and dispersion components of surface tension for both liquids are presented in **Table 1**. The calculated polar and dispersion components of surface free energies versus the plasma treatment time are presented in **Figure 8**.

4 DISCUSSION

The results summarized in **Figures 6 to 8** reveal some interesting features that are worth discussing. A fast drop of the water drop contact angle can be explained by characteristics of oxygen plasma applied at our experiments. As mentioned earlier the density of oxygen atoms in our plasma is $3 \cdot 10^{21}/m^3$. The flux of neutral oxygen atoms on the surface of a sample is calculated using basic equation

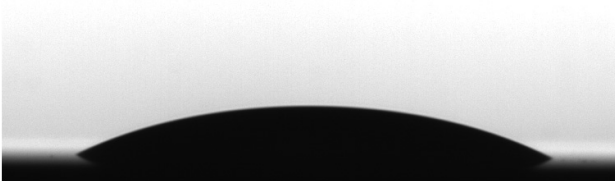


Figure 4: A photography of the diiodomethane dropon oxygen plasma treated PET sample for 1.5 s

Slika 4: Fotografija kapljice dijodometana na PET-vzorcu, ki je bil obdelan s kisikovo plazmo 1,5 s

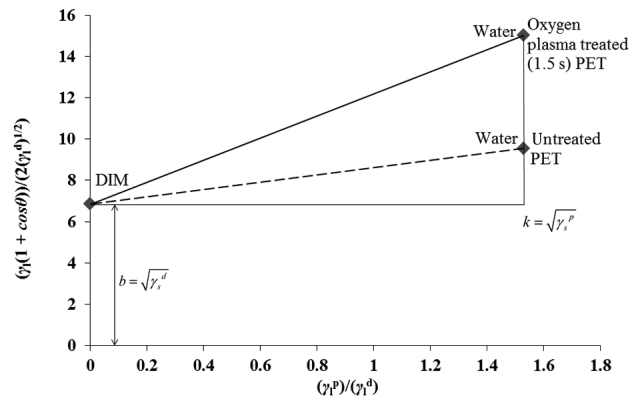


Figure 5: The OWRK model plot for SFE determination of PET surface

Slika 5: Graf OWRK modela za določitev površinske proste energije PET-površine

$$j = \frac{1}{4}nv \tag{4}$$

Where the n is the density of neutral oxygen atoms in the vicinity of our sample and v is the average of the thermal velocity of neutral oxygen atoms which is calculated as

$$v = \sqrt{\frac{8kT}{\pi m}} \tag{5}$$

Here, k is the Boltzmann constant, T the neutral gas kinetic temperature and m is the mas of one oxygen atom. Taking into account numerical values and assuming the gas is at room temperature the velocity is 630 m/s. The resultant flux of neutral oxygen atoms is about $5 \cdot 10^{23}/(m^2 s)$. This value is really high. The typical surface density of atoms in solid materials is in the order of $10^{19}/m^2$. If all oxygen atoms reaching the surface interacted with solid materials a monolayer of oxygen atoms would form in less than 0.1 ms. The reaction probability is, of course, never equal to 1, but the huge flux of atoms onto the surface of our samples allowed for a rapid saturation of polymer surface with

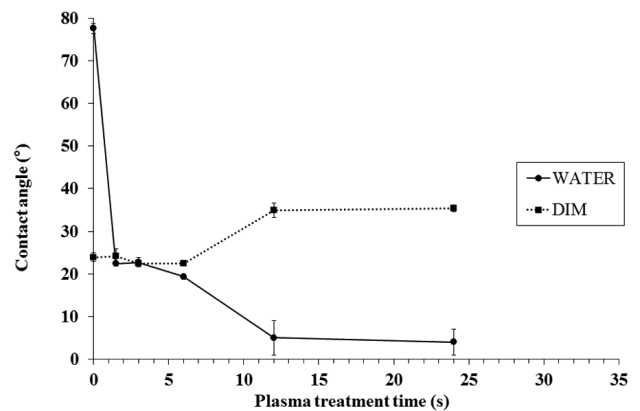


Figure 6: The contact angles of water and diiodomethane on model PET surface at various oxygen plasma treatment times

Slika 6: Kontaktni koti kapljic vode in dijodometana na modelnih PET- površinah pri različnih časih obdelave s kisikovo plazmo

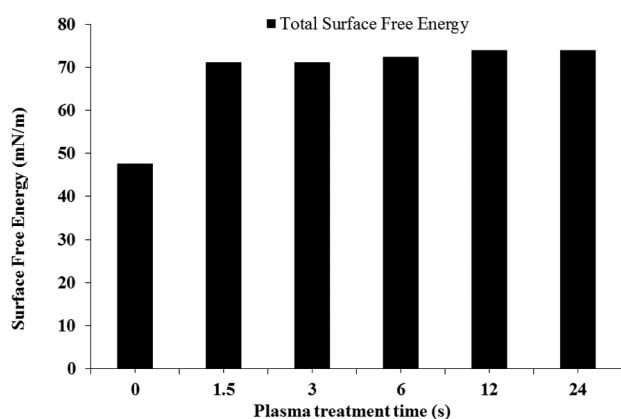


Figure 7: The surface free energies of PET versus the plasma treatment time

Slika 7: Površinska energija PET-vzorcev v odvisnosti od časa obdelave s kisikovo plazmo

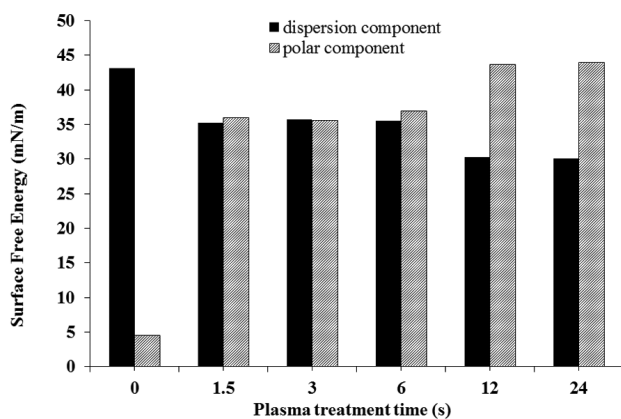


Figure 8: The calculated polar and dispersion components of surface free energies versus the plasma treatment time

Slika 8: Izračunane vrednosti polarne in disperzne komponente površinske energije v odvisnosti od časa obdelave s kisikovo plazmo

oxygen functional groups. Oxygen functional groups are known to be very polar and this explains a rapid increase of the polar component of SFE just after a brief exposure of the samples to oxygen plasma. **Figure 7** reveals that the SFE keeps increasing slightly with plasma treatment time even though the surface must have been already saturated with functional groups. Such increase can be explained by increased surface roughness. Namely, numerous authors have shown that the treatment of any material by oxygen plasma results in increased surface roughness.^{32–34}

The behavior of a DIM drop is completely different as shown in **Figure 6**. The measurements reveal that the contact angle of DIM drops remains practically unchanged for the first several second of plasma treatment and increases only slightly with prolonged treatment time. This behavior is not unexpected taking into account upper considerations. Namely oxygen plasma causes formation of polar functional group that definitely affects the polar component but has little effect on the dispersion component of SFE. Since DIM a non-polar liquid it cannot be affected by formation of polar

functional groups. **Figure 8** even reveals a continuous decrease of dispersion component. This effect can be explained by increased surface roughness. Namely, while the surface roughness increases, real surface area becomes larger and this causes a decrease of the dispersive component.

The total SFE is just a sum of the dispersive and polar components. It is presented in **Figure 7**. As expected, the total SFE increases rapidly when the samples are exposed to oxygen plasma but, since the saturation occurs quickly, the total SFE remains barely unchanged with prolonged treatment. From this point of view it is obvious that the very brief exposure of PET samples to oxygen plasma is efficient for modification of the surface properties of our samples. Such a rapid process allows for negligible modifications of the bulk properties. Neutral oxygen atoms are thermal so they cannot penetrate to any depth due to ballistic effects. They could penetrate into bulk material at elevated temperatures. As mentioned earlier, our plasma is kept at room temperature (in terms of neutral gas kinetic temperature), so the samples cannot be heated by accommodation of neutral oxygen atoms and molecules on the polymer surface. The samples could be heated by other effects. One of them is bombardment of the surface by oxygen ions. The density of ions in our plasma, however, is very low so this heating effect is easily neglected. More important should be heterogeneous surface recombination of neutral oxygen atoms. These atoms may represent a pretty important source of heating as showed by several authors.^{38–47} Happily enough, however, the required treatment time is only about 1 s so even this heating channel can be neglected. The temperature of our samples therefore remains close to the room temperature so any bulk modifications are absent.

5 CONCLUSION

The surface free energy can be determined rather precisely by measuring contact angles of testing liquids with a known surface tension against polymer surface. Surface free energy of PET surface was modified by treatment with oxygen plasma. The results show an increase of the surface free energy from around 47 mN/m to almost 75 mN/m even after a brief exposure of the polymer to oxygen plasma. The increase is due to increasing of polar component of surface free energy because oxygen plasma causes formation of polar functional group on a polymer. Such a surface is more hydrophilic than untreated one and it is expected that such a surface is by far more biocompatible than original material. The results of our experiments showed that optimal results were achieved even after a second of plasma treatment so the method is suitable for modification of surface properties of delicate organic materials that do not stand heating to elevated temperatures.

ACKNOWLEDGMENTS

The authors acknowledge the financial support from the Ministry of Higher Education, Science and Technology of the Republic of Slovenia through contract No. 3211-10-000057 (Centre of Excellence Polymer Materials and Technologies).

6 REFERENCES

- ¹ T. Vrlinic, A. Vesel, U. Cvelbar, M. Krajnc, M. Mozetic, *Surf. Interface Anal.*, 39 (2007) 6, 476–481
- ² M. Sowe, I. Novak, A. Vesel, I. Junkar, M. Lehocky, P. Saha, I. Chodak, *Int. J. Polym. Anal. Ch.*, 14 (2009) 7, 641–651
- ³ A. Vesel, *Inf. MIDEM*, 38 (2009), 257–265
- ⁴ M. Gorjanc, V. Bukosek, M. Gorenssek, A. Vesel, *Tex. Res. J.*, 80 (2010) 6, 557–567
- ⁵ A. Vesel, M. Mozetic, S. Strnad, K. Stana - Kleinschek, N. Hauptman, Z. Persin, *Vacuum*, 84 (2010) 1, 79–82
- ⁶ I. Junkar, A. Vesel, U. Cvelbar, M. Mozetic, S. Strnad, *Vacuum*, 84 (2010) 1, 83–85
- ⁷ A. Asadinezhad, I. Novak, M. Lehocky, F. Bilek, A. Vesel, I. Junkar, P. Saha, A. Popelka, *Molecules*, 15 (2010) 2, 1007–1027
- ⁸ A. Vesel, K. Elersic, I. Junkar, B. Malic, *Mater. Tehnol.*, 43 (2009) 6, 323–326
- ⁹ A. Asadinezhad, I. Novak, M. Lehocky, V. Sedlarik, A. Vesel, I. Junkar, P. Saha, I. Chodak, *Plasma Processes Polym.*, 7 (2010) 6, 504–514
- ¹⁰ A. Asadinezhad, I. Novak, M. Lehocky, V. Sedlarik, A. Vesel, P. Saha, I. Chodak, *Colloids Surf. B Biointerfaces*, 77 (2010) 2, 246–256
- ¹¹ A. Vesel, M. Mozetic, P. Panjan, N. Hauptman, M. Klanjssek - Gunde, M. Balat-Pichelin, *Surf. Coat. Technol.*, 204 (2010) 9/10, 1503–1508
- ¹² A. Drenik, A. Vesel, M. Mozetič, *J. Nucl. Mater.*, 386–388 (2009), 893–895
- ¹³ A. Vesel, M. Mozetic, A. Zalar, *Appl. Surf. Sci.*, 200 (2002), 94–103
- ¹⁴ A. Vesel, A. Drenik, M. Mozetič, A. Zalar, M. Balat - Pichelin, M. Bele, *Vacuum*, 82 (2007) 2, 228–231
- ¹⁵ A. Vesel, M. Mozetič, A. Drenik, S. Milosevic, N. Krstulovic, M. Balat - Pichelin, I. Poberaj, D. Babic, *Plasma Chem. Plasma P.*, 26 (2006), 577–584
- ¹⁶ R. Kulcar, M. Friskovec, N. Hauptman, A. Vesel, M. Klanjssek - Gunde, *Dyes Pigm.*, 86 (2010) 3, 271–277
- ¹⁷ U. Cvelbar, M. Mozetič, I. Junkar, A. Vesel, J. Kovač, A. Drenik, T. Vrlinič, N. Hauptman, M. Klanjssek - Gunde, B. Markoli, N. Krstulović, S. Milosevič, F. Gaboriau, T. Belmonte, *Appl. Surf. Sci.*, 253 (2007) 21, 8669–8673
- ¹⁸ A. Vesel, *Surf. Coat. Technol.*, 205 (2010) 2, 490–497
- ¹⁹ Z. Peršin, K. Stana - Kleinschek, T. Kreže, *Croatia Chemica Acta*, 75 (2002), 75–84
- ²⁰ Z. Peršin, K. Stana - Kleinschek, M. Sfiligoj-Smole, T. Kreže, V. Ribitsch, *Textile Research Journal*, 74 (2004), 74–81
- ²¹ K. Stana - Kleinschek, T. Kreže, L. Fras Zemljič, V. Ribitsch, *Mater. Res. Innov.*, 6 (2002), 13–18
- ²² K. Stana-Kleinschek, V. Ribitsch, T. Kreže, M. Sfiligoj-Smole, Z. Peršin, *Lenzing, Ber.*, 82 (2003), 83–95
- ²³ T. Kreže, K. Stana-Kleinschek, V. Ribitsch, Z. Peršin, M. Sfiligoj-Smole, *Mater. res. innov. (Internet)*, 9 (2005), 108–129
- ²⁴ A. Vesel, M. Mozetič, A. Hladnik, J. Dolenc, J. Zule, S. Milosevič, N. Krstulović, M. Klanjšek - Gunde, N. Hauptman, *J. Phys. D: Appl. Phys.*, 40 (2007) 12, 3689–3696
- ²⁵ M. Mozetič, U. Cvelbar, A. Vesel, A. Ricard, D. Babič, I. Poberaj, *J. Appl. Phys.*, 97 (2005) 10, 103308-1–103308-7
- ²⁶ M. Mozetič, A. Vesel, U. Cvelbar, A. Ricard, *Plasma Chem. Plasma Process.*, 26 (2006) 2, 103–117
- ²⁷ M. Mozetič, A. Vesel, A. Drenik, I. Poberaj, D. Babič, *J. Nucl. Mater.*, 363–365 (2007), 1457–1460
- ²⁸ M. Mozetič, A. Vesel, V. Monna, A. Ricard, *Vacuum*, 71 (2003) 1–2, 201–205
- ²⁹ A. Vesel, M. Mozetič, *Vacuum*, 61 (2001) 2–4, 373–377
- ³⁰ A. Drenik, U. Cvelbar, A. Vesel, M. Mozetič, *Inf. MIDEM*, 35 (2005), 85–91
- ³¹ A. Drenik, U. Cvelbar, A. Vesel, M. Mozetič, *Strojstvo*, 48 (2006) 1/2, 17–22
- ³² A. Vesel, A. Drenik, M. Mozetič, M. Balat - Pichelin, *Vacuum*, 84 (2010) 7, 969–974
- ³³ I. Junkar, U. Cvelbar, A. Vesel, N. Hauptman, M. Mozetič, *Plasma Processes Polym.*, 6 (2009) 10, 667–675
- ³⁴ A. Vesel, M. Mozetič, A. Drenik, N. Hauptman, M. Balat - Pichelin, *Appl. Surf. Sci.*, 255 (2008) 5, 1759–1765
- ³⁵ A. Vesel, I. Junkar, U. Cvelbar, J. Kovač, M. Mozetič, *Surf. Interface Anal.*, 40 (2008) 11, 1444–1453
- ³⁶ U. Cvelbar, Z. Chen, M. K. Sunkara, M. Mozetič, *Small*, 4 (2008) 10, 1610–1614
- ³⁷ M. Balat - Pichelin, J. M. Badie, R. Berjoan, P. Boubert, *Chem. Phys.*, 291 (2003), 181–194
- ³⁸ U. Cvelbar, K. Ostrikov, A. Drenik, M. Mozetič, *Appl. Phys. Lett.*, 92 (2008) 13, 133505-1–133505-3
- ³⁹ M. Balat - Pichelin, L. Bedra, O. Gerasimova, P. Boubert P, *Chem. Phys.*, 340 (2007), 217–226
- ⁴⁰ L. Scatteia, D. Alfano, F. Monteverde, J. L. Sans, M. Balat - Pichelin, *J. Am. Ceram. Soc.*, 91 (2008), 1461–1468
- ⁴¹ C. Guyon, S. Cavadias, I. Mabilie, M. M. Santillan, J. Amouroux, *Catalysis Today*, 89 (2004), 159–167
- ⁴² C. Guyon, S. Cavadias, J. Amouroux, *Surf. Coat. Technol.*, 142–144 (2001), 959–963
- ⁴³ S. Gomez, P. G. Steen, W. G. Graham, *Appl. Phys. Lett.*, 81 (2002), 19–21
- ⁴⁴ M. Mozetič, A. Zalar, *Appl. Surf. Sci.*, 158 (2000), 263–267
- ⁴⁵ M. Mozetič, U. Cvelbar, *Int. J. Nanosci.*, 6 (2007), 121–124
- ⁴⁶ A. Drenik, U. Cvelbar, K. Ostrikov, M. Mozetič, *J. Phys. D: Appl. Phys.*, 41 (2008), 115201-1–115201-7
- ⁴⁷ M. Balat - Pichelin, M. Passarelli, A. Vesel, *Mater. Chem. Phys.*, 123 (2010), 40–46

PROBABILITY OF RECOMBINATION AND OXIDATION OF O ATOMS ON a-C:H SURFACE

VERJETNOST ZA REKOMBINACIJO IN OKSIDACIJO ZA ATOME KISIKA NA POVRŠINI a-C:H

¹Aleksander Drenik, ²Kristina Eleršič, ²Martina Modic, ²Peter Panjan

¹Center of Excellence for Polymer Materials and Technologies, Tehnološki park 24, 1000 Ljubljana, Slovenia.

²Jožef Stefan Institute, Jamova 39, 1000 Ljubljana, Slovenia
aleksander.drenik@ijs.si

Prejem rokopisa – received: 2011-03-01; sprejem za objavo – accepted for publication: 2011-04-04

In the search for a sustainable energy source for future generations, thermonuclear fusion should not be left unconsidered. One of the important problems of current and near-future fusion devices is the formation of amorphous hydrogenated carbon deposits (a-C:H), which have to be removed regularly. Removal of a-C:H by atomic oxygen seems like a suitable candidate for a cleaning method. Efficiency of the cleaning method will depend on the efficiency of atomic oxygen delivery. This in turn will depend on the atom loss on reactor walls, which is predominantly governed by recombination. An experiment was performed to measure the recombination coefficient of a-C:H for neutral oxygen atoms. The source of atomic oxygen was an inductively coupled RF discharge, created in pure oxygen. The oxygen densities were measured by a nickel tipped FOCP. The a-C:H sample was prepared by thermionic arc sputtering of a graphite target in a mixed argon / acetylene atmosphere. The recombination coefficient was found to be of the order of 10^{-5} . Moreover, it was discovered that the a-C:H deposition was eroded by O atoms during the experiment. In a rough estimate, the probability of oxidation was found to be two orders of magnitude lower than the probability of recombination.

Key words: weakly ionised plasma, atomic oxygen, recombination, a-C:H, Fiber Optic Catalytic Probe

Pri iskanju trajnostnega energijskega vira za prihodnje generacije ne smemo prezreti termonuklearne fuzije. Ena od najpomembnejših težav sodobnih in prihodnjih fuzijskih naprav je nalaganje amorfnih hidrogeniziranih ogljikovih nanosov (a-C:H), ki jih je treba redno odstranjevati. Primeren kandidat za metodo čiščenja se ponuja odstranjevanje a-C:H z atomskim kisikom. Učinkovitost te metode bo odvisna od učinkovitosti dotoka atomskega kisika k površini. Ta pa bo odvisna od izgub atomov na stenah reaktorja, v katerih je največji delež rekombinacija. Izvedli smo eksperiment z namenom izmeriti rekombinacijski koeficient a-C:H za nevtralne kisikove atome. Vir atomskega kisika je bila induktivno sklopljena RF-razelektritev v čistem kisiku. Gostote atomskega kisika smo merili z nikljevo optično katalitično sondo. Vzorec a-C:H je bil pripravljen z razprševanjem grafitne tarče v atmosferi mešanice argona in acetilena s termionskim oblokom. Ugotovili smo, da je rekombinacijski koeficient reda velikosti 10^{-5} . Nadalje smo ugotovili, da je med eksperimentom nastala erozija a-C:H-vzorca zaradi delovanja O-atomov. Z grobo oceno smo ugotovili, da je verjetnost za oksidacijo dva velikostna reda nižja od verjetnosti za rekombinacijo.

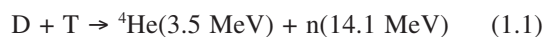
Ključne besede: šibko ionizirana plazma, atomarni kisik, rekombinacija, a-C:H, Optična katalitična sonda

1 INTRODUCTION

In the effort to satisfy the ever growing energy needs of the human civilization, mankind will have to look beyond the horizon of currently used energy sources, among which are fossil fuels are prevalent.¹ Resources of fossil fuels are known to be limited and moreover, the use of fossil fuels is linked to the emission of greenhouse gases, such as CO₂, which is also a very significant problem.^{2,3} While renewable sources offer production of energy without the high environmental costs, they are unfortunately not efficient enough to completely replace the fossil fuels.⁴ Nuclear fission seems like a powerful source of energy, which is also not linked to CO₂ emissions. However, the fission fuel reserves are limited and their use is associated to the problem of nuclear waste. In contrast, when obtaining energy from nuclear fusion, the reaction is fueled by isotopes of hydrogen and lithium that are plentiful in nature. Moreover, the end products of the fusion reaction are stable elements, so there is no problem of radioactive waste. Unfortunately,

the controlling the fusion reaction is much more difficult than the fission reaction. Despite the efforts invested in this field, so far there are no operating fusion power plants. However, individual experiments have shown that fusion can indeed be both achieved in a laboratory and controlled.⁵

The reaction that is most suitable for controlled fusion is:



where a deuterium and tritium nucleus join to form a helium nucleus and a neutron. In order to overcome the electrostatic potential of the positively charged nuclei, a substantial amount of energy must be invested into the reaction (0.4 MeV). This is most easily achieved by heating the fuel to a sufficiently high temperature, so that the thermal kinetic energy of the hydrogen isotopes is high enough – this is referred to as thermonuclear fusion. The required temperature is several thousands of Kelvin, at which the gas is ionized and becomes plasma. Currently, the most promising reactor type for achieving

thermonuclear fusion is the tokamak. It is a toroidal plasma reactor, where the plasma is confined by magnetic field. The confining magnetic field is produced both by external magnets, as well as the electric current of the plasma itself.

While the plasma is magnetically confined, certain contact between the plasma and reactor walls is required for the normal operation of the reactor. In most modern fusion devices, this takes place in the divertor. The heat loads on the surfaces of plasma facing components can be extremely high, in the forthcoming ITER, they are expected to rise up to 10 MW/m².⁶ For that reason, the plasma facing components are constructed using materials which can sustain such high thermal loads. One of such materials is carbon fiber composite (CFC), which features excellent thermal conductivity and can also withstand very high temperatures. The main drawback of the CFC is that it is highly susceptible to chemical erosion by hydrogen.

Hydrogen atoms from the plasma interact with carbon atoms in the PFCs and form carbohydrate molecules which are desorbed from the wall. This way, they can migrate throughout the reactor before they are finally re-deposited on the wall of the reactor. This gives rise to the formation of amorphous hydrogenated carbon deposits (a-C:H) in the walls of the reactor.⁷ Depending on the position of deposit formation, the hydrogen content in the deposit can be as high as 40 %. Because fusion reactors operate on a deuterium-tritium fuel mixture, the a-C:H layers also contain tritium, the radioactive isotope of hydrogen. The buildup of a-C:H layers inside the reactor cause the reactor vessel itself to become radioactive, which is a very much undesired effect, and a serious security risk. In order to ensure an uninterrupted operation of a fusion device, these deposits should be regularly removed.⁸

While there is – and most probably there will not be – one definite method, but rather a combination of various cleaning methods, oxidation of a-C:H deposits is certainly a very suitable candidate. So far, thermal oxidation (baking in O₂ atmosphere) has shown promising results, however the a-C:H removal rates are too low for application in modern day and future fusion devices. A much more efficient technique would be removal of a-C:H by atomic oxygen. Neutral oxygen atoms, which are the predominant species in weakly ionized oxygen plasma, are known to be very reactive, especially in interaction with organic (e.g. carbohydrate) materials.

The interaction of weakly ionized oxygen plasma with organic materials is spread over a very broad spectrum. The effect of oxygen atoms on materials can either be very non-invasive, modifying only the topmost atomic layers of the surface, such as is the case in surface activation,^{9–17} or it can be destructive, as it is with the application of weakly ionized plasma for destruction of bacteria (sterilization).^{18,19} However, it should be noted that even when atomic oxygen interacts destructively with the processed material, the destruction is very

selective. Indeed, the selective etching by neutral oxygen atoms is a well known and documented feature.^{20–24} The selectivity is believed to stem from the different erosion yields, based on different hydrogen content of the processed material. The general rule is that the more hydrogen the material contains (the "softer" it is), the higher is the erosion yield for neutral oxygen atoms.²⁵ The etching efficiency along with the selectivity of etching could allow for successful removal of a-C:H without causing significant damage to carbon based reactor components. Weakly ionized oxygen plasma has already been used as a source of atomic oxygen in experiments of a-C:H removal, yielding removal rates as high as 10 nm/s,²⁶ and in experiments dealing with interaction of oxygen atoms with tungsten containing a-C:H deposits at extreme conditions.²⁷

A successful technique for removal of a-C:H requires efficient delivery of atomic oxygen to the contaminated surface, which means that the density of oxygen atoms at the contaminated surface should be relatively high, even if that surface is not in the direct vicinity of the atom source. The transmission of atoms from the source to the target, so to speak, depends in a great way on losses of atoms on the surrounding reactor walls. Among the many possible reactions that can undergo during the interaction of atomic oxygen with solid materials,^{28–40} heterogeneous recombination, reaction in which two oxygen atoms join to form an oxygen molecule, is in most cases the most probable reaction. Due to the laws of conservation of momentum and energy, in gas phase it requires a three body collision, which is an extremely rare event at low pressures, so it is safe to assume it only takes place on surfaces of solid materials. Since recombination is the most important contribution to atom losses, it has a very significant effect on the atomic oxygen density inside the reactor. Thus, the probability of heterogeneous recombination, or recombination coefficient γ is of key importance when planning a-C:H removal systems.

In this paper, we present an experiment in which we observed both recombination of oxygen atoms on an a-C:H surface, as well as oxidation of a-C:H. Based on these observations, we compare the probability of recombination and the probability of oxidation.

2 EXPERIMENTAL

We performed an experiment in the afterglow of weakly ionized oxygen plasma with the intent to determine the recombination coefficient of a-C:H for oxygen atoms. The a-C:H sample was prepared in a thermionic arc sputtering system, by sputtering a graphite target in an atmosphere of argon and acetylene. The material used for the substrate, was aluminum foil, due to its favorable mechanic properties. The thickness of the deposited a-C:H film was 0.5 μm . The a-C:H covered foil was inserted into a side-arm of our plasma

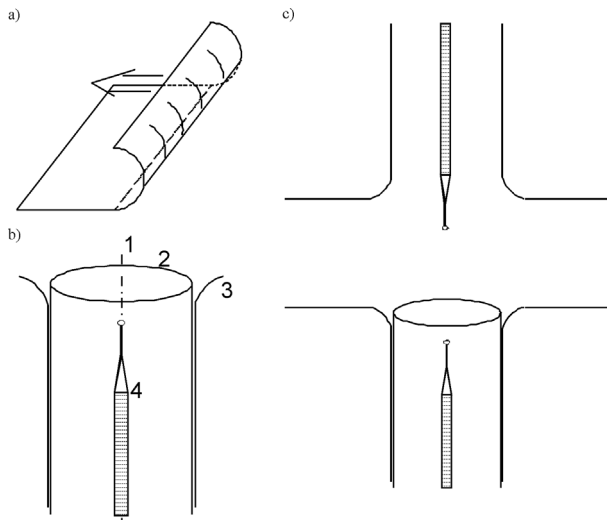


Figure 1: Experimental set-up: a) manipulation of the a-C:H covered foil, arrow indicates direction of folding; b) insertion of foil (2) and the FOCP (4) into the side-arm (2). The FOCP is used to measure the density of atomic oxygen along the axis (1) of the side-arm; c) position of the additional FOCP (top side) that measures the atomic oxygen density at a constant position.

Slika 1: Eksperimentalna postavitev: a) zvižanje folije, pokrite z a-C:H, puščica nakazuje smer zvižanja; b) vstavljanje folije (2) in optične katalitične sonde (4) v stransko cev (2). Z optično katalitično sondo merimo gostoto atomarnega kisika v osi (1) stranske cevi; c) položaj dodatne optične katalitične sonde (zgoraj), s katero merimo gostoto atomskega kisika na nespremenljivem položaju.

reactor, so that the a-C:H covered side was facing the inside of the tube, as seen in **Figure 1**. The reactor was powered by an inductively coupled radiofrequency generator, operating at 27.12 MHz with an approximately 100 W output power. Plasma was ignited in pure oxygen, leaked into the plasma reactor at pressures between 60 Pa and 180 Pa. The resulting atomic oxygen densities in the direct vicinity of the a-C:H sample were from $5 \cdot 10^{21} \text{ m}^{-3}$ to $2 \cdot 10^{22} \text{ m}^{-3}$. A spatially resolved measurement of atomic oxygen densities was performed using a nickel tipped fiber optic catalytic probe (FOCP).⁴¹⁻⁴⁷ The FOCP was used to measure the atomic

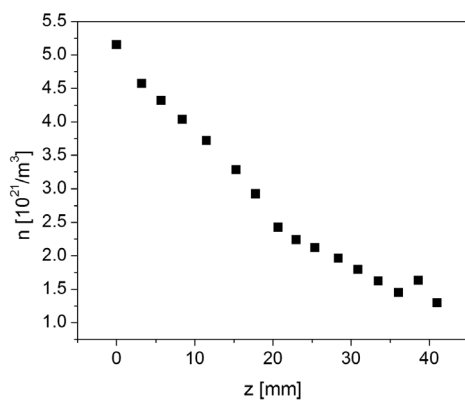


Figure 2: Atomic oxygen density profile recorded at 120 Pa. The term z denotes the distance from the probe tip to the opening of the side-arm.

Slika 2: Profil gostote atomskega kisika, posnet pri 120 Pa. Izraz z označuje razdaljo med ustjem stranske cevi in konico sonde.

oxygen density at several discretely spaced points along the axis of the side-arm, at different pressures. Simultaneously, another nickel tipped FOCP was kept at constant position in the reactor to monitor the fluctuations of the atomic oxygen density that might affect the results.

3 RESULTS AND DISCUSSION

An example of the recorded atomic oxygen density profile, recorded at a fixed pressure, is shown in **Figure 2**. A physical model, based on the diffusion equation,⁴⁸ was employed to determine the values of the recombination coefficient from the recorded atomic oxygen profiles. Fitting the model over the density profiles obtained at all the different pressures, we get the value of the recombination coefficient $\gamma = (1.0 \pm 0,3) \cdot 10^{-3}$.

When we removed the foil from the experimental system, we noticed that the a-C:H film had been partially eroded during the experiment. As seen in **Figure 3**, the deposit was removed from the substrate up to 2 cm away from the edge of the foil. This, of course, means that the obtained values of the recombination coefficient are not accurate, as during the measurement, the surface of the sample changed from a-C:H to aluminum. Using only the data obtained in the non-eroded region, the re-calculated value of recombination coefficient is $(9.9 \pm 0,2) \cdot 10^{-4}$. As the value does not greatly differ from the first calculation, we assume that the value of the recombination coefficient of the substrate (Al) is similar to that of a-C:H. However, that is not the only problem that has arisen due to the erosion of the sample. The model we used to determine the value of the recombination coefficient assumes that the only mechanism of atom loss on the walls is recombination when clearly, the oxygen atoms engage in oxidation as well. However,

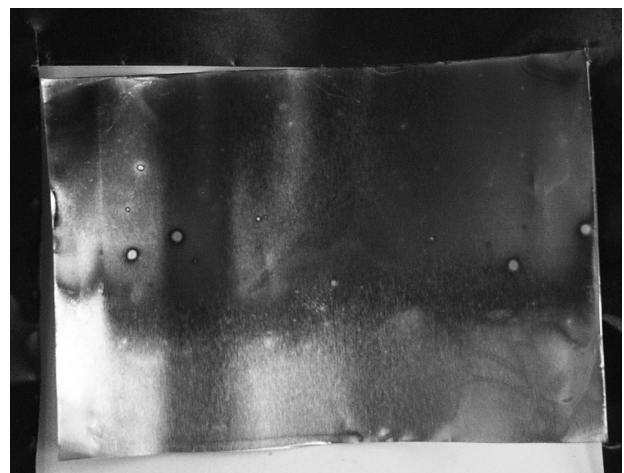


Figure 3: Aluminum foil with the deposited a-C:H thin film after the experiment. The foil used in the experiment was cut out from the piece that is framing it in the picture. The difference between the eroded and non-exposed a-C:H deposits are easily observable.

Slika 3: Aluminijeva folija z nanosom a-C:H po eksperimentu. Folija, ki smo jo uporabili pri eksperimentu, je bila izrezana iz večjega kosa folije, ki jo na sliki uokvirja. Razlika med pojedkanim in nespremenjenim vzorcem je očitna.

while determination of the erosion rate was not the primary aim of this experiment, we can nonetheless make a rough estimate of the erosion rate and subsequently the loss of atoms due to oxidation.

The topmost, eroded layer of the sample received, in approximately two hours of total operation time, a dose of neutral oxygen atoms:

$$\Gamma = 15 \cdot 10^{28} / \text{m}^3 \quad (1.2)$$

The thickness of the deposit was $h = 0.5 \mu\text{m}$, which results in an erosion rate of $\nu \approx 0.06 \text{ nm/s}$. Assuming the density of carbon atoms in the deposit to be the same as the density of carbon atoms in graphite, $n = 1.24 \cdot 10^{29} / \text{m}^3$, we get the number of removed atoms per square meter in those two hours, $N = 6 \cdot 10^{22} / \text{m}^2$. Further assuming that each eroded carbon atom reacts with one oxygen atom from the gas phase, the probability for oxidation is the ratio between the oxygen atoms that engage in oxidation and the total number of impinging oxygen atoms:

$$P = \frac{\Gamma}{N} = \frac{6 \cdot 10^{22}}{15 \cdot 10^{28}} = 4 \cdot 10^{-6} \quad (1.3)$$

which is for a factor of 250 lower than the probability of recombination. Thus, we can safely conclude that probability of the oxygen atom engaging in recombination is at least two orders of magnitude higher than the probability it would engage in an oxidation reaction. Moreover, since oxidation is only a minor contribution to the atom loss on the a-C:H surface, we see that the erosion hasn't further affected the results of this experiment.

4 CONCLUSION

An experiment was performed to determine the recombination coefficient of a-C:H for neutral oxygen atoms. The sample was prepared by thermionic arc sputtering deposition on aluminum foil. An inductively coupled radiofrequency discharge in pure oxygen was used as the source of atomic oxygen. Neutral oxygen atom densities were measured with a fiber optic catalytic probe. After the experiment, it was found that the a-C:H film had been eroded during the experiment. Using a rough estimate, we conclude that an impinging oxygen atom will take part in an oxidation reaction is $4 \cdot 10^{-6}$. The value of the recombination coefficient, obtained using a diffusion model, was found to be $(9.9 \pm 0.2) \cdot 10^{-4}$. Thus, we found the probability of recombination two orders of magnitude greater than the probability of oxidation.

ACKNOWLEDGEMENT

The authors acknowledge the financial support from the Ministry of Higher Education, Science and Technology of the Republic of Slovenia through the contract

No. 3211-10-000057 (Center of Excellence Polymer Materials and Technologies).

5 REFERENCES

- ¹ International Energy Annual 2004, www.eia.doe/international, accessed on: 2007
- ² BP-Amoco Statistical Review of World Energy, June 1999, www.bpamoco.com, accessed on: 2007
- ³ H. Inhaber, H. Saunders, *The Sciences* (1994) 20–25
- ⁴ M. Kleemann, *Elektrowärme International* 49 (1991) A2, A62.70
- ⁵ G. Van Oost, E. Rebhan, *Transactions of Fusion Science and Technology* 53 (2008) 2T, 17–26
- ⁶ J. Linke, *Fusion Science and Technology* 53 (2008) 2T, 278–287
- ⁷ A. Kirschner, D. Borodin, S. Droste, V. Philipps, U. Samm, G. Federici, A. Kukushkin, A. Loarte, *Journal of Nuclear Materials* 363 (2007) 91–95
- ⁸ G. Counsell, P. Coad, C. Grisola, C. Hopf, W. Jacob, A. Kirschner, A. Kreter, K. Krieger, J. Likonen, V. Philipps, J. Roth, M. Rubel, E. Salancon, A. Semerok, F. L. Tabares, A. Widdowson, *Plasma Physics and Controlled Fusion* 48 (2006) 12B, B189–B199
- ⁹ C. Canal, F. Gaboriau, A. Ricard, M. Mozetic, U. Cvelbar, A. Drenik, *Plasma Chemistry and Plasma Processing* 27 (2007) 4, 404–413
- ¹⁰ U. Cvelbar, M. Mozetic, I. Junkar, A. Vesel, J. Kovac, A. Drenik, T. Vrlinic, N. Hauptman, M. Klanjsek-Gunde, B. Markoli, N. Krstulovic, S. Milosevic, F. Gaboriau, T. Belmonte, *Applied Surface Science* 253 (2007) 21, 8669–8673
- ¹¹ I. Junkar, A. Vesel, U. Cvelbar, M. Mozetic, S. Strnad, *Vacuum* 84 (2009) 1, 83–85
- ¹² M. Mozetic, *Informacije Midem-Journal of Microelectronics Electronic Components and Materials* 33 (2003) 4, 222–227
- ¹³ A. Vesel, I. Junkar, U. Cvelbar, J. Kovac, M. Mozetic, *Surface and Interface Analysis* 40 (2008) 11, 1444–1453
- ¹⁴ A. Vesel, M. Mozetic, *Second International Workshop on Non-Equilibrium Processes in Plasmas and Environmental Science* 162 (2009), 12015–12015
- ¹⁵ A. Vesel, M. Mozetic, A. Hladnik, J. Dolenc, J. Zule, S. Milosevic, N. Krstulovic, M. Klanjsek-Gunde, N. Hauptmann, *Journal of Physics D-Applied Physics* 40 (2007) 12, 3689–3696
- ¹⁶ A. Vesel, M. Mozetic, S. Strnad, Z. Persin, K. Stana-Kleinschek, N. Hauptman, *Vacuum* 84 (2009) 1, 79–82
- ¹⁷ T. Vrlinic, A. Vesel, U. Cvelbar, M. Krajnc, M. Mozetic, *Surface and Interface Analysis* 39 (2007) 6, 476–481
- ¹⁸ U. Cvelbar, M. Mozetic, N. Hauptman, M. Klanjsek-Gunde, *Journal of Applied Physics* 106 (2009) 10, 103303
- ¹⁹ Z. Vratnica, D. Vujosevic, U. Cvelbar, M. Mozetic, *Ieee Transactions on Plasma Science* 36 (2008) 4, 1300–1301
- ²⁰ U. Cvelbar, M. Mozetic, M. Klanjsek-Gunde, *Ieee Transactions on Plasma Science* 33 (2005) 2, 236–237
- ²¹ M. K. Gunde, M. Kunaver, M. Mozetic, A. Hrovat, *Powder Technology* 148 (2004) 1, 64–66
- ²² M. K. Gunde, M. Kunaver, M. Mozetic, P. Pelicon, J. Simcic, M. Budnar, M. Bele, *Surface Coatings International Part B-Coatings Transactions* 85 (2002) 2, 115–121
- ²³ M. Kunaver, M. Klanjsek-Gunde, M. Mozetic, A. Hrovat, *Surface Coatings International Part B-Coatings Transactions* 86 (2003) 3, 175–179
- ²⁴ M. Kunaver, M. Mozetic, M. Klanjsek-Gunde, *Thin Solid Films* 459 (2004) 1–2, 115–117
- ²⁵ M. Mozetic, *Vacuum* 71 (2003) 1–2, 237–240
- ²⁶ A. Drenik, A. Vesel, M. Mozetic, *Journal of Nuclear Materials* 386 (2009), 893–895

- ²⁷ A. Vesel, M. Mozetic, P. Panjan, N. Hauptman, M. Klanjšek-Gunde, M. Balat-Pichelin, *Surface & Coatings Technology* 204 (2010) 9–10, 1503–1508
- ²⁸ U. Cvelbar, Z. Q. Chen, M. K. Sunkara, M. Mozetic, *Small* 4 (2008) 10, 1610–1614
- ²⁹ U. Cvelbar, K. Ostrikov, I. Levchenko, M. Mozetic, M. K. Sunkara, *Applied Physics Letters* 94 (2009) 21, 211502
- ³⁰ U. Cvelbar, K. Ostrikov, M. Mozetic, *Nanotechnology* 19 (2008) 40, 405605
- ³¹ A. Drenik, A. Tomelj, M. Mozetic, A. Vesel, D. Babic, M. Balat-Pichelin, *Vacuum* 84 (2009) 1, 90–93
- ³² M. Mozetic, *Vacuum* 61 (2001) 2–4, 367–371
- ³³ M. Mozetic, U. Cvelbar, *International Journal of Nanoscience*, 6 (2007) 2, 121–124
- ³⁴ M. Mozetic, U. Cvelbar, A. Vesel, N. Krstulovic, S. Milosevic, *Ieee Transactions on Plasma Science* 36 (2008) 4, 868–869
- ³⁵ M. Mozetic, A. Zalar, *Vacuum* 71 (2003) 1–2, 233–236
- ³⁶ M. Mozetic, A. Zalar, U. Cvelbar, D. Babic, *Surface and Interface Analysis* 36 (2004) 8, 986–988
- ³⁷ A. Vesel, A. Drenik, M. Mozetic, A. Zalar, M. Balat-Pichelin, M. Bele, *Vacuum* 82 (2007) 2, 228–231
- ³⁸ A. Vesel, M. Mozetic, M. Balat-Pichelin, *Vacuum* 81 (2007) 9, 1088–1093
- ³⁹ A. Vesel, M. Mozetic, A. Drenik, S. Milosevic, N. Krstulovic, M. Balat-Pichelin, I. Poberaj, D. Babic, *Plasma Chemistry and Plasma Processing* 26 (2006) 6, 577–584
- ⁴⁰ A. Vesel, M. Mozetic, A. Zalar, *Applied Surface Science* 200 (2002) 1–4, 94–103
- ⁴¹ D. Babic, I. Poberaj, M. Mozetic, *Review of Scientific Instruments* 72 (2001) 11, 4110–4114
- ⁴² U. Cvelbar, M. Mozetic, I. Poberaj, D. Babic, A. Ricard, *Thin Solid Films* 475 (2005) 1–2, 12–16
- ⁴³ U. Cvelbar, M. Mozetic, A. Ricard, *Ieee Transactions on Plasma Science* 33 (2005) 2, 834–837
- ⁴⁴ M. Mozetic, U. Cvelbar, *Plasma Sources Science & Technology* 18 (2009) 034002
- ⁴⁵ M. Mozetic, A. Ricard, D. Babic, I. Poberaj, J. Levaton, V. Monna, U. Cvelbar, *Journal of Vacuum Science & Technology A* 21 (2003) 2, 369–374
- ⁴⁶ M. Mozetic, A. Vesel, A. Drenik, I. Poberaj, D. Babic, *Journal of Nuclear Materials* 363 (2007), 1457–1460
- ⁴⁷ I. Poberaj, M. Mozetic, D. Babic, *Journal of Vacuum Science & Technology a-Vacuum Surfaces and Films* 20 (2002) 1, 189–193
- ⁴⁸ W. V. Smith, *The Journal of Chemical Physics* 11 (1943) 3, 110–125

HYDROTHERMAL GROWTH OF $Zn_5(OH)_6(CO_3)_2$ AND ITS THERMAL TRANSFORMATION INTO POROUS ZnO FILM USED FOR DYE-SENSITIZED SOLAR CELLS

HIDROTHERMALNA RAST $Zn_5(OH)_6(CO_3)_2$ S TERMIČNO TRANSFORMACIJO V POROZNO PLAST ZnO, UPORABLJENO ZA ELEKTROKEMIJSKE SONČNE CELICE

Marko Bitenc, Zorica Crnjak Orel

Center of Excellence for Polymer Materials and Technologies, Tehnološki park 24, 1000 Ljubljana, Slovenia
marko.bitenc@ki.si

Prejem rokopisa – received: 2011-02-14; sprejem za objavo – accepted for publication: 2011-03-15

Zinc oxide (ZnO) films, composed of nano-sheets, were prepared by the thermal decomposition of hydrozincite film precursor ($Zn_5(OH)_6(CO_3)_2$, ZnHC). The ZnO film kept the morphology on the microscale level during the heat treatment, while the thermal decomposition caused the formation of a nano-porous structure of the nano-sheets' surface. ZnHC precursor was hydrothermally synthesized on the conductive glass from zinc nitrate and urea. The influence of media (water or mixture of water/ethylene glycol), PVP-K additive and the concentration of the initial reagents, on the morphology of the film were observed. The growth and morphology of the ZnHC film was followed with FE-SEM microscopy and the formation mechanism of the ZnHC film, formed in the water, was proposed. The assumed growth mechanism follows the concept of a self-assembling mechanism of the nanometer-sized building units into nano-sheets of ZnHC with a thickness of ≈ 20 nm. These nano-sheets are further agglomerating into porous film. The thickness of the film was around (5, 8, 10 and 20) μm after (2, 3, 4 and 24) h of synthesis, respectively. The addition of PVP-K and ethylene glycol retards the growth of ZnHC film. Moreover, the addition of PVP-K affects the interactions between particles and the substrate, which enable the parallel growth of the nano-sheets on the substrate surface. As prepared ZnO films were used for DSSCs, where the conversion efficiency was $\approx 0.6\%$.

Keywords: ZnO, hydrozincite, hydrothermal, precipitation, particles growth, SEM, DSSCs

Cinkov oksid (ZnO) smo pripravili kot tako plast na prevodni podlagi s termično obdelavo prekursorja hidrocinkita ($Zn_5(OH)_6(CO_3)_2$, ZnHC). Tako pripravljena plast je bila sestavljena iz nanolističev, ki so po termični obdelavi obdržali svojo obliko na mikroskopskem nivoju, medtem ko so na njihovi površini nastale luknjice nanovelikosti. Plast ZnHC smo pripravili s hidrotermalno precipitacijo cinkovega nitrata s sečnino. Ob tem smo opazovali vpliv različnih koncentracij začetnih reagentov, medija (voda in mešanica vode/etilen glikola) in dodatkov (PVP-K) na rast in morfologijo nastalega produkta, ki smo ju spremljali z FE-SEM-mikroskopijo. Na osnovi rezultatov opazovanja vzorcev, pripravljenih v vodnem mediju, smo predpostavili mehanizem rasti plasti ZnHC. Ugotovili smo, da ta mehanizem sledi konceptu povezovanja nanogradnikov v večje urejene kristalne mikrostrukture z obliko nanolističev z debelino ≈ 20 nm. Nanolističi ZnHC se na podlagi aglomerirajo v porozno plast. Debelina plasti je bila približno 5 μm po 2 h, 8 μm po 3 h, 10 μm po 4 h in 20 μm po 24 h sinteze. Dodatek PVP-K in etilen glikol upočasnita rast plasti ZnHC. Poleg tega je dodatek PVP-K vplival na interakcije med lističi in podlago, ki omogočijo rast lističev vzporedno s površino podlage. Plasti ZnO smo uporabili za izdelavo elektrokemijskih sončnih celic, katerih učinkovitost pretvorbe sončne energije v električno je $\approx 0,6\%$.

Ključne besede: ZnO, hidrocinkit, hidrotermalno, precipitacija, rast delcev, SEM, elektrokemijske sončne celice

1 INTRODUCTION

ZnO nano-sheets have attracted increasing interest on account of their specific microstructure and potential applications in many areas, such as chemical sensors, photocatalysts, phosphors and dye-sensitized solar cells (DSSCs).¹⁻⁴ For these applications the ZnO particles are typically prepared as a film on various glass or polymer substrates, covered with transparent conducting oxides (TCO). ZnO films and powders, reported in the literature, are most commonly composed of particles with the hexagonal rod-like morphology^{2,5-9} and rarely with nano-sheet morphology prepared from the corresponding layered ZnHC precursor with the thermal decomposition.^{1,3,10} The hydrothermal precipitation of ZnHC from zinc nitrate with urea was presented in our papers, where the influence of the different additives on the final morphology of the particles was studied in a closed

reactor system.¹¹ The precipitated ZnHC decomposed into ZnO in only one relatively sharp step. The growth mechanism of the ZnHC particles based on the combination of in-situ SAXS measurement and ex-situ electron microscopy was also presented in our recently published paper.⁴

The interest in dye-sensitized solar cells (DSSCs) has increased due to reduced energy sources and higher energy production costs. For the most part, titania (TiO_2) has been the material of choice for dye-sensitized solar cells and so far have shown the highest overall light conversion efficiency $\approx 11\%$.¹² However, ZnO has recently been explored as an alternative material in DSSCs with great potential since it has a bandgap similar to TiO_2 at 3.2 eV and has a much higher electron mobility ($\approx (115-155) \text{ cm}^2/(\text{V s})$) than TiO_2 ($\approx 10^{-5} \text{ cm}^2/(\text{V s})$). In addition, ZnO has ability of simpler tailoring of the

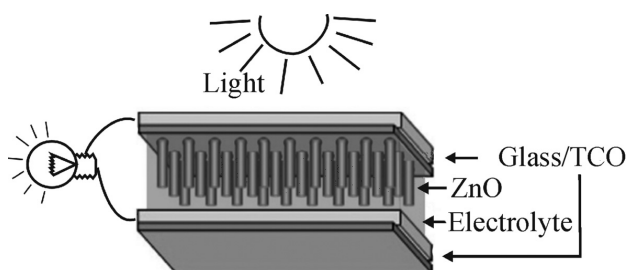


Figure 1: Schematic description of DSSCs applying ZnO nanoparticles as the electron transport material, dye for light-harvesting and electrolyte with a I^-/I_3^- redox couple

Slika 1: Shema elektrokemijske sončne celice, sestavljene iz ZnO-polprevodnika za transport elektronov, barvila na polprevodniku in elektrolita z redoks parom I^-/I_3^-

particles' morphology. Also it can not be neglected, that the initial compounds for the production of ZnO are much cheaper as compared to TiO_2 . The efficiency of the DSSCs prepared from the ZnO nano-sheet film is lower regarding DSSCs that use TiO_2 for their preparation.^{1,3} In the literature it was reported that DSSCs with the ZnO nano-sheets film electrode, prepared from ZnHC precursor, have the efficiency around 4 %.

Figure 1 shows a schematic representation of DSSCs applying vertically-aligned ZnO nanostructured electrode. The typical basic configuration is as follows: At the heart of the device is the mesoporous oxide layer composed of ZnO film. Typically, the film thickness is $\approx 10 \mu m$ and the porosity is 50–60 %. The mesoporous layer of ZnO is deposited on substrate (polymer or glass) coated with TCO, such as indium tin oxide (ITO) fluorine doped tin oxide (FTO) or aluminium doped zinc oxide (AZO). Attached to the surface of the ZnO film is a monolayer of the charge-transfer dye, mostly based on ruthenium. Photoexcitation of the later results in the injection of an electron into the conduction band of the oxide, leaving the dye in its oxidized state. The dye is restored to its ground state by electron transfer from the electrolyte, which is usually an organic solvent containing the iodide/triiodide redox system. The regeneration of the sensitizer by iodide intercepts the recapture of the conduction band electron by the oxidized dye. The I_3^- ions formed by oxidation of I^- diffuse because of a short distance ($< 50 \mu m$) through the electrolyte to the cathode, which is coated with a thin layer of platinum catalyst, where the regenerative cycle is completed by electron transfer to reduce I_3^- to I^- .

In this work we present the preparation of ZnHC film from zinc nitrate and urea in different media, such as water, water/EG mixture and in water with addition of PVP-K. The growth of the ZnHC film, which was later thermally decomposed into ZnO, was followed with FE-SEM microscopy. The formation mechanism of the ZnHC film, in water, is presented. As prepared ZnO films were used for DSSCs preparation.

2 EXPERIMENTAL

All reagents in the experimental work were of analytical reagent grade. To avoid hydrolysis upon storage, fresh stock solutions prepared from $Zn(NO_3)_2 \times 6H_2O$ (Aldrich) and urea (Aldrich) in millique water were used. The detailed experimental conditions for the preparation of samples are given in **Table 1**. The initial concentrations of Zn^{2+} ions were 0.1 M and 0.01 M and urea 0.5 M and 0.05 M. The concentration of urea was five times higher than Zn^{2+} in all experiments. As solvents water and a mixture of water and ethylene glycol (EG, Merck) with the volume ration 1 : 1, were used. Experiments were performed without and in the presence of PVP-K additive. The additive was dissolved in the initial reactive mixture before hydrolysis took place. The concentration of additive was 10 mg/mL throughout the experimental study.

Table 1: Experimental conditions for the sample preparations in water and water/ethylene glycol (EG) mixture, with and without additive

Tabela 1: Pregled eksperimentov za pripravo tanke plasti na prevodnem steklu v vodi in mešanici voda/etilen glikol (EG) brez dodatka in z njim

Sample	Medium	Solution mL	C (Zn^{2+}) M	PVP-K mg/mL	Time h
A	water	50	0.1	/	2, 3, 4, 24
B	water	50	0.01	10	24
C	water + EG	25 + 25	0.01	/	72

The experiments were carried out in laboratory bottles, where the total volume of reaction mixture was 50 mL. Borosilicate glass slides, with one side covered with the $SnO_2 : F$, were used as substrates for the film deposition. The substrates were placed into laboratory bottles filled with Zn/urea solution, sealed and kept at 90 °C for 2 h to 72 h in drying oven (Kambič, Easy) as presented in **Figure 2a**. During these experiments, the temperature was measured in the center of laboratory bottle with Pt100. The resulting temperature profile shows that maximum temperature was reached after around 100 min and was constant (85 °C) during the synthesis (**Figure 2b**). After the deposition, the obtained

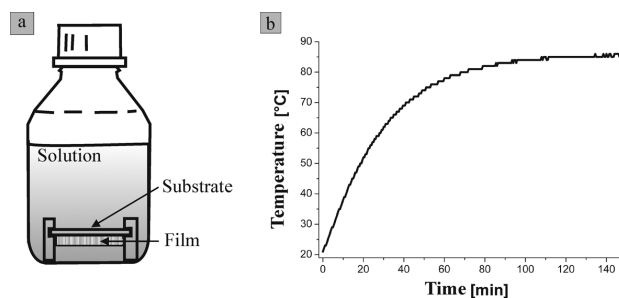


Figure 2: a – Schematic description of the film preparation. b – Temperature profile in laboratory bottle

Slika 2: a – Shema priprave delcev na podlagi; b – Temperaturni profil v laboratorijski steklenici

hydrozincite films were rinsed with ethanol and dried at room temperature. The films were thermally treated at 300 °C for 30 min in air. As prepared ZnO film were used for DSSCs preparation.

The DSSCs were prepared and characterized in Laboratory of Photovoltaics and Optoelectronics of the Faculty of Electrical Engineering (University of Ljubljana) as previously reported in their papers.^{13–15}

Samples were characterized by scanning field emission electron microscopy (FE-SEM, Zeiss Supra 35 VP). IR-spectra were obtained on an FTIR spectrometer (Perkin Elmer 2000) in the spectral range between 4000 cm^{-1} and 400 cm^{-1} with a spectral resolution of 2 cm^{-1} . The KBr pellet technique was used for the sample preparation.

3 RESULTS AND DISCUSSION

The FE-SEM microstructure of the hydrozincite (ZnHC) film marked as Samples A, which was prepared on the glass substrate coated with $SnO_2 : F$ in water medium after (2, 3, 4 and 24) h are presented in **Figure 3** (top-view) and **Figure 4** (cross-section). The porous spherical structures composed of nano-sheets with thickness around 20 nm was observed after 2 h of synthesis as presented in **Figures 3a and 4a**. The thickness of ZnHC film is round 5 μm after 2 h of the synthesis as presented in **Figure 4a**. From the particles' microstructure and morphology, we could propose that

ZnHC nano sheets begin to grow from one point (initial nucleus) on a substrate and not separately, which is typical for the growth of the pure hexagonal ZnO.^{16–18} The top-view and the cross-sectional micrographs of the substrate's microstructure of the Sample A, obtained after 3 h (**Figures 3b and 4b**) and 4 h (**Figures 3c and 4c**) are presented, respectively. The nano-sheets cover the entire surface of the substrate. The thickness of ZnHC film is about 8 μm after 3 h and about 10 μm after 4 h of the synthesis. The thickness of the film increases up to 20 μm after 24 h of synthesis (**Figure 4d**). We found that nano-sheets grow in the length and width, while the thickness of the nano-sheets was remaining constant about 20 nm (**Figure 3d**). The ZnHC film was found on substrate only on the conductive side and when this side was facing down (**Figure 2a**). Scratches and dirt on conductive side of the substrate retard and limited the growth of the particles.

The proposed growth mechanism of the ZnHC film on the TCO substrate is schematically presented in **Figure 5**. We propose that growth of the nano-sheets follows the growth mechanism of the ZnHC particles which was recently presented by our group. We explain the growth mechanism by the "non-classical crystallization" concept of a self-assembling mechanism. The growth mechanism predicts the rapid formation of nanometer-sized building units. The size of these nano building units, stable only in the reaction medium, remains nearly constant during the synthesis, as the concentration of the nano building units increases

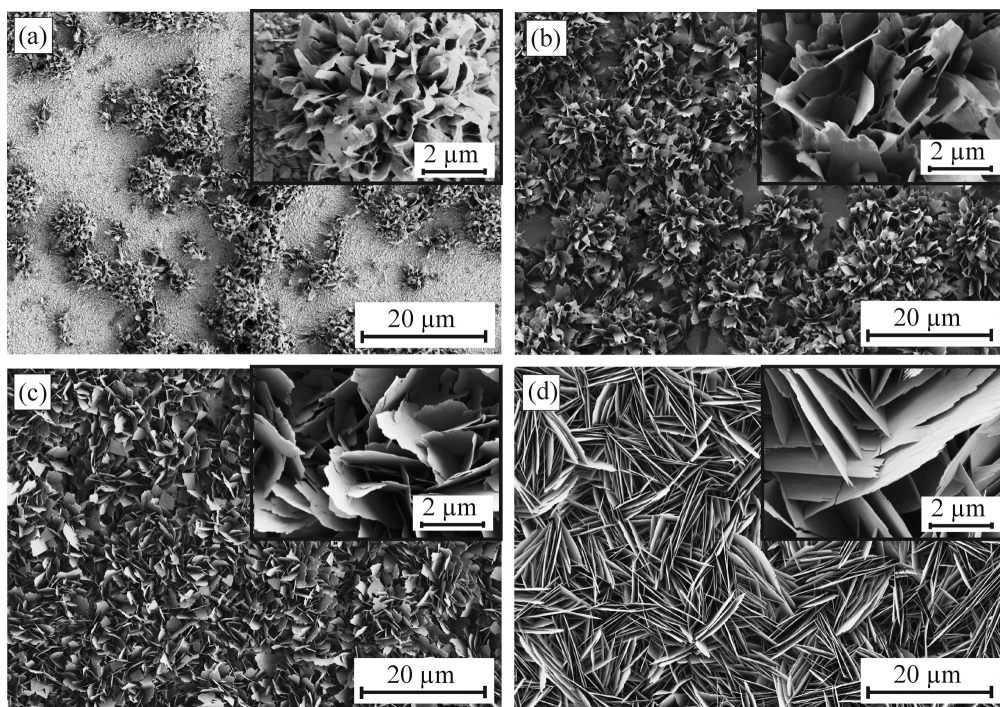


Figure 3: FE-SEM microstructure of the ZnHC of Sample A prepared on the glass substrate in water medium after (a) – 2 h, (b) – 3 h, (c) – 4 h in (d) – 24 h

Slika 3: FE-SEM-mikrostruktura ZnHC-vzorca A, pripravljenega na prevodnem steklu v vodnem mediju pri različnih časih: (a) – 2 h, (b) – 3 h, (c) – 4 h in (d) – 24 h

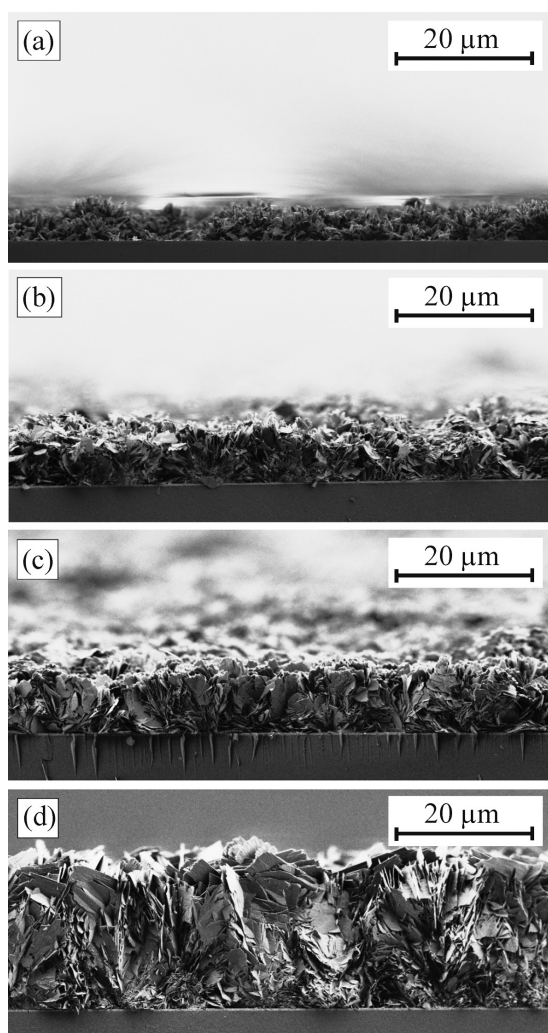


Figure 4: FE-SEM microstructure of the ZnHC film cross-section of Sample A prepared on glass substrate in water medium after (a) – 2 h, (b) – 3 h, (c) – 4 h in (d) – 24 h

Slika 4: FE-SEM-mikrostruktura prereza plasti ZnHC-vzorca A, pripravljenega na steklu v vodnem mediju ob različnih časih: (a) – 2 h, (b) – 3 h, (c) – 4 h in (d) – 24 h

throughout the reaction. These leaves of ZnHC are further agglomerated into porous, nano-sheet like film. The thickness of the film is increasing with time.

The influence of the medium (a mixture of water/EG at volume ratio 1/1), PVP-K additive and the concentration of the initial reagents, on the morphology and growth of the film were observed (**Figure 6**). Microstructure of Sample B, prepared with the addition of PVP-K (10 mg/mL) after 24 h of synthesis, is presented in **Figure 6a**. We found that the addition of PVP-K noticeably retard the growth of ZnHC film, since the microstructure of the particles is similar to the film of Sample A prepared in water after 2 h of the synthesis (**Figure 3a**). Additionally, we observed the parallel (according to substrate surface) formation of nano-sheets in the synthesis with the PVP-K, as it is presented in **Figure 6a**. We assume the addition of PVP-K affects

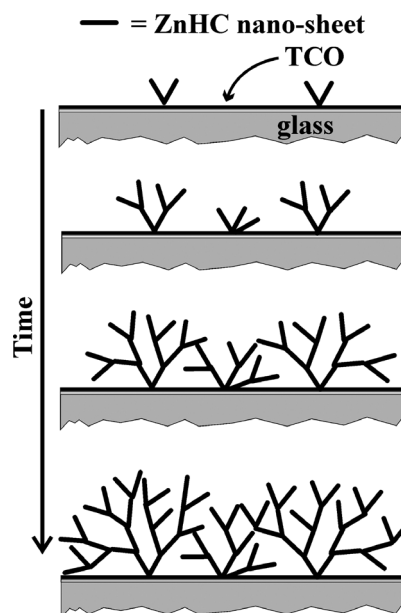


Figure 5: Schematic description of the growth mechanism of ZnHC film on the substrate

Slika 5: Shematično predstavljen mehanizem rasti plasti ZnHC na podlagi

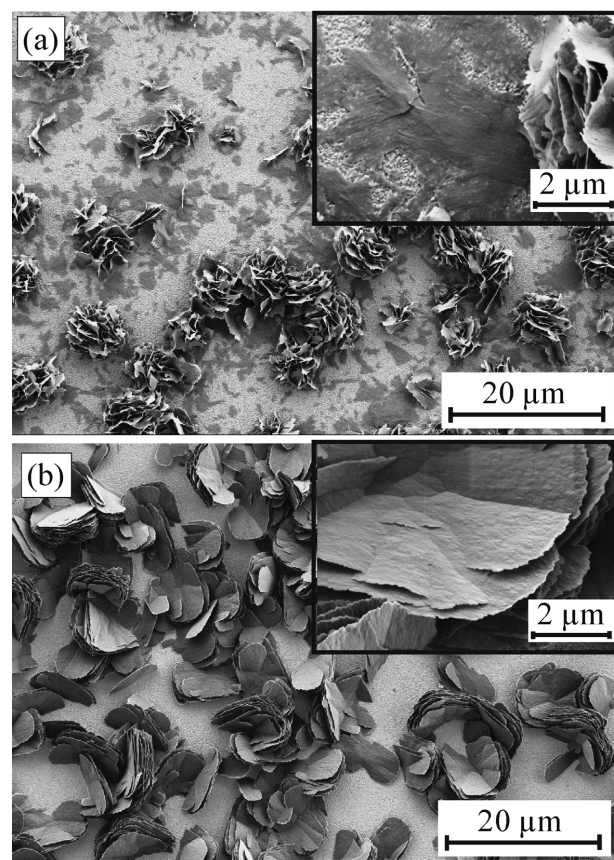


Figure 6: FE-SEM microstructure of the ZnHC samples prepared on glass substrate: (a) – Sample B, prepared in water with PVP-K additive and (b) – Sample C prepared in water/EG mixture

Slika 6: FE-SEM-mikrostruktura delcev ZnHC, pripravljenih na steklu: (a) – vzorec B, pripravljen v vodi z dodatkom PVP-K in (b) – vzorec C, pripravljen v mešanici voda/EG

hydrophilic/hydrophobic interactions between particles and the substrate, which enable the parallel growth of the nano-sheets on the substrate surface.¹ Microstructure of Sample C, prepared in the mixture of water/EG 1/1, after 72 h of synthesis is shown in **Figure 6b**. Particle growth is retarded even at a higher concentration of initial reagents.

As prepared ZnHC films on the TCO substrate were additionally heat-treated for 30 min at 300 °C. The FE-SEM microstructure of heat treated film of Sample A (4 h) is presented in **Figure 7** as an example. Similar effects were observed also in other samples (micrographs not presented in this paper). Generally the size and the morphology of the particles observed by FE-SEM remain practically identical on the micro scale during heat treatment (**Figure 7**). However, the annealing caused the formation of a nanoporous structure on the particles' surface, which revealed an increased specific surface area.¹¹

The samples were characterized by FTIR (**Figure 8**) before and after heat treatment to determine the chemical composition of the prepared films. The FTIR spectrum of Sample A, prepared after 24 h of synthesis and before heat treatment, is presented in **Figure 8a**. The presence of carbonate groups in the ZnHC product was confirmed

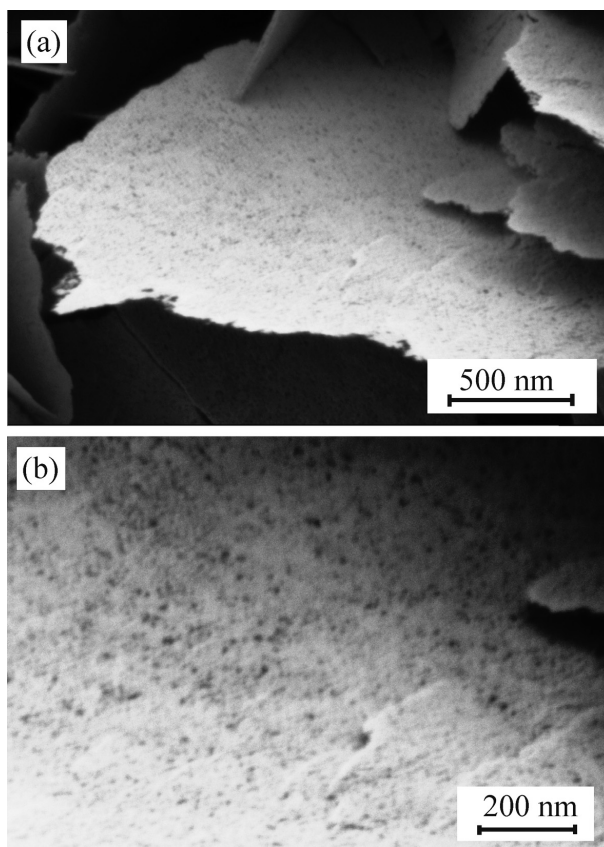


Figure 7: FE-SEM microstructure of ZnO film of Sample A (4 h) after 30 min of heat treatment at 300 °C

Slika 7: FE-SEM-mikrostruktura plasti ZnO-vzorca A (4 h) po 30 min termični obdelavi na 300 °C

by bands in the spectral range from 1600 cm^{-1} and 1200 cm^{-1} , i.e. the frequency at 1507 cm^{-1} and 1390 cm^{-1} , and additionally with the frequency at 1044 cm^{-1} , 956 cm^{-1} and at 708 cm^{-1} .^{4,19} After thermal treatment (300 °C) of this sample (Sample A, 24 h) the band at 421 cm^{-1} with a pronounced shoulder at 530 cm^{-1} in the IR spectra (**Figure 8b**) confirmed the presence of ZnO.

ZnO films, obtained after 4 h and 24 h of the synthesis and additionally heat treated for 30 min at 300 °C, were used for the preparation of DSSCs.^{12–15} Average current density-voltage characteristics of electrochemical solar cells under standard conditions (100 mW/cm^2 , 25 °C) are summarized in **Table 2**. The density-voltage characteristic curve of the best DSSCs, prepared from the ZnO film after 4 h of the synthesis is presented in the **Figure 9**.

Table 2: An average short-circuit photocurrent density (J_{SC}), open-circuit voltage (V_{OC}), fill factor (FF), and conversion efficiency (η) of the DSSCs evaluated under STC (100 mW/cm^2 , 25 °C) for the ZnO films prepared after 4 h and 24 h of synthesis

Tabela 2: Povprečne meritve kratkostične tokovne gostote (J_{SC}), napetosti odprtih sponk (V_{OC}), polnilnega faktorja (FF) in učinkovitost pretvorbe (η) za DSSCs, izmerjen pri standardnih pogojih (100 mW/cm^2 , 25 °C) in z uporabo plasti ZnO pripravljene po 4 h in 24 h sinteze

Synthesis time, h	$J_{SC}/mA/cm^2$	V_{OC}/V	$FF/\%$	$\eta/\%$
4	2.63	0.52	41.93	0.57
24	3.23	0.50	36.37	0.58

An average open-circuit voltage (V_{OC}) 0.52 V and 0.50 V, and conversion efficiency (η) 0.57 % and 0.58 % of the DSSCs, evaluated under STC (100 mW/cm^2 , 25 °C) and prepared from the ZnO films of the 4 h and 24 h synthesis, are comparable. However, the short-circuit photocurrent density (J_{SC}) is higher (3.23 mA/cm^2) in a cell made from the thicker ZnO film ($\approx 20 \mu m$) prepared after 24 h of the synthesis, compared to the J_{SC} of the

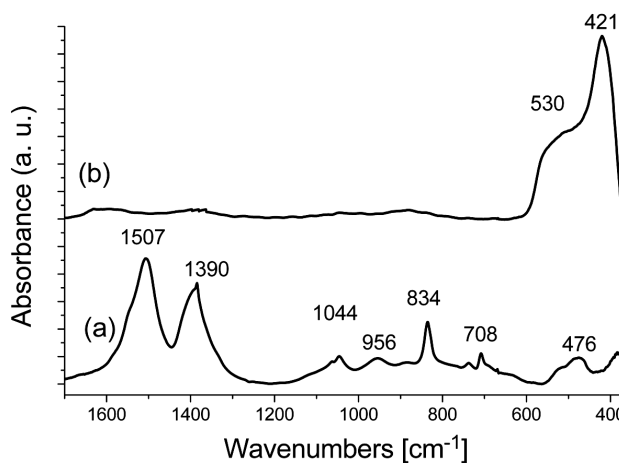


Figure 8: FTIR spectra of Sample A prepared after 4 h of synthesis (a) and with additional heat treatment (b)

Slika 8: FTIR-spekter vzorca A, pripravljenega po 4 h sinteze (a) in po dodatni termični obdelavi (b)

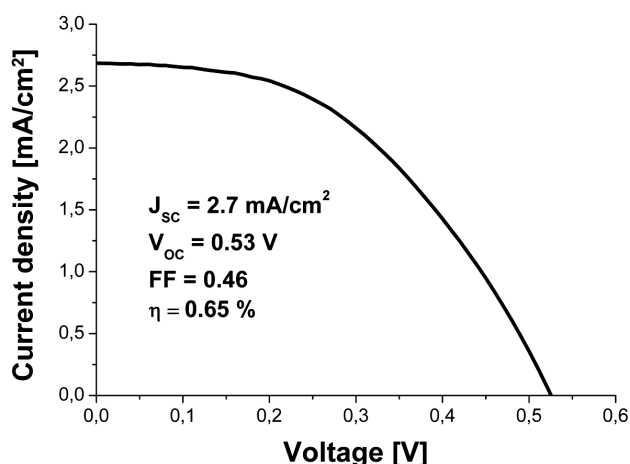


Figure 9: A current density-voltage curve of the dye-sensitized solar cell prepared from ZnO films of Sample A (4 h of synthesis)

Slika 9: Tokovno-napetostni odziv elektrokemijske sončne celice, pripravljen iz plasti ZnO vzorca A (4 h sinteze)

DSSCs prepared from the 10 μm thick ZnO film obtained after 4 h of synthesis. Contrary, the fill factor (FF) 41.93 % is higher in a DSSCs prepared from the thinner ZnO film (4 h synthesis), compared to the FF 36.37 % obtained in the DSSCs with thicker ZnO film. Results prove that larger film thickness increases the amount of adsorbed dyes, which leads to higher J_{SC} . On the other hand, increasing the film thickness decreases FF through diffusion-limited access.¹

The V_{OC} and FF of our DSC cells are comparable to results reported in the literature.^{1,3} On the other hand, the J_{SC} of cells is between 2.63 mA/cm^2 and 3.23 mA/cm^2 in a short circuit, which is almost one third of comparable measurements in literature.^{1,3} The low J_{SC} could be explained by the generation of the Zn^{2+}/dye aggregates. Ru-complexes dyes, such as N-719 (used in our case), are slightly acid, since they could have protons derived from the complex.³ Consequently, the dye-loading solution dissolves the surface of ZnO and makes Zn^{2+}/dye aggregates, which influence on the lower electron injection efficiencies and fill nano-scale pores. The optimization of various parameters including ZnO film fabrication, dyeing time, heating conditions, and so on, will result in the improvement of the conversion efficiency because the FF and V_{OC} in this work are reasonably high.

4 CONCLUSIONS

ZnO film with the nano-sheets porous microstructure was prepared by the thermal decomposition of ZnHC precursor, which was hydrothermally synthesized on the conductive glass from zinc nitrate and urea. The growth mechanism and the morphology of the ZnHC film was followed with SEM microscopy and the formation of the ZnHC film, is proposed by the "non-classical crystalli-

zation" concept of a self-assembling mechanism. The influence of a mixture of water/EG, surfactant additive PVP-K and the concentration of the initial reagents, on the morphology of the film were observed. ZnO films were used for the preparation of DSSCs with the average conversion efficiency around 0.6 %.

ACKNOWLEDGMENT

The authors would like to thank the colleges from Laboratory of Photovoltaics and Optoelectronics (Faculty of Electrical Engineering, UL) for their help regarding DSSC assembling and characterization. We acknowledge the financial support from the Ministry of Higher Education, Science and Technology of the Republic of Slovenia through the contract No. 3211-10-000057 (Center of Excellence for Polymer Materials and Technologies).

5 REFERENCES

- E. Hosono, S. Fujihara, I. Honna, H. S. Zhou, *Adv. Mater.*, 17 (2005) 17, 2091–2094
- I. Gonzalez-Valls, M. Lira-Cantu, *Energy & Environmental Science*, 2 (2009) 1, 19–34
- K. Kakiuchi, M. Saito, S. Fujihara, *Thin Solid Films*, 516 (2008) 8, 2026–2030
- M. Bitenc, P. Podbršček, P. Dubček, S. Bernstorff, G. Dražić, B. Orel, S. Pejovnik, Z. C. Orel, *Chem.–Eur. J.*, 16 (2010) 37, 11481–11488
- Z. Y. Fan, J. G. Lu, *J. Nanosci. Nanotechnol.*, 5 (2005), 10, 1561–1573
- Y. W. Heo, D. P. Norton, L. C. Tien, Y. Kwon, B. S. Kang, F. Ren, S. J. Pearton, J. R. LaRoche, *Materials Science & Engineering R-Reports*, 47 (2004) 1–2, 1–47
- M. Bitenc, P. Podbršček, Z. C. Orel, M. A. Cleveland, J. A. Paramo, R. M. Peters, Y. M. Strzhemechny, *Cryst. Growth Des.*, 9 (2009) 2, 997–1001
- M. Bitenc, G. Dražić, Z. C. Orel, *Cryst. Growth Des.*, 10 (2010) 2, 830–837
- G. Ambrožič, S. D. Škapin, M. Žigon, Z. C. Orel, *J. Colloid Interface Sci.*, 346 (2010) 2, 317–323
- P. Podbršček, Z. C. Orel, J. Maček, *Mater. Res. Bull.*, 44 (2009) 8, 1642–1646
- M. Bitenc, M. Marinšek, Z. C. Orel, *J. Eur. Ceram. Soc.*, 28 (2008) 15, 2915–2921
- T. P. Chou, Q. F. Zhang, G. E. Fryxell, G. Z. Cao, *Adv. Mater.*, 19 (2007) 18, 2588–2595
- M. Hočevar, M. Berginc, M. Topič, U. O. Krašovec, *J. Sol-Gel Sci. Technol.*, 53 (2010) 3, 647–654
- M. Berginc, U. O. Krašovec, M. Hočevar, M. Topič, *Thin Solid Films*, 516 (2008) 20, 7155–7159
- U. O. Krašovec, M. Berginc, M. Hočevar, M. Topič, *Sol. Energy Mater. Sol. Cells*, 93 (2009) 3, 379–381
- A. B. Djurisić, Y. H. Leung, *Small*, 2 (2006) 8–9, 944–961
- L. Schmidt-Mende, J. L. MacManus-Driscoll, *Materials Today*, 10 (2007) 5, 40–48
- A. S. Barnard, Y. Xiao, Z. Cai, *Chem. Phys. Lett.*, 419 (2006), 4–6, 313–316
- M. Bitenc, Z. C. Orel, *Mater. Res. Bull.*, 44 (2009) 2, 381–387